A metallogenetic model for carbonate-hosted non-sulphide zinc deposits based on observations of Mehdi Abad and Irankuh, Central and Southwestern Iran

Dissertation

zur Erlangung des akademischen Grades
Doctor rerum naturalium (Dr. rer. nat.)

vorgelegt der

Mathematisch-Naturwissenschaftlich-Technischen Fakultät
(mathematisch-naturwissenschaftlicher Bereich)
der

Martin-Luther-Universität Halle-Wittenberg

von

Jörg Reichert
geb. am 20.08.1971 in Anklam

Gutachter:
1. Prof. Dr. Gregor Borg
   (Institut für Geowissenschaften, Martin-Luther-Universität Halle-Wittenberg)
2. Prof. Dr. Bernd Lehmann
   (Institut für Mineralogie und Mineralische Rohstoffe, Technische Universität Clausthal

Verteidigt in Halle/Saale, 07.05. 2007

urn:nbn:de:gbv:3-000011883
[http://nbn-resolving.de/urn/resolver.pl?urn=nbn%3Ade%3Agbv%3A3-000011883]

ACKNOWLEDGEMENTS

I would like to thank the Geological Department of the Martin-Luther-University Halle-Wittenberg (MLU) for providing the resources for research throughout this Ph.D.

The author is grateful to the Federal State of Sachsen-Anhalt for financial support by a doctoral scholarship and is grateful to Anglo American for providing an additional funding.

The first person, I want to thank, is my supervisor Prof. Dr. Gregor Borg. His long-term interest in non-sulphide Zn-deposits and his ability to arouse my interest in this type of Zn-deposits was the decisive point for me to start this Ph.D.-Project. His enthusiasm, his many good advices, and his fair comment have always been a valuable help in finishing this project. His excellent didactic abilities and his competence in the field of non-sulphide Zn-deposits and economic geology also enriched this project. Lot's of thanks!

Thanks to Prof. Dr. Bernd Lehmann. The final published version of this study has profited from his comments.

I would like to thank Ian Willis, Nick Franey and Mike Buxton, and the staff of the Anglo Exploration Division for their support and the well-organised non-sulphide Workshop in Johannesburg. This workshop and the associated discussion have widened my understanding of non-sulphide zinc deposits and, in addition, it helped to see both sides: the scientific and the economic/financial aspects of non-sulphide zinc deposits from the point of view of a mining company.

I would like to thank PARS KANI Mineral Industries Research and Development Co, Iran and especially Zaker Salehi, A. Houshmand-Zadeh, and Rashidi Bahman for the hospitality, the logistical support, and stimulating scientific discussions, respectively, during the fieldwork in Iran.

The study has profited from scientific discussions with Thomas Johannes Degen (MLU), Christoph Gauert (University of the Free State, South Africa), Sabine Walther (MLU), Susanne Schmid (Geological Survey of Denmark and Greenland), and Prof. Dr. H. A. Gilg (Technical University, Munich).

An additional special thank is given to Sabine Walther. Her special dark and strong coffee and the discussions with her have become to an invaluable ritual.

Furthermore, I would like to thank the management and the staff of the BAMA Mining Co. of Esfahan for their hospitality and the great support of this project. I want to thank Mr Farshid Esmaeil, Mr. Saedy Mr. Saheban, Mr. Alameh.

I want to thank the management of the Mehdi Abad project for their great hospitality and the support of the fieldwork: Mr. Shamsi and Mehdi Kohi.

My deepest gratitude belongs to Katja. Her patience, encouragement, and love were essential for the work at this Ph.D. project. I am lucky to have a person like her by my side.

The last note and the final words in my acknowledgments are in honor of my father and my mother, who always encouraged me to go one step further. They accompanied me during the most important time of my life and had to go much too early.

LIST OF ABBREVIATIONS

a = activity [mol*l^{-1}]

c = concentration [mol*l^{-1}]

CL = cathodoluminescence

EDX = energy dispersive X-ray

Eh = oxidation-reduction potential

eV = electron Volt

ga = galena

HFO = hydrous ferric oxide

HREE = heavy REE

hy = hydrozincite

K = Kelvin

kPa = kilo Pascals

Loga_ = log of activity of an aqueous species [mol·l^{-1}]

LOI = loss on ignition

LPE = Law of Proportional Effect

LREE = light REE

m = mass

M = molar mass

m.a.s.l. = metres above sea level

Ma = million years

MOB = Mountain Ore Body (Mehdi Abad)

MPa = mega Pascals

P = partial pressure in kPa

P_{CO2} = partial pressure of CO_2

P_{H2O} = partial pressure of water vapour

P_{O2} = partial pressure of O_2

ppl = plane polarised light

ppm = part per million

py = pyrite

SEM = scanning electron microscopy

Si [mineral name] = saturation index

sm = smithsonite

stdev = standard deviation

SX-EW = solvent extraction-electro winning

T = temperature

V_m = molar volume

VOB = Valley Ore Body (Mehdi Abad)

X = molar fraction

XN = crossed nicols

XRD = X-ray diffraction

°**C** = degree Celsius

Table of content

Abstract

The general metallogenetic model presented here is based on observations from the Iranian combined non-sulphide/sulphide zinc deposit Mehdi-Abad and the non-sulphide Koladahrvazeh mine in the Irankuh mining district (Iran). The resulting geochemical model has been tested and refined by the simulation of complex hydrochemical models using the PHREEQC software developed by PARKHURST & APPELO (1999).

The non-sulphide zinc ore spectrum has two end members: red zinc ore, rich in Zn (>20%), Fe (>7%), Pb - (As) and white zinc ore with typically high zinc grades (up to 40%) but low concentrations of iron (<7%) and lead. These typically high concentrations of iron and lead in red zinc ore can be observed in many non-sulphide zinc deposits in Iran and elsewhere (e.g. Sierra Mohada, Mexico) and have been described by other authors as well (e.g. CABALA, 2001). Common minerals of the red zinc ore are Fe-oxyhydroxides, goethite, hematite, hemimorphite, smithsonite and/or hydrozincite, and cerrusite. These minerals are also common within the 'white zinc ore' although in different proportions. Metal separation is caused by a gradual change from an acidic oxidation zone to alkaline conditions in the adjacent carbonate wall rock. The establishment of an acidic oxidation zone within carbonate host rock is facilitated by the "armouring" of calcite by gypsum and hydrous ferric oxides (HFO) (HUMICKI, 2004; HUMINICKI & RIMSTIDT, 2004) and by several pH-buffering reactions (BLOWES & PTACEK, 1994). Iron precipitates within the oxide zone mostly as immobile HFO, which additionally adsorbs various amounts of Pb and Zn, depending on pH (MARTINEZ & MCBRIDE, 2001; DZOMBAK & MOREL, 1990). The high activity of SO_4^{2-} ions during the oxidation stage immobileises lead and leads to the precipitation of (under theses conditions) highly insoluble anglesite. A major portion of the zinc (up to 80% at pH 6 or 97% at pH 5) leaves the oxidation zone and precipitates as zinc carbonates in adjacent parts of the carbonate host rock. The neutralisation of the sulphuric acid by reaction with the carbonates of the host rock during the 'oxidation stage' liberates CO_2. Consequently, the CO_2 partial pressure (P_{CO2}) increases drastically and forms a CO_2-halo around the active oxidation zone. Thus, most of the zinc precipitates as smithsonite, which occurs exclusively in a high P_{CO2} environment. Subsequent to the oxidation process, i.e. during the 'post-oxidation stage', the P_{CO2} decreases and reaches the level of atmospheric P_{CO2}. Now, hydrozincite becomes stable and starts to replace smithsonite. Most of the stage-I smithsonite becomes corroded and altered to stage-II hydrozincite. The 'post-oxidation stage' is also associated with the successive local formation of zinc silicates, according to the availability of SiO_2 within the solution and the partial mobilisation of lead and the replacement of anglesite by cerussite.

In general, an arid climate provides the best conditions for the preservation of non-sulphide deposits. The limited availability of meteoric water and deep to very deep water tables protect the sulphide ore from subsequent dissolution.

The Mehdi Abad zinc-lead deposit is located in central Iran and is one of the largest zinc deposits of the region. The orebody consists of both primary sulphide and supergene non-sulphide ore. The deposit comprises a main sulphide/non-sulphide combined orebody (Valley Orebody, VOB), and an exclusively non-sulphide orebody (Mountain Orebody, MOB). The VOB is located in a valley and is covered by alluvial overburden. The exclusively non-sulphide MOB is located on the flanks of a mountain, separated by faults from the VOB. The non-sulphide ore of the MOB occurs as a matrix of fault- and karst breccias. Ore minerals comprise hemimorphite, hydrozincite, smithsonite, goe-

thite, as well as small amounts of mimetite, hetaerolite, and sauconite. Two separate types of the non-sulphide ore of the MOB can be distinguished: red zinc ore and white zinc ore. The red zinc ore is characterised by high Fe, Mn, Pb, and Zn concentrations. The white zinc ore, in contrast, is very high in Zn but low in Fe and Pb. Both types of zinc ore occur spatially (i.e. laterally and/or vertically) separated from each other. The formation of the two distinct non-sulphide ore types of the MOB is due to a rapid oxidation process. One of the main controlling factors was a high pyrite concentration of the sulphide protore, which generated a high acidity during the oxidation process. The above-mentioned geochemical processes led to a metal separation resulting in the formation of white and red zinc ore. The VOB, in contrast is covered by alluvial overburden. Its deep location prevents oxygen to reach the orebody in large quantities. The oxidation process is slow, produces only minor acidity, and thus has limited ability for metal separation processes. The still active oxidation of the VOB has produced Fe-rich non-sulphide ore without a differentiation into white and red zinc ore type.

The Kolahdarvazeh pit in the Irankuh mining district is dominated by white non-sulphide zinc ore and minor amounts of sulphide ore. The main portion of the non-sulphide mineralisation occurs as cement of a dolomite (karst-) breccia, but it also occurs as filling of faults and fractures. Smithsonite, hydrozincite, hemimorphite, cerussite, leadhillite, malachite, calcite, goethite, hematite, limonite, coronadite, and barite have been detected within the non-sulphide ore. The ore is hosted in Cretaceous dolomites. The sulphide ore is still observable in several bore holes and consists predominantly of sphalerite and galena. Pyrite and other Fe-(Cu-) bearing minerals are rare. In the Kolahdarvazeh mine the red zinc ore is absent. There is no evidence, that the white zinc ore of the Koladahrvazeh mine has been formed due to metal mobilisation and differentiation. The main portion of the white zinc ore is proposed to be a result of in situ replacement of sulphide protore by non-sulphide minerals. Only a small portion has been successively mobilised by meteoric water and has locally formed a high quantity of white zinc ore as cement of karst breccias. The formation of the non-sulphide ore has been supported by the proximity of a footwall aquitard (shales) where the metal bearing fluids became ponded. The location of the Kolahdarvazeh pit between two important faults and impermeable shales below likely played an important role in the genesis of this deposit. The shales acted as an impermeable and insoluble barrier for both the ore-delivering fluids and the ground water system. This hydraulic barrier stopped the fluid-flow, which caused a long lasting and effective enrichment process that affected the dolomite and the limestone adjacent to the Kolahdarvazeh fault and the shales.

1 Introduction

The utilisation of and the industrial/economic interest in non-sulphide zinc ore has changed through time and reflects the ability to process different types of Zn-Pb – ore as well as the industrial capability to use different types of Zn-Pb ores for the winning of zinc and lead. Non-sulphide zinc deposits were the principal source of zinc in the world until the 20th century (LARGE, 2001; BONI, 2003). The dominance in mining of non-sulphide zinc deposits reaches from Roman times up to the 18th century. Different types of non-sulphide zinc ores have been used depending on their availability. Zn-(hydro-)silicates as well as Zn-(hydro-)carbonates or a mixture of these have been used as zinc source for the production of brass (a zinc-copper-tin alloy) (BONI & LARGE, 2003). During the nineteenth and early twentieth centuries, zinc metal was recovered almost entirely from smithsonite-bearing non-sulphide ores in so-called 'Wälz' kilns (HITZMAN ET AL., 2003). However, the development of floatation techniques and the ability to process zinc sulphides, such as sphalerite, has resulted in the dominance of sulphide ores in zinc metal production. The (renewed) commercial interest for non-sulphide zinc ore and its associated deposits is due to the availability of improved solvent-extraction methods with coupled electro-winning. This combination of hydrometallurgical techniques provides the possibility to produce zinc with very high purity. Thus, it is possible to produce 'medical-grade' zinc with a purity of 99.99 % zinc with relatively low energy input by solvent-extraction and electro-winning processes (SX-EW), generating higher economic value on site (BORG, 2002 B).

Non-sulphide zinc deposits combine several important advantages. One of the most important advantages is the high concentration of zinc in several types of non-sulphide zinc ores. Average cost-effective zinc concentrations of carbonate-hosted non-sulphide zinc ores range from 10 % up to 35 % zinc and more. Furthermore, some non-sulphide ore types are characterised by low concentrations of lead, arsenic, cadmium and other toxic and/or unwanted metals. The mining of these non-sulphide zinc ore is highly profitable without detrimental effects on the environment by toxic metals and/or emmsion of sulphur bearing gasses into the atmosphere (SO_2, sulphuric acid, and associated acid rain) or process residuals that need storage in waste dumps .

Countries, which are mining non-sulphide zinc (-lead) ores, are Brazil, Iran, Namibia, China, and Thailand (WELLMER, 2002, LARGE, 2001). Additional projects in Kazakhstan, Jemen, and Australia will start production in the near future.

The technical progress turned the non-sulphide zinc ores into attractive exploration targets due to a number of advantages such as low metal recovery costs and favourable environmental aspects such as the obvious absence of sulphur (LARGE, 2001, BORG, 2002B, HITZMAN ET AL., 2003). This unusual group of sediment-hosted zinc deposits comprises a number of very significant ore deposits or prospects, compared to both carbonate-hosted and clastic-hosted massive sulphide deposits (DALIRAN & BORG, 2004).

The world zinc production from non-sulphide zinc deposits in 2002 is approximately 2 % (WELLMER, 2002) related to all zinc sources (sulphide zinc deposits). However, the annual production of zinc from non-sulphide zinc ores could in future exceed 10 % of the total global zinc metal production (LARGE, 2001). Non-sulphide zinc deposits contain approximately 11 % of the world's known zinc reserve (BORG, 2002B). This shows the enormous economic potential of this type of Zn-deposits

and reflects its attractivity for industry and, as a result, the need for a more comprehensive understanding of these zinc deposits. Since the mining of non-sulphide zinc deposits depends on sufficient resources (WELLMER, 2002) improved knowledge about the geochemical characteristics of non-sulphide zinc deposits offer the chance for a more specific and successful exploration of such deposits.

1.1 Non-sulphide zinc deposits in carbonate host rocks

The majority of the known non-sulphide zinc deposits occur in carbonate rocks (LARGE, 2001; HITZMAN ET AL., 2003). This is a result of the specific geochemical behaviour of the carbonates. The ability to form (solution-) cavities, karst-breccias, and the high pH-values within a carbonate-dominated environment offer ideal conditions for the accumulation, enrichment, and emplacement of both sulphide ore and non-sulphide zinc ore. The highly reactive nature of carbonate rocks favors efficient chemical reactions and accumulation of precipitated minerals.

Non-sulphide zinc deposits have been often (sensu stricto incorrectly) termed as zinc-oxide and/or calamine deposits in historic literature. The term 'calamine' comprises all types of non-sulphide zinc ores: carbonates and silicates as well. Non-sulphide zinc deposits have been described by numerous authors, but in depth scientific research started with the economic interest in this type of mineralisation in the last years. Thus, a comprehensive Special Issue of Economic Geology (2003, 98-4) has bee published. Numerous authors, such as BORG (2002B), HEYL & BOZION (1960), HITZMAN (2001), HITZMAN ET AL. (2003), and LARGE (2001) described and classified non-sulphide zinc deposits. Basically, two major subclasses of supergene- and one class of hypogene non-sulphide zinc deposits are distinguished according to their geological setting and mineralogical aspects, although HEYL AND BOZION (1960, 1962) focused mainly on supergene ore.

These two major classes of non-sulphide zinc ore are: Group A: Supergene deposits, which formed by supergene oxidation, and Group B: hypogene deposits. Group-A supergene non-sulphide zinc deposits are the most common type and are associated with hydrated zinc-silicates and carbonates such as hemimorphite ($Zn_4Si_2O_7(OH)_2 \cdot H_2O$) and hydrozincite ($Zn_5(CO_3)_2(OH)_6$) or other carbonates (mainly smithsonite, $ZnCO_3$). Group-B hypogene deposits in contrast, consist dominantly of anhydrous zinc silicates and oxides, such as willemite (Zn_2SiO_4), zincite (ZnO), franklinite ($ZnFe_2O_4$), and others, locally with minor amounts of sulphide minerals. Group-B mineralisation is considered to be of primary hydrothermal origin and has been formed at low sulphur and high oxygen activities (BONI & LARGE, 2003; HITZMAN, 2001). Thus, silicates dominate the mineralogy of group-B hypogene deposits, with a typical prevalence of willemite. The (rare) metamorphosed non-sulphide zinc deposits (Franklin Furnace and Sterling Hill, New Jersey) probably belong to this class as well (BONI & LARGE, 2003), and are characterised by metamorphic non-sulphide zinc minerals such as franklinite and gahnite.

Beside these classifications of non-sulphide zinc deposits several authors have studied the broad field of geochemical aspects associated with the genesis of non-sulphide zinc deposits, starting from the sulphide protore up to the oxidation and the preservation conditions. However, most of these studies focus on specific detail, but lacking in the implication of these specific geochemical reactions into a broad model for the genesis of (supergene) non-sulphide zinc deposits in a car-

bonate environment and their preservation is lacking.

1.2 Aims and objectives of this study

The aim of the present thesis is an improved understanding of the mechanisms of the formation and preservation of carbonate-hosted non-sulphide zinc deposits. The concentration and the limitation of this study to carbonate environments and host rocks is the result of completely different behaviours of geochemical processes within carbonate rocks compared to siliceous host rocks.

One part of this thesis focuses on geological, mineralogical, and geochemical aspects of this type of deposits considering as example the non-sulphide and sulphide combined zinc deposits Mehdi Abad and Irankuh. Variations in mineralogy, geochemistry, and the distribution of the non-sulphide zinc minerals as well as their relationship to the sulphide protore have been analysed with respect to supergene oxidation processes of the sulphide protore, transportation and separation processes of metal ions, and the precipitation of the non-sulphide minerals. The second half of this thesis combines the results of these examinations and develops a general geochemical model for the genesis of carbonate-hosted non-sulphide zinc deposits. This implies the investigation and numerical simulation of the related geochemical processes and the development of a generalised geochemical model.

1.3 Outline of this study

The thesis has been divided into 6 chapters. The first and second chapter addresses the basic fundamentals of non-sulphide zinc deposits and the methods that have been used for this study. The third chapter introduces the regional geological setting of Iran and the examined areas. The fourth chapter presents the results of the examination of two non-sulphide zinc deposits: Mehdi Abad and Irankuh. The main geological and geochemical features have been examined with a special focus on non-sulphide ore related processes.

Chapter 5 presents a general geochemical model for the genesis of carbonate hosted non-sulphide zinc deposits, which includes the results of the observations of both deposits and theoretically geochemical modelling. The model is used to explain the formation of the non-sulphide ore of Mehdi Abad and Irankuh.

The final chapter six summarises the outcome of this research and the appendix includes analytical results from ICP-MS analysis.

1.4 Study area

Iran hosts numerous important non-sulphide and mixed sulphide/non-sulphide zinc deposits, such as Angouran, Mehdi Abad, Kuh-e-Surmeh, and Iran-Kuh, which are well exposed and relatively easily accessible. Either the examined deposits are active mines with well-developed open pits and

adits (Iran-Kuh, Mountain Ore Body –MOB- of Mehdi Abad) or extensively drilled exploration projects (Valley Ore Body –VOB- of Mehdi Abad).

Thus, Iran is the ideal region to study different non-sulphide zinc deposits for a detailed geochemical and mineralogical analysis and comparison of variations among them.

2 Materials and methods

2.1 Sample material

Samples have been obtained and collected from Irankuh and Mehdi Abad zinc deposits. Here, the first step of the field campaign was the comprehensive geological examination and evaluation of each deposit as a condition precedent for an effective sample collection. The fieldwork comprised both surface- and underground work.

The geochemical analyses are based on samples from both drill cores and hand specimen. The drill cores were obtained from the local mines/exploration camps and were selected according to their geological position and potential geochemical relevance. The lithological descriptions of the sedimentary host rocks and local core logs have been used on site for the selection of samples. In addition, hand specimen from selected adits, trenches, and surface outcrops have systematically sampled.

Field work in Iran was from May 24th to June 19th 2002. The purpose of this visit was to establish a general overview of the geology of Iran and to visit and sample the main Iranian Zn-Pb deposits Mehdi-Abad and Irankuh. The work comprised general geologic fieldwork and sampling. An additional visit at Teheran has been made in December 2003 (December 13-21, 2003). The purpose of this visit was the scientific exchange with the Geological Department of the Shahid Beheshti University of Teheran and to give talks about the results of this research project. An additional visit was made at the Geological Survey of Iran.

A total number of 202 specimens with a total weight of approximately 130 kg have been sampled during the field campaign from May 24th to June 19th 2002. The following tables Tab. 1 and Tab. 2 show the specific number of samples:

Tab. 1: Overview of the sampled drill cores from Mehdi Abad and Iran-Kuh.

Core	Origin	Depth of drill core	Samples
M5204	Mehdi Abad	245 m	7
M5308	Mehdi Abad	445 m	11
M7006	Mehdi Abad	352 m	9
M7008	Mehdi Abad	417 m	10
M7010	Mehdi Abad	348 m	8
M7016	Mehdi Abad	327 m	5
M7018	Mehdi Abad	402 m	10
M7101	Mehdi Abad	452 m	7
DDH10G	Iran-Kuh	119 m	15
DDH40K	Iran-Kuh	151 m	11
DDH64	Iran-Kuh	129 m	16

Tab. 2: Summary list of 202 rock samples. The table includes samples from drill cores and 'other' types of specimens, such as hand specimens from mines and outcrops.

Origin	Type of sample	Number of samples
Mehdi Abad	Drill core samples	67
Mehdi Abad	Other sampling	60
Iran-Kuh	Drill core samples	42
Iran-Kuh	Other sampling	33

These samples and data provide the basis for the research activities of this thesis. The samples were prepared for further investigations at the Martin-Luther-University Halle-Wittenberg. This comprises the cutting and formation of rock samples for the preparation of thin sections for light microscopy, SEM and SEM-EDX analyses. Additionally, crushing and milling of the specimen have been carried out for XRD, RFA, and ICP-MS analyses.

2.2 Methods

2.2.1 Sampling and sample preparation

The drill cores have been selected and cut either to half-sized or to quarter-sized cores by usage of a rock saw. One part remained on site, whereas the other part was used as sample for further analytical work. The sample sizes of drill cores reach from 10 up to 30 cm in length and were taken after a careful examination of the drill core from both geochemically relevant zones and wall rocks.

Hand specimens have been geo-referenced by using a GPS or by the use of geo-referenced maps of local adits and shafts of the sampled mines. Mineral paragenesis and relevant sediment structures have been studied in detail in selected core segments and have been documented using a digital photographic camera.

2.2.2 XRD analyses

X-ray diffraction (XRD) measurements were performed at the Institute for Geological Sciences of the Martin-Luther-University Halle-Wittenberg on a Bragg-Brentano-Diffractometer of the type Siemens D 5000, with a Cu X-ray tube (CuKα) and Ni monochromator operated at 40 kV and 30 mA.

The diffraction patterns were compared with a set of standard patterns compiled by the Joint Committee on Powder Diffraction Standards (JCPDS). A full description of the X-ray diffraction methodology, analytical settings, and applications can be found in BRINDLEY & BROWN (1980) and MOORE & REYNOLDS (1997).

Powder samples were prepared from the same slabs of rock used to make thin and double polished sections. Rock pieces of vein minerals and host rock were initially crushed by hand using a metal hammer to reduce the samples to cm-sized fragments. Finally, the material has been ground with a tungsten disc mill to approximately 600-μm grain size. The powder obtained was scanned in the 2θ range from 10° to 60° with increments of 0.04° 2θ. Counting time was 2 seconds.

2.2.3 SEM and SEM-EDX analyses

Scanning electron microscope investigations were made on both Au- and C-coated samples using a JEOL JSM-6300 scanning electron microscope. This SEM is coupled with an X-ray energy dispersive spectrometer. Analytical EDX settings were 20 kV beam voltage and count time of 60 seconds (peaks).

2.2.4 Light microscopy

From most representative samples of sulphide ore, non-sulphide ore and the host rocks polished and unpolished thin sections were prepared. The thin sections were studied under transmitted and reflected light. Photographs of the thin sections were made by using the Microscope Zeiss Axiophot and the coupled digital camera Nikon DS-5M.

2.2.5 ICP-MS analysis

Whole-rock analysis of the major, trace, and rare earth elements by ICP-AES and ICPMS were done by Acme Analytical Laboratories, Vancouver, British Columbia (Canada). The raw samples were milled by using a tungsten carbide shatter box, involving tungsten contamination during sample preparation. Therefore, the tungsten data cannot be used for geochemical interpretation.

Elements are expressed as common oxides for each element (i.e. Al_2O_3, CaO, Cr_2O_3, Fe_2O_3, K_2O, MgO, MnO, Na_2O, P_2O_5, TiO_2). Other element concentrations are given in ppm. Total abundances of the major oxides and several minor elements are based on a 0.2 g sample analysed by ICP-emission spectrometry following a lithium metaborate/tetraborate fusion and dilute nitric digestion. Loss on ignition has been determined by weight difference after ignition at 1000°C.

2.2.6 Stable isotope analyses

The term ‘stable’ refers to isotopes, which are not radioactive. Radioactivity is an evidence for nuclei affected by decaying processes. Thus, stable isotopes show a long-term stable behaviour and are not influenced by decaying processes. In most cases, one stable isotope is predominant and other isotopes only occur in traces.

The different masses of the isotopes of each element lead to differences in physicochemical properties of each isotope. The chemical properties of molecules differing only in isotopic substitution are qualitatively the same, but quantitatively different. These differences in chemical properties can lead to considerable isotope effects in chemical reactions. The partitioning of isotopes between two substances or two phases of the same substance with different isotope ratios is referred to as isotope fractionation.

The isotope fractionation is caused by isotope exchange reactions and kinetic processes. These processes depend on the reaction rates of (isotopic) molecules. Other factors may be the chemical composition or the crystal structure.

The detection of different isotopes of a specific element is based on the different masses of each isotope. The most effective way to detect isotopes is a mass spectrometer, which separates the isotopes due to the behaviour of their charged ions within magnetic fields.

The δ-values reflect the fractionation mechanisms and processes predominant for each specific element during geological evolution. The oxygen isotope ratio $\delta^{18}O$ provides a useful tool for the study of water/rock interaction in carbonate minerals and rocks, as this ratio shifts for both phases away from their initial values during interaction. The carbon isotope ratios $\delta^{13}C$ can be used to trace the carbon source and the carbonate evolution during diagenesis and very low-temperature metamorphism. Thus, the carbon and oxygen isotope studies on carbonate minerals of the non-sulphide zinc ore and the carbonate host rock have been used to determine the conditions of non-sulphide ore formation and the source of the fluids and the carbonate ions.

For a more complete description of the theoretical background, analytical techniques, and common applications of stable isotopes the reader is referred to HOEFS (1997), SHARP (1999), VALLEY ET AL. (1986), and ATTENDORN ET AL. (1997).

2.2.7 Geochemical modelling and calculations

The results of the examined deposits have been tested by using the PHREEQC code (PARKHURST & APPELO,1999). PHREEQC is a well established modelling program and has been successfully used by numerous authors, such as SALMON & MALMSTRÖM (2002), APPELO ET AL (1998), and others to describe, simulate, and solve hydro-geochemical problems. PHREEQC is capable to model equilibrium reactions of aqueous solutions. These solutions can interact with other phases, such as minerals, gases, or model processes like sorption and non-electrostatic surface-complexation processes. The calculations are based on an extensible database and give results for saturation indices, as well as pH, redox calculations and 1-D transport simulations as well. Thus, this program is an excellent tool to test geochemical assumptions and to calculate parameters of equilibrium reactions.

The PHREEQC calculations are based on the thermodynamic database 'thermo.com.V8.R6.230' compiled at the Lawrence Livermore National Laboratory, USA. PHREEQC was used for the calculation of equilibrium reactions and data, the calculation of the 1-D transport/titration model and the calculation of metal sorption effects onto ferrihydrite. The calculation of the metal sorption uses the generalised two-layer model of DZOMBAK AND MOREL (1990). The equilibrium constants for the adsorption of all species onto ferrihydrite were derived from adsorption experiments on ferrihydrite (DZOMBAK AND MOREL, 1990).

The adsorption calculation is based on a hypothetical (Fe-Zn-Pb) metal-rich aqueous solution, which includes the mobile elements and corresponding precipitated immobile Fe-oxihydroxides, which remained immobile within the oxide zone. The metal concentration values are based on values from acid mine drainage (AMD) waters. These waters are the result of an oxidation process of sulphides and one can assume that the metal concentration and the pH values of non-neutralised AMD waters are similar to an initial metal-rich fluid, which originated from oxidising sulphide ore. The range of metal concentrations for AMD waters is given in Tab. 3:

Tab. 3: Typical metal concentrations of AMD [mg/l^{-1}] (values from GAZEA ET AL., 1996).

	Fe	Zn	Pb	pH
mg/l^{-1}	8.5 – 3200	0.04 – 1600	0.02 – 90	1.7-7.9
mol/l^{-1}	$1.5 \cdot 10^{-4} – 5.7 \cdot 10^{-2}$	$6.1 * 10^{-7} – 2.41 \cdot 10^{-2}$	$9.6 * 10^{-8} – 4.3 \cdot 10^{-4}$	1.7-7.9

The zinc concentrations are based on values given by GAZEA ET AL. (1996). The composition of the model-solution is based on the zinc concentration of Tab. 3. Zinc concentrations are assumed to be on the higher side of the typical range to take into account the high sulphide concentration within sulphide ore compared to mine dumps. The initial hypothetical solution comprises only the metals Fe^{3+}, Zn^{2+}, Pb^{2+} and SO_4^{2-} ions at an initial pH=2 and the elements should be in their highest oxidation state, according to an oxygen-path oxidation process. Ferric iron Fe(III) is mostly immobile at pH=2 due to the precipitation of insoluble Fe-oxihydroxides. Thus, the value of iron within the supergene fluid is presumed to be relatively low with $1.7 \cdot 10^{-3}$ $mol \cdot l^{-1}$ according to the solubility of HFO.

The predominant portion of the iron remains immobile within the oxidation zone as insoluble Fe-

oxihydroxides. As a first approximation, the amount of the immobile iron can be estimated by using the relative amounts of Fe, Zn, and Pb in the sulphide protore. The amount of iron (mainly associated with pyrite) within the sulphide protore have been estimated by using analyses of the sulphide ore of the Mehdi Abad, Valley Ore Body. The mean mass% for selected elements within the sulphide ore are: 7.2 % Zn (in sphalerite), 2.3% Pb (galena) and 20% Fe (pyrite) with a ratio of Zn/(Zn+Pb) of 0.75. Calculations (using the molar masses: M_{Zn}=65.39, M_{Pb}=207.2, and M_{Fe}=55.85 g*mol^{-1}) show the relative molarities between these metals:

1_{Fe}:0.38_{Zn}:0.028_{Pb}.	Relative molarities between Fe, Zn, and Pb within the sulphide ore of Mehdi Abad.

Pyrite is the most reactive mineral with respect to oxygen-path reactions (JAMBOR, 1994, KAKOVSKY & KOSIKOV, 1975) but zinc is also highly reactive and soluble at pH=2. The amount of oxidised pyrite can be estimated by using the relative molarity of these minerals under the assumption of a sulphide ore with homogeneously distributed pyrite, sphalerite and galena. Thus, the assumed oxidation of sphalerite and the concentration of $2.4 \cdot 10^{-2}$ mol·l^{-1} Zn within the metal-rich fluids is associated with $6.3 \cdot 10^{-2}$ mol oxidised pyrite (=$6.3 \cdot 10^{-2}$ mol Fe(III)), from which the biggest portion precipitates as HFO and is thus removed from the solution.

The calculated concentration of cation-associated sulphate ions is similar to those values given in numerous analytical results of AMD systems (FORSTNER & WITTMANN, 1983, FERREIRA DA SILVA ET AL. 2005, and other authors).

The calculations include the geochemical behaviour of the zinc minerals smithsonite, hydrozincite, and willemite. Hemimorphite is not included although it is the most common zinc silicate mineral in the examined Iranian deposits. However, it is difficult to determine the field of stability of hemimorphite, since presently no thermodynamic data are available for this mineral. Several authors (e.g. INGWERSEN, 1990) attempted to estimate the thermodynamic data from solubility curves (provided by TAKAHASHI, 1960 and others). These results were not used due to high experimental uncertainties of these data. These uncertainties are caused by the usage of acetate-buffered solutions during the pH-dependent hemimorphite solubility experiments. The presence of acetate leads to the formation of zinc-acetate complexes. The binding of zinc as acetate complexes decrease the activity of free Zn cations within the solution (VOEGELIN ET AL., 2003). This phenomenon should increase the solubility of hemimorphite and thus distort the solubility curves of hemimorphite towards to an apparently higher solubility.

Tab. 4: Hypothetical acidic solution on which the modelling is based upon. Most of the iron is bound to HFO, which remains within the oxidation zone.

pH	2	**Fe^{3+}**	$1.7 \cdot 10^{-3}$ mol·l^{-1}
pe	4	**Zn^{2+}**	$2.4 \cdot 10^{-2}$ mol·l^{-1}
Temperature	25 °C	**Pb^{2+}**	$1.6 \cdot 10^{-5}$ mol·l^{-1}
CO_2	0.0 mol·l^{-1}	**SO_4^{2-}**	$3.7 \cdot 10^{-2}$ mol·l^{-1}
HFO	$6.1 \cdot 10^{-2}$ mol	insoluble, remains within the oxide zone	

The hypothetical continuous reaction/neutralisation of the initial acidic aqueous solution with the carbonate host rock was modelled by applying up to 200 reaction steps to the aqueous solution

(Fig. 1). At each reaction step a specific and constant amount of 0.01 moles of limestone or dolomite (or a mixture of both) were added irreversibly to one litre of solution. Then the solution equilibrated with local mineral assemblages and gas phases. After equilibrium reaction and precipitation, the resulting solution was used again to react in a further reaction step.

The solution reacts with the wall rock minerals (dolomite and/or calcite) in 200 incremental steps. The change in pH and saturation indices of different minerals and the metal- and anion concentration within the aqueous solution have been studied and analysed over these steps. The following minerals

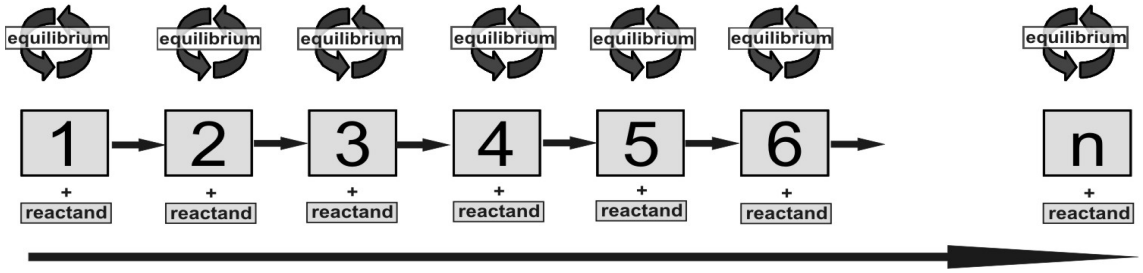

Fig. 1: Titration model used for neutralisation- and precipitation reactions of acidic fluids within carbonate host rocks and precipitation of secondary minerals. An initial solution reacts in “n” steps with a specific amount of additional reactants (e.g. limestone), the system equilibrates and, after reaching the equilibrium, is followed by the next reaction.

were included to precipitate from the solution: anglesite, cerussite, hydrocerussite, hydrozincite, smithsonite, willemite, gypsum, goethite, ferrihydrite, hematite, calcite, dolomite, schwertmannite, magnesite and aragonite. These minerals represent the most common and relevant secondary minerals within carbonate-hosted non-sulphide zinc deposits and show stabilities, which may be realistically reached during the numeric simulation.

As a consequence, all or one of these minerals are allowed to precipitate if they become thermodynamically stable and the saturation index $Si_{\_[mineral]}$ of these phases is reached (a value of 0). If the saturation index $Si_{\_[mineral]} < 0$ then the solution is undersaturated, with respect to this specific mineral and, consequently, it would not precipitate from the solution. If $Si_{\_[mineral]} = 0$ then the concentration has reached the maximum value and the specific mineral will precipitate. A saturation index $Si_{\_[mineral]} > 0$, which indicates oversaturated solutions, is not allowed in this modelling process. A mineral, once precipitated, becomes removed from the fluid and does not participate in further reactions. This simulates a one-dimensional irreversibly progressing fluid migration through reactive limestone.

Tab. 5: Overview about important mineral phases, aqueous species and oxidation processes.

Primary minerals
galena (PbS), sphalerite (ZnS), pyrite (FeS_2), calcite ($CaCO_3$), dolomite ($CaMg(CO_3)_2$), quartz (SiO_2)
Precipitating minerals
gypsum ($CaSO_4 \cdot 2H_2O$), ferrihydrite* ($FeO[O,OH_{1-x},Y_x]$, goethite ($FeO(OH)$), hematite (Fe_2O_3), jarosite ($KFe_3(SO_4)_2(OH)_6$), smithsonite ($ZnCO_3$), hydrozincite ($Zn_5(CO_3)_2(OH)_6$), hemimorphite ($Zn_4Si_2O_7(OH)_2{}^*H_2O$), willemite ($Zn_2SiO_4$), anglesite ($PbSO_4$), cerrusite ($PbCO_3$), hydrocerussite ($Pb_3(CO_3)_2(OH)_2$) , anglesite ($PbSO_4$), calcite ($CaCO_3$), dolomite ($CaMg(CO_3)_2$), schwertmannite ($Fe_{16}O_{16}(OH_{12})(SO_4)_2$), magnesite ($MgCO_3$), aragonite ($CaCO_3$)
Main aqueous species
Fe^{2+} , Fe^{3+} , H^+ , Ca^{2+} , Mg^{2+} , Zn^{2+} , Pb^{2+} , $O_{2(aq)}$, $CO_{2(aq)}$, CO_3^{2-} , HCO_3^- , OH^- , HSO_4^- , SO_4^{2-} , $Fe(OH)_{3(aq)}$, $Fe(OH)_2^+$,$ZnOH^+$, $ZnHCO_3^-$, $ZnCO_3^0$, $PbOH^{+,-}$, $PbCO_3^0$
Gases (equilibrium)
CO_2 , O_2

3 Geological situation of Iran

The geology and especially the tectonic style of Iran is highly influenced by the development and history of the Tethyan region (Fig. 2). The tectonic events, which occurred around the Iranian Plate margins, are related to rifting processes of Gondwana and subsequent collision with the Arabian plate from the WSW. These important processes affected the Iranian Plate and the adjacent plates, such as the African, Indian, Arabian, and Eurasian Plates, during Mesozoic to Tertiary times (ALSHARHAN ET AL., 2001; ALAVI, 2004).

The Tethyan region, which includes the Iranian Plate and the adjacent areas, underwent three major evolutionary stages. The first stage was the closing of the Paleo-Tethys and rifting of the Neo-Tethys from early Permian to late Triassic times. With the second stage, the subduction process of the Neo-Tethys and the collision of the Indian Plate with the Eurasian Plate from the Jurassic to the early Lower Tertiary began. The third and last stage is associated with the collision between the Arabian plate and the Eurasian plate from early Tertiary to the present (SHUFENG, 2002).

The first step, the Gondwana break-up, was associated with tensional basins and basement highs. The central Iranian segment separated from the Arabian plate along the line of the present High Zagros Zone (ALSHARHAN ET AL., 2001). The result of this process was the opening of the Neotethys. The closure of Neotethys started with the Late Cretaceous and proceeded into Cenozoic times. This phase is marked by the emplacement of a number of prominent ophiolithes in Oman, Iran, Syria, and southeast Turkey.

The final orogenic phase is due to the Arabia–Eurasia convergence and takes place first in southern Iran starting at the end of Eocene (HESSAMI ET AL. 2001). This process affected the Arabian and Iranian Plates and results in the Zagros orogenic phase of Late Miocene to Pliocene age. The suturing began approximately 12 Ma in Turkey and subsequentely progressed southeast. The suturing process has not yet occurred along the Gulf of Oman and the Makran. In these regions the subduction continues (McCall, 1998).

Latest Tertiary to Holocene events included strong uplift processes (Fig. 3), magmatism (Alavi, 1994) and volcanism, erosional processes, and the associated deposition of extensive alluvial fans from the uplifted mountains (ALSHARHAN ET AL., 2001).

The non-sulphide zinc deposits at Iran-Kuh, and Mehdi Abad studied and analysed in this thesis, are each situated in different tectono-sedimentary units. STÖCKLIN, 1968 and others have presented detailed investigations about the tectonic and geological setting of the Iran. Most of the tectono-sedimentary units are distinguished from the adjacent regions by faults and transitional zones (RASTAD, 1981). Mainly three structural trends (Fig. 4) can be distinguished in Iran: (i) a N-S trend, (ii) a NW-SE trending system, which follows the alpine trend, and (iii) a NE-SW trend.

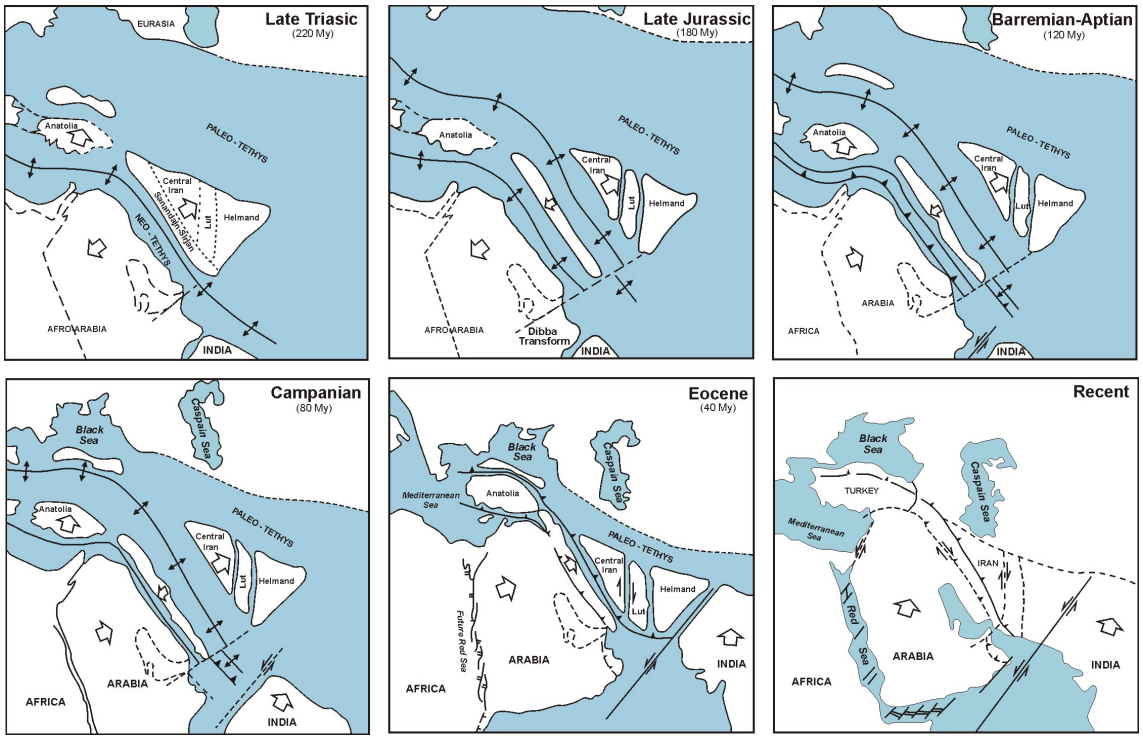

Fig. 2: Continental Drift of the Arabian Plate beginning in late Triassic to present. (modified from GLENNIE, 1992)

The following major structural zones can be distinguished in Iran (STÖCKLIN, 1968; BERBERIAN & KING, 1981) (Fig. 4): Folded Zagros, High Zagros, Sanandaj-Sirjan Ranges, Central Iran, Alborz Mountains, Kopet Dagh, Lut Block, and East Iran/Markran Ranges. The Mehdi Abad Zn-Pb deposit is located at the Central Iranian zone and the Zn-Pb deposit Irankuh is located at the Sanandaj-Sirjan zone (Esfandagheh-Marivan), whereas the Kuh-e-Surmeh is located in the Folded Zagros

zone. These deposit-specific zones will be explained in more detail due to their relevance for this research project.

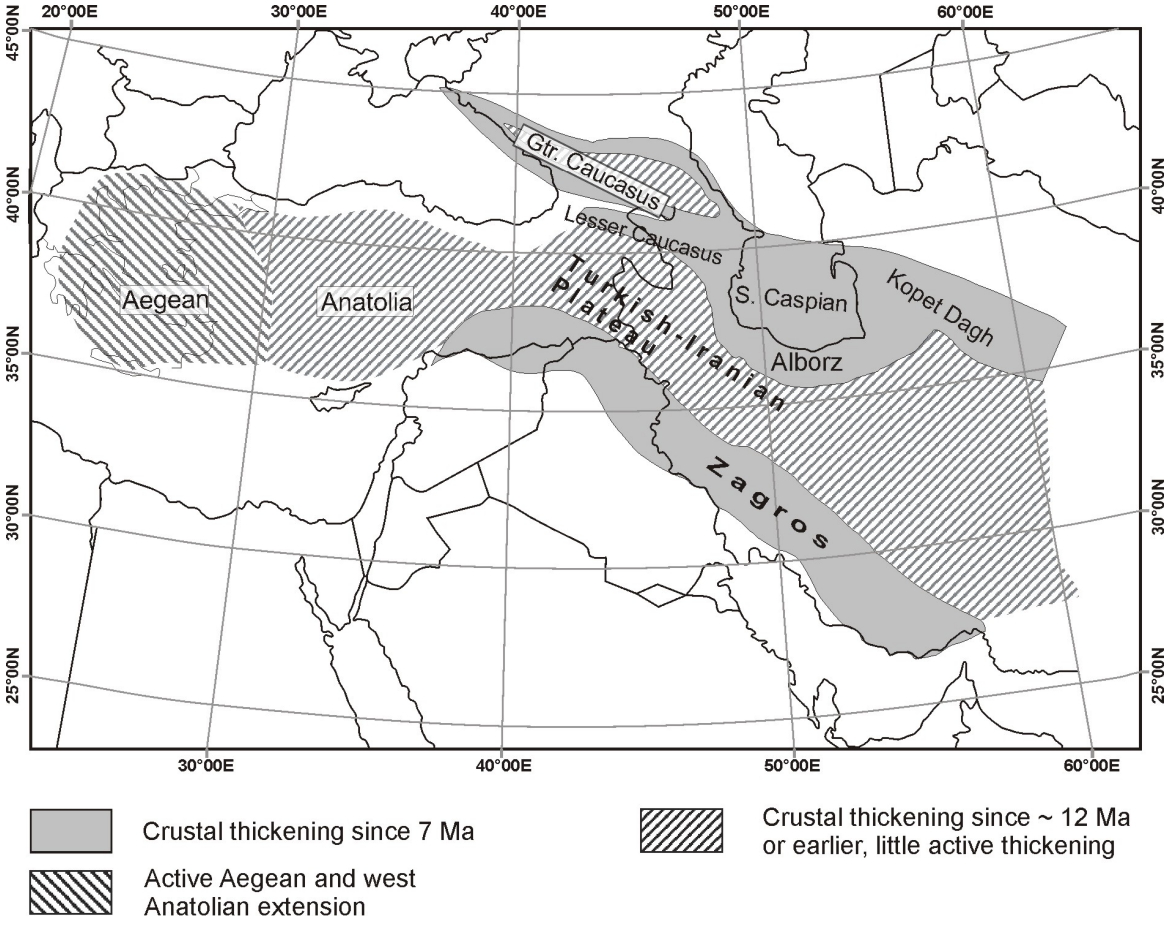

Fig. 3: The Arabia-Eurasia plate collision resulted in crustal thickening and uplift. The crustal thickening in the 12Ma highlighted area show no significant thickening processes at present (e.g. Turkish-Iranian plateau), whereas the 7 Ma marked area is still active (e.g. Zagros Simple Folded Zone, Alborz) (After ALLEN ET AL. 2004)

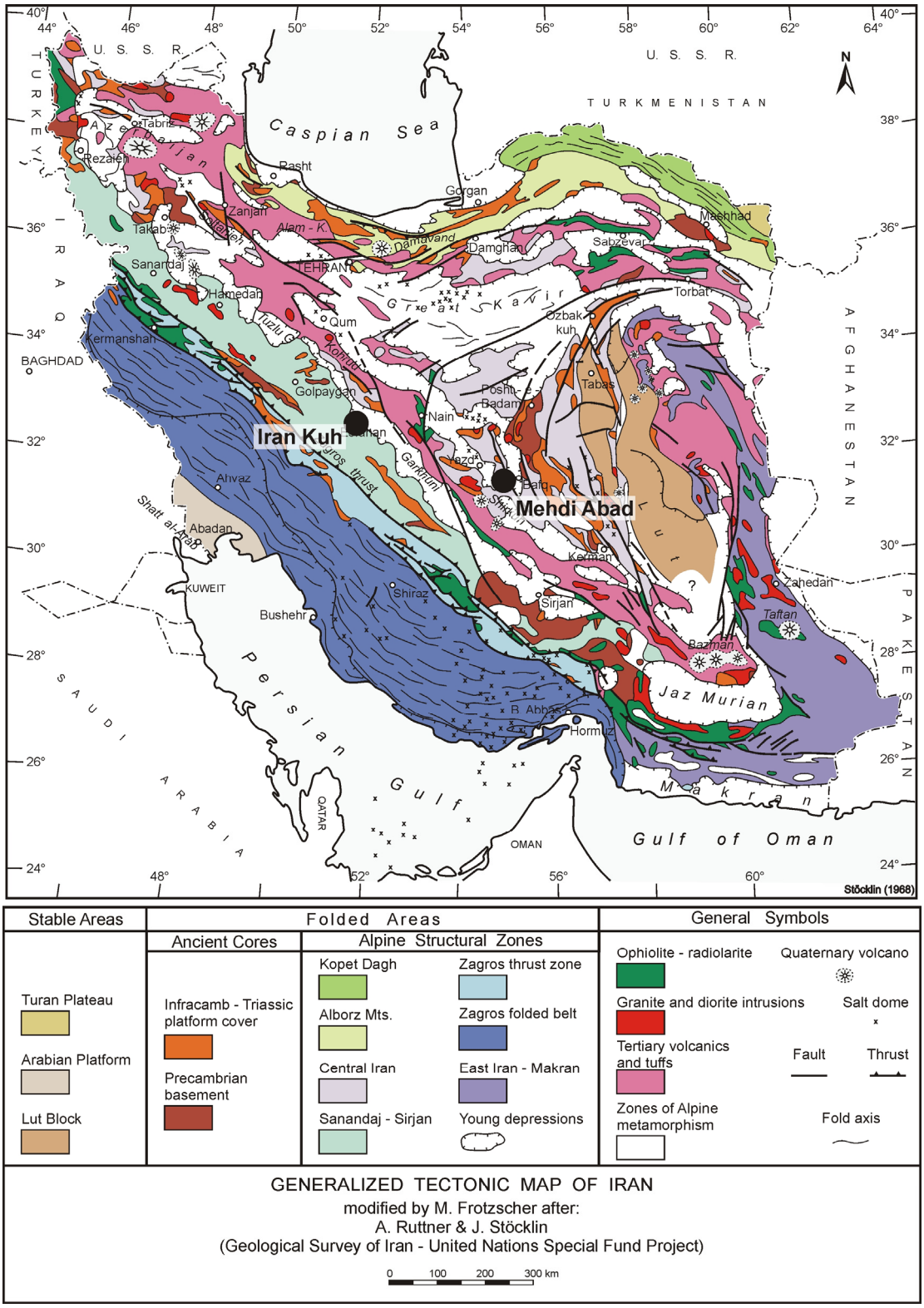

Fig. 4: Generalised geological and tectonical map of Iran with the location of the examinated non-sulphide zinc deposits: Mehdi Abad and Irankuh. Modified after STÖCKLIN (1968).

3.1 The Zagros structural zone

The predominant structural style of the Zagros Mountains is a characteristic set of NW-trending open, parallel anticlines and synclines. The main orientation of the fold-axis is NW-SE, which reflects the characteristic orientation of the Zagros Fold Belt. The Zagros Structural Zone comprises the main structure units: Folded Zagros in the southwestern part of the Zagros, the High Zagros, and following to Northeast the Sanandaj-Sirjan Ranges (Fig. 5).

The Zagros Mountains are the result of complex deformation processes, which started in Late Cretaceous time. These deformations are due to the collision of the Arabian and Iranian Plates. The deformation rate increased during the Pliocene time due to increased convergence rate by the opening of the Red Sea (SATTARZADEH, 2002). The sedimentary cover and the underlying metamorphic basement decouple along an important detachment horizon, the Hormuz Salt Formation. The irregular distribution and the thickness of this horizon play an important role in determining the geometry of the deformation belt (SATTARZADEH, 2002).

The Folded Zagros consists mainly of thick marine sediments of several thousand meters depth. The stratigraphic sequence comprises sediments of Mesozoic and Neogene ages, which have been deposited in a basin. These sediments were folded and uplifted mainly during the Upper Miocene/Lower Pliocene (ALLEN ET AL. 2004) to the Pleistocene. As a result, the Zagros fold-belt has been formed.

The High Zagros (historically known as Zagros Crushed Zone and Zagros Thrust Zone e.g. STÖCKLIN, 1968) marks the plate boundary between the Arabian Plate to the west and the Iranian plates to the east. The Arabian plate is subducted beneath the Iranian plate along the High Zagros zone. Both, the Central Iranian strato-volcanoes and important ore deposits are related to this High Zagros thrust zone (DABIRRAHMANI, 1984). Sedimentation and magmatism within the High Zagros are similar to those of the Folded Zagros (BERBERIAN & KING, 1981). The width of this structural zone varies around 10 to 65 km.

This collisional setting and the thrust- and folding-processes caused a rapid uplift of the overriding Iranian plate and high level magmatic-volcanic activity along the Urumieh-Dokhtar Volcanic Belt as well (STÖCKLIN, 1968; ALAVI, 1994). This uplift and provided a favourable environment for the exhumation and oxidation of several primary sulphide ore bodies and the preservation of the resulting non-sulphide ore.

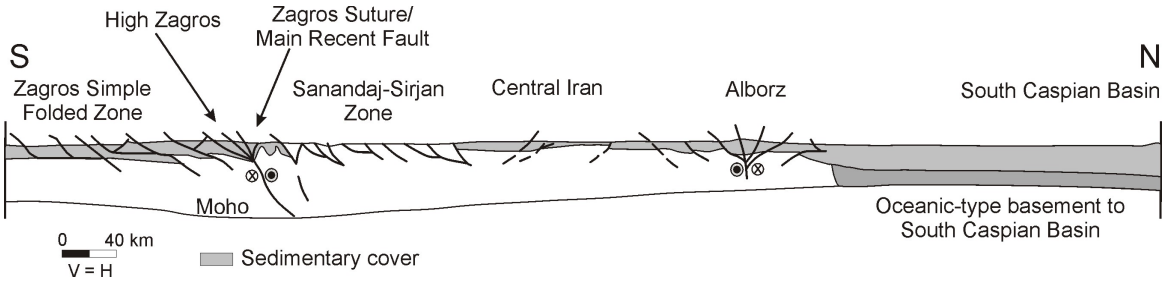

Fig. 5: Structural units of Iran and tectonic relations (after ALLEN ET AL. 2004)

The Sanandaj-Sirjan Zone (SSZ) extends over 1200 km length and is located between the Central Iranian zone to the northeast, and the Tethyian ophiolitic zone of Zagros in the south-west. The SSZ has been formed in the late Cretaceous during the closure of the Neo-Tethys and the subsequent collision of the Arabian- with the Iranian plate. The SSZ can be subdivided in several zones, which comprise Triassic to Cretaceous shallow to deep marine sediments, ophiolit^ es, volcanics (MOHAJJEL, 1997).

3.2 Central-Iran structural zone

The Central Iranian Terrane is located northeast of the Zagros-Makran Neo-Tethyan suture and its sub-parallel Cenozoic magmatic arc, between the convergent Arabian and Eurasian plates. Thus, due to the collision setting, continuous continental deformation processes affect Central Iran. The Central Iranian platform was a stable platform during Paleozoic times, but late Triassic movements caused the creation of horsts and grabens. Central Iran comprises three major crustal domains: the Lut Block, the Kerman-Tabas Block, and the Yazd Block. The area of the Central Iranian terrane is surrounded and limited by faults and fold-and-thrust belts and Upper Cretaceous to lower Eocene ophiolite and ophiolitic melange (DAVOUDZADEH, 1997). Adjoining fault separated areas and tectonical units are the Alborz and Kopeh-Dagh region, which ranges to the north, Makran and Zagros ranges to the west and south, and the East Iran Ranges, which borders this terrane to the east.

The structural components (Lut Block, Kerman-Tabas, Yazd) of the Central Iranian Terrane are characterised by distinct horst (e.g. Lut block) and graben (e.g. Kerman-Tabas region) structures. The grabens are characterised by fillings of thick Jurassic sediments. However, the stratified cover rocks are largely correlatable among these blocks, but with locally significant facies and/or thickness variations across the block boundaries. The Blocks are characterised by an individual deformation style and seismicity, which makes them distinguishable from the adjacent regions (BERBERIAN, 1981).

3.3 Magmatic intrusions

In Mesozoic and Tertiary times tectonic activities affected particularly Central Iran. These movements were accompanied by folding, uplift processes, metamorphism, and magmatism (KHALILI, 1997). In Late Jurassic times, the tectonic activity affected a great part of the Iranian region, which resulted in regional unconformities. In some areas, such as Central Iran, the Sanandaj-Sirjan belt and the Lut block these tectonic movements were associated with felsic intrusions (KHALILI, 1997). The most important intrusions of the Lut block are the granodiorites of Kuh-e-Bidmeshk, Shah-Kuh, and Sorkh-Kuh, where the Shah-Kuh granite represents the largest intrusion in the Lut region. Other important intrusions, especially in Central Iran are the Shir-Kuh granite, the Esmael-Abad biotite granite, the Airakan granites and the Kolah-Quazi S-type granitoides, located 50 km SE of Esfahan. These intrusive bodies intruded in Jurassic sediments and were overlain by basal conglomerate of Cretaceous age.

Tectonic movements in Late Cretaceous and Tertiary times were accompanied by magmatism and metamorphism as well. The Tertiary plutonic activity had a climax in the Eocene and continued into Neogene and Quaternary times. This activity caused numerous felsic intrusions (granites and diorites) in the Sanandaj-Sirjan Zone/Esfahan, Central Iran zone, the southeast areas, and the north and north-west areas of Iran.

Tectonism, magmatism, and implications for metallogenetic processes

Iran and the adjacent areas are composed of composite subduction-collisional belts. These collisional belts are the result of the closure of the (Neo-) Tethys and successive episodes of volcano-plutonism. As the result of these tectonics and magmatism the Tethyan Eurasian Metallogenic Belt (TEMB) was formed during Mesozoic and post-Mesozoic times. The TEMB is located in the area of the former Tethyan Ocean on the southern margin of Eurasia and extends from the western Mediterranean to the Alps and southeastern Europe, the lesser Caucasus, the Hindu Kush, and the Tibet Plateau, Burma, and SW Indonesia (Fig. 6).

In Triassic times, the Neo-Tethys began to open as a series of back-arc basins. Subduction activities during Cretaceous times and extensive submarine volcanism and collisional tectonics between the Arabian and the Iranian plates began to result in formation of important ore deposits.

The most important types of deposits relating to these collisional processes are: (i) Porphyry copper, (ii) chromite and related deposits, (iii) lead-zinc deposits, and others (DIXON & PEREIRA, 1974).

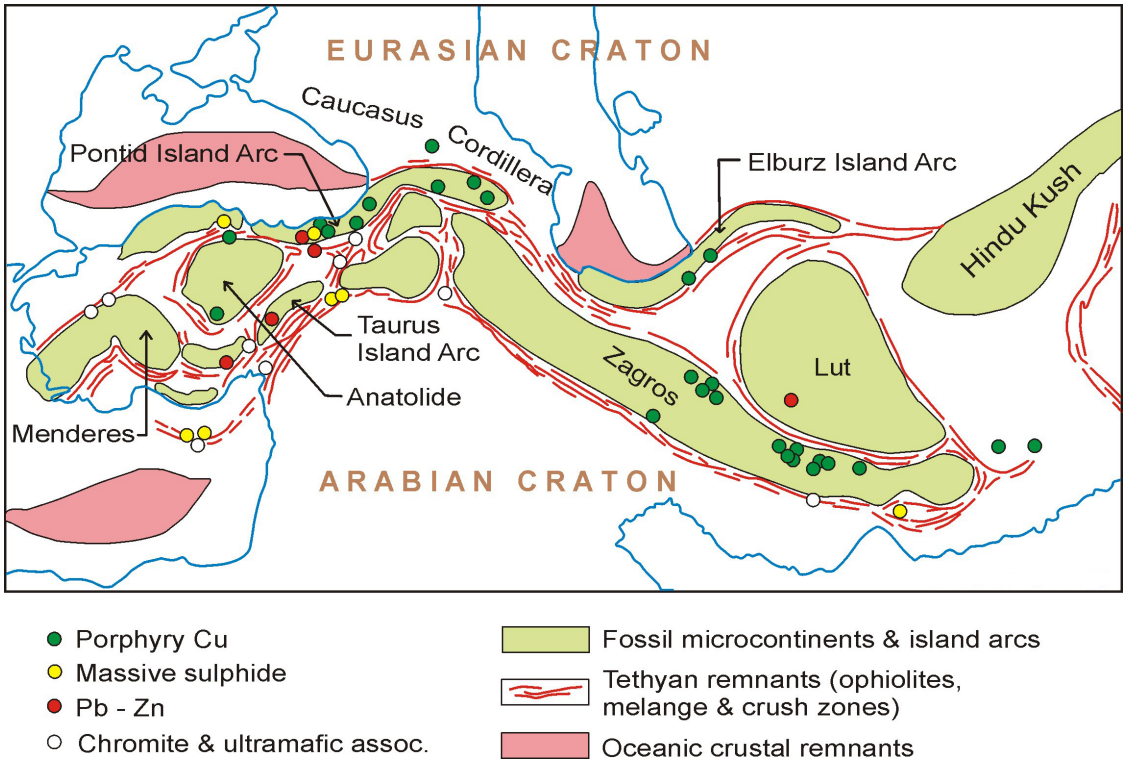

Fig. 6: Microcontinents in the Tethyan region and their relationship to important mineral deposits. (modified after DIXON & PEREIRA, 1974)

(i) Porphyry copper deposits

The emplacement of large porphyry copper deposits in Iran is the result of major mineralising events in Late Oligocene-Miocene times. These events are caused by the continental arc-style tectono-magmatism (LEAMAN & STAUDE, 2002). This zone extends through Turkey and into the Balkan as the north Anatolian Metallogenic Belt. Important Iranian porphyry copper deposits are Sar Cheshmeh, Meduk, Kal-e-Kafi, and the Sungun deposit, which is located in the Azerbaijan-Tarom belt in the north of the Iran. Sungun contains a resource of 860 Mt @ 0.6%Cu. Other Tethyan-related porphyry copper deposits are Gumushane, Guzelyayla, Derekoy, Ulutas (Turkey), and Saindak, and Reko Diq in Pakistan.

Some other deposits are probably associated to these porphyry copper systems. DALIRAN & BORG (2004) have suggested that the primary sphalerite-rich ore of the important (non-sulphide) zinc deposit Angouran is probably related to a hidden porphyry copper system.

(ii) Chromite and related deposits

Peridotites are common both in the melange zones and in the ophiolite complexes and are often associated with lens-shaped massive or disseminated bodies of chromite. However, in contrast to the porphyry copper deposits the occurrence of chromite deposits is much less common. Nevertheless, several distinct provinces occur in the Taurus zone in Turkey, and some small deposits in Iran, such as Fariab, Esfandoqeh, Makran, Khash-Nehbandan belt, Sabzevar, and Neyriz.

(iii) Lead-zinc deposits

Lead-zinc deposits occur widely in Iran and presently about 600 Zn-Pb deposits and occurrences are known. Only a small portion of these ist actually explored and/or exploited to variable degree and 10 deposits are actually mined (GHORBANI ET AL., 2000). It is probable, that the full range from exhalative sedimentary to Mississippi Valley types occur (DIXON & PEREIRA, 1974). The most important metallogenetic provinces for zinc mineralisation are Central Iran, the Sanandaj-Sirjan zone, and the Alborz region (GHAZANFARI, 1999). The time for the mineralisation events ranges from Upper Proterozoic, Upper Cretaceous up to Tertiary (Oligocene-Miocene). The age of the host rocks ranges from Upper Proterozoic up to Tertiary rocks. However, most of the host rocks are Paleozoic and especially Cretaceous carbonates. Provinces with the greatest potential for zinc-lead mineralisation are Central Iran and the Sanandaj-Sirjan Zone.

In the past, the exploration and scientific interest has been focussed mainly on sulphide ore deposits. Only a small amount of non-sulphide zinc deposits is actually in an active mining process, such as Angouran, Iran-Kuh, Kuh-e-Surmeh (REICHERT & BORG, 2002). Thus, the scientific data about non-sulphide zinc deposits in Iran are very preliminary (DALIRAN & BORG, 2004). However, numerous non-sulphide zinc deposits are known at this time in Iran (Fig. 7) and several of these prospects can be probably turned into significant resources of zinc, and thus they hold an enormous economic potential.

Literature research of DALIRAN & BORG (2004) has showed that most of the non-sulphide zinc deposits have been formed in Jurassic to Cretaceous carbonate rocks within the overriding Iranian plate. This overriding plate has undergone strong uplift and exhumation, which are an important factor for the formation of non-sulphide zinc deposits.

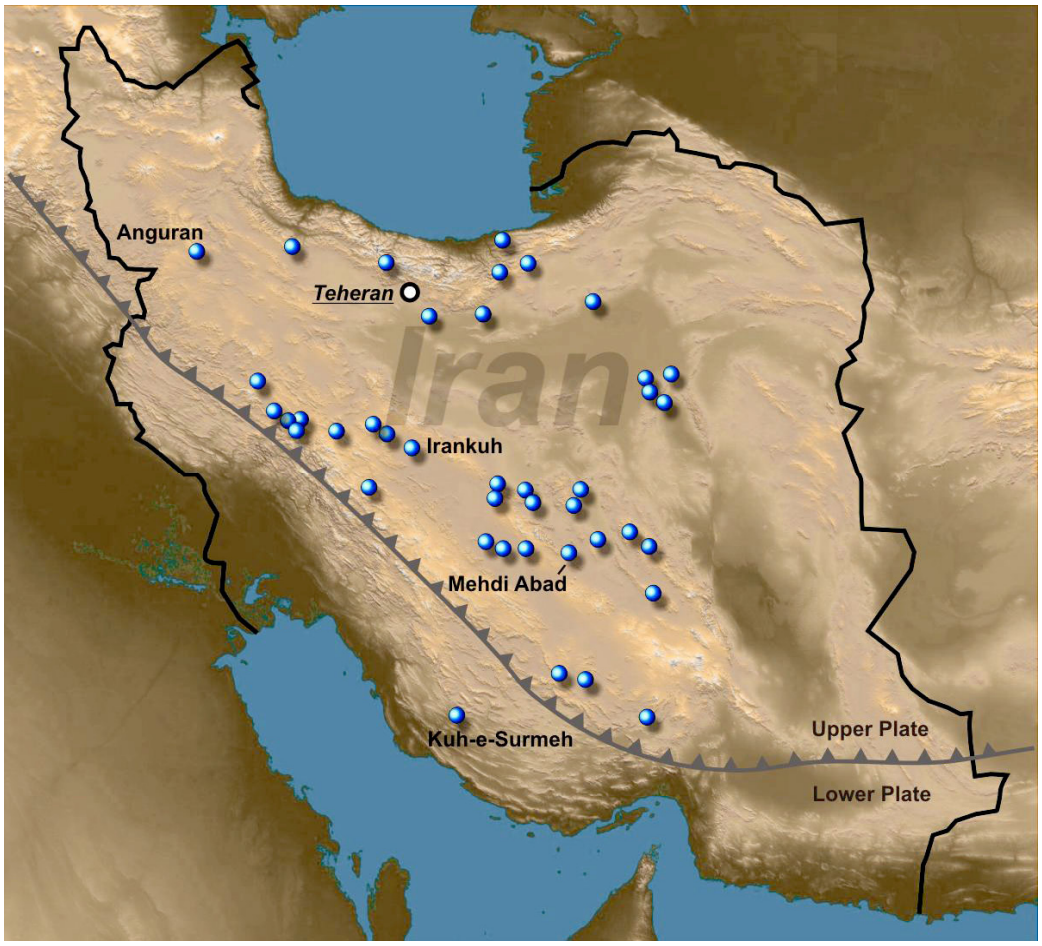

Fig. 7: Regional distribution of the non-sulphide zinc deposits. Most of these deposits are located on the upper (Iranian) plate. This plate has undergone strong uplift, exhumation, and erosion. (BORG ET AL. IN PREP.)

4 Results

4.1 The combined sulphide/non-sulphide Zn-Pb deposit Mehdi-Abad

4.1.1 Introduction and geographic location

The Mehdi Abad Project is located approximately 100 km southeast of the city Yazd and about 500 km southeast of Teheran in central Iran. The mine can be reached by the Yazd-Kerman Highway. Starting from Yazd, after 90 km a gravel road turns off to Bahadoran, and further on to the mine site. The UTM coordinates are 40R 0310158; 3484911. The altitude of this area is about 1850 m. The climate is semi-arid. There is no considerable vegetation within this area, only some bushes and little grass.

The main part of the ore body, the so-called Valley Ore Body (VOB) is located in a depression surrounded by hills and mountains with an altitude of up to 2500 metres (Fig. 8). A second ore body, the Mountain Ore Body (MOB) represents the highest parts of the oxide ore mineralisation (Fig. 9). The altitude of the MOB above the main Mehdi Abad ore body ranges from 2000 up to 2300 metres.

Fig. 8: View to the south at the Mehdi Abad deposit. The location of the VOB is traced by the dashed line. The VOB is covered by alluvial overburden. Point of view is near the MOB (see also Fig. 9)

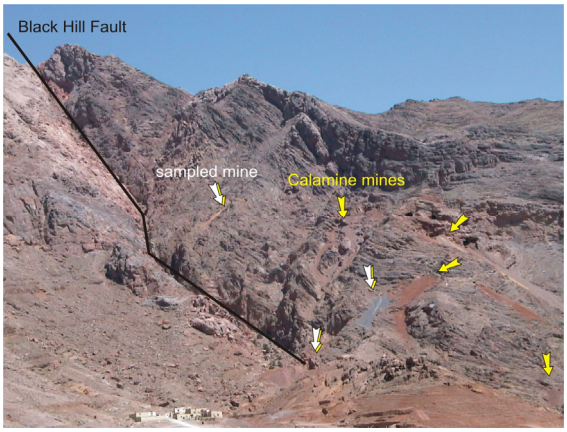

Fig. 9: Position of several adits of the MOB (yellow arrows) in the north-western part of the Mehdi-Abad deposit. The white arrows point to the sampled adits.

4.1.2 Geological overview

The Mehdi Abad zinc-lead deposit is located in the Central Iranian Shield. Here, Cretaceous limestones and sandstones were deposited over Jurassic rocks. The marine transgression started with the beginning of Cretaceous times with orbitulina-bearing carbonates and shales. Major faults became active during the Kimmerian Orogeny and resulted in horst and graben structures in Central Iran (AZARI & SETHNA, 1994). These grabens acted as sedimentary basins. The sedimentary basin, in which the Mehdi Abad deposit occurs is between the Chapedony fault to the east, and the Nain-

Deshir fault to the west (AZARI & SETHNA, 1994).

Except for the mountains and ridges, the area of Mehdi Abad is covered by alluvial overburden. The Cretaceous strata can be subdivided to the Sangestan Formation as the lowest, the Taft Formation in the middle, and the Abkou Formation on top of this stratigraphic sequence. These formations consist of detrital siliciclastic rocks and carbonates with an increase in carbonates towards the top. Mehdi-Abad has two separate ore bodies.

The VOB is located in a valley and is covered by an alluvial overburden (up to 250 m), whereas MOB locates on a rough mountainside in the northwestern part of the deposit. The MOB is completely oxidised, whereas the main portion of the VOB consist of sulphides. The non-sulphide ore of the MOB is hosted in the Abkouh Formation whereas both the sulphide ore and the non-sulphide ore of the VOB are hosted in the Taft formation (Fig. 10). The fact that the mineralisation of the Mehdi Abad ore body sensu stricto occurs in the Taft Fm. and the calamine ore in the Abkou Fm. documents the large vertical (stratigraphic) extent of the mineralisation.

The Sangestan Formation is the lowest and oldest Formation exposed in the mine area. It consists of shales and siltstones with interlaced calcarenite layers and fine- to coarse-grained quarzitic–feldspathic sandstones, sandy shales, and limestones (with fragments of corals).

The Taft Formation consists mainly of dolomite and dolomitic to ankeritic limestone. The zinc and lead mineralisation occurs within this formation, but the ore body is lateral limited by faults. Outside these terminating faults the same ore bearing Formation shows no notable lead and zinc mineralisation. Generally, the sulphide ore of the VOB is associated with dolomite or ankeritic limestone.

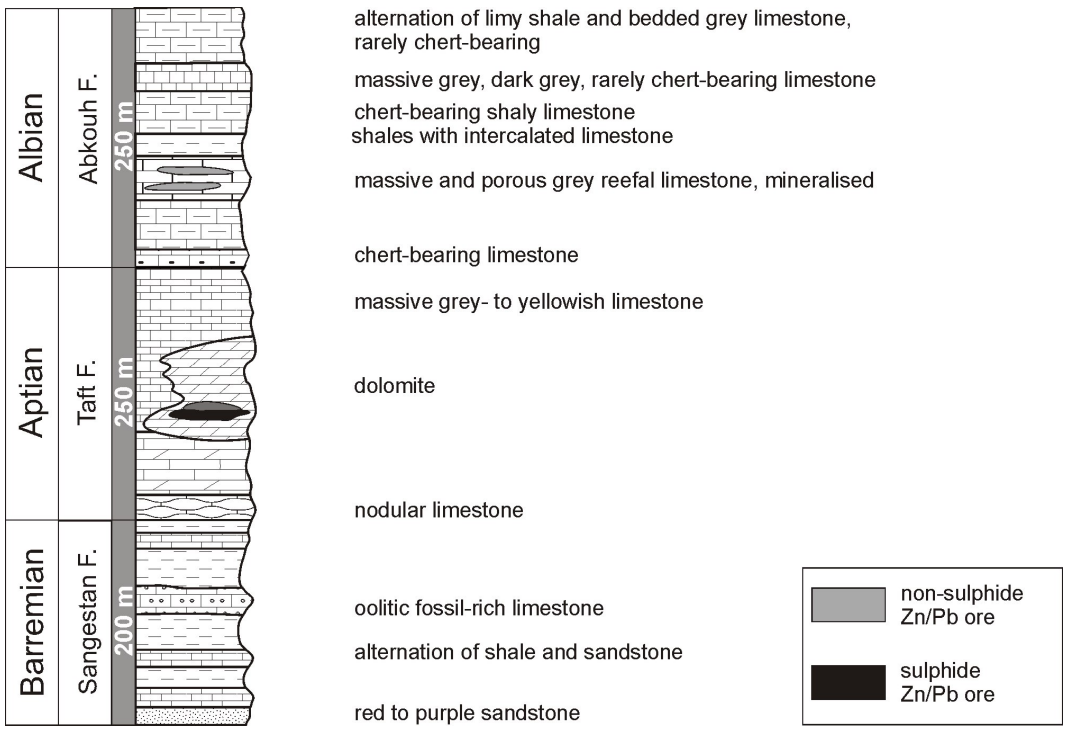

Fig. 10: Stratigraphic column of the Mehdi Abad deposit (modified after GSI, 1988)

The uppermost unit is the Abkou Formation. It can be found in the north, northwest, and west of the mine area (Fig. 11). This sequence overlies the Taft Formation and consists of a succession of limestone, marly limestone, calcareous shales, and dark limestones. The thickness of this formation is about 250 m. The mineralisation of the MOB occurs within the Abkou Formation in brecciated karstic limestones overlying a sequence of limy shales and marly limestones. The mineralisation occurs only in the brecciated limestones, but is repeated by folding (G.S.I., 1988). The folding of this part of the Abkou Formation is due to movements of the two adjoining faults. Besides this location, the Abkou Fm. and other formations are not folded in the area of Mehdi Abad ore body. The same stratigraphic unit within the Abkou sequence shows no mineralisation in other non-folded and non-brecciated regions.

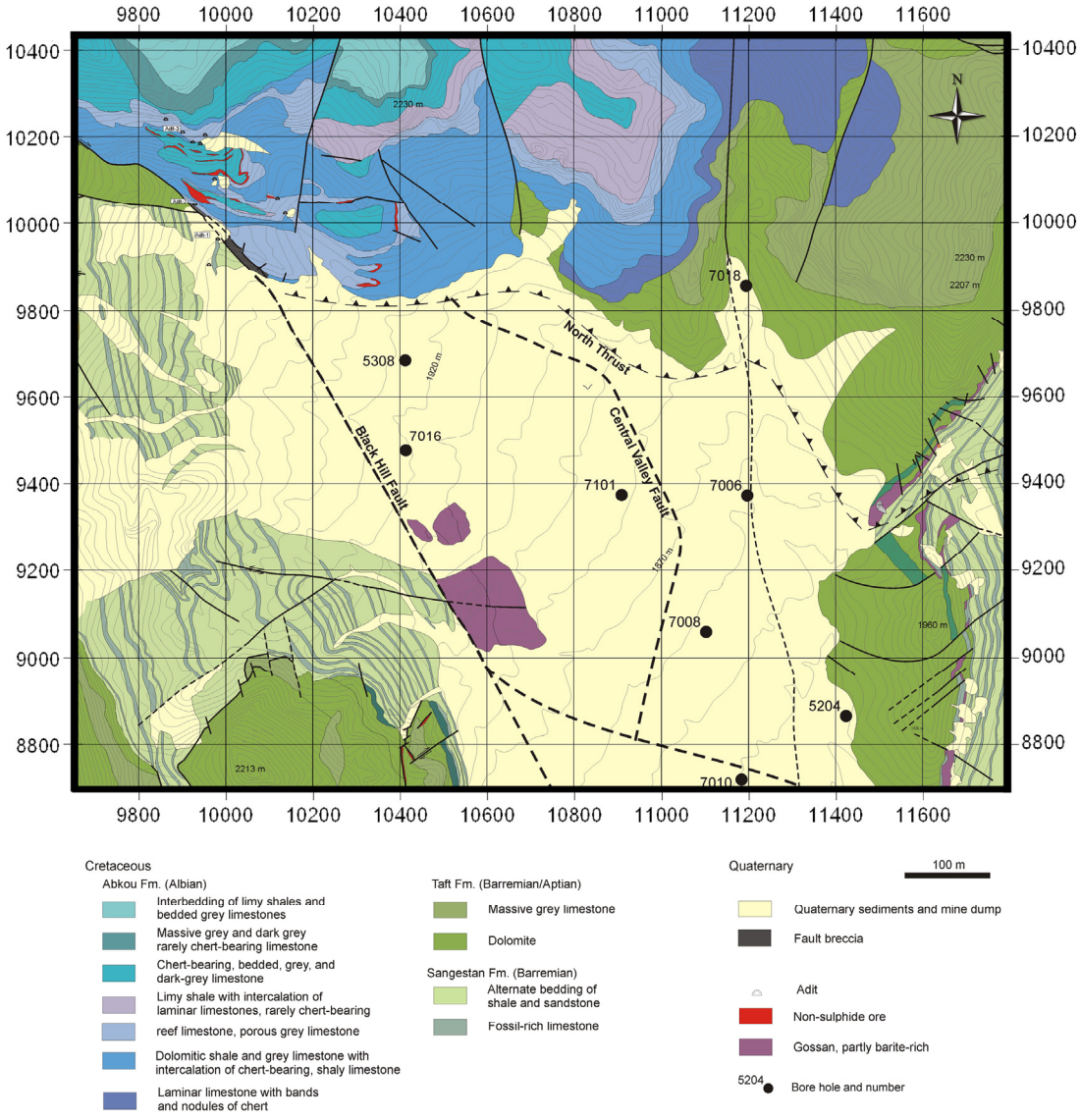

Fig. 11: Geological map of the Mehdi Abad Zn-Pb deposit and the adjoining area. (After Nosratian, 1991)

The structural geology is controlled by three main fault systems striking N-S, NE-SW, and NW-SE. The geologic map of the Mehdi Abad deposit (Fig. 11) shows the position of the main faults in this area. Apparently, these faults represent one of the main controlling factors of mineralisation.

4.1.3 The Mountain Ore Body (MOB) of Mehdi Abad

The altitude of the Mountain Ore Body (MOB) (locally also called 'Calamine Mine'), which is separated by faults from the main sulphide/non-sulphide Valley Ore Body (VOB), ranges from approximately 2000 up to 2300 m and represents the highest parts of the exposed mineralisation of Mehdi Abad. In contrast to the mixed main sulphide/non-sulphide orebody of the VOB, the MOB contains no zinc- and lead sulphides. The MOB consists of numerous adits, which follow the folded and duplicated ore horizon at different levels (Fig. 13). Three adits, on the 2006 m-, 2080 m-, and 2230 m-level have been sampled from W to E and a total of 36 specimens have been analysed by light microscope, XRF, ICP, XRD, SEM, and SEM-EDX.

Geology of the MOB

The geological map of the Mehdi Abad zinc-lead deposit shows the position of the MOB, wedged-in between two important faults (Fig. 12): limited to the west by the Black Hill Fault, and in the east by the Forouzandeh Fault. The Black-Hill-Fault is one of the main and principal faults of the Mehdi-Abad zinc-lead deposit. The zinc-lead mineralisation occurs exclusively in the strata to the east. The Black Hill Fault is a normal dip slip fault, which strikes NNW-SSE and dips approximately 65°-70° to NE. The Forouzandeh Fault is a dextral strike-slip fault with a strike of approximately 60° to NE and a dip of approximately 50°- 80° to the NW. No folding can be recognised away from these two major faults. The enclosed strata within this fault-bounded area are intensively folded. The folding in this area is due to the displacing movement of the two above-mentioned faults and is unique within the area of the Mehdi-Abad zinc-lead deposit.

The non-sulphide zinc-lead ore occurs on mainly three different levels within the Abkouh Formation (Fig. 13), which is the result of fold repetition (GSI., 1988). Overall, the mineralisation is predominantly hosted within the massive limestone of the K_a^{l2} member of the Abkouh Formation (Albian) and particularly at the contact of the K_a^{l2} to the K_a^{sh2} member. The K_a^{sh2} member consists of yellow to greenish dolomitic and calcareous shales and laminated limestones. The zinc-lead mineralisation consists exclusively of non-sulphide minerals, such as hemimorphite, smithsonite, and hydrozincite. No sulphide minerals have been observed. The MOB is the main location of the Mehdi-Abad zinc-lead deposit, hosted within the Abkouh Formation. In contrast, the predominant portion of the zinc-mineralisation of the VOB of the Mehdi-Abad zinc-lead deposit is hosted in strata of the Taft Formation (Barremian/Aptian) (G.S.I., 1988). The host rocks to the MOB are intensively faulted, brecciated, and locally mylonitised.

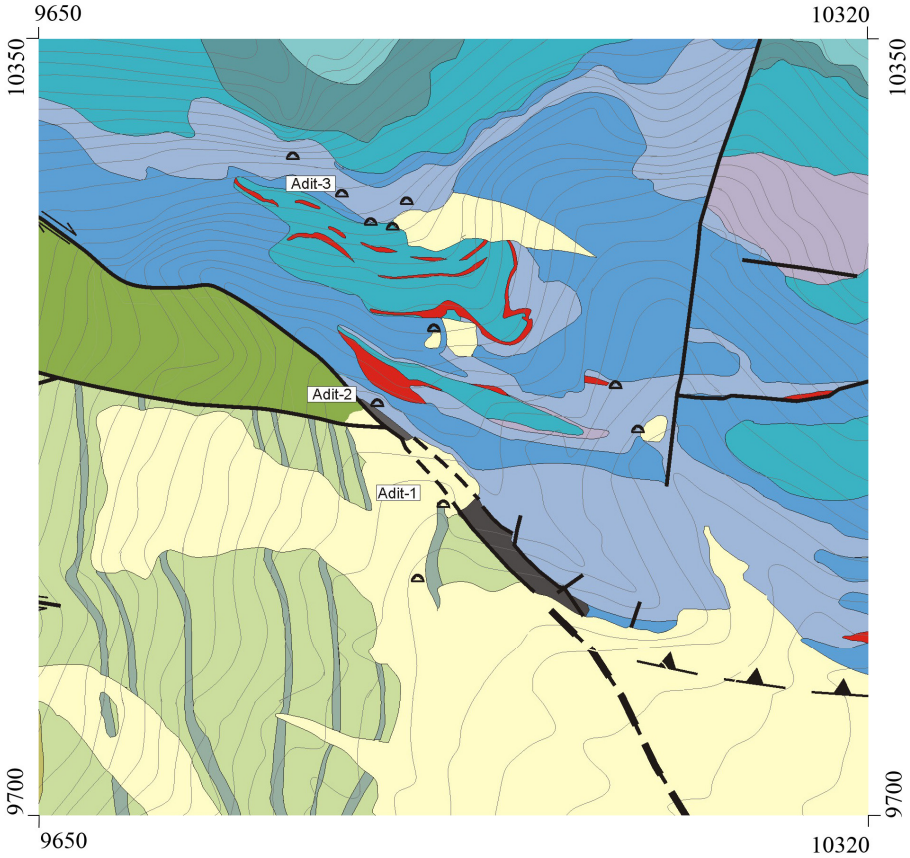

Fig. 12: Regional geological map of the of Mountain Ore Body , which is located in the northwestern part of the Mehdi-Abad zinc-lead deposit. The ore is hosted within the strata of the Abkou Fm. The rocks between the Black-Hill Fault and the Forouzandeh Fault are folded. The strata and the ore bearing horizons are stacked by folding, faulting, and thrusting. (Redrawn after NOSRATIAN, 1991)

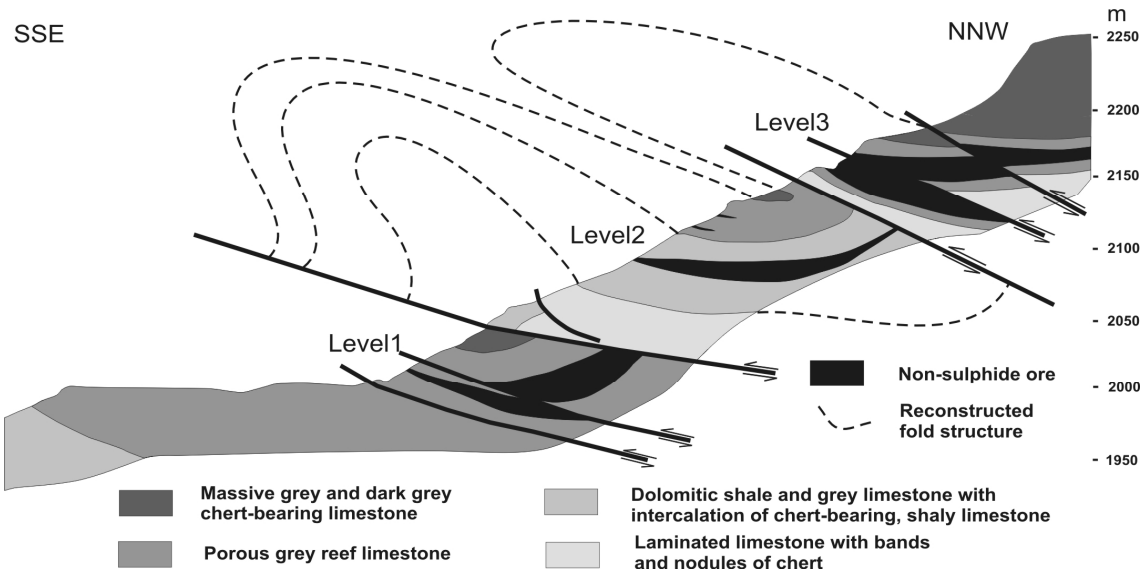

Fig. 13: Schematic NNW-SSE section of the folded and faulted strata at the Calamine Mine area. The ore-bearing strata are stacked in three main units due to folding, faulting, and thrusting. The dotted line indicates reconstructed fold shapes. (Modified after NOSRATIAN, 1991).

Examinations of the Mountain Ore Body (MOB)

Three adits on different levels of the MOB have been examined and sampled for the investigation of the metal distribution and genesis of the non-sulphide ore of the MOB. The Fig. 12 and Fig. 13 show the location of these adits. The course, direction and the sample-points of adits no. one and two are given in the appendix (Fig. A. 1 and Fig. A. 2). The total length of the adits decreases on the upper levels. The uppermost adit no. 3 has a length of 20 meters only and is not shown separately due the limited length of from this adit. The underlying principle for the selection of the adits was to get information's about the spatial distribution of elements, the distribution of metal concentrations, and the different styles of mineralisation within this mine-area.

The base-level adit (no. 1) and mid-level adit No. 2 (Fig. 12, Fig. A. 1, and Fig. A. 2, appendix) are part of a network of several galleries and branches, which ead to big cavities of mined-out non-sulphide zinc-ore. The top-level adit no. 3 is not connected to other tunnels or galleries and represents a locally limited region of historical non-sulphide ore searching – and mining activities.

The level of the adit no.1 is at 2006 m.a.s.l. and starts in strata of medium-thickly bedded, shaley and grey limestone with an average dip-direction of 268/35. The strata consisting of limestone and dolomitic limestone show clearly determinable bedding and an extensively and intensively faulting. Several major intensively and extensively faulted zones are recognisable within these adits. They mainly consist of highly brecciated limestone and/or dolomite with a reddish-brown coloured matrix. The metal concentrations within these fault-zones reaching from no mineralisation or even increased metal-concentrations up to high-grade Zn-(Pb)-concentrations. The strata in between these faults are less brecciated. The stope walls of several fault zones show up to 1 cm thick layers of a coating by white gypsum and a leakage of small amounts of water dripping from the fault. The ICP-analysis of specimen of most of these fault zones give elevated heavy metal contents compared to the wallrock, with zinc showing the highest concentrations (Zn: 2933 ppm, Pb: 90.9 ppm, Sample M02104), but no substantial economic mineralisation. However, several faults as well as highly (karstic-) brecciated areas, which are already mined out, show high Zn-(Pb-) concentrations and the metal bearing minerals occur as a cement of fault- and karst-breccias. Main minerals within these ore-bearing zones are hemimorphite, hydrozincite, calcite, quartz, and iron oxi-hydroxides, such as goethite and hematite.

The mid-level adit no.2 is located on a level of 2027 m.a.s.l. and belongs to another huge and complex system of galleries and caverns, which document extensive mining activities in former times. The entry of this adit is located close to the Black-Hill Fault. The rock, which consists of a mid-grey limestone and dolomites, is massive to highly brecciated on a regional scale and is probably due to karst effects. The fragment-sizes range from cm to dm-scale. Numerous faults cross the rock of this adit, similar to the base level adit. The metal distribution is rather similar to the base level adit. Most of the faults show only slightly increased metal concentrations. However, some of the sampled faults are characterised by high metal concentrations.

The top-level adit no. 3 is the shortest sampled adit with a length of 20 meters on level 2173 m. The limestone of this adit is highly brecciated and is riddled with numerous faults. The non-sulphide zinc ore occurs furthest in the back of this gallery, associated with a fault-system within a range of 8 meters.

Water occurs rarely at all examinated levels. Most of them are dry; except several fault related zones with a wettish appearance.

Ore-mineralogy and style of mineralisation of the Mountain Ore Body

The non-sulphide zinc ore of the MOB is hosted by limestone and low magnesium dolomitic limestone. The primary sulphide ore is completely oxidised. Based upon the composition of the sulphide ore of the VOB the supposed main sulphide mineral association of the MOB zone was galena-sphalerite-barite-pyrite.

The distribution of the mineralisation and the ore textures are highly dependent on the scale of observation. The occurrence of the ore is strata-bound on a regional scale, but underground the mineralisation is spatially related to faults, fault-breccias, and possibly to localised (karst-) solution collapse breccias. The non-sulphide zinc ore of the MOB can be subdivided into a red zinc ore and a white zinc ore. The red zinc ore is rich in Zn (up to approximately 30%), iron (Fe app. 17%) and other metals such as Pb - (As). The white zinc ore in contrast shows typically high zinc grades (up to 40%) but low concentrations of iron (<7%) and lead and arsenic.

The most important non-sulphide zinc minerals are hydrozincite and hemimorphite. Smithsonite is also common and is detectable by XRD analyses within nearly all non-sulphide ore samples. However, smithsonite occurs only in traces. The most common XRD-detected minerals and their position within the genetic sequence of the non-sulphide ore are (Tab. 6):

Tab. 6: Genetic sequence of main minerals within the non-sulphide zinc ore of the MOB. Detected by XRD and indirectly detected by SEM-EDX analyses

Mineral	Formula	Occurrence	Early	Late
Calcite	CaCO3	common		
Dolomite	$(Ca,Mg)CO_3$	common		
Quartz	SiO_2	minor/traces		
Barite	$BaSO_4$	common		
Goethite/Hematite	$FeO(OH)$, Fe_2O_3	common		
Hydrozincite	$Zn_5(CO_3)_2(OH)_6$	common		
Smithsonite	$ZnCO_3$	traces		
Hemimorphite-I	$Zn_4Si_2O_7(OH)_2 \cdot H_2O$	common		
Hemimorphite-II	$Zn_4Si_2O_7(OH)_2 \cdot H_2O$	common		
Cerussite	$PbCO_3$	minor		
Gypsum	$CaSO_4 \cdot H_2O$	traces		
Coronadite	$Pb(Mn(IV),Mn(II))_8O_{16}$	traces		
Hetaerolite	$ZnMn_2O_4$	traces		
Secondary calcite	$CaCO_3$	minor		
Kaolinite	$Al_2Si_2O_5(OH)_4$	traces		
Sauconite	$Na_{0,3}Zn_3(Si,Al)_4O_{10}(OH)_2 \cdot 4(H_2O)$	traces		
Mimetite	$Pb_5(AsO_4)_3Cl$	traces		

The **red zinc ore** (Fig. 14) occurs over the full spatial range of the MOB area as lenses or irregular shaped bodies with varying dimensions that range from several metres up to several 10's metres. The amount of red zinc ore compared with the white zinc ore increases at the upper levels. Com-

mon minerals of the red zinc ore are Fe-oxyhydroxides, goethite, hematite, hemimorphite, hydrozincite, smithsonite, and cerrusite. These minerals occur as a matrix of a carbonate breccia with limestone clasts of a broad size range (cm up to several dm). Hemimorphite, a zinc-hydro-silicate, is one of the most important zinc minerals of this ore-type, although the ore is carbonate-hosted.

Fig. 14: Red zinc ore from MOB, adit no. 2. The reddish-brown colour is due to the high Fe-concentration of this ore type. Common minerals are goethite, hematite, hemimorphite, hydrozincite and traces of smithsonite.

Fig. 15: White zinc ore from the MOB, adit no. 1. Host rock carbonate clasts with fine-grained hydrozincite and traces of smithsonite occur as cement of this breccia.

The occurrence of the **white zinc ore** (Fig. 15) is similar to the red zinc ore. The ore zones are irregular shaped and varying form several meters up to several 10's of metres. The size and occurrence of this ore increases with depth and is most common at the base level adits of the MOB. Most common minerals of this ore type are hydrozincite, smithsonite, and hemimorphite. Iron-bearing minerals are rare compared with the red zinc ore. Hemimorphite is less common compared with the red zinc ore. These minerals occur as a fine-grained cement of a carbonate karst-collapse breccia. The size of the breccia clasts is similar to the red zinc ore and ranges form cm to several dm.

Hemimorphite occurs as two different types: hemimorphite-I and hemimorphite-II. Hemimorphite-I represents sub- to anhedral crystals and masses within the matrix of the breccias. The size of the crystals is up to 200 µm. This hemimorphite-I is highly corroded, partly dissolved, and associated with fine-grained coatings, which mainly consist of hydrozincite, smithsonite and traces of goethite, hematite, and other Fe-oxihydroxides (Fig. 16, Fig. 17, and Fig. 20). Locally, goethite and hematite are absent, and here the highly corroded hemimorphite-I is associated with white, fine-grained hydrozincite and minor amounts of smithsonite. Fe-oxihydroxides (goethite, hematite etc.), associated with hemimorphite-I, show partly high concentrations of zinc (approximately 15 %, SEM-EDX), which is probably the result of high dispersed hydrozincite or due to zinc adsorption by goethite (ANKOMAH, 1992). Several mechanisms are proposed by ANKOMAH for the adsorption of Zn by goethite: (i) the adsorption of the metal on external surfaces, (ii) solid-state diffusion of the metal from external to internal binding-sites, and (iii) metal binding and fixation at positions within the goethite particles.

Hemimorphite-II occurs commonly in veins and open spaces of fault zones and –breccias (Fig. 18

and Fig. 21), and in the matrix of fault breccias as euhedral crystals, which have grown perpendicular to the underlying surface of fractures and spaces. The size of the hemimorphite-II is up to 300 µm. The occurrence of hemimorphite II is mainly limited to the red zinc ore and hydrozincite and/or smithsonite-mineralised zones and grows preferentially onto these Zn-rich minerals. Thus, hemimorphite is related to relatively late stages of the formation of the MOB.

Hydrozincite is another major component within the non-sulphide ore of the MOB and is the main mineral of the breccia matrix within the white zinc ore but is also common in the red zinc ore and occurs commonly as 10 to 100 µm euhedral crystals. Hydrozincite occurs also within the red zinc ore as one of the main zinc minerals and is often associated with highly corroded hemimorphite-I. Additionally, hydrozincite is the predominant zinc mineral within several cm/dm sized faults and fault-related breccia zones. Smithsonite is rare at the MOB. It can be detected with XRD-analyses, but was not found with SEM and microscope. Thus, the occurrence of smithsonite is presumably high-disperse, fine crystalline and occurs only in traces.

Cerussite and mimetite are the main lead-bearing minerals of the MOB, whereas segnitite occursonly in traces. Cerussite occurs predominantly as crystals related to late-stage precipitations within fractures and pores of the red zinc ore, especially regionally bound and limited to fault- and fracture zones. However, cerussite occurs also rarely within the white zinc ore, preferentially within fractures and pores. Mimetite occurs commonly as yellow needles and aggregates (Fig. 22). Other zinc minerals, such as hetaerolite, coronadite, willemite, or sauconite are rare and are also associated with both ore types. Black coloured hetaerolite forms mm-thick crusts and masses within pores and fractures, suggesting a late stage-related precipitation

The supergene, non-sulphide ores are characterised by very high Zn-, varying Pb-, and very low Ag-contents (Tab. 7). However, unexpectedly high concentrations of As, Sb, Tl, and Sr within the red zinc ore, point to (a) complex and exotic metal source(s) than expected for typical carbonate-hosted Zn-Pb deposits. A hydrothermal input from a magmatic source appears to be likely.

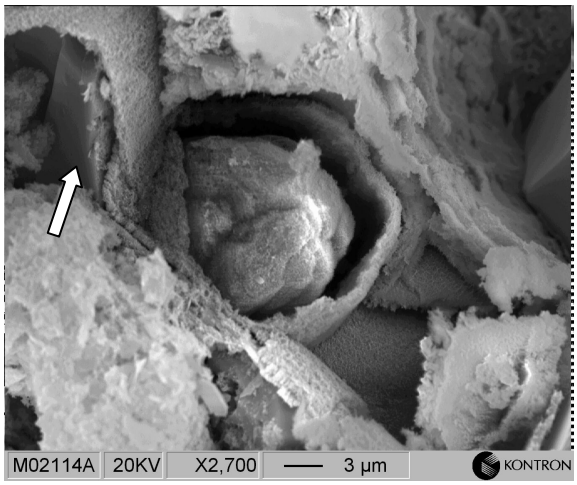

Fig. 16: SEM-photograph of a boxwork structure, which consists of zinc (hydro-)carbonates (hydrozincite/smithsonite) and porous goethite. Hemimorphite-I occurs commonly in the centre of the boxwork structures (arrow). Sample M02114.

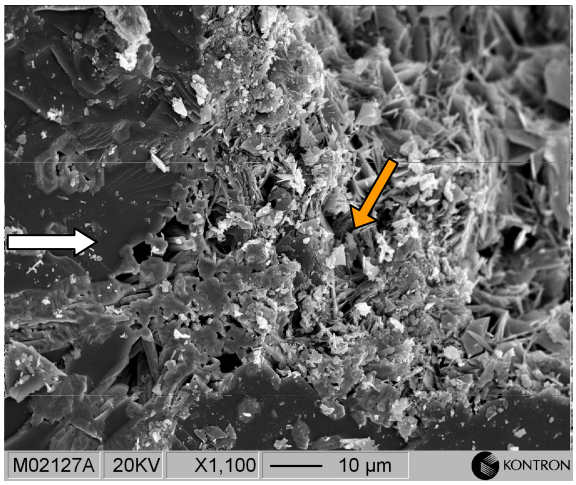

Fig. 17: SEM-photograph of a boundary between hemimorphite-I (white arrow) and hydrozincite (orange arrow). The boundary surface is irregular and porous and due to as an alteration and replacement of hemimorphite-I with hydrozincite. Sample M02127.

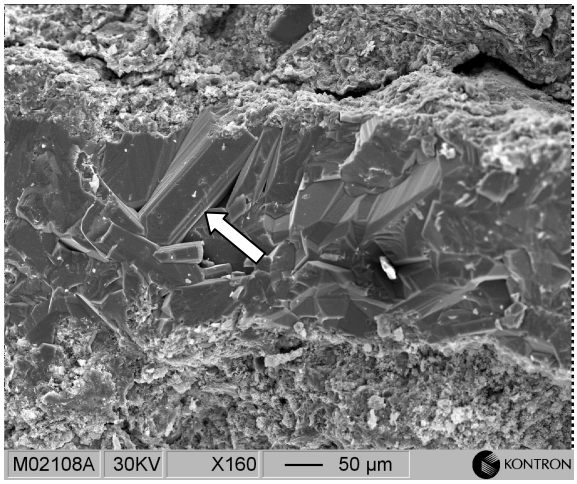

Fig. 18: SEM-photograph of euhedral hemimorphite-II (arrow) growing in vugs and fractures of the breccia matrix, which consists of fine-grained goethite, hydrozincite and hemimorphite-I. (Sample M02108)

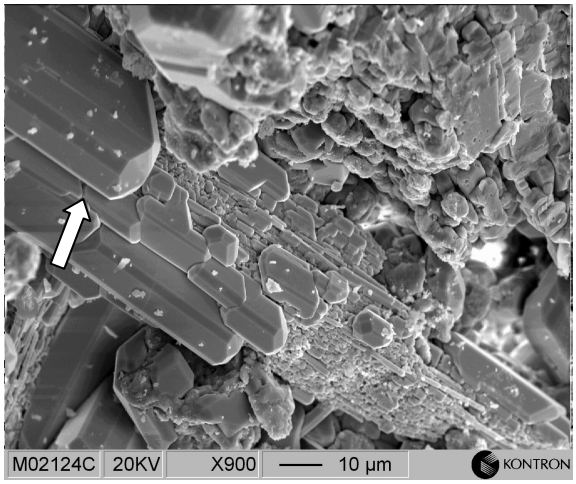

Fig. 19: SEM-photograph of a mimetite aggregate (arrow) and small grains of anhedral barite. The mimetite aggregate consists of small euhedral crystals (white arrow). Sample M02124.

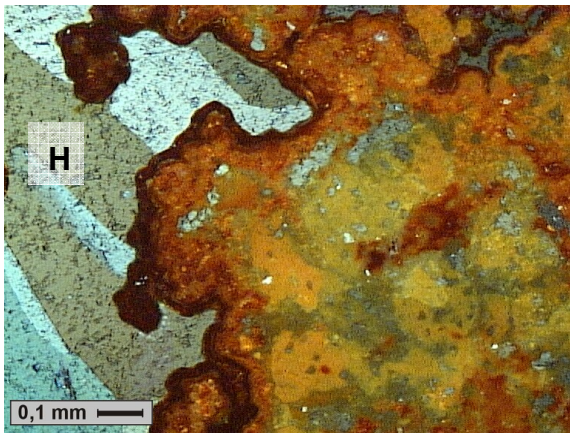

Fig. 20: The thin section shows hemimorphite-I (H), which is replaced by goethite, hydrozincite, and smithsonite. Sample M02132, reflected light.

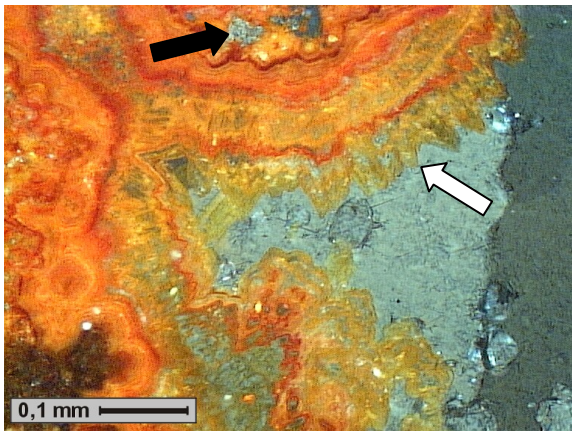

Fig. 21: Hemimorphite-I (black arrow) botryoidally overgrown by layers of goethite and hematite and late stage euhedral hemimorphite-II (white arrow) within a vug. Sample M02133, reflected light.

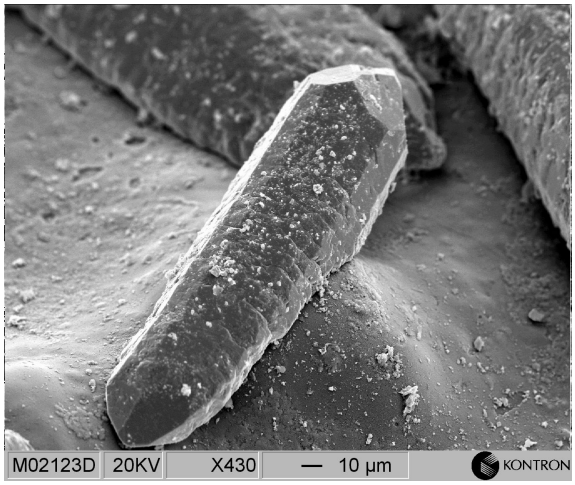

Fig. 22: SEM-picture of euhedral mimetite, which appears to be partly embedded within a sub-mm thick coating of an unidentified fine-grained (amorphous?) Fe-oxide/hydroxide. A XRD analysis of this Fe- bearing mineral shows no unequivocal results. Sample M02123

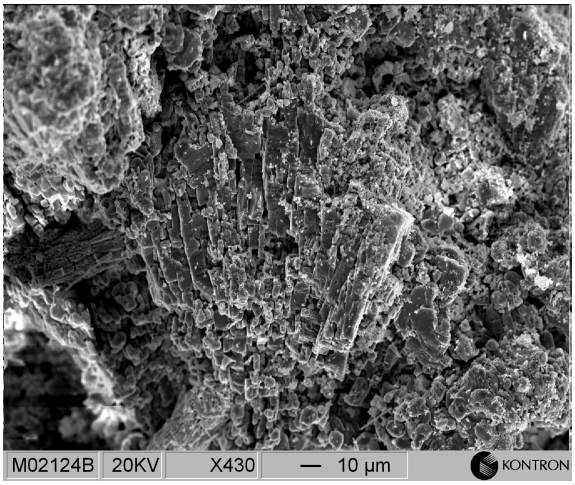

Fig. 23: SEM-photograph of linear ordered small, subhedral grains, which consist of barite. The barite is probably weathered and coroded into numerous rounded grains. Sample M02124.

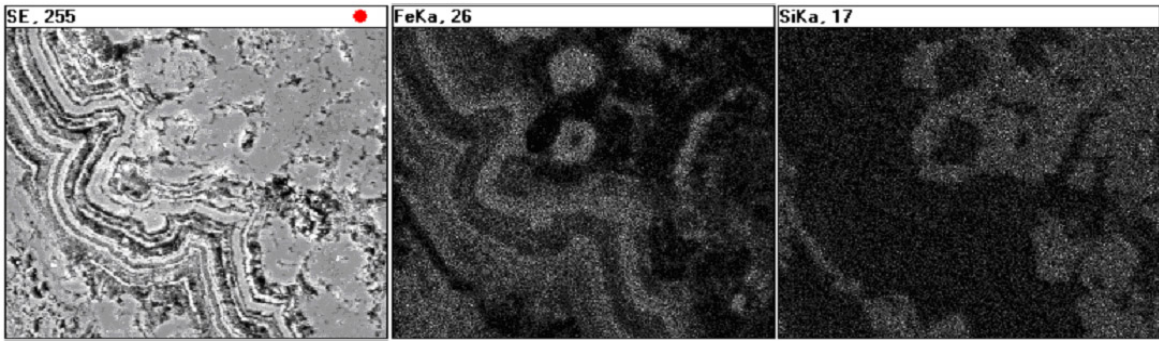

Fig. 24: SEM-EDX element distribution maps of a polished thin-section of sample M02133. Hemimorphite is overgrown by layers of goethite and hematite. The picture, which is marked by “SE”, shows a secondary electron image, and the other two images show element distribution maps of iron (FeKa) and silica (SiKa). The FeKa-picture points to the Fe-bearing layers, whereas the SiKa marked picture indicates the distribution of the Si-bearing hemimorphite. The width of the field of view is 120 µm. Hemimorphite (high Si concentration) in the innermost part of botryoidal-shaped aggregates is probably alterated to goethite/hematite (high Fe concentration), which occurs as several, parallel layers. Lighter grey colours indicate a high amount of a specific element. All pictures show the same area.

The minerals and their occurrence suggest several stages of non-sulphide zinc ore genesis, during which formation, dissolution, and re-precipitation appear to have been competing processes with hemimorphite and hydrozincite being the ore minerals.

Tab. 7: Average concentrations of typical, goethite-rich non-sulphide ore samples (n = 9, ICP-MS¸ all concentrations in ppm). For more details, see also appendix.

Cu	Pb	Zn	Co	Ni	Ag	Cd	Sb	Mo	Sr	As
44	17518	360003	25	72	7	365	339	4	694	7217

Hemimorphite-I and hemimorphite-II represent different stages of the ore-forming process of the MOB. After TAKAHASHI (1960) and INGWERSEN (1990), the precipitation of hemimorphite can be described as an equilibrium reaction between hemimorphite and smithsonite/hydrozincite, which is mainly controlled by the partial pressure of CO_2 (P_{CO2}), pH, and the concentration of H_2SiO_4. Hemimorphite becomes more stable under relatively low P_{CO2} (< 10^{-2} bar) and low pH (< 6.9) conditions. After the formation of a hemimorphite-dominated ore, the geochemical conditions have apparently changed. Hemimorphite became unstable under these new conditions, and was (partly) replaced by hydrozincite. The stability of hemimorphite and the equilibrium reaction between hemimorphite and smithsonite/hydrozincite are shown in detail in chapter 5.4.1 (page 90).

C-O stable isotope geochemistry of carbonates of the MOB

Carbon and oxygen isotope measurements have been applied to samples of the MOB. These samples comprise limestones of the barren host rock, hydrozincite from the non-sulphide zinc ore, and euhedral calcites, which fill open spaces and fractures. The results of the isotopic measurements are presented in Tab. 8 and depicted in Fig. 25. The isotope compositions are expressed as delta values in $^{0}/_{00}$ relative to V-SMOV for oxygen and relative to V-PDB for carbon.

Tab. 8: δ13C and δ18O values of selected samples of the MOB from Mehdi Abad

Sample	δ ^{18}OV-PDB ‰	δ ^{18}O V-SMOW ‰	δ ^{13}C V-PDB ‰	
M02109	-14	16.5	2.0	calcite
M02109	-7.7	23.0	2.9	dolomite
M02113b	-15.3	15.1	1.1	calcite
M02113b	-5.9	24.8	2.8	limestone
M02117	-9.2	21.4	-0.4	calcite
M02120	-13.7	16.8	0.7	calcite
M02120	-8.3	22.4	2.2	limestone
M02127	-10.2	20.4	-1.8	hydrozincite
M02129	-8.7	21.9	-0.4	hydrozincite
M02129	-5.7	25.0	2.6	dolomite
M02134	-9.1	21.5	-3.8	hydrozincite

The diagram (Fig. 25) shows three separate clusters: (1) limestone samples of the host rock, (2) samples of calcite crystals, which occur as fillings in fractures and open spaces of the carbonate host rock, and (3) hydrozincite/smithsonite samples of the MOB. However, the hydrozincite cluster

comprises an additional single calcite sample, which plots within in the area of the hydrozincite.

The hydrozincite samples have not a monomineralic composition, since the mineralogy of the zinc-carbonates is relatively complex. Hydrozincite is commonly contaminated by traces of smithsonite and in most cases it is not possible to separate hydrozincite from smithsonite impurity, due to its microcrystalline intergrowth with hydrozincite. Thus, the result of the isotopic measurement of the hydrozincite may be influenced by the isotopic composition of smithsonite.

The analysed limestone samples of the MOB form a separate cluster (Fig. 25) and show a restricted range of both $\delta^{13}C$ (between 2.2 and 2.9 $^{0}/_{00}$) and $\delta^{18}O$ values (between 22.4 and 25 $^{0}/_{00}$) . The calcite samples form a second cluster. Calcite occurs as euhedral crystals, grew in open spaces and fractures of the limestone. These calcites show an close range of $\delta^{13}C$ (between 0.7 and 2 $^{0}/_{00}$) and $\delta^{18}O$ (between 15.1and 16.8 $^{0}/_{00}$). The third field consists of samples of hydrozincite of the non-sulphide ore from the MOB. The hydrozincite samples show a restricted range of $\delta^{18}O$ values between 20.4 and 21.9 $^{0}/_{00}$. The $\delta^{13}C$ values are more variable and range between -0.4 and -3.8 $^{0}/_{00}$. A single calcite sample fits in this field of hydrozincite samples.

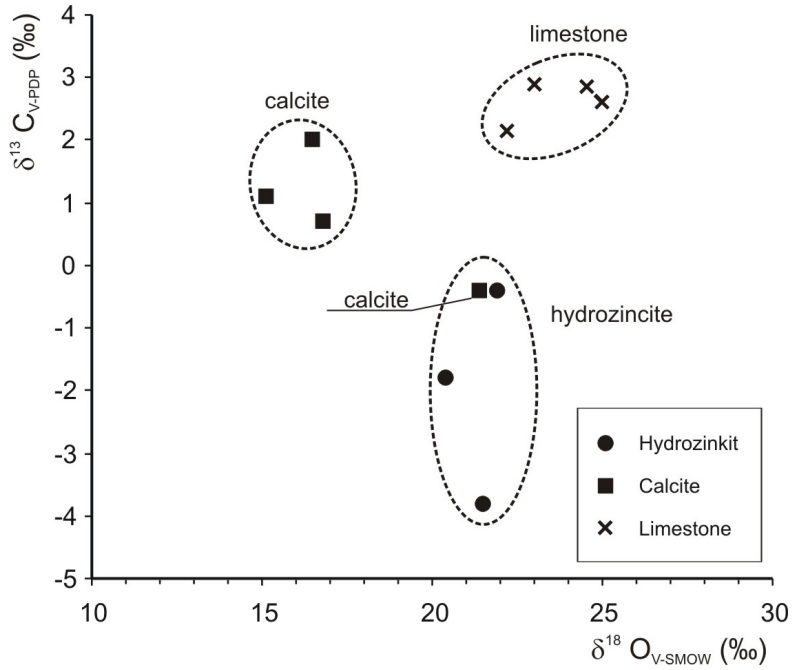

Fig. 25: Stable carbon and oxygen isotope composition of hydrozincite, late-stage related calcite, and limestone from the MOB of the Mehdi Abad Zn-Pb deposit.

The isotope values of the limestone correspond to the range of values, which has been established as typical for marine Cretaceous limestones (VEIZER & HOEFS, 1976).

The calcites of the MOB plot within two distinct regions. Thus, the isotopic composition of the calcites from the MOB suggests two different possible genetic sources. Three samples of calcite show lower $\delta^{18}O$ (15.1-16.8 $^{0}/_{00}$) and higher $\delta^{13}C$ (0.7-2.0 $^{0}/_{00}$) compared to a single calcite sample, which is relatively high in $\delta^{18}O$ (21.4 $^{0}/_{00}$) and low in $\delta^{13}C$ (-0.4 $^{0}/_{00}$). The $\delta^{18}O$ of a carbonate precipitated from water depends on the $\delta^{18}O$ composition of the water and the temperature. Increasingly lighter

$\delta^{18}O$ values tend to be associated with a decreased salinity and with higher temperatures, whereas the $\delta^{13}C$ composition reflects the source of the bicarbonate, which is dissolved in the water (NELSON & SMITH, 1996). Thus, the only slightly decreased $\delta^{13}C$ values of the calcite veins are due to a buffer effect from the limestone. The negative trend in the $\delta^{18}O$ values of the calcites may reflect precipitation at higher temperatures and is typical for burial (CHOQUETTE & JAMES, 1990; NELSON & SMITH, 1996).

The single calcite sample, which plots within the field of the zinc carbonates, suggests an influence of meteoric water, which delivered isotopically light carbon from the decomposition of organic matter. The $\delta^{13}C$ is moderately depleted and the calcite has been presumably precipitated under the influence of meteoric waters, which are variably buffered by water-limestone interaction. (ALLAN & MATTHEWS, 1982; NELSON & SMITH, 1996).

The isotopic pattern of the hydrozincite samples shows a narrow range of $\delta^{18}O$ values and a more variable range of $\delta^{13}C$ data. This behaviour is similar to smithsonite samples, which have been analysed by GILG & BONI (2004) and BONI ET AL. (2003). This probably indicates at least two isotopically different sources of carbon. The roughly constant $\delta^{18}O$ values and the variably low- to medium depleted $\delta^{13}C$ values match the idealised trend of a meteoric carbonate precipitation. Thus, wide variability in $\delta^{13}C$ and narrow variability in $\delta^{18}O$ most likely reflect the influence of meteoric water associated with subaerial exposure (ALLAN & MATTHEWS, 1982, LOHMANN, 1988) and point to the precipitation of the zinc carbonates within the vadose and/or phreatic zone (ALLAN & MATTHEWS, 1982). The isotopically light component of the carbon is the result of dissolved CO_2 derived from the decay of organic matter (CRISS, 1995).

4.1.4 The Valley Ore Body (VOB) of Mehdi Abad

Geology of the Valley Ore Body

The strata of the Taft and Abkou Formation overlie the Sangestan Formation and host the sulphide ore of the Valley Ore Body (VOB) (AZARI & SETHNA, 1994). The Sangestan Formation consists mainly of partly cross-bedded sandstone (Fig. 26), limestone, and shales. The strata of the Taft Formation consist mainly of dolomitic and ankeritic limestone, whereas the Abkou Formation comprises marl stone with conglomeratic intervals, and massive limestone.

The contact zone between the Sangestan and Taft Formation is characterised by an unconformity, which shows an irregular surface with shallow water sediments between the para-reef limestone (Fig. 27) at the top of the Sangestan Fomation and the limestone of the Taft Formation. These shallow water sediments consist of red and green mudstone with worm tubes, nodular limestone, and cross-bedded limestone (BRGM, 1993). This zone probably reflects a period of emergence and has been used as a marker horizon in the drill cores. Most of the drill cores of Mehdi Abad stop at this horizon.

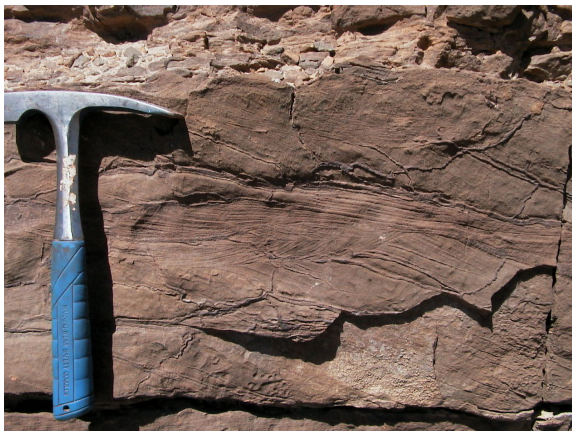

Fig. 26: Cross-bedded sandstone of the Sangestan Formation at the East Ridge of Mehdi Abad.

Fig. 27: Reefal limestone near the contact zone of the Sangestan- and Taft Formation.

The strata of the Taft Formation, which host the main portion of the sulphide ore of the VOB are characterised by an intensive and extensive brecciation. This brecciation is common within most of the VOB drill-cores of Mehdi Abad (BRGM, 1993) and is probably the result of emergence, paleo-carstification, and finally collapse of these strata. The breccia fragments are angular and the fragment-size ranges from a cm- to dm-scale.

The contact zone between the Taft- and the overlaying Abkou Formation is characterised by an unconformity, similar to the contact zone of the Sangestan- and Taft Formation. Here, the cherty limestone of the Taft Formation shows a channelled surface, overlain by a conglomeratic bed, which consists of limestone and chert clasts (BRGM, 1993) and can be interpreted as a renewed period of emergence and probably the stage, during which karstification and collapse of the Taft Formation occurred.

Ore mineralogy of the VOB

Examinations of several samples and detailed investigations of bore holes no. 5308, 5204, and no. 7008 (Fig. 11) show, that the sulphide ore of the VOB consists of several subordinate mineralised zones, which are separated by barren dolomite of the Taft Formation as well as several faults.

The most abundant minerals within the **sulphide ore** are galena, sphalerite, barite, pyrite, and traces of chalcopyrite. The sulphide ore of the VOB occurs as impregnation of the Taft Formation breccia and fills the interstitial space between the breccia fragments (Fig. 28). Sample examination and literature data as well (e.g. AZARI & SETHNA, 1994) show, that the main sulphide minerals of the VOB are sphalerite, galena, pyrite and traces of chalcopyrite, and other sulphides. Other sulphides, such as marcasite or chalcopyrite in subordinate traces. Disseminated sulphides occur commonly as low-grade mineralisation within the barren dolomite and the adjacent strata. The sulphide mineralisation is not associated with conventional vein-system or with synsedimentary stratiform horizons, but occurs as matrix in a complex fracture and breccia system (Fig. 28). In some cases, the sulphide ore itself occurs as breccia fragments (Fig. 29). Pyrite occurs as angular crystals and masses accompanied with Zn and Pb sulphides or as spherical framboidal pyrite within dolomite and limestone.

It appears that sphalerite and galena have been partly replaced the barite of the dolomite breccia (Fig. 31 and Fig. 32). The sulphide mineralisation occurs as fine-grained crystals in a wide range from euhedral to anhedral crystals. The observed sphalerite/barite ratio changes irregularly but is generally between 1/1 and 2/1, which is in general agreement with the reported ratio of 1 (BRGM, 1993).

Barite is ubiquitous within the mineralised dolomite breccia as well as in fractures, veins, and veinlets within the non-brecciated barren dolomite and limestone of the Taft Formation and Abkouh Fm. Additionally, massive barite occurs in the Black Hill area, but only with a slight amount of sulphide mineralisation. In most cases, the barite tends to have grown with a euhedral habit but occurs also as anhedral patches or skeletal crystals. The size of barite crystals varies over a wide range from microcrystalline sub-mm to cm-sized euhedral crystals. The barite grew in pores and open spaces of dolomite. The crystal-size has been probably controlled by the space of the hosting cavities. Locally, barite occurs as broken crystals and is observable in several thin sections. The space between these barite fragments is filled with fine-grained carbonate cement (Fig. 30). The observable barite deformation and the subsequent carbonate cementation of the barite fragments are probably due to a pre- or syn-collapse barite-mineralising event. The barite crystals grew in pores and open spaces of the karstic carbonate and have been deformed and crushed as a result of collapse and compaction of this karst-breccia.

The **dolomite**, which hosts the sulphide ore, is probably secondary and the result of a dolomitisation process. This dolomitisation of the carbonate host rock is possibly either associated with the barite mineralisation or with the sulphide-ore delivering fluids. It is supposed that the dolomitisation was associated with the ore fluids, since the adjacent carbonate strata (Abkou Formation) to the massive barite rock ‘Black Hill’ is not affected to any dolomitisation (Fig. 117 and Fig. 118).

Tab. 9: Genetic sequence of main minerals of the VOB. Detected by XRD and indirectly detected by SEM-EDX /analyses

Mineral	Formula	Occurrence	Early		Late
Calcite	$CaCO_3$	common			
Dolomite	$(Ca,Mg)CO_3$	common			
Quartz	SiO_2	minor/traces			
Barite	$BaSO_4$	common			
Pyrite	FeS_2	common			
Sphalerite	ZnS	common			
Galena	PbS	common			
Goethite/Hematite	$FeO(OH)$, Fe_2O_3	common			
Hydrozincite	$Zn_5(CO_3)_2(OH)_6$	common			
Smithsonite	$ZnCO_3$	traces			
Hemimorphite	$Zn_4Si_2O_7(OH)_2 \cdot H_2O$	traces			
Cerussite	$PbCO_3$	minor			
Gypsum	$CaSO_4 \cdot H_2O$	traces			
Coronadite	$Pb(Mn(IV),Mn(II))_8O_{16}$	traces			
Hetaerolite	$ZnMn_2O_4$	traces			
Secondary calcite	$CaCO_3$	minor			
Mimetite	$Pb_5(AsO_4)_3Cl$	traces			

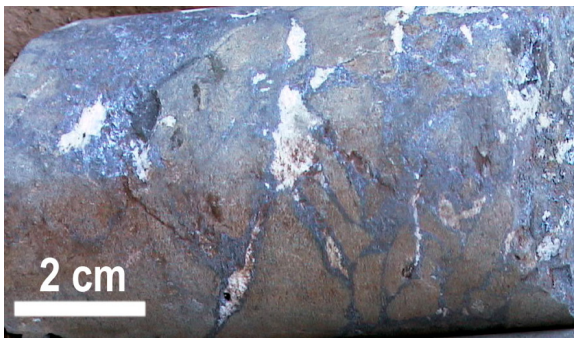

Fig. 28: Highly brecciated ore-bearing dolomite of bore hole no. 5308 at 212 m. The space between the fragments is filled by a grey coloured matrix of fine-grained sphalerite, galena, and barite and traces of chalcopyrite.

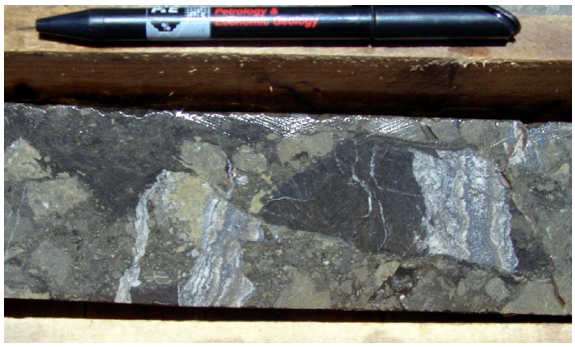

Fig. 29: Angular breccia fragments. The fragments consist of sulphide ore and sulphide ore-mineralised dolomite. (Fotograph: G. Borg).

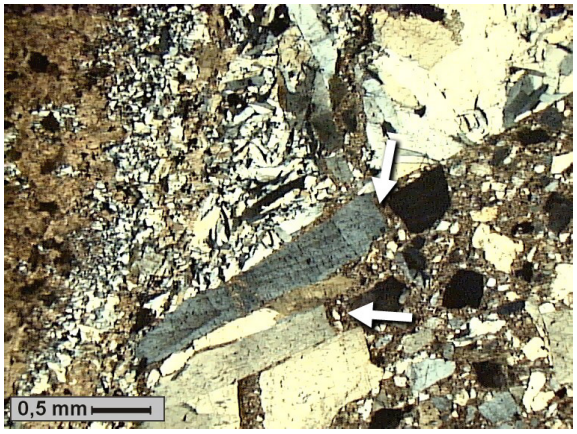

Fig. 30: Barite crystals in dolomite (brown colours) breccia. Some large barite crystals are broken. The space between the barite fragments (white arrows) is filled by small irregular barite fragments and a carbonate matrix. Bore-hole no. 5308 at 226 m. (transmitted light, XN)

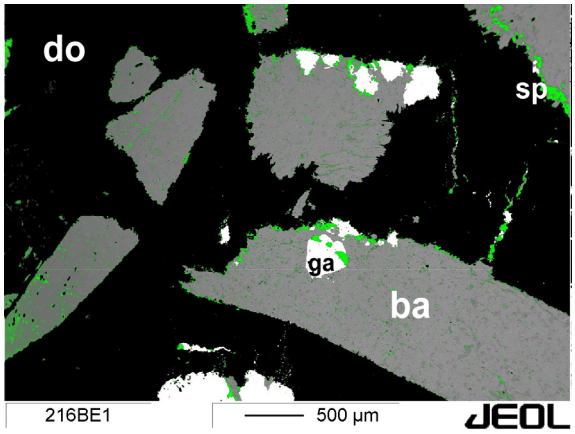

Fig. 31: Barite crystals of bore-hole 7008 at 216 m in dolomite (do). Most of barite-crystals (ba) show a euhedral to subhedral shape. In some cases, the barite has been incompletely replaced by galena (ga) and sphalerite (green coloured, sp). Pyrite is rare at this depth and absent in this field of view. (SEM-BSE photograph)

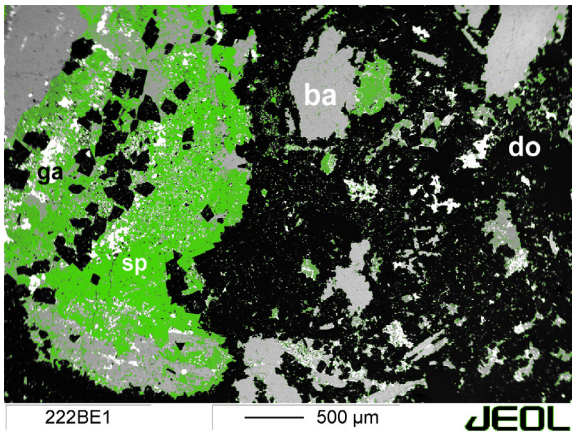

Fig. 32: Barite (ba) is partly replaced by sphalerite (green colour, sp) and galena (ga). Sphalerite and galena are the most common sulphides. Pyrite and other sulphide minerals are generally rare and absent in this thin-section. In some cases, dolomite occurs as euhedral rhombs with crystal sizes up to 200 µm. SEM-BSE photograph of borehole 7008 at 295 m.

4.1.5 Geochemical investigations of the MOB and the VOB

A total of 19 samples of the MOB (hand specimen) and 109 samples of the VOB (drill core and hand specimen) have been analysed by ICP-MS.

Cadmium in the sulphide ore and in the non-sulphide ore

Cadmium is associated with most Pb-Zn deposits (SCHWARTZ, 2000). In particular, the behaviour of Cd during oxidation and the formation of non-sulphide ore are very interesting. The Cd-concentration within the sulphide ore of the VOB was examined in several sulphide mineralised samples. The measured concentration varies in a wide range from 0.3 ppm up to 583 ppm. The relationship of cadmium to other elements has been tested by plotting several graphs, but exclusively the Zn-Cd plot shows a significant positive correlation (Fig. 33). The incorporation of Cd into sphalerite is a common phenomenon (DOMÈNECH et al., 2002) and based on these results, it can be assumed that sphalerite, which is the main zinc-bearing mineral, is the predominant host mineral to cadmium within the sulphide zone. The Cd-Zn ($R_{Cd/Zn}$) ratio is nearly constant and gives results of approximately $R_{Cd/Zn}$ = 0.004 (n=19, stdev = $9.1 \cdot 10^{-4}$). With the molar masses of zinc, sulphur, and cadmium (M_{Zn}=65.38, M_S=32.06, M_{Cd}=112.4 g/mol) it is possible to calculate the concentration of cadmium in a simplified $(Zn_{(1-x)},Cd_x)S$ - sphalerite (formula F1).

$$C_{ppm} = \frac{m_{Cd}}{\left(\frac{m_{Zn}}{M_{Zn}} + \frac{m_{Cd}}{M_{Cd}}\right) * M_S + m_{Zn} + m_{Cd}} * 10^6 \qquad \text{F1}$$

with n=molarity, M=molar mass of Cd, S, and Zn

This calculation gives an average concentration of 2682 ppm cadmium in sphalerite or 0.27% Cd. However, in most cases the real cadmium concentration of sphalerite is smaller than the calculated value, due to additionally incorporated iron and other elements into the sphalerite crystal lattice. Nevertheless, the calculated (maximum-) concentration of cadmium within the sphalerite is comparable to MVT-type deposits (Tab. 10) (SCHWARTZ, 2000) and fits also within this range even at lower Cd-concentration values. However, this value fits also to a wider spectrum of deposit types within the range of Cd concentrations of each type. According to Tab. 10, Mississippi-Valley type (MVT) deposits show the significantly highest concentrations of Cd in sphalerite (Cd_{Sph}). The high Cd_{Sph} is caused by the high $R_{Cd/Zn}$ of basinal brines, which can be considered to be the recent equivalents of MVT fluids (Schwartz, 2000). The Cd-content depends on the $R_{Cd/Zn}$ ligand activities, and temperature of the ore forming fluid. Thus, exhalative systems with their low $R_{Cd/(Zn+Cd)}$, and high temperature form deposits with lower Cd concentration in sphalerite (SCHWARTZ, 2000).

The average Cd concentration of the non-sulphide ore of the MOB is similar compared with the sulphide zone of the VOB. However, several extreme values of MOB non-sulphide-related Cd-concentration can be as high as 2004 ppm in whole rock ore samples.

Tab. 10: Basic statistical concentrations for Cd concentration in sphalerite of different deposit types (after Schwartz, 2000)

Type of deposit	min	max	mean	median	st. deviation	n of deposits
VMS	100	10000	2360	1890	1.777	87
SEDEX	50	6250	2560	2200	1735	19
Skarn	300	9900	3540	3180	2192	54
Veins in low carbonate rock	15	46480	410	3110	4212	155
Veins in limestone/dolomite	1000	20000	7260	5000	6256	31
MVT	390	50000	4850	3630	5668	106
Sandstone lead-zinc	2570	-	-	-	-	1
Unclass., in limestone/ dolomite	560	21500	4300	2540	4830	27

$Cd_{Sphalerite}$ concentration in ppm

A possible host mineral for cadmium within the non-sulphide ore is smithsonite. Similar to sphalerite, smithsonite is able to hold up to 45500 ppm Cd (SCHWARTZ, 2000). Smithsonite occurs only in traces in the MOB and, in contrast to Cd within VOB sulphide ore, the cadmium in MOB non-sulphide ore shows no significant correlation with Zn (Fig. 34). One reason might be the high density of faults and the associated alteration, oxidation and mobilisation of zinc minerals, which might have led to a partial separation of zinc from cadmium and, as a result of this process; to a poor correlation. Another possible explanation might be two different generations of Cd-bearing minerals, associated with the major non-sulphide ore types of MOB, the Fe-rich and the Fee-poor ore. Greenockite (CdS) could not be detected as a Cd-bearing mineral that is commonly associated with supergene zinc mineralisation (TAKAHASHI, 1960). The abundance of greenockite within the alteration and non-sulphide zone can be explained by the scavenging of zinc during (re-) crystallisation from non-sulphide zinc minerals, such as smithsonite, hemimorphite, and hydrozincite (SCHWARTZ, 2000).

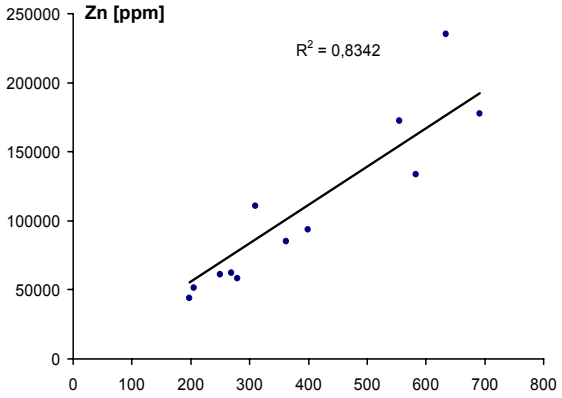

Fig. 33: Zn-Cd concentration plot of specimen from the sulphide ore of the VOB. The Cd concentration correlates with Zn. and is bound to sphalerite of the sulphide ore. (criteria: sulphide-bound sulphur >3%)

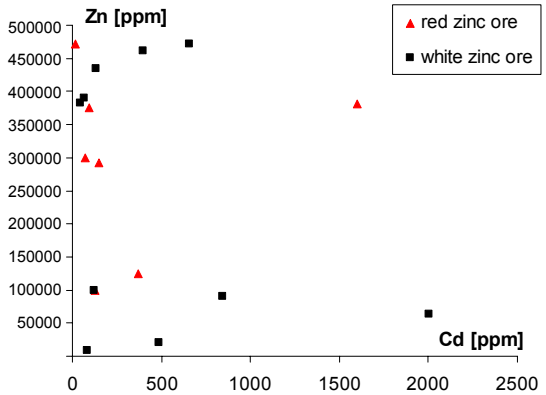

Fig. 34: Zn-Cd concentration plot of specimen from the red zinc ore (red triangles) and white zinc ore of the MOB. In contrast to Fig. 33, no correlation is determinable between the zinc and cadmium contents.

Arsenic in sulphide and non-sulphide ore

Arsenic occurs in the sulphide ore of the VOB as well as in non-sulphide ore of VOB and MOB. The arsenic concentration within the non-sulphide ore of the MOB $C_{As\text{-}Ox\text{-}MOB}$ is up to factor 30 higher than concentrations in the non-sulphide ore $C_{As\text{-}Ox\text{-}VOB}$ respectively. Similar to cadmium, sphalerite is able to incorporate arsenic into its crystal structure (LEACH ET AL., 1986) but no correlation to sphalerite could be found within the sulphide bearing samples of the VOB. This phenomenon is supported by additional SEM-EDX examinations of sphalerite. The measurements show no arsenic content. Another possibility is the incorporation of As within pyrite. Here, the overall theoretic possible compositional range for arsenic in pyrite is approximately up to 100000 ppm (KOLKER & NORDSTROM, 2001). However, the measurements of sulphide ore samples show bad or no correlation of iron with arsenic. Thus, the arsenic of the sulphide ore is probably bound to pyrite, but with a broad varying range of As-concentrations and is probably also bound to minerals such as arsenopyrite (FeAsS).

The plots of As vs. Pb give a hint of an As-Pb bearing mineral within the non-sulphide ore of the MOB. The ratio $C_{As\text{-}Ox}/C_{Pb\text{-}Ox}$=0.18 of white zinc ore of the MOB is apparently related to mimetite. The $C_{As\text{-}Ox}/C_{Pb\text{-}Ox}$ of mimetite can be calculated by using the formula and the molar masses of As and Pb and is calculated as $C_{As\text{-}mimetite}/C_{Pb\text{-}mimetite=}$ 0.22. This value is close to the As/Pb ratio of the white zinc of the MOB that suggests mimetite as one As-bearing mineral. In addition with cerussite, which is also detectable in the white zinc ore one can achieve the lower As/Pb ratio of 0.18 from Fig. 36.

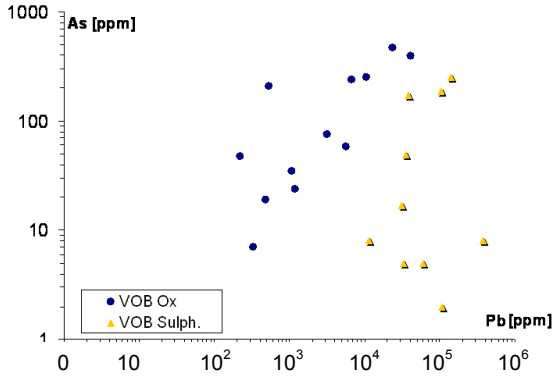

Fig. 35: Bivariate graph of As vs. Pb of non-sulphide zinc ore, and sulphide ore samples of the VOB. The value of R^2 gives no positive correlation between these elements, but a rough trend is visible, especially at samples of the Oxide zone.

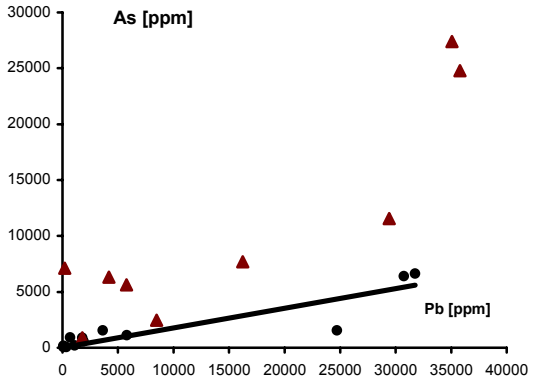

Fig. 36: Concentration of arsenic in relation to lead of non-sulphide ore-samples from the MOB. The red dots represents specimen, which are characterised by high Fe_2O_3 (>10%). The black dots represent ore, which is low in Fe_2O_3 (<5%).

Fe-concentrations in sphalerite of the VOB

The iron-concentration in sphalerite has been measured in sulphide-ore thin-sections of bore-hole No. 5308 and 7008 by SEM-EDX. All data of bore-hole 5308 show a continuous trend of increasing iron-concentrations with depth (Fig. 37). The highest Fe-concentration has been measured at a level of 275 m of borehole 5308. Here the Fe-content of sphalerite ranges from 6.3 % up to 11.8 % with a mean of 8 %. The iron-concentration at each level of borehole 5308 varies on a wide range of approximately 5 % of the mean.

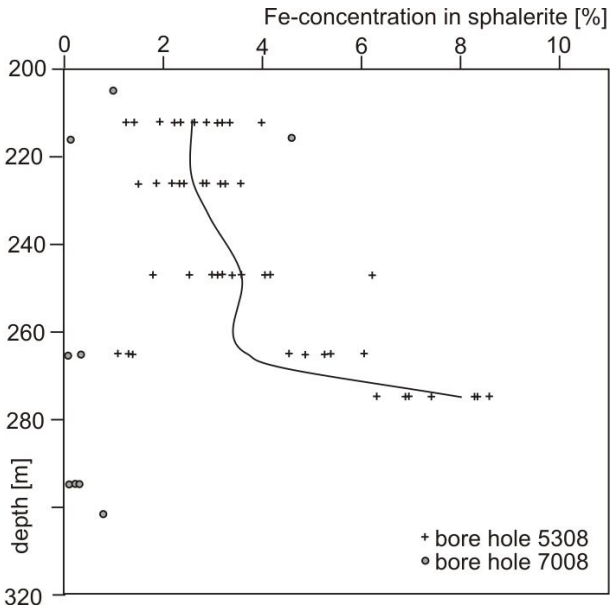

Fig. 37: Iron-concentration in sphalerite, measured by SEM-EDX. Samples of bore hole 5308 show an increasing Fe-content with increasing depth, whereas bore hole 7008 is characterised by low Fe-concentrations over the entire depth.

The Fe-concentration pattern of borehole 7008, which intersects the sulphide ore body approximately in its centre, is completely different from borehole 5308. Nearly all samples of borehole 7008 show a low Fe-concentration within sphalerite (Fig. 37) with no apparent visible trend.

The iron content of sphalerite depends on the geochemical parameters of the system pyrite – pyrrhotite – sphalerite and is very sensitive to pressure, sulphur fugacity, and temperature (BARTON & TOULMIN, 1966). As a result of these different variables, this system is only useful in geothermometry for three-phase assemblages of sphalerite – pyrite – pyrrhotite in which the sulphur fugacity is fixed at a given temperature by the coexisting iron sulphides under equilibrium conditions (SCOTT & BARNES, 1971).

Examinations of specimen from bore hole 7008 and 5308 has shown a dominance of galena and sphalerite, but only small amounts of pyrite and no pyrrhotite. Since the Fe-content of sphalerite is quite variable in the absence of pyrite and/or pyrrhotite (CRAIG & SCOTT, 1974), the iron concentration within the sphalerite cannot be used for geothermometry in this case.

The iron concentration within the sphalerite is controlled over a wide range only by the activity of FeS (a_{FeS}). High values of a_{FeS} result in sphalerite with high Fe-concentrations (CRAIG & SCOTT, 1974). This leads probably to decreasing a_{FeS}, which is associated with decreasing Fe concentrations of sphalerite.

Since the Fe-concentration of most ore-fluids increases with higher fluid-temperatures (MARIE ET AL., 2001), the gradient of the Fe-concentration with depth could additionally be the result of decreasing temperature during the hydrothermal pulse of the ore-mineralising event. Lower temperatures (probably more distal to the vent) decrease the Fe-concentration of the fluids and leads to the crystallisation of sphalerite with lower Fe content relative to the more proximal high-temperature

sphalerite.

The increase of Fe-concentration with an increase of depth in borehole 5308 is probably an indication for an upward directed hypogene ore fluid-flow within this ore body. Fe-rich sphalerite crystallised when the Zn-bearing fluids reached the (collapse-) breccia. This led to an iron depletion of the mineralising fluid, associated with the crystallisation of sphalerite at higher levels, which is low in Fe. The same mechanism of Fe-depletion is probably active during the lateral fluid flow. Therefore, the low Fe-concentration in sphalerite in borehole 7008 could point to a lateral mineralisation process with its origin in the western part of the sulphide ore body.

Based on the gradient of the Fe-concentrations within the ore body, a possible source (vent) for the ore fluids might have been located at the western outskirt of the sulphide ore body, probably near the Black Hill Fault.

Another possible explanation for diverse Fe-contents in sphalerite could be different generations of Zn-Pb-Fe delivering fluids that could cause these different Fe-fingerprints of sphalerite. The examined boreholes show completely different Fe-concentration patterns. The Fe-content of bore hole 5308 increases continuously with depth, whereas nearly all samples of bore hole 7008 show very low iron concentrations, which are absent in bore hole 5308. The exclusive occurrence of low-Fe sphalerite in borehole 7008 suggests at least two different fluid generations with a spatially independent occurrence. The controlling factor for the spatial separation could be probably faults.

Occurrence of zinc and lead

The main zinc mineral of the VOB is sphalerite and subordinately non-sulphide zinc minerals, such as hydrozincite, smithsonite, willemite, and hemimorphite. In contrast to the completely oxidised MOB, the VOB comprises both sulphide ore and non-sulphide ore as well. However, the occurrence and the style of the non-sulphide ore are different from that of the MOB. The actual data of the calculated Zn-Pb reserves are (Tab. 11):

Tab. 11: Zn-Pb reserves of Mehdi Abad.

oxide reserve	45.2 Mt at 7.15% Zn, 2.47% Pb
sulphide reserve	116.5 Mt at 7.3% Zn, 2.3% Pb

data: MEHDI ABAD ZINC COMPANY, 2005

Typical zinc and lead concentrations of the VOB are given in Tab. 12. The non-sulphide zinc ore of the VOB reaches Zn concentrations of approximately 8.4 % Zn and 2 % Pb. The zinc concentration of the VOB- non-sulphide ore is neither significantly increased nor is the Zn/Pb ratio significantly changed with regard of the sulphide protore, in contrast to the MOB, where both mentioned effects are observable.

Tab. 12: Element concentrations of the VOB and MOB

Element	VOB NS [1] (low grade)	VOB NS [1] (high grade)	VOB[1] Sulphide ore	MOB NS red zinc ore	MOB NS white zinc ore
Zn %	2.8	8.4	7.2	30	40
Pb %	2.5	2	1.6	1.6	1
Cu %	0.11	0.03	0.16	<0.01%	<0.01%
Ag [ppm]	45.9	23	52	8	5
As [ppm]	112	305	269	11613	1985
Cd [ppm]	87	182	1634	307	480
Fe %	23	21	20	17.5	1.89
Mn [ppm]	4.6	7.6	3.9	0.07%	<0.01%
SiO_2 %	5	5	16.2	15	14

NS = non-sulphide ore, ([1]) Data : ITOK INTERNATIONAL, 2005

The occurrence of zinc within the sulphide zone of the VOB is generally similar to- and associated with that of lead, but concentrations are of a higher magnitude. In borehole no. 5308, zinc and lead concentrations increase generally from a depth of 450 to 256 m (Fig. 38) to a maximum of approximately 10000 ppm. The Zn-Pb content increases rapidly within the sulphide zone up to approximately 100000

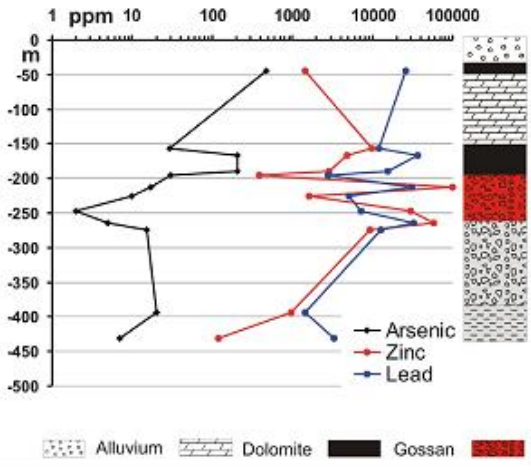

Fig. 38: Variation diagram of Zn, Pb, and As in drill core no. 5308. The reverse orientated changing of Zn-Pb concentration at 150-200 m marks the oxidised gossan zone.

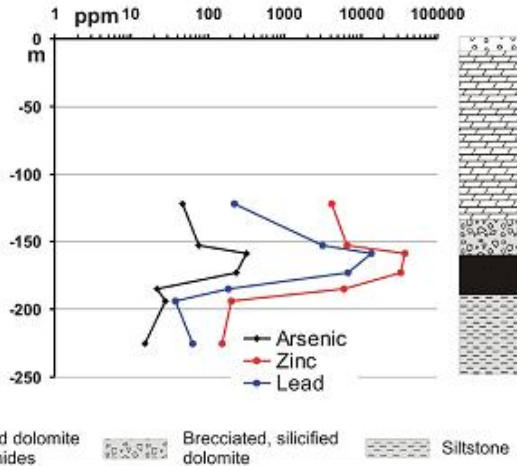

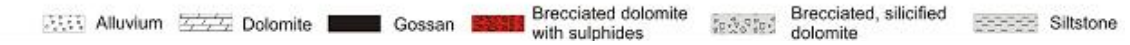

Fig. 39: Downhole variation of Zn, Pb, and As for drill core no. 5204. This core contains no sulphide ore. The increase of Lead and the moderate increasing Zinc marks the gossan zone.

ppm for zinc and 31000 ppm for lead. With the transition to the gossan zone, the similar trends stops and lead concentration increases much more than those of zinc do. Here, the graph can be interpreted as retention of (relatively immobile) lead and arsenic and a remobilisation or loss of (soluble) zinc. This is probably an effect of a diverse mobility of these elements during alteration processes and is well known for gossan zones in general (BOYLE, 1993).The most common zinc-bearing mineral within the sulphide zone is sphalerite, but in the non-sulphide, and gossan zone hemimorphite, smithsonite, and hydrozincite are the most common Zn-minerals. Lead occurs as

galena within the sulphide ore, and within cerussite, mimetite, and minor amounts of coronadite in non-sulphide ore.

The non-sulphide zinc ore overlays the sulphide ore (Fig. 38) and is mainly restricted to fault-zones (BRGM, 1994) or is well developed at these zones. The concentration of zinc within these oxidised zones is low compared to the equivalent ore type of the MOB. The non-sulphide ore of the VOB is predominately Fe-(Mn)-rich and shows no distinct tendencies of metal-separation and differentiation into a red zinc ore and a white zinc ore.

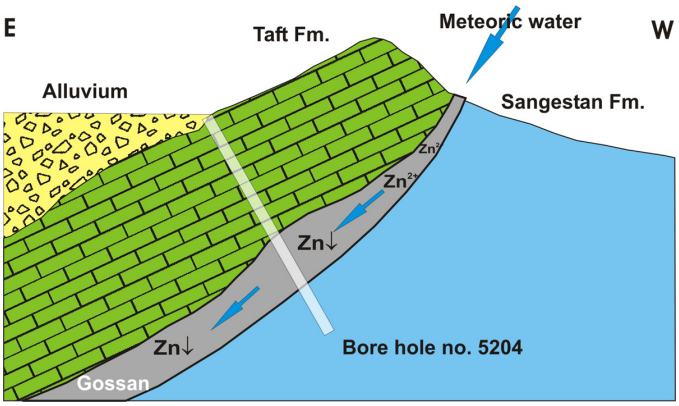

Fig. 40: Schematic cross section of drill core no. 5204 and its related strata. The meteoric water is guided along the oxidised, 'gossanous', and porous contact zone between the Taft Fm. and Sangestan Fm.. Zinc has probably been dissolved in the upper parts and (re-) precipitated in lower portions of the gossanous horizon.

The geochemical data of borehole no. 5204 show an unusual pattern (Fig. 39). Here, the concentration of zinc is consistently higher than the concentration of lead, despite the presence of a continuously oxidised zone without sulphide intercalations.

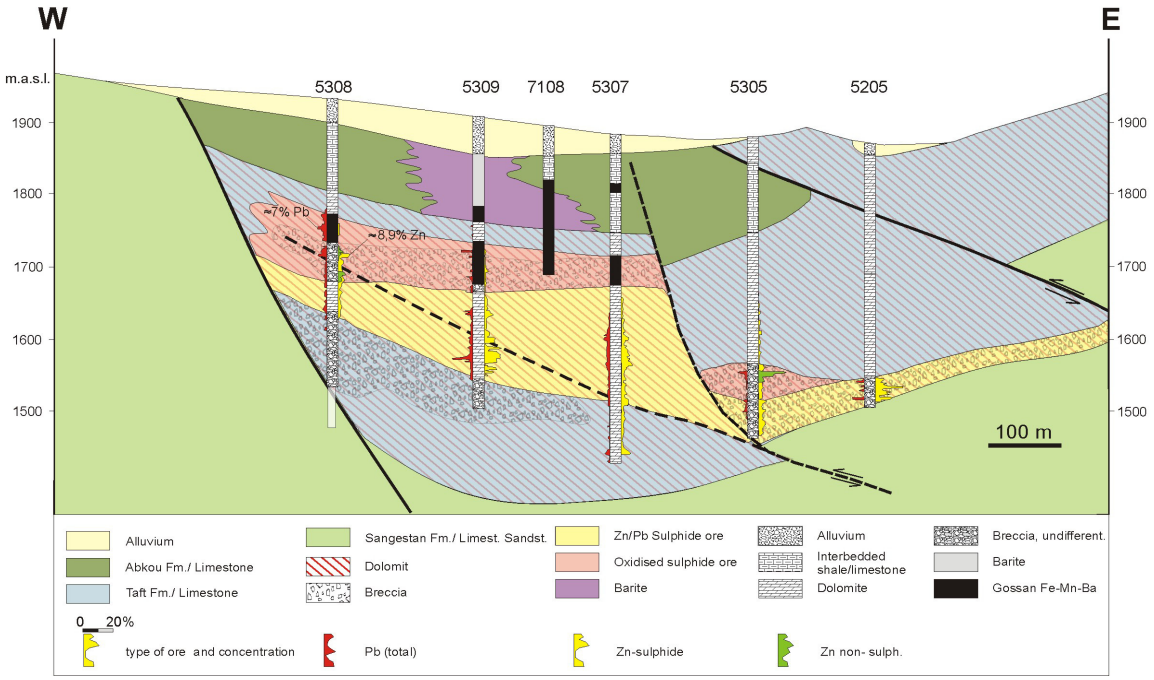

Fig. 41: Cross-section of the VOB. Boreholes and the Zn (sulphide and oxide) and Pb concentrations are plotted to illustrate the occurrence of the sulphide and non-sulphide ore types. The non-sulphide mineralised zone overlays the sulphide ore. The overall Zn-concentration of the non-sulphide zinc ore is limited to relatively low Zn-concentrations (2-8% Zn) compared with the MOB. (modified after BRGM, 1994)

This effect of increasing Zn concentrations and a lead-zinc ratio Zn/Pb>1 within the gossan can be explained by the geologic position of this bore hole (Fig. 40). The gossan is restricted to the contact between the Taft Formation And the subjacent Sangestan Formation. The gossan and the contact zone dip to the west. It can be assumed, that meteoric water migrated along this path through the porous gossan. Thus, it is proposed that the dissolved zinc has been transported from upper parts of the gossan to lower regions where it became re-precipitated. This supergene process leds to an enrichment of zinc within the lower parts of this gossan section and is probably an important factor for Zn-enrichment in similar regions of this deposit. The geochemical conditions of zinc mineral dissolution and precipitation in carbonate host rocks are described in detail in Chapter 5.4 (page 90).

The non-sulphide ore of the MOB shows no level-dependent systematic vertical trend in its Zn/Pb distribution. The ratio remains relatively constant at approximately Zn_{ox}/Pb_{ox}= 15-20 except for few extreme values. Under the assumption of a decreasing mobility of the metals Zn>>As>>Pb (BOYLE, 1993) and a Zn/Pb ratio of a supposed sulphide protore Zn_{sulph}/Pb_{sulph}=2, the non-sulphide ore of MOB must have been affected by an enrichment process for zinc, which has led to a contemporaneous decreasing concentration of Pb and Fe_2O_3 (Fig. 42). The result of this process is a non-sulphide ore with a wide range of Fe_2O_3, but small amounts of lead only. The Zn-rich zinc-rich cluster of Fig. 42 marks a non-sulphide ore, which is probably the result of Zn-mobilisation, displacement and reprecipitation, whereas iron remained as a relative immobile element.

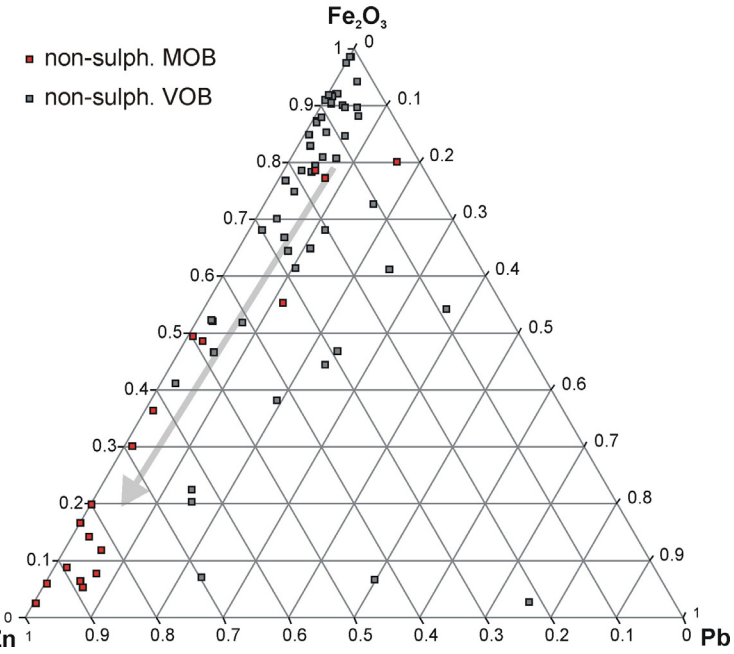

Fig. 42: Ternary Zn-Pb-Fe_2O_3 plot of non-sulphide ore samples of the MOB and VOB of Mehdi Abad. The non-sulphide ore is characterised by a wide range of Fe_2O_3 with a remarkable cluster of high-Zn and low Fe/Pb samples that represent the white zinc ore. The samples of the VOB do not show such a distinct differentiation.

Copper

The copper concentration in the examined drill core samples of sulphide ore is much higher than in non-sulphide ore samples of the MOB. The concentrations within the non-sulphide ore of the MOB range up to 200 ppm. These values are very low, compared to the gossanous zone of the VOB, which shows Cu concentrations up to 2.000 ppm. In contrast to the low Cu content of non-sulphide MOB ore, the examined drill core of sulphide ore contains up to 2400 ppm Copper. The copper

within the sulphide zinc ore is commonly related to chalcopyrite and the carbonate mineral malachite, whereas copper of the gossan zone seems to be bound to malachite.

Occurrence of silver in the sulphide ore of MOB

The sulphide ore of the Valley Ore Body (VOB) of Mehdi Abad shows silver concentrations up to 350 ppm. In contrast to these relatively high concentrations, the non-sulphide ore of both the VOB as well as the non-sulphide ore of the Mountain Ore Body (MOB) show only minor or background concentrations of silver. The occurrence of silver is intimately associated with the sulphide ore of the VOB, whereas the non-sulphide zone of the VOB only shows small concentrations related to the sulphide ore (approximately 10 ppm Ag). Since no specific silver bearing minerals was detectable, the purpose of the actual study was to investigate the geochemistry and the mineralogy of this silver.

Silver is common in a wide range of concentrations in different types of massive-sulphide deposits, such as MVT-, SHMS-, Irish-type and others. In these deposits, Ag occurs as Ag-bearing minerals or is predominantly associated and incorporated in sphalerite, marcasite, pyrite, and/or galena (HANGI & PAARLBERG,1996; MATTHES, 1996).

The analyses of sulphide ore samples of the VOB show a moderate positive correlation of the silver concentrations with lead (galena) (Fig. 44).

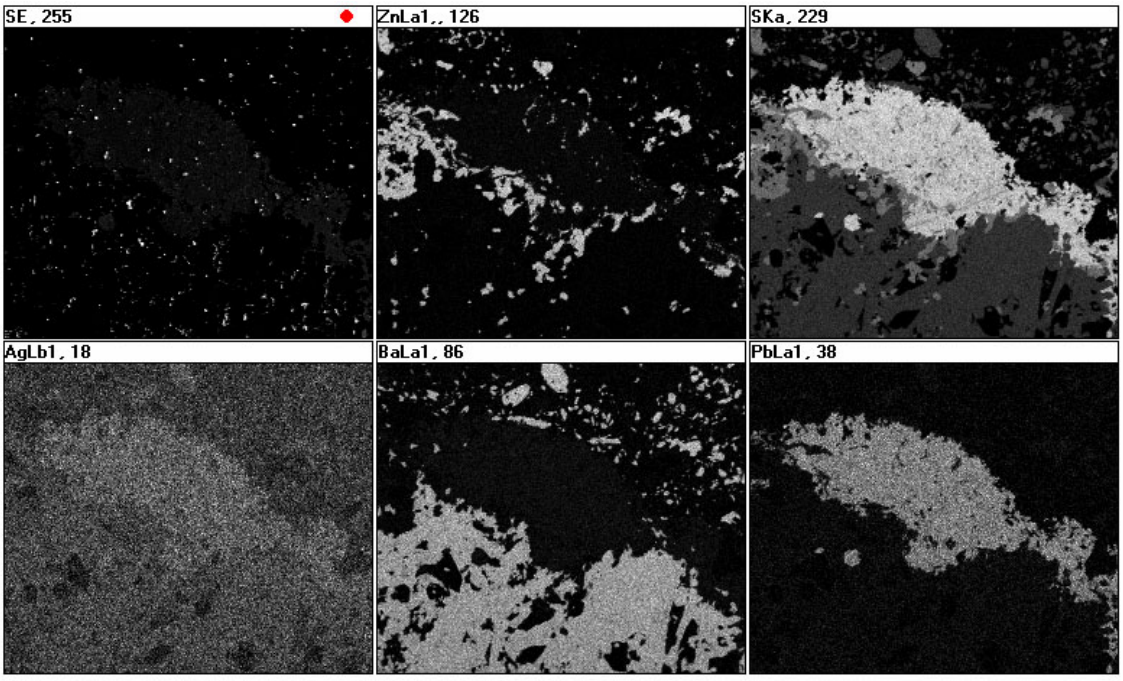

Fig. 43: SEM-EDX element distribution maps of sample 5308-226. Bright areas indicate the presence of a specific element. The low Ag concentration results in a higher background noise within the Ag-element distribution map. However, silver is associated with the occurrence of lead, indicated by light colours within the galena.

The diagrams, which are shown in Fig. 44, Fig. 45, and Fig. 46 indicate a binding of silver to both Pb (galena) as well as Sb and not to As. but the detailed interelement correlation plots (Fig. 4 & 5) show only for Sb a good correlation. Arsenic correlates nor or probably within a small range with silver and is highly variable. Based on these results one can assume that silver is probably bound to a Sb (and As ??) bearing mineral, such as argentian tetrahedrite ($(Cu,Fe,Ag,Zn)_{12}Sb_4S_{13}$ and/or freibergite $(Ag,Cu,\ Fe)_{12}(Sb,As)_4S_{13}$. Freibergite forms a series with tetrahedrite $(Cu,Fe,Ag,Zn)_{12}Sb_4S_{13}$ with a variable Sb/As ratio. This could be one reason for the highly variable Ag/As ratio within the sulphide ore. Most of these Ag-Sb-(As) minerals probably occur within galena as µm-sized inclusions within the galena (ZENG ET AL., 2000). This explains the visible correlation of Ag with Pb in Fig. 44.

An association of silver and silver bearing minerals with sphalerite and/or pyrite could not detected by using SEM-EDX and as a positive correlation in a Zn-Ag diagram.

The silver grade of the VOB ranges from 330 ppm (borehole 5308) down to approximately 30 ppm in several other boreholes. This value is highly dependent from the galena content of the sulphide ore. However, BRGM investigations (MONTHEL, 1994) have shown up to 300 ppm Ag for the western and central part of the VOB and up to 92 ppm for the eastern part.

Fig. 44

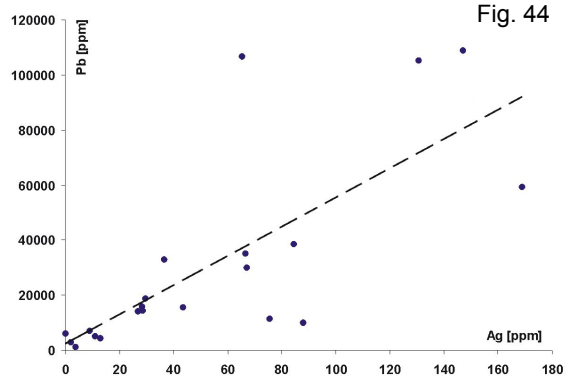

Fig. 45

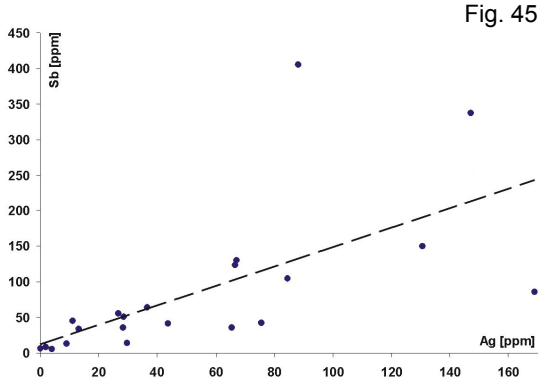

Fig. 44: Ag-Pb variation diagram for the sulphide ore of the VOB. Silver is associated with the occurrence of lead/galena within the sulphide ore and shows a moderate correlation.

Fig. 45: Ag-Sb variation diagram for the sulphide ore of the VOB. Silver shows a moderate correlation to Sb, which is probably due to a Sb-Ab bearing mineral.

Fig. 46: Ag-As variation diagram for the sulphide ore of the VOB. Silver shows no correlation of Sb related to Ag within the range from 0 to 180 ppm Ag.

Fig. 46

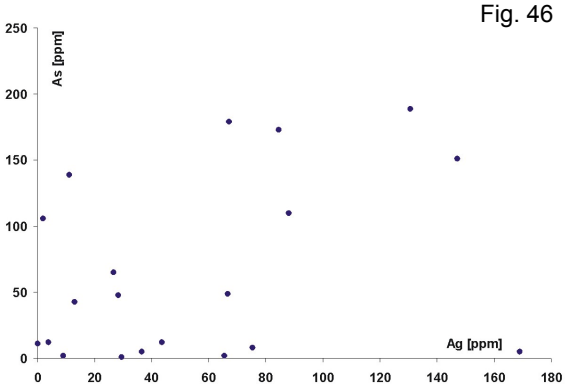

TiO_2, Al_2O_3, and Zr in the Valley and Mountain Ore Body

Regardless to their origin, all samples show nearly the same Ti/Al ratio (Fig. 48). This constant ratio applies to both samples of the MOB as well as samples of the sulphide- and the oxide-zone of the VOB.

Zr correlates with both Ti and Al (Fig.47). All element pairs of Zr, Al, and Ti show a positive significant interelement correlation within the sulphide as well as the non-sulphide zone of VOB and MOB. The interelement correlation is probably the result of the occurrence of a Zr-Al-Ti bearing mineral. These elements are characteristically present in detrital aluminosilicate minerals, such as clays (PETER & GOODFELLOW, 1996), which could be a component of the siliciclastic sediments, carbonates, and limestones of Taft- and Abkou Formation. There is no correlation with SiO_2, which is probably the effect of multiple sources of SiO_2 within the limestone, dolomite, siliciclastics, and the Zn-Pb ore such as quartz grains, chert, zinc-silicates (hemimorphite) and other minerals.

Since Ti, Al, and Zr are highly immobile elements in most alteration zones (MACLEAN & BARRET, 1993; JUN ET AL., 1996), these elements could be residuals of a Ti-Al-Zr mineral. The Ti/Al/Zr ratio remained constant during and after the alteration of this precursor mineral, which is due to the immobility of these elements.

Fig.47: The inter-element correlation between Zr and Al_2O_3 is similar to the TiO_2 - Al_2O_3 diagram. The concentrations of nearly each specimen from both the VOB (blue dots) and MOB (red triangle) show a significant positive correlation. This probably reflects the clastic component in the chemical sediments (limestone).

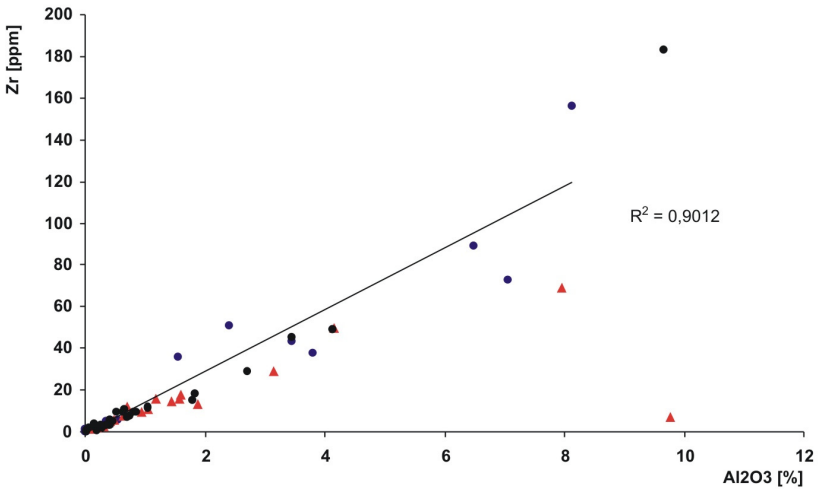

Fig. 48: The concentration of TiO_2 and Al_2O_3 show a highly significant correlation. All samples from the MOB as well as the VOB show nearly the same Ti/Al ratio. This is probably due to the occurrence of a Ti-Al bearing mineral or it is a relict pattern of a former Ti-Al bearing mineral. (blue=VOB, red=MOB)

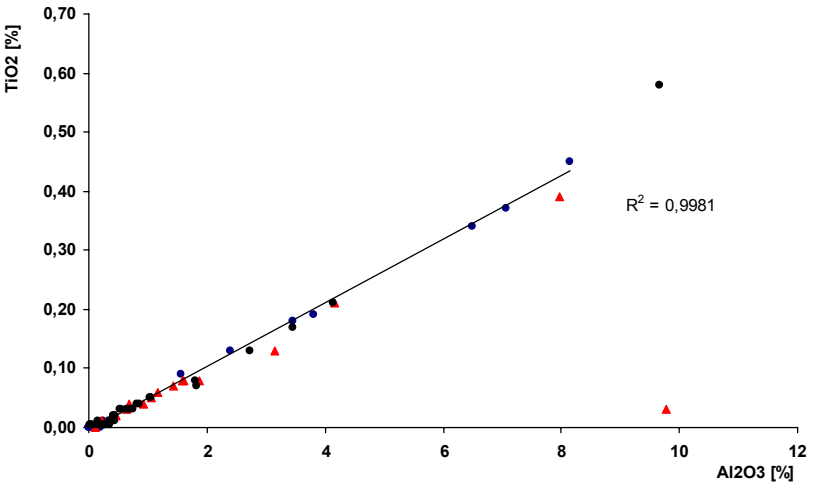

Thallium content in VOB and MOB

Thallium occurs within different types of Zn-Pb deposits as a trace element and is commonly associated with sphalerite (LEACH ET AL. 1986), pyrite, marcasite, and other sulphides (DUCHESNE ET AL., 1983), of hydrothermal mineralisation. The thallium concentration of the Mehdi Abad deposit varies on a wide range (Tab. 13). The highest concentration can be found within the non-sulphide ore body of the MOB. Here the concentration of Tl reaches up to 348 ppm whereas the concentration of Tl within the non-sulphide ore of the VOB shows values of about 1 ppm (Tab. 13). Thallium seems not to be associated with zinc or Iron – but is probably linked with As. As DOMÈNECH et al. (2002) has shown Tl is probably also associated with galena, which indicates its inclusion as trace element into the mineral galena.

Tab. 13: As and Tl mean values and their standard deviation for different ore types of Mehdi Abad.

Ore-Type and Location	As [ppm]	As stand.dev.	Tl [ppm]	Tl stand.dev.	n
VOB: sulphide ore	176	408	2.6	3	15
VOB: non-sulphide ore	145.9	153.9	5.0	6.6	8
MOB: red ore	11623.7	11042.6	105.9	125.1	7
MOB: white ore	2034.4	2576.1	37.9	16.3	9

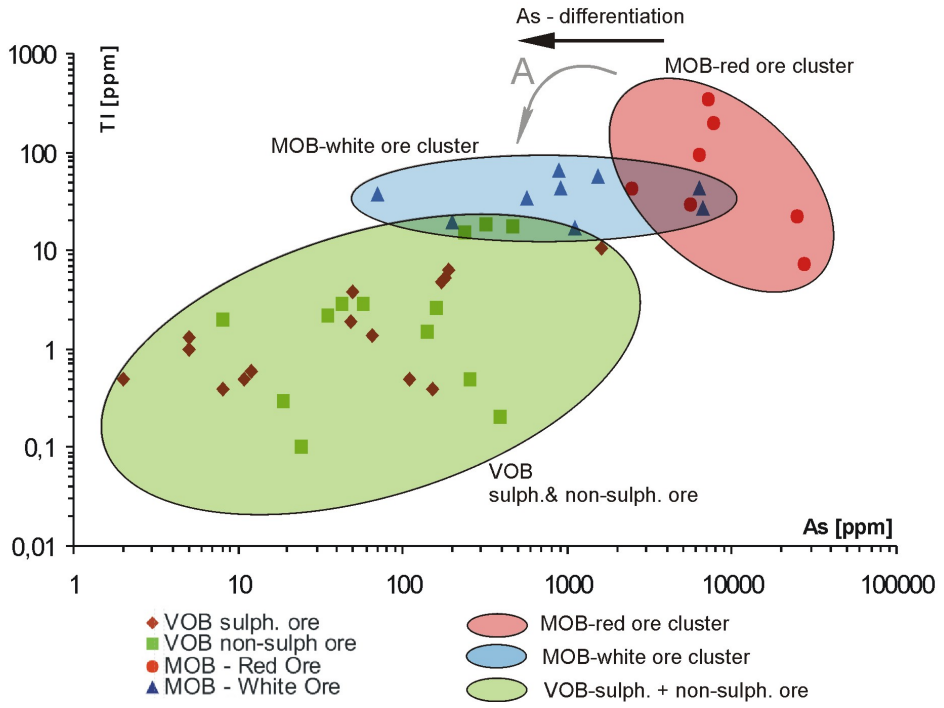

Fig. 49: Thallium concentrations of the non-sulphide zone of the MOB and sulphide- and non-sulphide ore of the VOB. Both ore bodies are highly distinguishable by their Tl and As concentrations, which form three clusters. The Tl and As concentrations of the MOB are approximately 80 times higher than the concentrations of the VOB. The As-(Tl-) concentrations of the white ore of the MOB are low with regard to the red zinc ore. In contrast to that, the non-sulph. ore and the sulphide ore of the VOB show no differentiation in As and Tl.

The samples of the MOB and the VOB plot at least within three different clusters (Fig. 49). These three clusters are due to by highly different Tl- and As-Sb-Cd concentrations within these two non-sulphide ore bodies. To explain this effect one can assume three different models:

(i) The source of both Tl and As of these non-sulphide ore-bodies was a sulphide protore, which was formed during **one** mineralising event for both the protore of the VOB as well as the protore of the MOB. During the oxidation of the sulphide ore As and the Tl remained as immobile elements within the MOB and have been concentrated during the process of carbonate dissolution and sulphide oxidation. However, calculations of this process, which are based on values of Tab. 13 give a factor for the As-accumulation of approximately 26 and the factor for the Tl enrichment is about 19. These rates are obviously to high to be realistic and they are in contrast with investigation of the As- and Tl concentrations of the oxide-zone of the VOB. Here, calculations have shown that there is no obvious enrichment in these elements (Fig. 49). Due to this fact, a highly immobile behaviour of As- and Tl during the oxidation of the protore of the MOB is improbable.

(ii) Both ore bodies, the MOB and the VOB are the result of at least **two** different mineralising events. These events were associated with different As and Tl concentrations.

(iii) Both ore-bodies are the result of one mineralising event, but the MOB was influenced by an earlier or later stage hydrothermal As- and Tl-delivering event.

Further investigations have to focus the source and the mechanisms, which are responsible for the different As and Tl concentrations of the MOB and the VOB.

REE elements

All REE data of the ore samples have been normalised to chondrite composition (data source: TAYLOR & MCLENNAN, 1985) except the data of the carbonate host rock, which is normalised to NASC (data source: HASKIN ET AL., 1968). The chondrite-normalisation for both non-sulphide and sulphide mineralised samples has been chosen to make these graphs comparable with other authors, which mostly use chondrite normalised data to describe sulphide mineralised samples (MVT, SHMS, VMS, and other styles of mineralisation). A normalisation of the REE data by using a $CaCO_3$ reference (e.g. a marble) would be possible, but is only useful for a regional comparison of the samples among themselves.

The REEs are relatively immobile during weathering, low-grade metamorphism, and hydrothermal alteration (ROLLINSON, 1993) and offer a good possibility for comparing and analysing the host rock and its mineralisation, which has been partly affected by intensive and extensive alteration processes. Sample analyses, which show REE values under the detection limit, have been estimated by using the method of half detection limit (HAAS & SCHEFF, 1990). All values below detection limit are assigned a value of the detection limit divided by 2. This procedure becomes necessary for some purposes, such as calculation of Eu/Eu* anomalies. Only two samples of an unaltered dolomitic host rock of MOB has been analysed yet. Because of this reason, these data will represent the unaltered and unmineralised carbonate host rock of both the sulphide ore of VOB and the non-sulphide ore of MOB. The criterion, which is used for a classification, as an unaltered host rock, is self-determined. The criteria for the classification as an unaltered and unmineralised carbonate

host rock are (i) a distance of at least 5 meters to ore-bearing rocks, (ii) a widely spaced fracture pattern and thus a minimised influence of alteration/meteoric fluids, and (iii) an apparent local background of Pb-Zn, Pb, and Fe. Four samples have been chosen to represent the limestone host rock (Fig. 50). The REE patterns of these specimen show roughly parallel trends with an erratic change of element concentrations. Elevated light REEs (LREE) relative to lower heavy REEs (HREE) can be recognised. Both specimen show a Eu/Eu* ratio, which ranges from 0.95 to 2.47. The Eu/Eu* anomaly is calculated by using the formula F 2 (McLennan,1989):

$$Eu/Eu^* = Eu_N \Big/ \sqrt{Sm_N * Gd_N} \qquad \text{F 2}$$

(*N = normalised*)

REE patterns of samples from the VOB

The REE pattern of the VOB sulphide ore (Fig. 51) shows higher REE concentrations, in relation to the unmineralised carbonate host rock (Fig. 50). The trend of lower HREEs is visible within most sulphide ore samples. The LREE contents are highly variable within the sulphide ore and La/Lu ranges from 84.2 to 19.7. A significant negative Ce/Ce* anomaly is not visible. Most of the sulphide ore samples show a strong positive Eu/Eu* anomaly.

The REE pattern of all examined oxide zone samples of the VOB are similar to patterns from the VOB sulphide ore (Fig. 52). Most gossan samples of the boreholes show a positive Eu/Eu* anomaly. The less mineralised samples of the sulphide and gossan zone of the boreholes show a characteristic high values of LREEs, and relatively constant and low values within the HREE range, witch effects an nearly x-axis parallel graph (Fig. 50). The sulphide ore samples show a distinctive positive Dy/Dy* anomaly (Fig. 51) which ranges from 1 to 5.3. This anomaly seems to be limited to the sulphide ore-bearing strata. The non-sulphide ore as well as the dolomite and the limestone as well seems to be not affected by a Dy/Dy* anomaly.

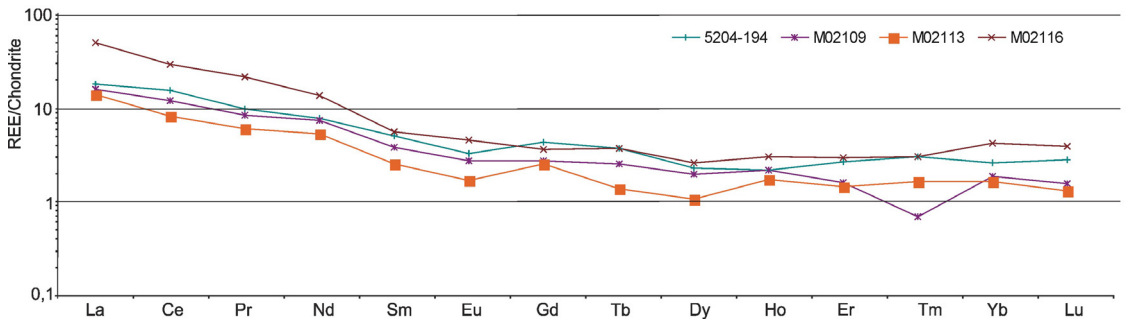

Fig. 50: Chondrite-normalised REE pattern of undolomitised limestone of Mehdi Abad.

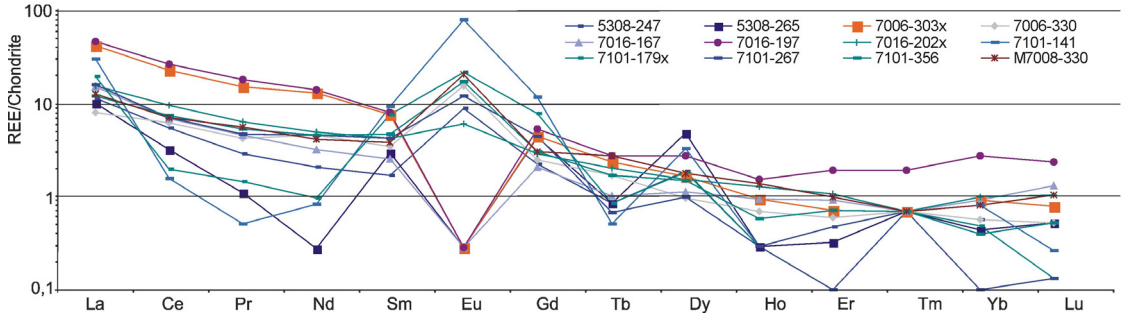

Fig. 51: Chondrite-normalised REE patterns for sulphide-rich dolomites of the VOB with [Zn]>2%, [Fe_2O_3]>10%. Most of these dolomites show a distinct Eu/Eu* anomaly.

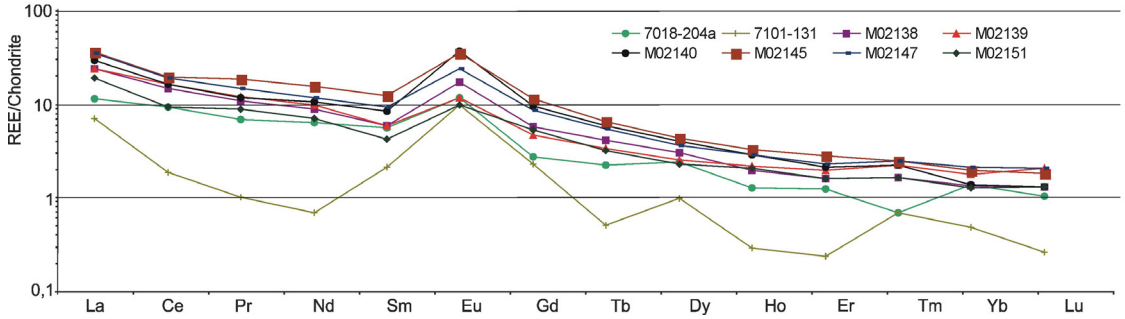

Fig. 52: Chondrite-normalised REE pattern of samples from the oxidised zone of the VOB with [Zn]>3%, [Fe_2O_3]>6%. All samples show high Fe concentrations and thus, belong to the class of the 'red zinc ore'. A well developed positive Eu/Eu* anomaly is visible in all samples of the oxidised zone.

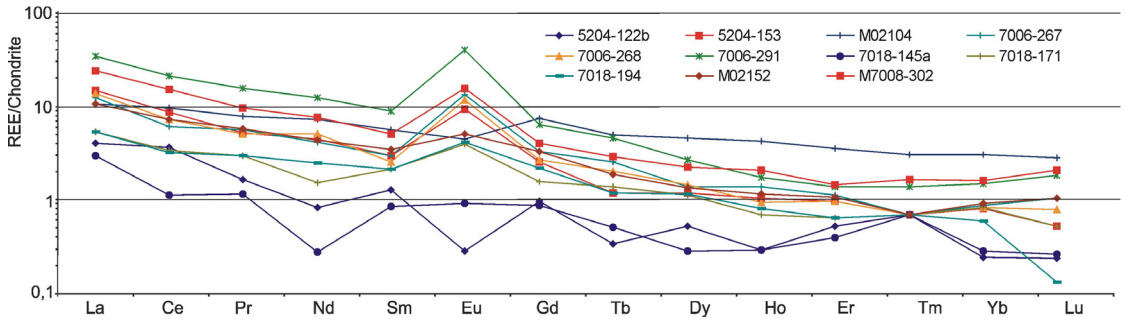

Fig. 53: Chondrite-normalised REE pattern of dolomites of the VOB. Most of the samples show a characteristic positive Eu/Eu* anomaly and are high in LREEs, whereas HREEs decreasing.

REE pattern of non-sulphide ore from MOB

In contrast to the oxidised zones of the examined drill cores from the VOB, the specimen of the non-sulphide ore of MOB can be divided into two specific types. These types are based on their concentration of Fe_2O_3, and Zn. The main non-sulphide ore-types are (i) an ore with high concentration of Fe_2O_3 (>10%) and Zn (red zinc ore) and (ii) an ore, low in Fe_2O_3 (<7%) and high in zinc, the white zinc ore. Both types of non-sulphide ore show completely different REE patterns (Fig. 54 and Fig. 55). The REE patterns of the red zinc ore of the MOB are comparable to the oxidised zone overlying the main sulphide ore body of the VOB. The samples show the characteristic high contents in LREEs with lower HREEs (Fig. 54), but no distinct Eu/Eu* anomaly. Except one sample, the La/Lu ratio shows high values, which ranges from 3.6 to 11.8 (mean=8.4, n=7).

The samples of the white zinc ore show relatively low values of LREEs and HREEs with regard to the red zinc ore samples. The values vary around 12 for the LREEs and 1.2 for the HREEs. The La/Lu ratio ranges from 0.8 to 40 (mean=10, n=9). Another marked feature is a significant Eu/Eu*anomaly (mean =0.55). The typical and good determinable positive Dy/Dy* anomaly that is detectable at the sulphide ore and in the overlying oxidised zone of the VOB, is missing here. (Dy/Dy* mean=1.02, n=9).

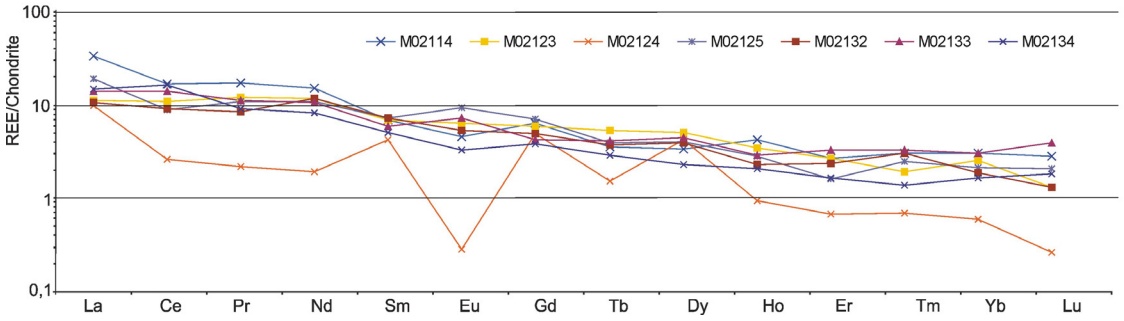

Fig. 54: Chondrite-normalised REE pattern of high-Fe non-sulphide ore samples from MOB. (These samples are characterised by Fe_2O_3 > 10% and Zn > 5000 ppm values). All samples show a characteristic decreasing value toward the HREEs.

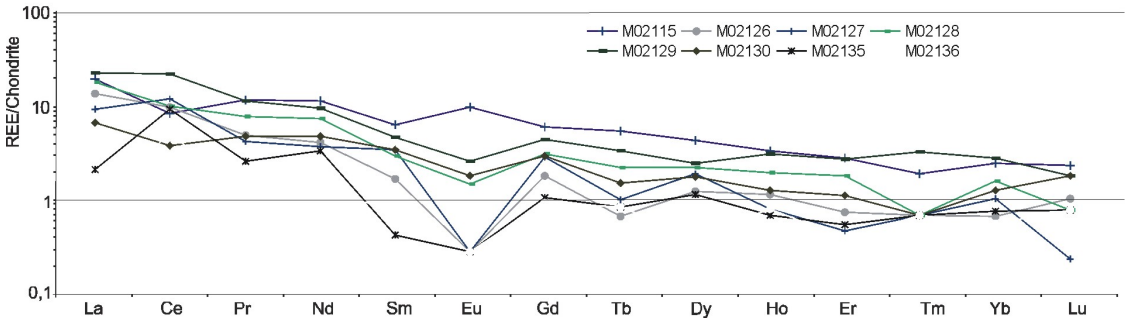

Fig. 55: Chondrite-normalised REE patterns of the white zinc ore from MOB. (The plotted samples are Fe-poor with Fe_2O_3<7% and zinc-rich with Zn values >50000 ppm). The graphs show an x-axis parallel pattern and, referred to the Fe-rich ore, low REE values.

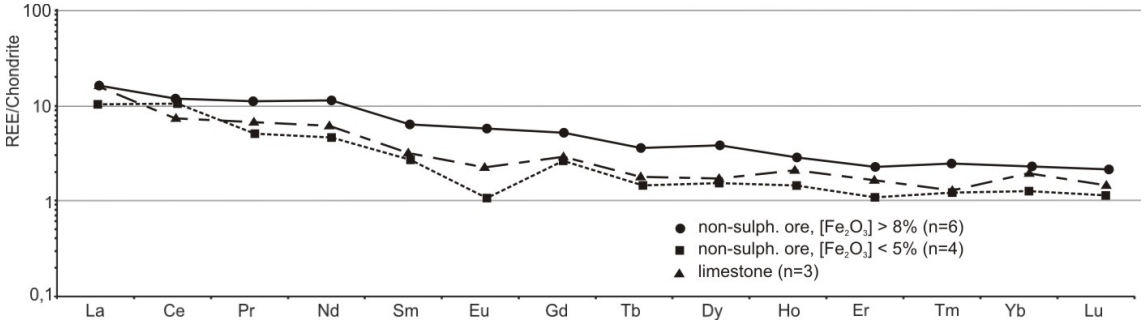

Fig. 56: Chondrite-normalised REE patterns of low-Fe non-sulphide ore samples from MOB. (The plotted samples are Fe-poor with Fe_2O_3<4% and zinc-rich with Zn values >100000 ppm). The graphs show an x-axis parallel pattern and, referred to the Fe-rich ore, low REE values.

Discussion and interpretation of the REE patterns

The limestone, dolomite and the sulphide ore show a distinct enrichment in light REE when normalised against chondrite. This pattern is typical for marine chemical sediments and platform carbonates (MAZUMDAR ET AL., 2003). The dolomitisation process should not necessarily influence the REE composition of the precursor limestone and the pattern of the limestone should be visible at the dolomites after the dolomitisation process (MIURA & KAWABE, 2000; QUING & MOUNTJOY, 1994). Thus, it is probable that the similar REE pattern especially the enrichment of the LREE and the decreasing values towards to the HREEs is due to the original limestone.

However, at least one process, the dolomitisation process or the ore mineralising event should be accompanied with the generation of the distinct positive Eu/Eu* anomaly. Most samples of the sulphide ore, of the oxidised zone overlying the sulphides, and of the dolomite samples of VOB show this marked Eu/Eu* anomaly and has its highest peaks within the sulphide ore, but also with significantly positive values in oxide zones and dolomite of the VOV. The MOB in contrast does not show such a Eu/Eu* anomaly. Here, most samples show a slightly negative Eu/Eu* anomaly, which is also common in marine carbonates (MAZUMDAR ET AL., 2003).

A possible explanation for the characteristic REE fractionation pattern, reflected by relatively high La/Lu ratios, is the preferential removal of LREEs from the fluid by carbonates, due to a replacement of Ca within the crystal structure of the carbonate (DAVIES ET AL., 1998). Accordingly, carbonate minerals should be more enriched in LREEs than in HREEs and $La/Lu_{carbonate} > La/Lu_{fluid}$ (DAVIES ET AL., 1997). Hydrothermal fluids are enriched in LREEs and show a low content of HREEs (PARR, 1992). These fluids could increase La/Lu by regional mixing with seawater. Because of this reason, hydrothermal fluids are another important factor for the La/Lu ratio of seawater, which could influence the REE pattern toward to high HREEs and decreasing LREEs of the carbonates.

A positive Eu/Eu* anomaly can be due to an enrichment of Eu^{2+} related to Eu^{3+} (PARR, 1992). The stability of Eu^{2+} and Eu^{3+} is dependent on the pH and Eh. An anomalously high concentration of total Eu in chondrite-normalised samples may reflect hydrothermal fluid temperatures of above 250 °C and reducing hydrothermal conditions (PARR, 1992). Additional to the high La/Lu ratio, the marked positive Eu anomaly in both Zn-Pb sulphide and non-sulphide ore of the VOB supports the thesis of a hydrothermal (T>250 °C, and reducing conditions) genesis of the sulphide ore (PARR, 1992). One possible explanation for the wide-ranging Eu/Eu* anomaly could be changes in proximity to an active hydrothermal vent.

However, the Eu/Eu* ratio within the sulphide ore and the oxide zone of the VOB is an indication of a hydrothermal signature. The lacking Eu/Eu* annomalie at the MOB might document an vent-distal position during the ore mineralising event. Another explanation could be the influence of two separate ore delivering events.

The observed phenomenon of relatively low LREE and HREE values of the white zinc ore of the MOB related to the red zinc ore and the carbonate host rock of MOB (Fig. 56) is probably a result of zinc mobilising, transport and reprecipitation. REE are immobile for most types of weathering and alteration processes (ROLLINSON, 1993) and remain in the original rock and the oxidation zone from where the zinc has been remobilised or dissolved. Thus, the high REE values of the red zinc ore are an effect of REE-enrichment within the oxidation zone (red zinc ore) due to carbonate dissolution and zinc mobilisation. The migrating Zn-rich fluids are poor in REEs and thus the resulting

white zinc ore shows lower REE values compared with the barren host rock.

Barium and strontium

Barium is an abundant element in both the samples of drill cores and specimen of MOB. Barite is the chief host of barium in non-sulphide ore of MOB as well as sulphide and oxide zones of VOB. The highest concentration of barium occurs within the sulphide ore, but elevated values occur also within oxidised zones of the main sulphide ore body as well as the non-sulphide ore of MOB. The bivariate plot of Barium versus Strontium correlates positively over a wide range (Fig. 57). This is due to the Sr-compatibility in the barite crystal lattice. It appears that the Zn-Pb mineralisation is at least regional associated with high concentrations of barite, which is characterised by high contents of strontium. The sample of a felsic intrusive body shows also high Ba and Sr concentrations. The Ba/Sr ratio is similar to the samples of the Mehdi Abad ore. This fact supports the thesis of a hydrothermal overprint derived from the emplacement of a felsic magmatic rock. A second possible explanation might be a separate event, which has delivered barite to both the felsite and Mehdi Abad.

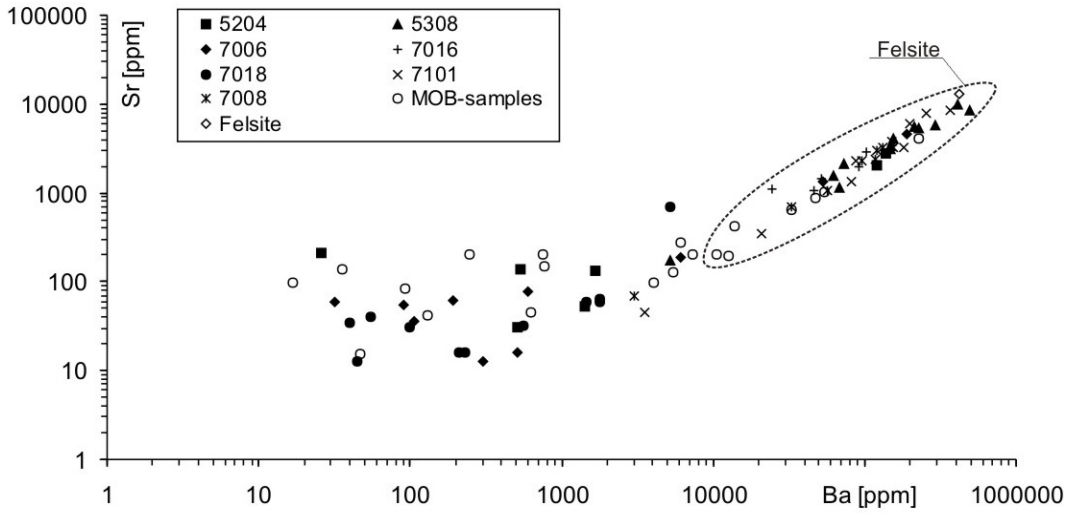

Fig. 57: Bivariate plot of Barium versus Strontium of all samples (numbers indicate different bore holes, which has been sampled, all other specimen are grab samples). Both calamine specimen as well as drill core samples correlate over a wide range, which is characterised by high Ba and Sr concentrations. A poorly correlated field of samples can be assumed for low concentrations of Sr (10 to 300 ppm), and even lower concentrations of Ba (15 to 2000 ppm). The sample of a felsic intrusion plots perfect in the linear trend.

Mass balance calculations

A mass balance calculation can give an estimation either if the non-sulphide ore of VOB was formed by oxidation processes of a sulphide ore without additional Zn sources, or if an additional Zn-source was necessary. The model, which has been developed for the oxidation process of the

sulphide protor comprises several chemical assumptions as follow:

- The oxidation of the sulphide protor of MOB is due to the influx of oxygen, which acts as an electron donator. Iron and sulphur are electron acceptors and were oxidised.
- Other components that exclusively delivered to the sulphide ore were H_2O and CO_2.
- The sulphide ore system looses calcium, sulphur, and carbonate, which is due to solution processes.
- The mass-balance calculation comprises for quantitative results the elements Ca, Pb, Zn, Fe, Ba, C, O, and S, but ignores elements that occur in traces.

The LREE's La and Ce has been used for an estimation of the mass-loss factor of the non-sulphide ore. Both elements are immobile within a wide range of geochemical conditions (CHRISTIDIS, 1998, MIDDELBURG ET AL. (1988), CRAMER & NESBITT, 1983, FEDO ET AL. (1995)).

The applicability of the system La – Ce is given if the ratio between these phases is constant and not affected by dissolution and/or weathering effects. The La – Ce ratio of relevant samples (sulphide ore and non-sulphide ore) of Mehdi Abad VOB are plotted in Fig. 58 to prove this assumption. The graph shows a linear correlation between the sample data regardless of their origin within the ore body. The La-Ce system agrees with the required stability and will be used here as reference for further calculations.

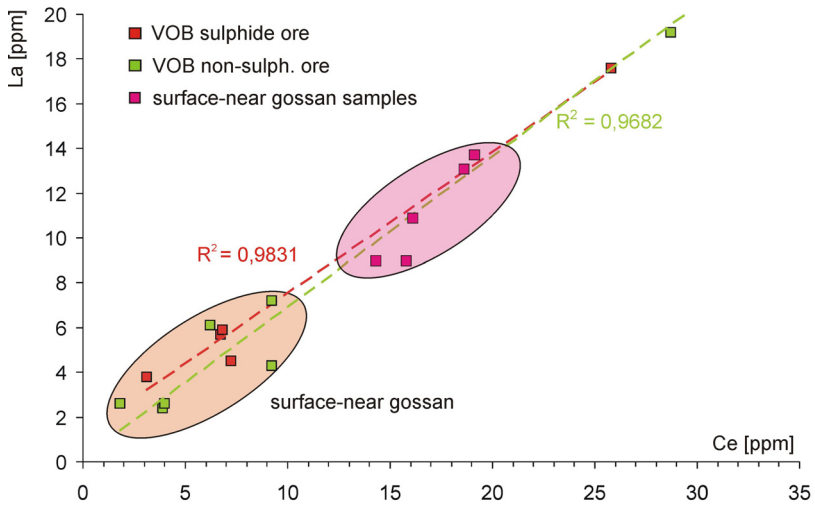

Fig. 58: La-Ce plot of both sulphide and non-sulphide ore samples of Mehdi Abad VOB. The red marked cluster represents samples from both high-grade sulphide ore (app. 8 % Zn) and igh-grade non-sulph. ore according to Tab. 12. The magenta coloured cluster is build by surface-near and surface gossan samples. All data show a linear correlating trends with R^2=0.97 and R^2=0.94. Both interpolated graphs overlaying each other with low variation only. Thus, no effect of selective mobility of either La or Ce can be estimated.

The here used method describes the non-sulphide ore of the MOB as a restit of the sulphide protor. This restit was formed by dissolution and oxidation processes, which include element influx and escape. However, immobile elements such as La or Ce remain in the restit and were not additionally supplied to this system. Therefore, the enrichment of La-Ce within the 'restit' should be inversely proportional to its mass reduction respectively directly proportional to the difference of the protor-mass and 'restit'-mass. This factor is necessary for further mass balance calculations.

The surface and surface-near gossanised samples plot into separate cluster. Here, the alteration process was associated with a significant mass loss. The mass-loss factor f_{ml} has been determined by using the graph of Fig. 58. The quotient $Ce_{nonsulph} / Ce_{sulp}$ results in f_{ml} = 2.8, whereas the La values gives an value of f_{ml} = 2.3. Thus, the average mass-loss factor can be estimated as f_{ml} = 2.5.

The data of the sulphide and non-sulphide ore overlying each other and form a single cluster at the La-Ce diagram (Fig. 58). Thus, the usage of the La-Ce data of both the sulphide and non-sulphide ore of the VOB is not appropriate to calculate a specific mass loss factor, but hints to an f_{ml} that is near 1. An mass loss factor around 1 would suggests that the non-sulphide zinc ore of the VOB is the result of an in-situ oxidation of the protore and the non-sulphide zinc ore as been presumably formed without an additional Zn-source. This hypothesis is supported by similar metal concentrations of both ore-types; especially the high-grade non-sulphide ore and the sulphide ore show similar values of Zn, Pb, and Fe concentrations.

4.2 The non-sulphide Zn-Pb Kolahdarvazeh deposit at the Irankuh district

The Irankuh district comprises several zinc-lead deposits. They are located in the Irankuh Mountain Range, 20 km south of Esfahan (Fig. 4) in West-Central Iran. The elevation of the mines is approximately 1700 m. Similar to Mehdi Abad, this region is influenced by a hyper-arid climate with a low-levelled rainfall and high temperatures. There is virtually no vegetation within this area.

The Irankuh district comprises several Zn-Pb deposits: the Goushfil pit (sulphide ore), the Kolahdarvazeh pit (non-sulphide ore), the small Tappeh-Sorkh pit, and some others. The UTM coordinates of the Goushfil pit are 40R 558444; 3598117 and the coordinates of the Kolahdarvazeh pit are: 40R 559169; 3597867.

The summarised ore reserve of these mines is estimated at approximately 10 million tonnes with 7.5% zinc and 2.4% lead (Tab. 14). The $\frac{Zn}{(Zn+Pb)}$ ratio is relatively high with an average of approximately 0.76 (GHAZBAN ET AL., 1994). The Mines within this district produce both a sulphide concentrate as well as an oxide concentrate.

The main difference between the Goushfil- and the Kolahdarvazeh pit is the chemistry of their ores. The ore of the Goushfil pit is characterised by high amounts of sulphide ore and a minor amount of non-sulphide zinc ore only. The Kolahdarvazeh mine is an open pit mine, which produces a concentrate of non-sulphide zinc ore and shows only small amounts of sulphides.

The origin of the ore has been discussed by several authors. ZAHEDI (1976) attributed the dolomitisation and mineralisation of the Esfahan area to the Alpine orogeny. However, the first study attributed to the Irankuh district deposits itself was written by RASTAD ET AL. (1980) and RASTAD, E. (1981). These studies consider that the ore mineralisation is a part of a Crateceous transgressive series and interpret the ore emplacement as sedimentary and diagenetic. More recent isotope based examinations on the sulphides of RASTAD ET AL. (1980) suggest an epigenetic model for the Irankuh deposit. Their model is supported by regional geological observation, such as the discordant nature of the sulphide ore and its emplacement along the Iran-Kuh Fault as well as by isotopic data.

The **Goushfil pit** (Fig. 59) is the most important Zn-Pb deposit within this area, which produces a sulphide concentrate. Beside the mined sulphide ore, they have approximately two million tons of tailings with a low-grade non-sulphide ore. This ore contains approximately 8 % Zn hosted in dolomite rocks. However, the non-sulphide ore of the Goushfil pit is not utilisable for the solvent extraction process, since the concentration of zinc is too low for the acid leaching process that is used for the extraction of zinc from the ore.

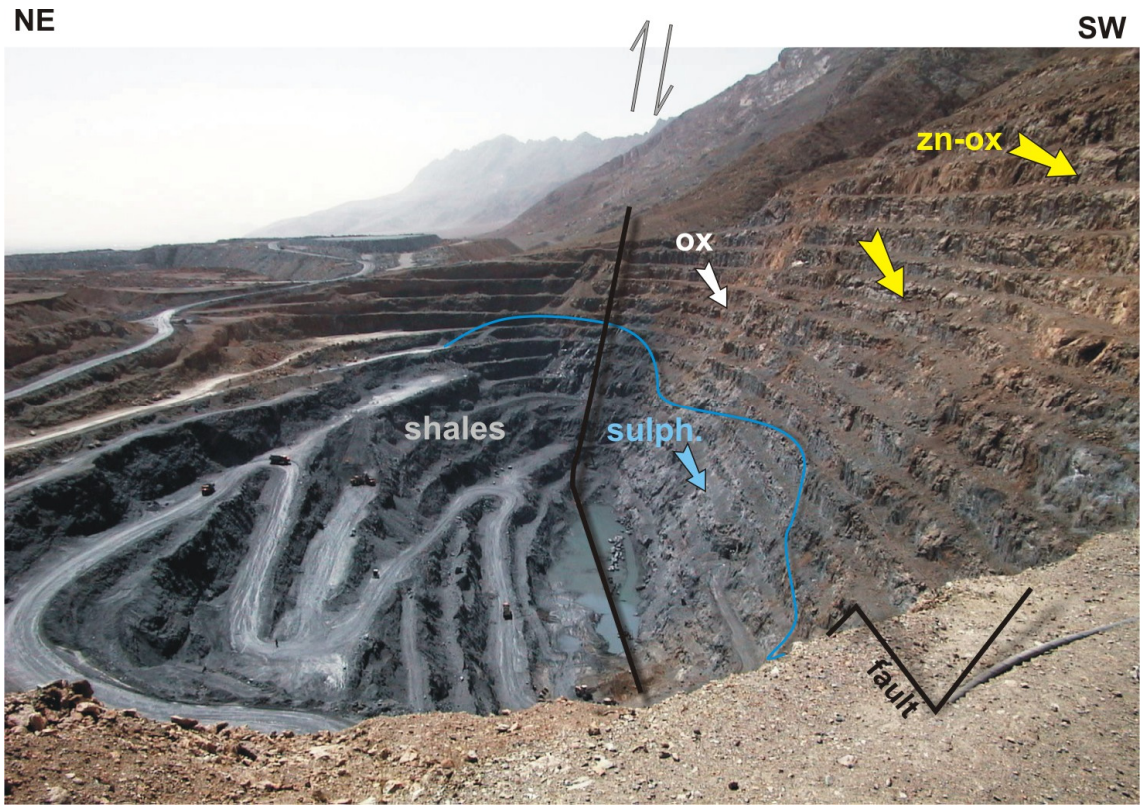

Fig. 59: View of the Goushfil pit at the Iran-Kuh district. Cretaceous dolomite in the south and Jurassic shales in the north are separated by a W-E trending fault. The vertical zonation (marked by the blue line) separates a non-oxide zone (dark grey colours) in the lower parts of the deposit and an oxide-zone (brown colours) in the upper parts. The sulphide ore is mainly hosted in the dolomite (blue arrow). The non-sulphide ore occurs within the oxide zone as secondary mineralisation predominantely in the vicinity of faults and fractures (yellow arrows).

The **Kolahdarvazeh pit** is under exploration and mining since 1962 and produces a high-grade non-sulphide zinc concentrate. The industrial mining has stopped and only some small adits are currently mined by artisan miners.

Tab. 14: Important Zn-Pb mines of the Irankuh district, west-central Iran

Mine	sulphide ore & mean grade (% Zn)	non-sulph.-ore & mean grade (% Zn)
Tappeh-Sorkh	5.046.431 (5.4%)	825.142 (6.6%)
Goushfil	4.299.500 (11.6%)	713.479 (10.8%)
Kolahdarvazeh	no reserve	mined out, approximately 30 %

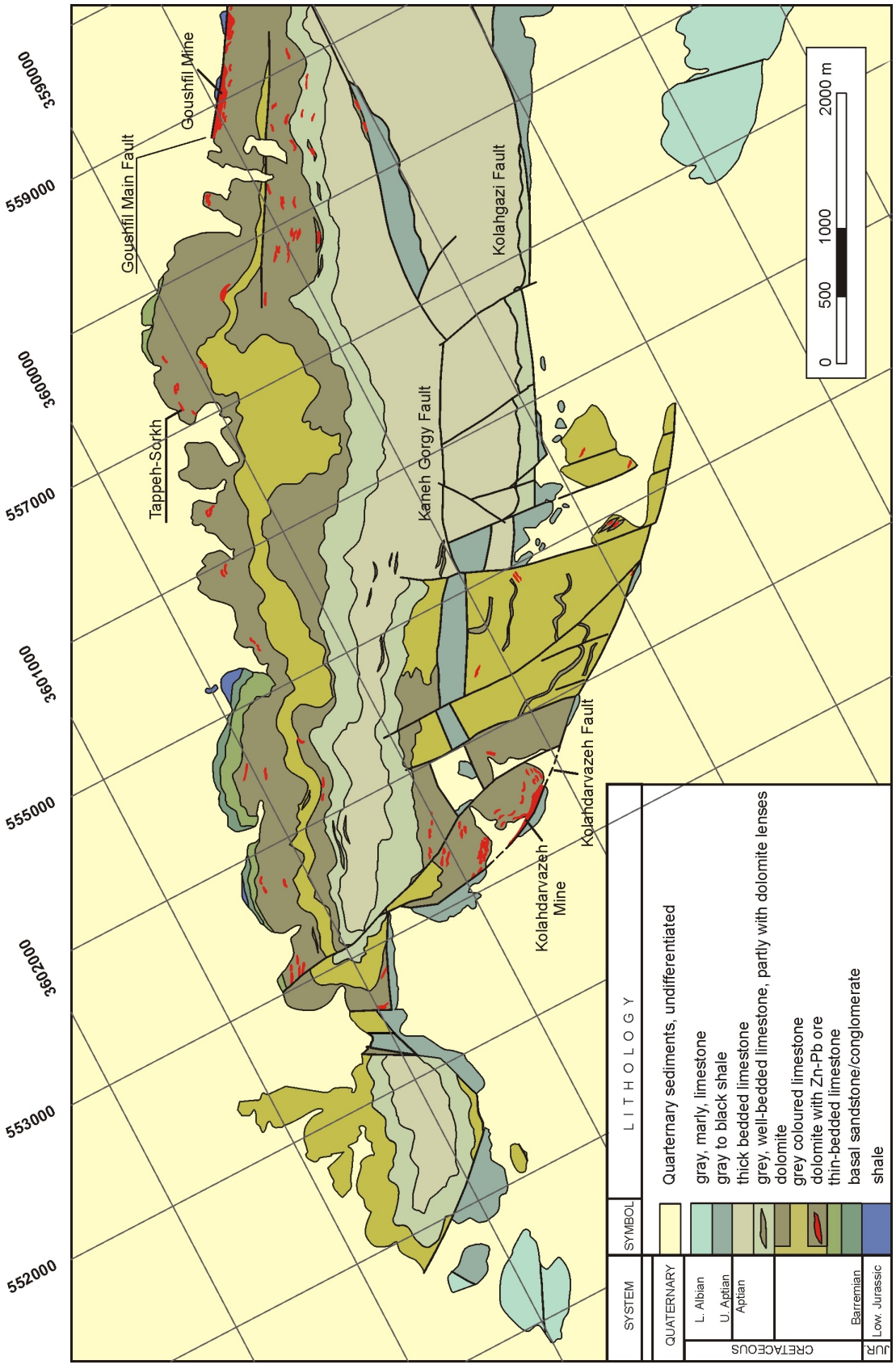

Fig. 60: Schematic geological map of the Irankuh mining district. (modified unpubl. geological map, BAMA Mining Corp.)

4.2.1 The Kolahdarvazeh Mine

Stratigraphic setting

The regional stratigraphic sequence of the Irankuh area (Fig. 62) starts with Lower Jurassic shales at the lowermost position, followed by Lower Cretaceous strata (Barremian-Aptian), Upper Aptian sediments, and on top of this sequence sediments of the Oligo- and Miocene. Two major stratigraphic gaps can be found within this stratigraphic sequence. The first separates the Lower Jurassic shales from the Lower Cretaceous strata. The second gap is located between the Cretaceous- and the Oligocene strata (RASTAD, 1981).

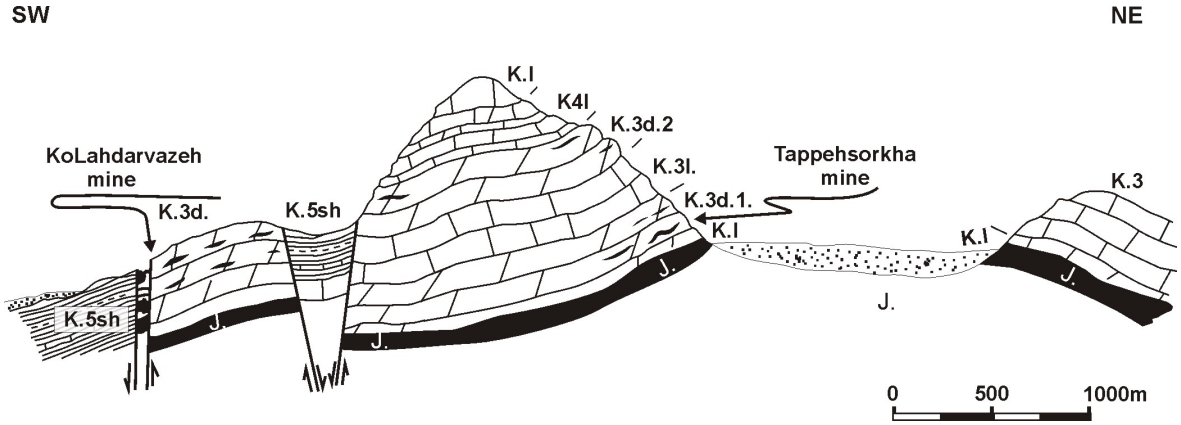

Fig. 61: Cross section of the Irankuh area. (modified after RASTAD, 1981)

The oldest rocks of the Irankuh area are the Jurassic shales, which are exposed in the northwestern part of the area, near the Goushfil pit. These strata are composed of dark grey shales with intercalations of silt- and sandstone (MOMENZADEH, 1976).

The sediments of the Lower Cretaceous overlying unconformably the Jurassic shales and form a continuous sequence beginning from the Barremian up to the Upper Aptian sediments. The total thickness of this sequence is approximately 800 m. These Cretaceous strata comprise mainly dolomite, limestone, and minor amounts of shales and marbles.

The strata of the Barremian and Lower Aptian sediments are the host rocks of the sulphide/non-sulphide ore mineralisation, which forms two discrete ore-bearing horizons within the K3 unit: the Goushfil-Kolahdarvazeh Horizon and the Goushfil-Gowdezendane Horizon (RASTAD, 1981).The K3 unit mainly consist of yellowish to brownish coloured dolomite and grey limestone. The limestone is medium to thick bedded with fossils, whereas the dolomite is massive to thick bedded.

The general structural setting of the Kolahdarvazeh pit is similar to the Goushfil pit. A sub-vertical, NW-SE trending fault (Kolahdarvazeh fault), which is located in the southern most part of the deposit, separates Cretaceous black shales from Cretaceous dolomites and limestones (Fig. 63). The main difference between the Kolahdarvazeh- and the Goushfil pit are the age of the shales (Kolahdarvazeh Mine: Cretaceous shales, Goushfil: Jurassic shales).

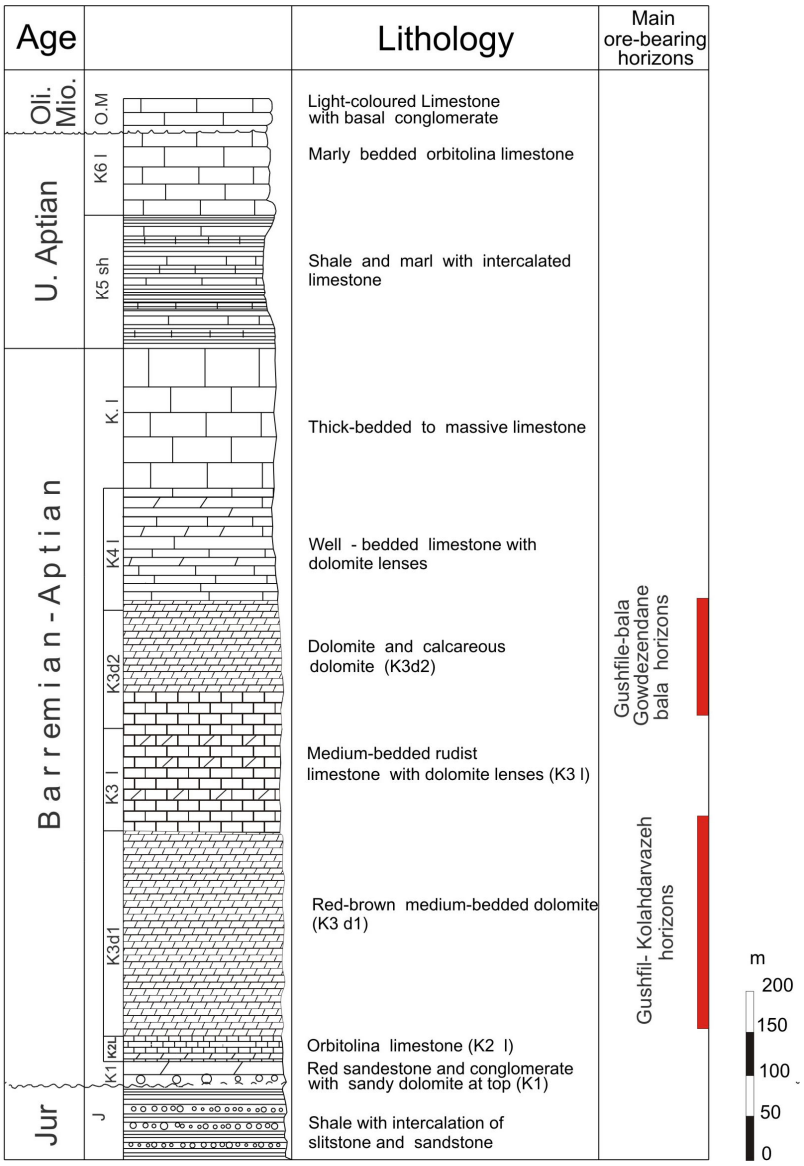

Fig. 62: Regional stratigraphic sequence of the Irankuh area, which comprise Jurassic and Cretaceous strata. The ore of the Irankuh district is hosted within the Cretaceous K3d1 and the K3d2 unit. (after RASTAD, 1981)

The ore of the Kolahdarvazeh mine is hosted within the strata of the Cretaceous K3d unit, which is cut by the sub-vertical Kolahdarvazeh- and Tofangchiha faults. The Kolahdarvazeh fault restricts the occurrence of mineralised rocks and the deposit to the South, whereas the Tofangchiha fault limits the deposit to the North. The most portions of the non-sulphide (and subordinate amounts of sulphide ore) occur between these two Faults.

The limestone and the dolomite of this area dip approximately 17° - 30° to the South. The whole area shows an intensive and extensive faulting.

The Irankuh district is mainly controlled by three different fault systems. The Kolahdarvazeh-, the Tofangchiha- as well as the Irankuh fault. Most of these faults as well as the folded strata of this region show a parallel trend to the Zagros Fold Belt and the Zagros Thrust zone, which is the result of the convergence of the Arabian and the Iranian plates.

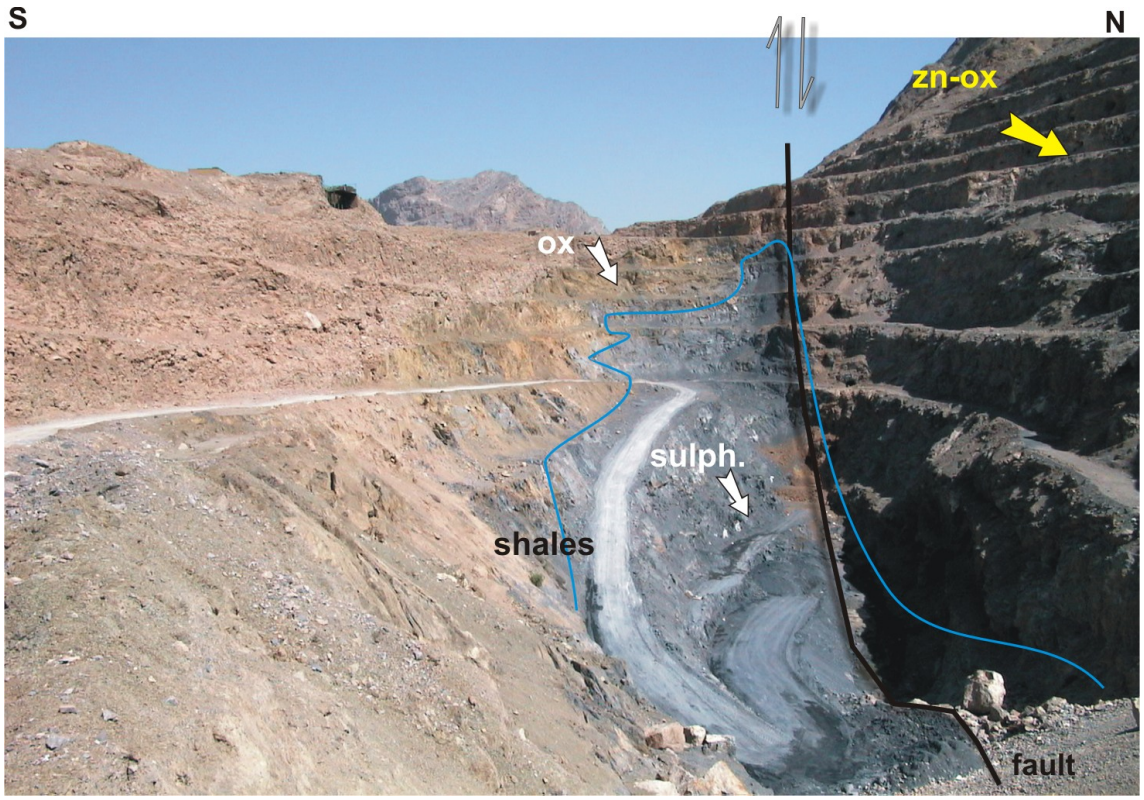

Fig. 63: Overview of the Kolahdarvazeh mine. Non-sulphide zinc ore ('zn-ox') (mainly hydrozincite/smithsonite) occurs in the oxide zone ('ox') of the Cretaceous rocks (above the blue line). The non-sulphide zinc minerals precipitated as a matrix of karst-breccias within dolomite and limestone and as mineralisation in faults and fractures. Mainly sphalerite, galena, and pyrite can be found within a small area in the sulphide-zone of the shales (close to the main fault) and in the ore lens between the main fault and the dolomite unit.

Style of mineralisation

The sulphide ore

Both the sulphide mineralisation as well as the non-sulphide ore of the Kolahdarvazeh mine occurs within Cretaceous dolomite and limestone. Sulphide mineralisation occurs in a number of locations in the proximity or especially at the contact to the shales. Most of the detectable sulphide ore occurs discordant to the hosting dolomite within the not oxidised zone near to- or directly at the contact to the shales. The most portion of the dolomite hosted precursor sulphide protor is oxidised and sulphide sulphides occur rarely within the dolomite. Unoxidised dolomite-hosted sulphide ore from the Kolahdarvazeh mine is only visible at drill cores and rarely at several adits.

In most cases, the sulphide ore is partly oxidised and only local relics of sulphides (mainly galena) are visible. The primary sulphide mineralisation consists of sphalerite, galena, subordinate amounts of pyrite, traces of marcasite, and chalcopyrite. Associated minerals are barite and calcite mainly as veins and fillings of fractures. The majority of the sampled sulphide ore is at least partially oxidised. In an advanced state of oxidation most of the sulphide minerals are oxidised and only galena

is present as the most oxidation-resistive mineral. The reddish to yellowish sphalerite occurs in minor amounts as fillings in fractures and spaces. The most portion of the sphalerite occurs as semi-massive replacements of the dolomite. Galena and pyrite are relatively minor and are associated with the occurrence of sphalerite. However, pyrite occurs in traces also as sub-mm sized framboids within the dolomite without any other (Zn-Pb-) mineralisation.

Sulfides, in particular sphalerite and galena, have replaced barite. Barite has probably formed both prior to and during the main period of sulfide mineralisation. Later barite crosscuts early sulphides and shows no corrosion or replacement by sulphides.

The mining district of the Irankuh area and especially the Kolahdarvazeh mine is characterised by low Fe concentrations. Pyrite as the main important Fe-bearing mineral is a minor component of the sulphide ore reflected by the arithmetic mean values of Fe_2O_3 = 1.5 % (Tab. 15).

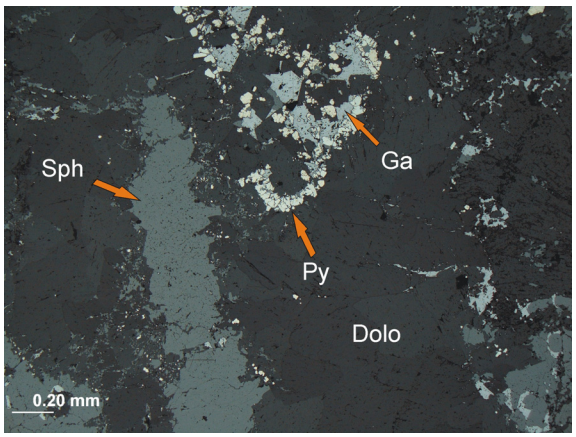

Fig. 64: This photomicrograph of a thin section from a sulphide ore zone of borehole DDH40. Dolomite (Dolo) has been replaced by sphalerite (Sph) and galena. Pyrite occurs in subordinate amounts as euhedral crystals. (reflected light, sample IK02155 at 45 m, borehole DDH40).

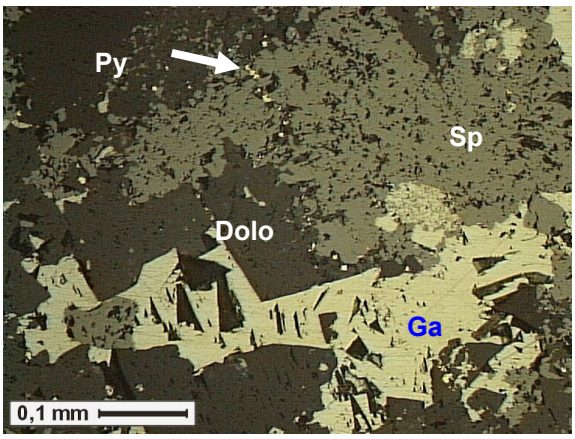

Fig. 65: Photomicrograph of sulphide mineralisation within the dolomite host rock. Main minerals are sphalerite, galena and subordinate amounts of pyrite. The ore occurs as filing between dolomite crystals and as a cement of dolomite fragments. IK02144, DDH64 at 111m.

The occurrence of dolomite-hosted sulphide ore is restricted to small zones, which ranges from dm to several metres (rare). These sulphides occur preferentially in the proximity of overlying shales or within massive and undisturbed dolomites (Fig. 73), which are not influenced by faults.

The non-sulphide ore

The majority of the non-sulphide ore is associated with karst-breccias within the dolomite and limestone (Fig. 66), but non-sulphide mineralisation occurs also within faults and fractures. In contrast to the Goushfil pit, which shows mainly sulphide mineralisation, the amount, and especially the grade of the non-sulphide zinc-ore of the Kolahdarvazeh pit is very high and the fraction of sulphide-ore is much smaller. Smithsonite, hydrozincite, hemimorphite, cerussite, malachite, calcite, goethite, hematite, limonite, and barite are the main minerals in the oxide-zone.

The non-sulphide ore occurs predominantly as a matrix of karst- and fault breccias (Fig. 68). Most of these breccias consist of angular fragments (2 cm up to several metres in diameter) set in a fine- to medium grained matrix. In some breccias, the fragments can be seen to match along their opposed sides, indicating only modest disturbance. The matrix mainly consists of zinc- (lead-) carbonates, such as smithsonite, hydrozincite, cerussite and minor amounts of zinc-silicates and zinc-manganese minerals: hemimorphite or coronadite $Pb(Mn^{4+},Mn^{2+})_8O_{16}$, and others. Goethite, hematite, and iron (hydro-) oxide minerals are not common, but occur in most samples as traces. The occurrence of high concentrated iron-bearing minerals is regionally limited.

Fig. 66: Typical occurrence of the non-sulphide ore within the Kolahdarvazeh pit. The non-sulphide ore occurs predominantly as matrix of karst- and fault-breccias and is characterised by a high Zn/Pb ratio and low concentrations of goethite and other iron hydroxides.

Most of the breccias within the Kolahdarvazeh region seem to be karst-breccias with varying size and dimensions. The diameter of these karst-breccias varies from some meters up to 10 meters and more (Fig. 67).

Fig. 67: Typical system of large dimensional slope, which is the result of the mining of a non-sulphide cemented karst-breccia. The caverns, which are 10 and more meters in diameter, show the wide extension of the karst-breccia and their related karst-conduits.

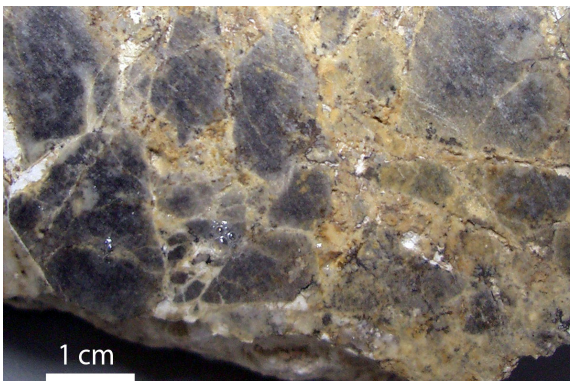

Fig. 68: Angular fragments of a breccia, cemented by non-sulphide Zn-(Pb-) minerals (hydrozincite, smithsonite, cerussite and subordinate amounts of iron hydroxides).

Non-sulphide zinc-(lead-) mineralisation is common as a filling of fracture planes and fault-zones and occurs in the region of the Kolahdarvazeh pit as well as in the Goushfil pit and their vicinity.

The non-sulphide Zn-(Pb-) minerals occur as mainly four types and styles at the Kolahdarvazeh mine. The first type **(Type-A)** occurs as filling of (more or less) planar faults and fractures (Fig. 69). The contact between the non-sulphide ore and the barren rocks is commonly sharp. Most of the secondary (non-sulphide) minerals grew normal to the fault- and fracture planes. Iron-oxide minerals, such as goethite and others are rare, which is according to their immobile behaviour during weathering and alteration processes. The grade of this type of non-sulphide zinc ore is relatively low, which is due to the limited surface- and fracture-size. Common minerals are secondary calcite, hydrozincite, smithsonite, hemimorphite, cerussite, traces of manganese minerals (coronadite), and traces of Fe-oxides and Fe-hydroxides.

The second type **(Type-B)** of non-sulphide zinc mineralisation occurs as a matrix of fault- and karst-breccias and is characterised by fine-grained cement. The fragments of the breccia are angular and show a sharp contact between the dolomite fragments and the cement (Fig. 70). Similar to Type-A, the common minerals are hydrozincite, smithsonite, hemimorphite, cerussite, and minor concentrations of Mn- or Fe-bearing minerals. However, this type of breccia is not common and occurs regionally limited as small karst-breccia systems or as fault-breccia.

One possible interpretation of this ore-type is a rapid mineralisation process. During this process, the breccia fragments had no time to interact with the ore-delivering fluids. The breccia fragments have not been altered chemically and/or mechanically. The edges remained sharp and angular. This hypothesis is supported by the fact of a fine-grained cement, which is probably also due to a rapid mineralisation and precipitation process. Another reason for these sharp edges of the breccia clasts could be the inert behaviour of some types of dolomite to the mineralising fluids.

The third type, **Type-C**, of non-sulphide zinc mineralisation is similar to Type- B. The non-sulphide ore occurs as a matrix of fault- and karst-breccias. However, the fragments of this type of breccia are not angular but (sub-) rounded. They lost their sharp contact between the non-sulphide matrix and the dolomite/limestone fragments. The matrix consists of fine-grained to coarse-grained (layered) crystals/masses, which commonly show a (concentric) zonation (Fig. 71). The size of these zones varies from a sub-mm scale up to several cm and dm. Common minerals are hydrozincite, smithsonite, hemimorphite, cerussite. Manganese and iron-bearing minerals are rare.

This type of breccia is common within the Kolahdarvazeh pit. In contrast to the formation of Type-B ore, here the mineralisation was probably a long lasting process. An intensive period of interaction between the breccia-fragments and the ore delivering fluids led to a (partial to total) dissolution and replacement of calcite and/or dolomite of the breccia-fragments. The edges of the dolomite/limestone fragments became round and irregular.

The **Type-D** non-sulphide ore consists of both non-sulphide minerals as well as varying amounts of sulphides. Within this ore-type, galena is the most common sulphide mineral (Fig. 72). This is probably the result of a higher reactivity of sphalerite during the oxidation process. The spaces between the breccia fragments are filled with hydrozincite, smithsonite, and cerussite. The adjacent regions of the galena bearing mineralisation are rich in cerussite and leadhillite $Pb_4(SO_4)(CO_3)_2(OH)_2$. This type is common at deeper levels of the Kolahdarvazeh mine and can be investigated exclusively in drill-cores.

Fig. 69: Type-A non-sulphide ore on fracture-planes. The non-sulphide ore minerals occur exclusively on the fractures planes (arrow). The adjacent massive dolomite is not mineralised. Sample No. IK02114.

Fig. 70: Matrix supported breccia, which is characterised by angular fragments with a sharp contact to the fine-grained non-sulphide cemented. The fragments match along their opposed sides, indicating only modest disturbance.

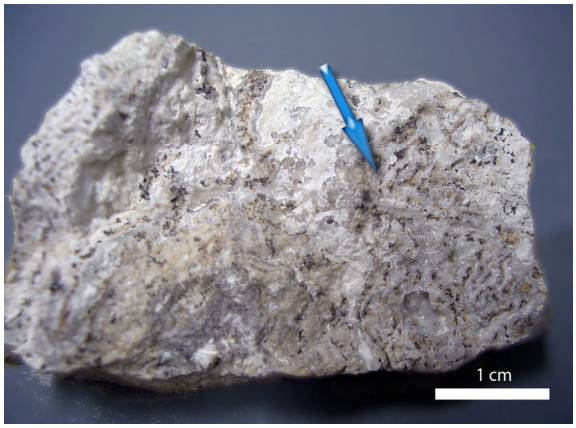

Fig. 71: The breccia clasts of the Type-C ore are replaced by non-sulphide minerals (smithsonite, hydrozincite). These minerals show a (concentric) zonation around the dolomite fragments (arrow). The contact between the matrix and the dolomite fragments is diffuse.

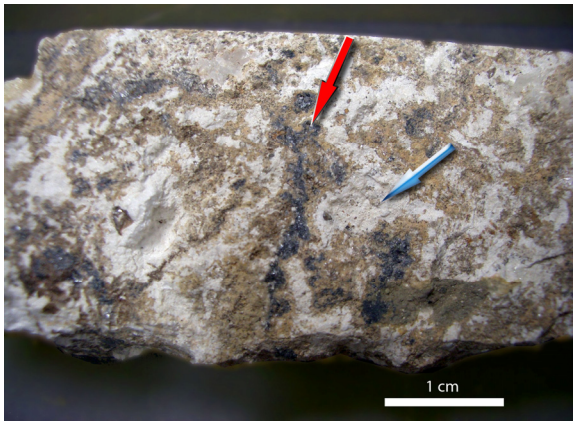

Fig. 72: Type-D non-sulphide/sulphide ore. The dolomite fragments of the non-sulphide cemented breccia show relicts of a sulphide mineralisation, mostly galena (red arrow). The dolomite clasts are highly altered and show diffuse edges, partly replaced by white-coloured smithsonite and hydrozincite (blue arrow).

Detailed investigations on sulphide and non-sulphide ore samples of the Kolahdarvazeh mine have been performed on borehole DDH64 and DDH40 (Fig. 73 and Fig. 74) and on several samples of the Kolahdarvazeh mine and artisanal-mined adits. The sampled boreholes are located within the area of the Kolahdarvazeh pit. The position of the DDH64 is (UTM 3598421.092; 553313.532) at an elevation of 1670 m. The total depth of DDH64 is 129.2 m with an inclination of 80° and a dip-direction of 251°. The DDH40 is located at position UTM 3598484.102; 553174.822 at an elevation of 1620 m. The depth of DDH40 is 151.2m and a dip of 65° to a dip-direction of 70°. The boreholes cross dolomites of the Cretaceous K3 unit and Cretaceous shales of the K5 unit.

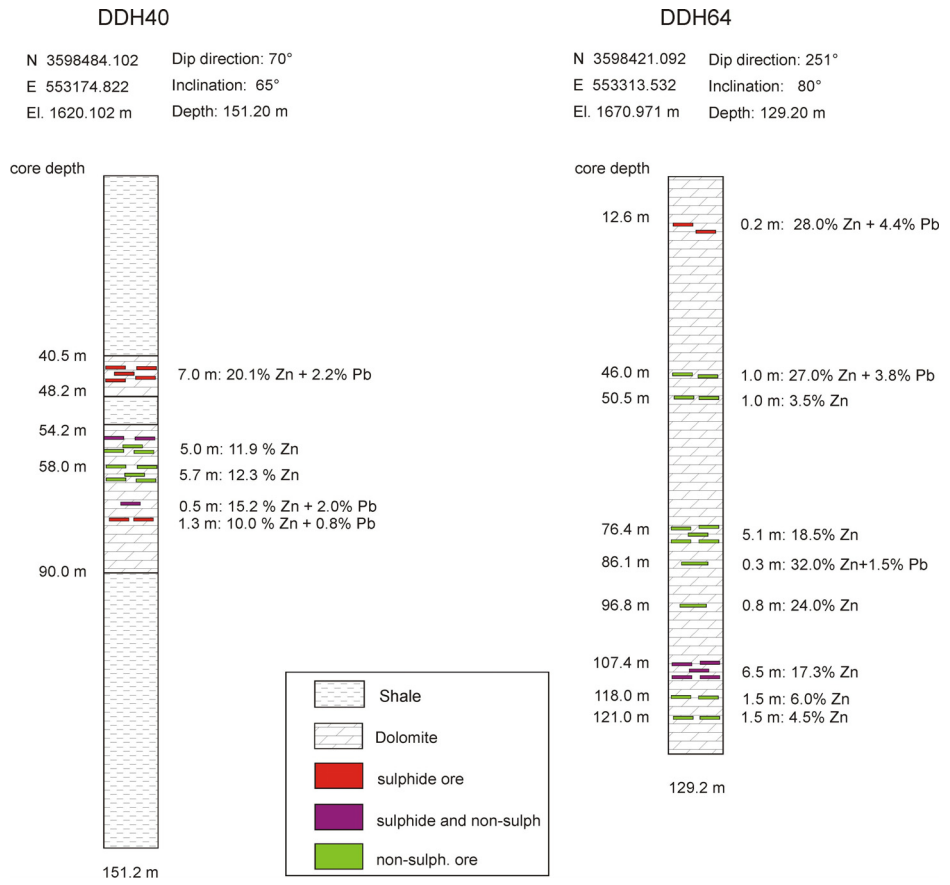

Fig. 73: Profiles of boreholes DDH 64 and DDH 40. The borehole DDH40 is located nearby the main vertical fault that limits the Kolahdarvazeh mine to the south. The shales of borehole DDH40 are fault-related and regionally sheared in the carbonates. (unpubl. data of the Bama Mining. Co., Esfahan)

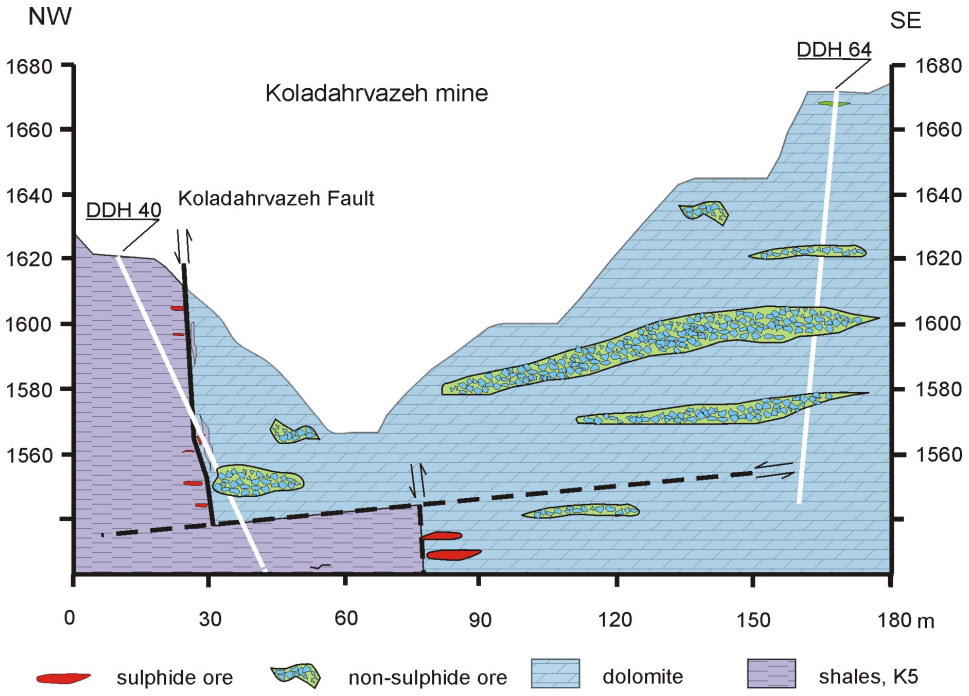

Fig. 74: Schematic cross section of the Koladahrvazeh mine and the location of the bore holes DDH40 and DDH64. (Modified after internal and unpublished data of the Bama Mining Co., Esfahan)

Fig. 75: Dolomite of DDH64 at 12 m. The dolomite is gray to dark grey coloured. Fractures are coated with Fe-hydroxides.

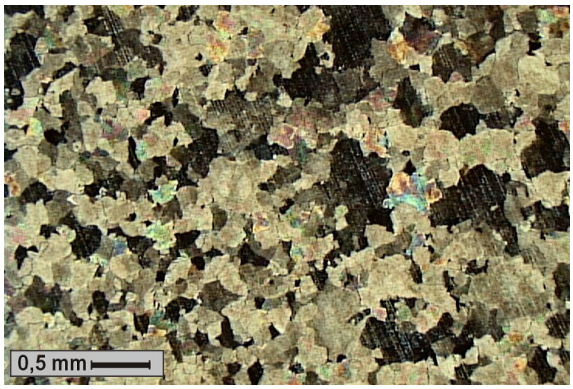

Fig. 76: Photomicrograph of a thin-section of a typical dolomite of borehole DDH64. The crystals show a perfect 120° angle at the triple-points, tat points to a dolomitised limestone. (xn) Sample IK02134

Fig. 77: Typical drill core sequence of borehole DDH64 with a zone of high-grade non-sulphide ore at 110 m (red marked). The non-sulphide ore consists mainly of cm-sized dolomite fragments that show a replacement by mainly smithsonite and hydrozincite, which also build the matrix of this breccia.

Fig. 78: DDH64 at 111 m. The dolomite is brownish-reddish coloured. The brownish dolomite clasts are (if visible) and remnants of them are highly altered and show diffuse edges due to replacement by smithsonite and hydrozincite (the dark red coloured area is caused by Zinc Zap, an indicator for non-sulph. zinc minerals).

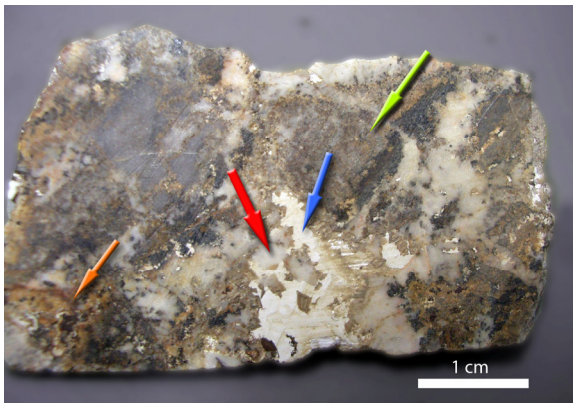

Fig. 79: Detail of a non-sulphide ore mineralised zone of DDH64 at 50 m. Breccia clasts (green arrow), consisting of dolomite surrounded by cement of smithsonite and hydrozincite (blue arrow). Goethite occurs in a microscopically scale as concentric botryoidal shaped layers (orange arrow) and as a constituent of the breccia matrix.

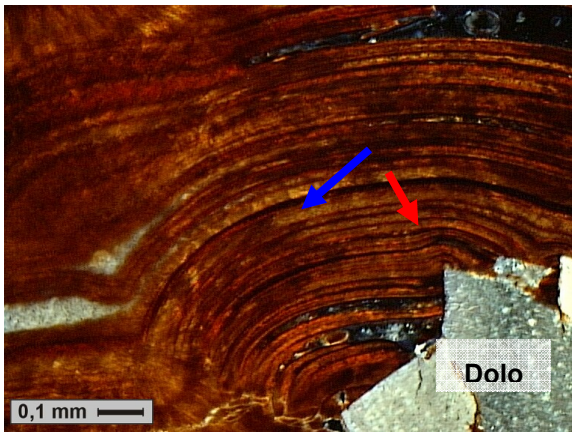

Fig. 80: Photomicrograph of a concentric growth banding due to the precipitation of hematite/goethite and smithsonite/hydrozincite (blue arrow) on dolomite fragments (Dolo) of a (karst-) breccia. A deformation of the bands and an unusual contact to the dolomite (red arrow) are probably due to a late stage movement of the dolomite clasts. IK02135 (xN), borehole DDH64

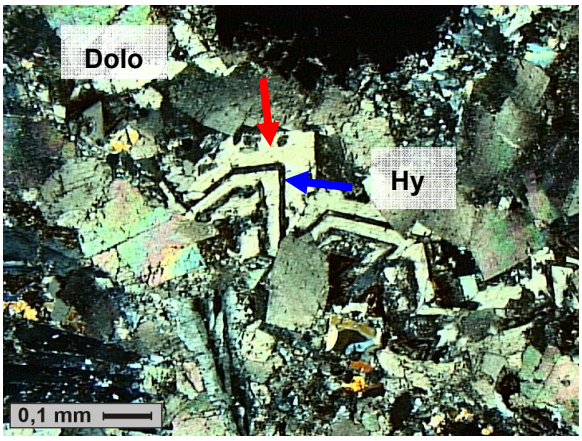

Fig. 81: The Photomicrograph shows smithsonite crystals (red arrow) in which hydrozincite (Hy) has developed and replaced smithsonite along crystallographically preferred planes (blue arrow). The dolomite (Dolo) is highly fractured and brecciated. The fragments are cemented by hydrozincite. IK02135 (xn), borehole DDH64

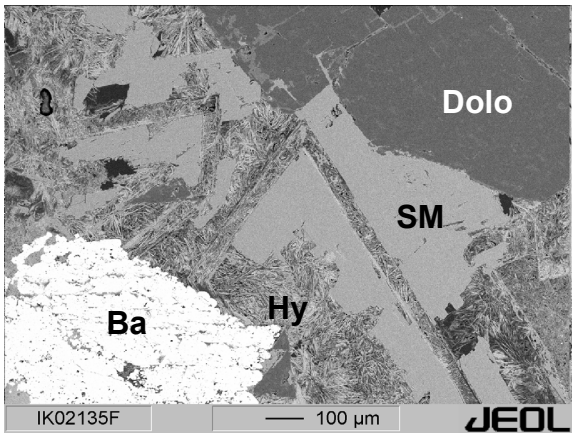

Fig. 82: BSE-image showing smithsonite and its replacing along preferred planes. Breccia fragments of dolomite (Dolo) and barite (Ba) have been cemented by hydrozincite (Hy) and smithsonite (SM). The space between the dolomite crystals is filled by hydrozincite/smithsonite. IK02135 (xN), borehole DDH64

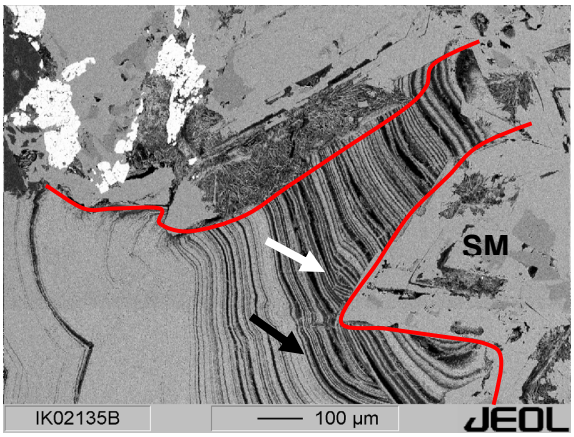

Fig. 83: BSE-image of a layered sequence of smithsonite (black arrow) and a Fe-Mn bearing mineral (probably Mn-bearing hematite) (white arrow). Due to the perpendicular contact of the layers to the Smithsonite (red line) it can be assumed that this sequence is probably subsequent brecciated or has been intergrown with smithsonite and hydrozincite (SM). IK02135 (xN), borehole DDH64

The dolomite host rock shows grey to brownish colours and has a medium grain size of approximately 0.2 mm. The grains are tightly interlocking. Most of the dolomite crystals show a perfect 120° angle on their triple points, which indicates a recrystallisation, probably due to a dolomitisation process of a pre-existing limestone (Fig. 77 and Fig. 76). Pyrite is rare and occurs as sub- to euhedral crystals (< 50 µm) and masses (Fig. 64). The fractures of the dolomite are filled by calcite and/or minor amounts of Fe-hydroxides, hydrozincite, and smithsonite. Barite occurs as veins within the dolomite.

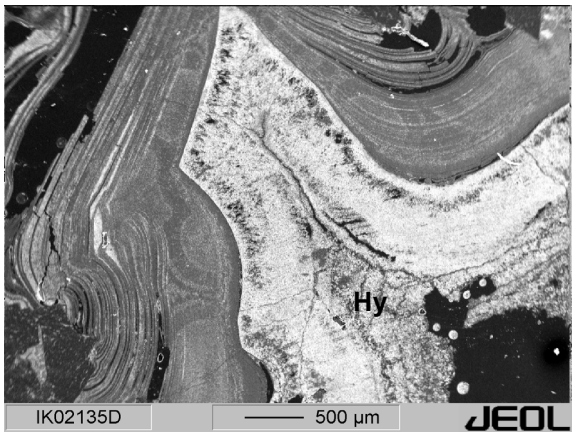

Fig. 84: BSE-image of a lamination consisting of smithsonite and a Fe-Mn bearing mineral, which is overgrown by hydrozincite (Hy). The hydrozincite represents the last stage of the mineralisation process. IK02135, DDH64@50m, DDH64

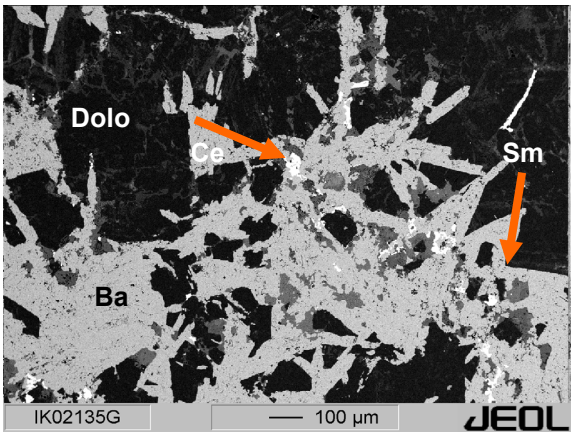

Fig. 85: BSE-image of a dolomite-clast with dolomite (Dolo), and acicular barite (Ba), which is probably partly replaced by cerussite (white spots, Ce), and smithsonite (Sm). IK02135, DDH64@50m

The examination of the drill cores DDH40 and DDH64 has shown several zones (approximately 10 to 30 cm) with high concentrations of non-sulphide ore (predominantly Zn-minerals) with subordinate amounts of lead minerals (Fig. 78 & Fig. 79). One of these zones has been sampled at a depth of 50 m. The most abundant Zn-minerals are hydrozincite and smithsonite. Lead occurs as cerussite and iron precipitated as fine-grained coating on fractures, and as intergranular filling of the non-sulphide ore minerals as well as concentric grown Fe-hydroxide aggregates (Fig. 80). Other minerals are barite, dolomite, and calcite. The non-sulphide ore-bearing zone at 50 m is probably a regional limited fault related breccia or a debris-filled karst-conduit. A collapse breccia would be improbable with regard of the limited dimension of this zone.

The layered sequence of iron-hydroxides and smithsonite shows fractures and indicates a subsequent brecciation after its precipitation (Fig. 83). These fragments are intergrown by euhedral smithsonite. This smithsonite is probably affected by alteration- and corrosion-processes, in which the smithsonite was partly replaced by hydrozincite (Fig. 82). Hydrozincite cements the breccia fragments and fills vugs and open spaces of this examined sample. Here, hydrozincite represents the final stage of the mineralising and cementation process (Fig. 84).

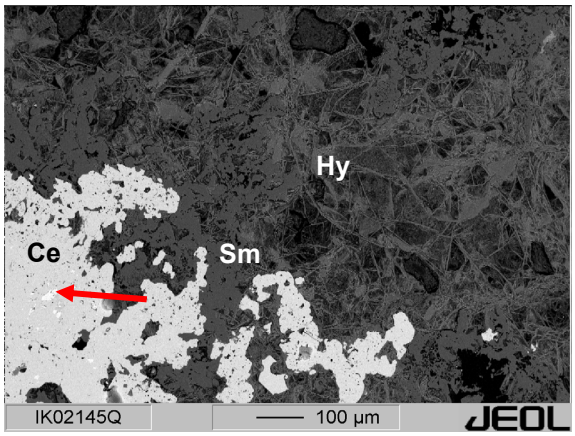

Fig. 86: BSE image of an oxidised region of a sulphide ore. Relicts of the pre-existing galena are preserved in the centre of the cerussite (white spots, red arrow). The cerussite is surrounded by massive anhedral smithsonite, which is overgrown (or was altered to) hydrozincite (Hy). IK02145, DDH64 at 119m

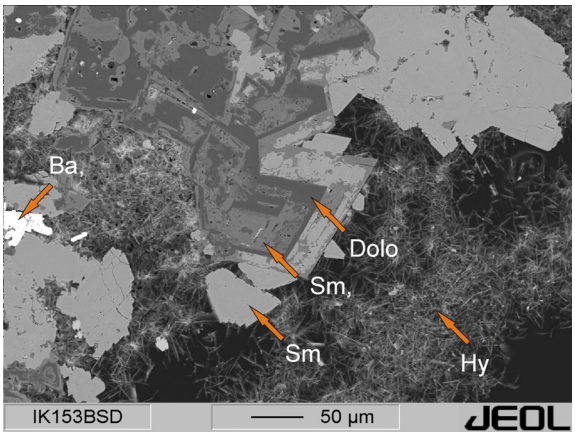

Fig. 87: BSE-image of a non-sulph. mineralised zone. The sulphides are oxidised. Dolomite (Dolo) is partly replaced by smithsonite (Sm). Hydrozincite (Hy) occurs as late stage mineral that overgrowths dolomite and smithsonite. (Sample IK02153 at 64 m, DDH40).

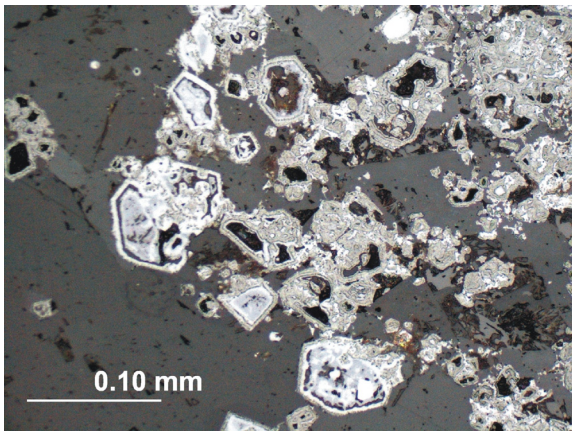

Fig. 88: Photomicrograph that shows an atoll texture similar to that of Fig. 87. Sphalerite and pyrite are oxidised. Brownish colours indicate Fe-oxihydroxides from oxidised pyrite or derived from Fe-bearing sphalerite. (Sample IK02158)

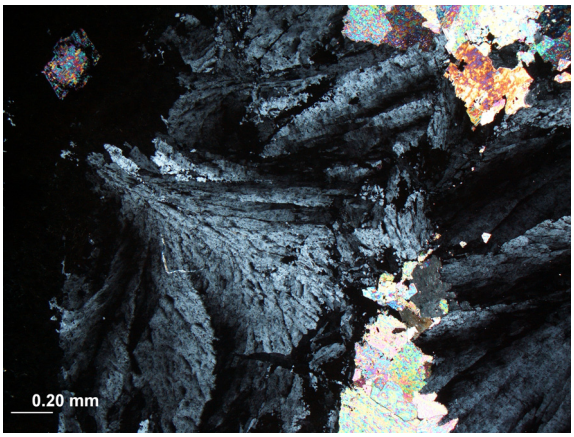

Fig. 89: Photomicrograph of euhedral barite. Barite occurs predominantly as filling of vugs and open spaces and replaces also the dolomite of the host rock. Sample IK02155, XN, borehole DDH40.

The occurrence of sulphides and their concentration increase with depth of borehole DDH64. Sphalerite and galena is commonly associated with pyrite (Fig. 65). The sulphides occur as fillings of the interstitial spaces of the dolomite crystals as well as cement of dolomite clasts. Most of the examined sulphide zones show a more or less extensive oxidation.

The oxidation of galena is associated with the formation of cerussite (Fig. 86) and small amounts of leadhillite, $Pb_4(SO_4)(CO_3)_2(OH)_2$. Sphalerite has been oxidised to smithsonite, which is altered/transformed at a later stage to hydrozincite.

The oxidation of sphalerite is associated with the forming of massive anhedral smithsonite and acicular shaped hydrozincite. Hydrozincite overgrew most of these minerals, fills pores, and open spaces of the oxidised ore and the adjacent regions. Similar to other samples of this borehole, it can be assumed that hydrozincite is associated with the last stage of oxidation and non-sulphide ore forming processes.

Geochemical investigations on samples from the Kolahdarvazeh mine

The calculation of the Zn/(Zn+Pb) ratio from sulphide ore samples of the Kolahdarvazeh mine (Tab. 15) gives a Zn/(Zn+Pb) value of 0.84. This value is similar to values for this mining district, which are given by GHAZBAN ET AL., 1994. They calculated a Zn/(Zn+Pb) value of 0.76. However, the Zn/(Zn+Pb) ratio is relatively invariant. The values of both the sulphide ore and the non-sulphide ore are similar with $Zn/(Zn+Pb)_{sulph}=0.84 \approx Zn/(Zn+Pb)_{ox}=0.82$ and are an evidence for a lacking metal separation process between Zn and Pb.

Tab. 15.: ICP-MS data of selected metals. Comparison between sulphide- and non-sulphide ore samples of the Irankuh-district/Kolahdarvazeh mine. (Sulphide ore: n=7, non-sulphide ore n=14)

	Cu_{sulph}	Cu_{ox}	Pb_{sulph}	Pb_{ox}	Zn_{sulph}	Zn_{ox}	As_{sulph}	As_{ox}
	ppm	ppm	ppm	ppm	ppm	ppm	ppm	ppm
Mean	71.7	90.7	47660.4	77494.5	253500	349890.9	127.4	320.3
Min	7.3	13.5	932.2	1334.5	153100	16400.0	13	10.0
Max	241.7	256.2	234700	239800.0	329400	517800.0	441	1362.0
Stdev.	81.7	81.4	84059.5	93504.1	67073	175998.2	152.3	382.4
	Cd_{sulph}	Cd_{ox}	Ag_{sulph}	Ag_{ox}	$Fe_2O_{3\ sulph}$	$Fe_2O_{3\ ox}$	MnO_{sulph}	MnO_{ox}
	ppm	ppm	ppm	ppm	%	%	%	%
Mean	641.6	482.0	4.66	19.8	1.6	2.0	0.12	0.2
Min	223.2	18.8	0.1	0.5	0.42	0.1	0.02	0.0
Max	1332	1706.8	11.1	87.1	3.81	6.6	0.21	0.9
Stdev.	419.5	545.1	4.3	26.8	1.15	2.0	0.07	0.2

The red zinc ore is a common type at Mehdi Abad and other non-sulphide zinc deposits (e.g. Sierra Mojada), but observations at the Kolahdarvazeh mine and the examination of drill cores have shown that here the “red zinc ore” is absent. . Most of the non-sulphide zinc ore samples of the Koladahrvazeh mine are poor in iron. The colour of the non-sulphide ore is bright white to yellow-ish- and brownish white and even the oxidised sulphides do not show a deep red colour but brown to ochre colours. The ternary diagram in Fig. 90 also reflects the above-mentioned dominance of zinc and lead, especially related to iron. In contrast to Mehdi Abad, the Fe-Zn-Pb values show no clear differentiation process. The white zinc ore is dominating at the Kolahdarvazeh mine. Both the sulphide protore and the non-sulphide ore show similar characteristics in these elements.

The cadmium concentration of the sulphide ore is approximately 641 ppm. In contrast to Mehdi Abad, where Cd correlates with Zn, the sulphide ore of the Kolahdarvazeh mine shows not such a relationship between these elements. Without a positive correlation between Zn and Cd it was not possible to calculate the Cd in sphalerite. In fact, cadmium is probably not only incorporated in sphalerite, but also occurs probably with other minerals.

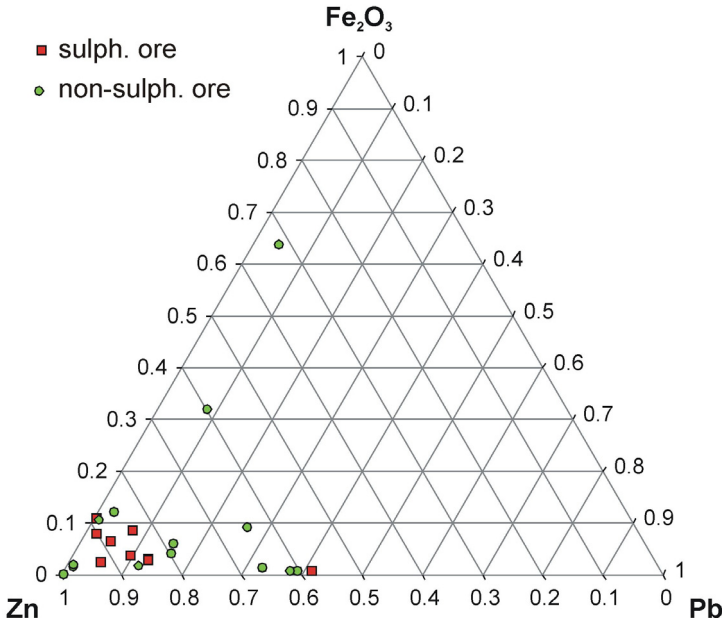

Fig. 90: Ternary Zn-Pb-Fe_2O_3 plot of sulphides and non-sulphide ore samples of the Kolahdarvazeh mine. Both ore types are characterised by low Fe_2O_3 values with the exception of two samples.

C-O stable isotope geochemistry of carbonates from the Kolahdarvazeh mine

Carbon and oxygen isotope measurements were applied to hydrozincite and dolomite samples of the Kolahdarvazeh mine and the results of the isotopic measurements are presented in table Tab. 16 and depicted in Fig. 91. The same limitation as used in Mehdi Abad is also valid for hydrozincite samples from the Kolahdarvazeh mine. The hydrozincite samples have not a monomineralic composition. XRD analyses point to an additional phase within the hydrozincite samples, which was detected as smithsonite. However, according to SEM (-EDX) analyses smithsonite occurs only in traces and should not influence the data of the hydrozincite importantly.

Tab. 16: δ13C and δ18O values of selected samples of the Kolahdarvazeh mine

Sample	18OV-PDB ‰	18 OV-SMOW ‰	13CV-PDB ‰	
IK02136	-8.2	22.40	-3.8	hydrozincite
IK02129	-8.3	22.3	-4.3	hydrozincite
IK02145	-9.1	21.6	-4.2	hydrozincite
IK02115	-7.8	22.9	-4.7	hydrozincite
IK02134	-8.1	22.6	-5.7	hydrozincite
IK02123	-7.9	22.8	-7.1	hydrozincite
IK02119	-8.7	21.9	-4.9	hydrozincite
IK02136	-9.5	21.1	2.1	dolomite
IK02150	-10.4	20.1	3.5	dolomite
IK02134	-8.2	22.4	1.6	dolomite

The hydrozincite samples plot in a similar region as the hydrozincite data from Mehdi Abad. The hydrozincite samples show a range of $\delta^{18}O$ (SMOW) values between 21.9 and 22.9 $^{0}/_{00}$. The $\delta^{13}C$ values range between -3.8 and -7.1 $^{0}/_{00}$. The dolomite samples intersect with the cluster of limestone samples from Mehdi Abad.

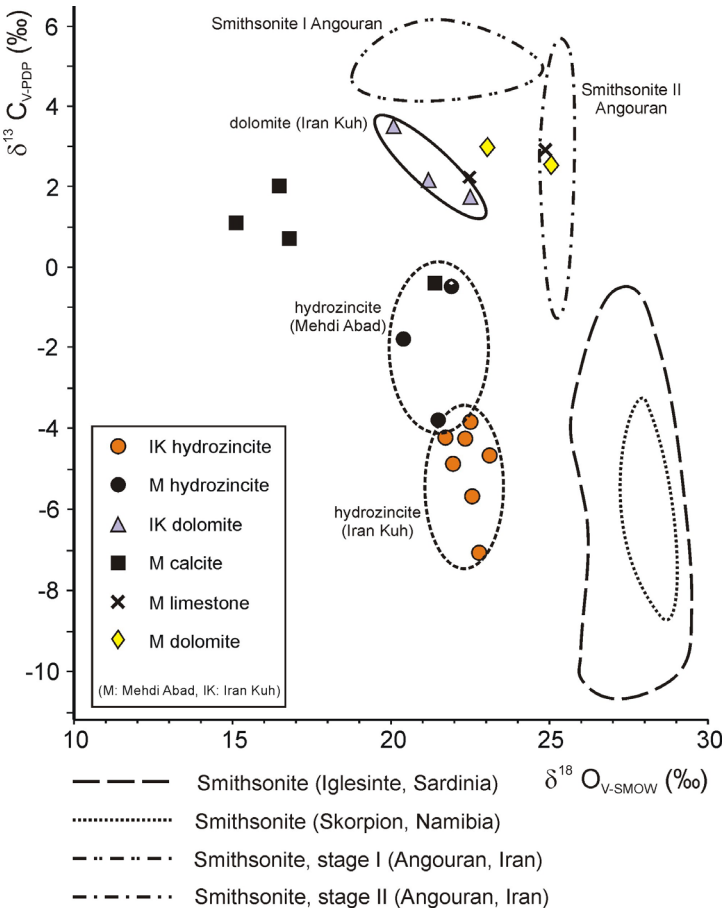

Fig. 91: Stable carbon and oxygen isotope composition of carbonates and hydro-carbonates from Irankuh compared with smithsonite isotope compositions worldwide. Data: Sardinia and Angouran: GILG & BONI (2004); Skorpion: KÄRNER (2006)

The isotopic pattern of the hydrozincite samples show close-ranged $\delta^{18}O$ values and a more variable range of $\delta^{13}C$ data. The $\delta^{13}C$ values are up to 3.3 ‰ lower than those from hydrozincite of Mehdi Abad. This behaviour of hydrozincite samples to tend to homogeneous $\delta^{18}O$ values and varying values of $\delta^{13}C$ is similar to the hydrozincite samples of Mehdi Abad and leads to a similar interpretation. At least two isotopically different sources of carbon are assumed for the formation of hydrozincite. The formation of the hydrozincite should be potentially influenced by an isotopically light component of carbon as a result of dissolved CO_2 derived from the decay of organic matter. However, the hydrozincite of the Kolahdarvazeh mine shows lower $\delta^{13}C$ values than its pendant from Mehdi Abad. This suggests a more important role of organic and meteoric CO_2 than in Mehdi Abad. A possible reason is a variable contribution of carbonate carbon from the limestone and/or the dolomite host rock and reduced organic carbon derived from the overlying soils and is comparable to pedogenic carbonates (CERLING 1984, CONIGLIO ET AL., 1996).

The isotopic values for smithsonite from different locations, especially from Sardinia (GILG & BONI, 2004) and Skorpion/Namibia (BORG ET AL., 2003; KÄRNER, 2006) shows a similar behaviour as the hydrozincite samples from Mehdi Abad and the Irankuh/Koladarvazeh mine. The interpretation of the smithsonite data points also to a supergene genesis and the influence of meteoric water combined with dissolved CO_2 derived from the decay of organic matter. However, the $\delta^{18}O$ values of smithsonite are shifted to higher values. This might indicate a different isotope fractionation factor between hydrozincite and CO_2 related to the smithsonite and is secondly related to the additional amount of water within the crystal structure, which also influences the $\delta^{18}O$ to lower values.

REE element analyses

Rare earth elements (REE) were determined for the dolomite host rock, the carbonate hosted sulphide ore and the non-sulphide ore. The REE distribution of the Koladahrvazeh mine is characterised by low to extremely low REE/C1 values. Numerous samples show that the concentration of different REE are below the detection limit and thus they are not plotted in the digrams. The lowest REE concentrations are detectable in the dolomite host rock. The data show no enrichment in LREE's or HREE's. The sulphide ore in contrast shows slightly higher REE values. The LREE's are slightly enriched compared to a moderate depletion of HREE's. However, the number of values below detection limit is still high and thus no clear statement about an Eu anomaly is possible.

The data of the measured samples show a relative high fluctuation. The barren dolomite host rock only gives relatively low values for REE/Chondrite varying around 0.5 (Fig. 93). However, the samples of the sulphide ore and the non-sulphide ore show around up to 3 times higher REE values, but they also show a high variation (Fig. 94). Thus, the presence of sulphide-mineralised dolomites is associated with increased REE element concentration with a tendency to higher LREE concentrations and decreasing values towards the HREE. The non-sulphide ore samples plot apparently within the same region as the non oxidised sulphides (Fig. 95). The graph of the non-sulphide ore is also influenced by a high variability of the REE values. A minor decrease in REE concentrations can be probably read and interpreted from the mean value diagram Fig. 96.

Most samples of the dolomite host rock show La, Ce and Lu values below the detection limit. In contrast to these dolomite samples, the majority of the sulphide ore as well as the non-sulphide ore samples have detectable La, Ce, and Lu values and thus are clearly distinguishable from the barren host rock. The nearly identical REE concentrations of the sulphide ore and the non-sulphide ore of the Koladahrvazeh mine suggest that the non-sulphide minerals replaced the sulphides. Only a minor fraction of the non-sulphide ore is probably the result of a metal dissolution– transport– and subsequent precipitation process. This process is associated with decreasing REE-concentrations due to their immobile behaviour (as shown for Mehdi Abad). In addition, the La-Ce plot for sulphide- and non-sulphide samples indicates no enrichment/depletion process, which should be a possible indication for a restit high in REE and a new formed distal non-sulphide ore that is low in REE. However, the close position of the REE data of the sulphide-, the non-sulphide, and the dolomite complicate the interpretation. According to the measured REE data two scenarios are possible. Firstly, the non-sulphide ore could have been formed in situ as a direct replacement of the sulphide protor or secondly the non-sulphide ore has been precipitated after an aqueous transport and thus as a distal precipitation.

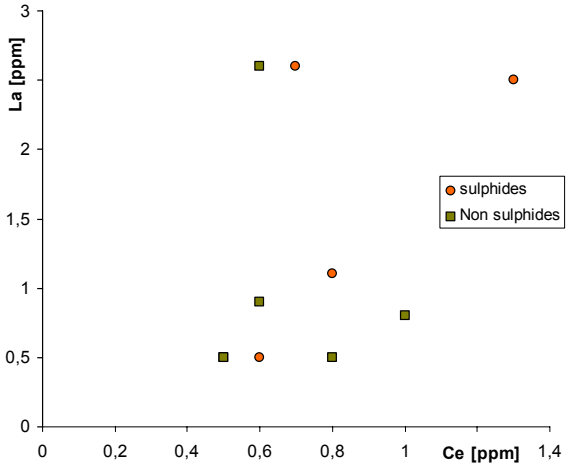

Fig. 92: La-Ce plot showing both sulphide and non-sulphide ore samples from the Koladahrvaze mine. All samples plot within one cluster which suggests a direct replacement of the sulphide protor with the non-sulphide minerals that form the non-sulphide ore.

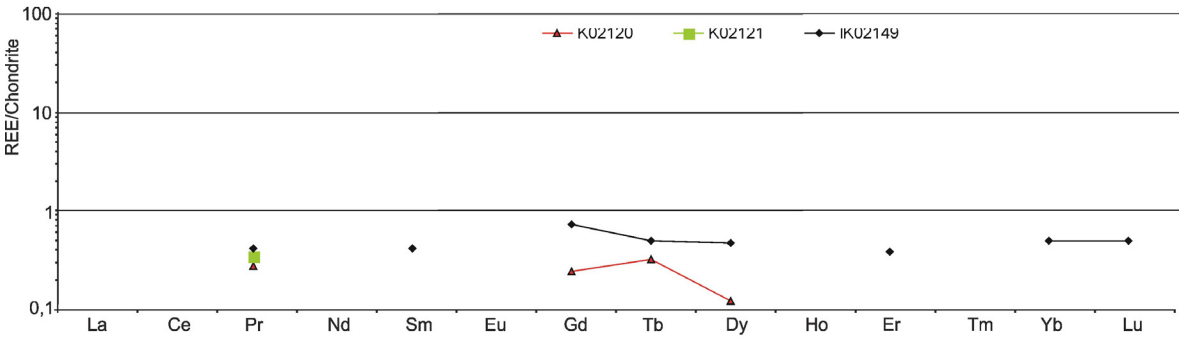

Fig. 93: REE data of the dolomite host hock from the Kolahdarvazeh mine. Not plotted data are below detection limit.

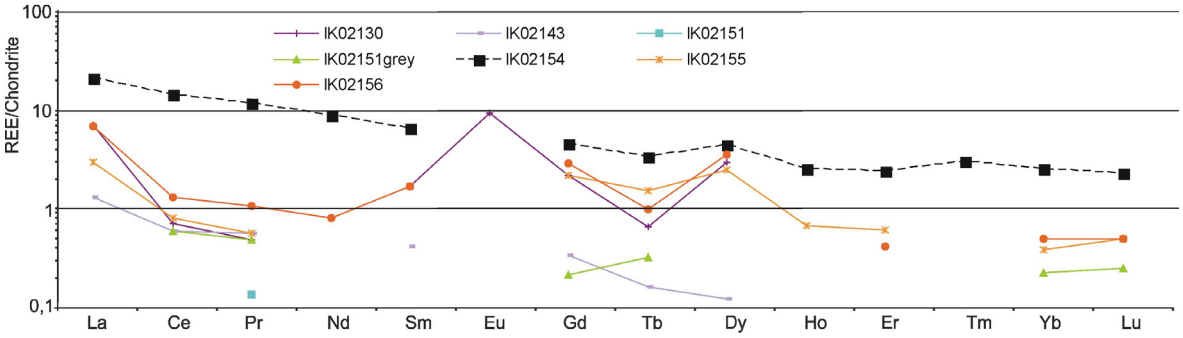

Fig. 94: REE data of the sulphide ore from the Kolahdarvazeh mine. The dashed line is a sulphide ore that is hosted in black shales.

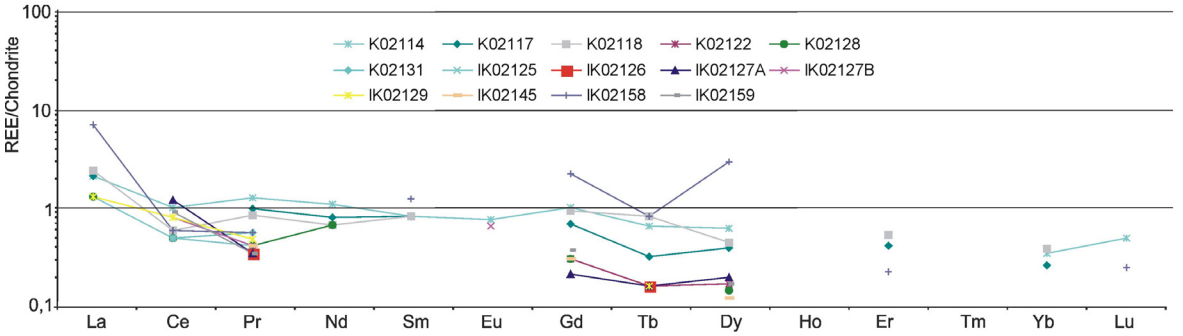

Fig. 95: REE data of the non-sulphide ore of the Kolahdarvazeh mine.

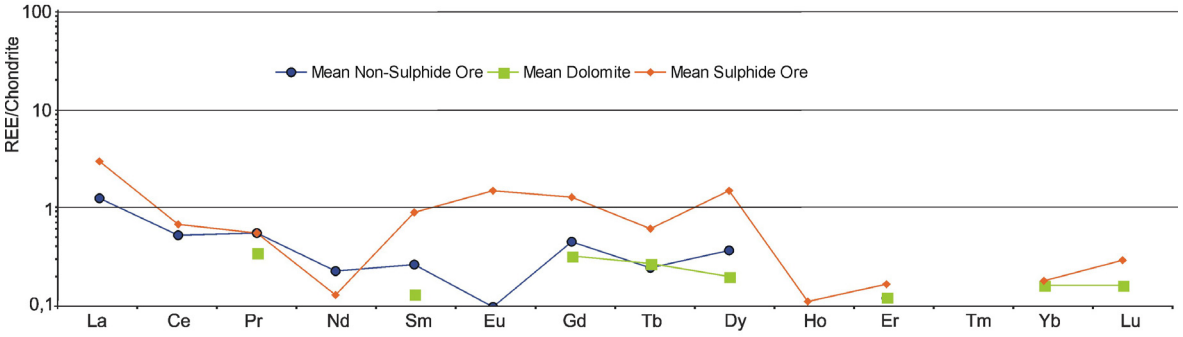

Fig. 96: Mean values of each REE classes: dolomite host rock, sulphide ore, and non-sulphide ore.

4.3 Comparison of the Kolahdarvazeh Mine and Mehdi Abad

The examination of both the Kolahdarvazeh mine and the Mehdi Abad deposit shows similarities as well as differences between them.

Similarities:

In both cases, the sulphide ore as well as the non-sulphide ore are hosted in Cretaceous limestone and dolomite. The occurrence of dolomite is predominantly spatially associated with the sulphide ore and is most likely due to a dolomitisation process during the Zn-Pb-(Cu) mineralisation. The location of sulphide- and non-sulphide ore is controlled and limited by faults (Kolahdarvazeh fault at Irankuh, and Black Hill Fault in Mehdi Abad).

The emplacement of the sulphide protore is laterally limited by faults. Outside these terminating faults the same ore bearing formation shows no notable lead and zinc mineralisation.

The exclusively non-sulphide ore of the Mountain Ore Body in Mehdi Abad, is hosted within topographically higher and exposed located Cretaceous strata, without an alluvial overburden. The non-sulphide ore of the Mountain Ore Body occurs as a matrix of a karst- and fault-breccia as well as a filling of fracture planes. These features are similar to the Kolahdarvazeh ore body, in which a high percentage of the sulphide ore has been oxidised. The mineralised area of the Kolahdarvazeh pit is located on the southern flank of the Irankuh Mountains and is not overlain by an alluvial overburden.

The non-sulphide ore body of both the Koladarvazeh mine as well as the ore body of the MOB at Mehdi Abad is underlyn by less or not permeable strata (MOB: shaly limestone, Kolahdarvazeh mMine: shales).

Differences:

The sulphide ore of Mehdi Abad shows high concentrations of iron and arsenic, which are still present within the oxidised ‘red zinc ore’, due to the immobile behaviour of Fe and As. In contrast to the ‘red zinc ore’ of Mehdi Abad the in-situ oxidised non-sulphide zinc ore of the Kolahdarvazeh pit shows only subordinate amounts of arsenic and iron. A typical non-sulphide ‘red zinc ore’ is absent at the Kolahdarvazeh mine.

The main non-sulphide zinc minerals of the Kolahdarvazeh mine are smithsonite and hydrozincite. Hemimorphite occurs only in subordinate amounts, whereas the non-sulphide ore of the Mehdi Abad MOB consists of both high amounts of hemimorphite and smithsonite/hydrozincite as well.

The MOB of Mehdi Abad shows two main types of non-sulphide ore. The red zinc ore as a result of an in-situ oxidation of a sulphide ore. The ‘white ore’ is the result of a complex dissolution, remobilisation, and reprecipitation process of zinc, which led to a white non-sulphide zinc ore with traces of iron and arsenic. At the Koladahrvaze mine the white zinc ore dominates.

The data and observations of both deposits will be used in the following chapters to develop a comprehensive geochemical model of carbonate-hosted non-sulphide zinc deposits.

5 Data interpretation and numerical modelling of carbonate-hosted non-sulphide zinc deposits

5.1 Limitations of the geochemical model

This geochemical model describes the most important processes of formation of carbonate-hosted non-sulphide zinc deposits and the results of these theoretical assumptions and processes are in agreement with observations that have been made at Mehdi Abad and Irankuh. The model and the assumptions are limited exclusively to a carbonate host rock environment.

The mechanisms of metal separation and the formation of two distinct types of non-sulphide zinc ore are highly dependent on the iron/pyrite content of the sulphide protore. Sulphide ore without pyrite would result predominantly in 'white zinc ore'. On the other hand, a sulphide ore, which fulfils the ideal conditions and consists of pyrite and sphalerite/galena but is influenced by a slow oxidation process, associated with large quantities of water will most likely result in a 'red zinc ore'-dominated non-sulphide deposit. Slow oxidation leads to a limited armoring process and the neutralisation occurs faster – probably just within the oxidation zone. In this case no mentionable metal transport and separation will occur.

Iron is assumed to be immobile within the oxidation zone for the presented general model of metal separation and non-sulphide ore formation: once precipitated as HFO it should remain within this zone. However, the neutralization of the acidic solution leads to a subsequent formation of various amounts of hydrous iron-oxide colloids (RUNNELLS AND RAMPE, 1989). Here, the most important mechanism for transport within the aqueous solution is the mechanical transport of iron as suspended colloidal particles (KIMBALL ET AL 1995). This behaviour is also known from processes similar to the sulphide oxidation, such as the oxidation of sulphide mine tailings and others (FERRERIA DA SILVA ET AL., 2005). The HFO colloid particles are able to transport adsorbed metals (As, Pb, Zn and other) into adjacent regions of the host rock. It is difficult to estimate this effect with regard of the final composition of the white zinc ore.

Thermodynamic data of hemimorphite are not available in literature. Willemite is the exclusive zinc-silicate mineral included in these calculations. Willemite occurs within a wide variety of geological environments and conditions. It can be formed under low-temperature conditions during alteration and oxidation processes of zinc sulphides, and can be found also in supergene non-sulphide zinc deposits (BONI, 2003), e.g in arid environments such as Goodsprings district in Nevada (TAKAHASHI, 1960) as well as under humid climates (JEONG & LEE, 2003), and is also associated with magmatic-hydrothermal processes (BRUGGER ET AL., 2003).

5.2 Important geochemical processes related to the oxidation-zone

The oxidation of the sulphide protore and the related geochemical reactions are highly complex. The most important process is the direct oxidation of solid sulphides by molecular oxygen. Another important process of sulphide (and especially pyrite-) oxidation is the reaction of sulphides with Fe(III)-ions and/or -complexes. Here, Fe(III) acts as an electron acceptor instead of oxygen. Fe(III) is generated by the oxidation of Fe(II) by oxygen or by microbially-driven oxidation of Fe(II) to Fe(III). Finally, other oxidants may be present in the sulphidic mineralised rocks, such as nitrate or manganese (IV) (HERBERT, 1999). However, other oxidation processes than oxygen-driven reactions may occur, but are negligible due to the commonly low concentrations of these other oxidants.

5.2.1 Oxidation of pyrite

The oxidation rate of pyrite is well documented in the work of numerous authors, which studied the oxidation processes of pyrite under different conditions, such as DOMENÈCH et al. (2002). These authors have studied the dissolution rate of pyritic sludge with flow-through experiments. WILLIAMSON & RIMSTIDT ET AL. (1994) presented a dissolution rate law of pyrite as a function of oxygen concentration and pH using data of other authors and studied the dissolution of pyrite by Fe^{3+} (ferric iron).

The oxidation of pyrite and the subsequent hydrolysation of ferric iron play an important role in the genesis of non-sulphide ore deposits. The reaction of oxygen with pyrite generates the highest portion of the sulphuric acid, according to the chemical reactions R1 and R2, whereas the oxidation of sphalerite will generate only minor amounts of sulphuric acid (dependent on the Fe-concentration within the sphalerite, according to reaction R9 (BERTORINO ET AL., 1995)) and the oxidation of galena will produce no acidity at all. Thus, the oxidation of pyrite is the most important factor and source for low pH values within the active oxidation zone of a sulphide ore body.

The following reactions show the oxidation of pyrite by oxygen (reaction R1) and the oxidation of pyrite by ferric iron (reaction R2) (DOLD, 2003):

$$FeS_2 + 7/2\, O_2 + H_2O \rightarrow Fe^{2+} + 2SO_4^{2-} + 2H^+ \qquad \text{R1}$$

$$FeS_2 + 14Fe^{3+} + 8H_2O \rightarrow 15Fe^{2+} + 2SO_4^{2-} + 16H^+ \qquad \text{R2}$$

The oxidation of Fe^{2+} by O_2 (R3) has to precede reaction R2 and is an important part of the iron redox-cycle (SALMON, 2003). Ferric iron leads to the precipitation of Fe-oxihydroxides (reaction R4 and R5) due to a hydrolysation reaction, which, in turn, is coupled with the release of 3 mole H^+ related to 1 mole Fe(III).

This acid-generating step of the oxidising process is followed by a neutralisation reaction, in which the released protons react with the carbonate of the dolomite and/ore limestone or with other minerals, which are capable to neutralise acidic solutions (e.g. feldspar). The elimination of most of the protons will shift the hydrolysation equation R4 and R5 to their right side and will thus stabilise the precipitated Fe-oxihydroxides.

$$2Fe^{2+} + \tfrac{1}{2} O_2 + 2H^+ \rightarrow 2Fe^{3+} + H_2O \quad \text{R3}$$

Fe(III) hydrolysis and release of protons (3mole H^+ per 1 mole Fe(III))

$$Fe^{3+} + 2H_2O \rightleftarrows FeOOH \downarrow +3H^+ \text{ (goethite)} \quad \text{R4}$$

$$2Fe^{3+} + 12H_2O \rightleftarrows Fe_2O_3 * 9H_2O \downarrow +6H^+ \text{ (ferrihydrite)} \quad \text{R5}$$

after STUMM & MORGAN (1996)

Ferric iron is also a strong oxidant of pyrite. At low pH (< 4.5) Fe^{3+} oxidises pyrite faster than oxygen (HERBERT, 1999). The oxidation of pyrite by ferric iron might be an important factor for the oxidation processes at deeper (O_2 undersaturated or O_2 free) levels of a sulphide ore body. The Fe^{3+} can be transported (dissolved as a complex or colloid) to these deeper levels where it probably leads to a widening of the oxidation front. However, this process is highly dependent on the availability of oxygen for the oxidation reaction of Fe^{2+} to Fe^{3+} and the limiting factor for the oxidation of pyrite by both the oxidation by ferric iron and the oxidation by oxygen is the availability of oxygen.

The transport of gasses, especially O_2 dissolved in water, is much less effective than the gaseous transport due to diffusion processes. The diffusion of oxygen is the main parameter governing the dissolution/oxidation of pyrite and other sulphides and the release of metals. Thus, ore bodies, which are influenced by hydraulically unsaturated conditions, are characterised by high metal concentrations within the aqueous solutions (SAALTINK ET AL., 2002). Examinations of oxidation processes of mine tailings have shown that dissolved oxygen may be completely consumed by passing through an organic-rich cover by microbial respiration and organic matter oxidation (HERBERT, 1999). In that case, the oxidation of the sulphides is limited to anoxic microbial activity or the oxidation of pyrite by Fe^{3+}, which slows down the rate of oxidation dramatically.

Another important factor for the oxidation of pyrite is the presence of oxidising bacteria, such as *thiobacillus ferrooxidans*. The presence of these and similar bacteria can increase the oxidation rate of sulphides by several orders of magnitude in an acidic environment. Under low pH (<4) the oxidation of pyrite by acidophilic, chemolithoautotrophic Fe(II) and sulphur/-compound oxidising bacteria predominates over chemical oxidation, obove pH 4 metal sulphides are chemically oxidised predominantly by O_2. The organisms are not attached onto the mineral surface, but the sulphides are being oxidised via the electron shuttle Fe(II)/Fe(III) (SCHIPPERS, 2003). At a pH below 4, Fe(III)-hydroxides become soluble and Fe(III) ions or complexes act as an effective electron acceptor for the oxidation of pyrite. The oxidation of Fe(II) to Fe(III) by micro-organisms is highly dependent on the presence of O_2, which is the predominant primary electron acceptor for all the oxidation processes within the sulphide ore body.

5.2.2 Oxidation of sphalerite and galena

Sphalerite and galena are, beside pyrite, the most important Zn- and Pb-bearing minerals within most types of carbonate-hosted Zn-Pb sulphide deposits. In contrast to the oxidation of pyrite,

which generates the largest volumes of sulphuric acid, the oxidation of galena and sphalerite produces no or only subordinate amounts of protons/acidity. However, during the oxidation process of sulphides, the concentration of SO_4^{2-} ions is highly increased due to the oxidation of galena, sphalerite (reactions R6 to R9) and the associated generation of sulphuric acid due to the oxidation of pyrite (reaction R1).

In case of sphalerite, Fe is able to substitute Zn within the sphalerite up to 15 mol %. This Fe-bearing sphalerite will be an additional source for the generation of acid due to the hydrolysis reactions (R9).

$$PbS + 2O_2 \rightarrow PbSO_4 \downarrow \quad \text{R6}$$

$$PbS + HCO_3^- + 2O_2 \rightarrow PbCO_3 \downarrow + SO_4^{2-} + H^+ \quad \text{R7}$$

$$ZnS + 2O_2 \rightarrow Zn^{2+} + SO_4^{2-} \quad \text{R8}$$

$$4(Zn_{0,75}Fe_{0,25})S + 8O_2 + 2H_2O \rightarrow FeO(OH) \downarrow + 3Zn^{2+} + 4SO_4^{2-} + 3H^+ \quad \text{R9}$$

[Reactions R6 to R9 after BERTORINO, 1995)

5.2.3 Neutralisation reactions and precipitation of secondary minerals

The acid generated during the oxidation process is able to react with other minerals, such as carbonates and several silicates. This dissolution can lead to “acid hyper karst” and generates significant secondary permeability and thus pathways for fluids. Important minerals for the neutralisation of the acid are carbonates such as calcite and dolomite. In many carbonate-hosted deposits, both minerals occur closely intergrown with sulphide ore minerals. However, silicate minerals such as feldspar, muscovite, pyroxene, and amphibole) are rare and thus lead only subordinately to mineral dissolution and the generation of secondary porosity and, subsequently, an enhanced permeability.

Without any neutralisation, the acid, which is produced during the oxidation of pyrite and other sulphides, would results in pH values ranging between 1 and 4 and lower (SEAL ET AL., 2002). However, rare non-sulphide ore deposits do exist, in which the neutralisation has been mainly controlled by the neutralisation reactions from the break-down of feldspar and mica. One prominent example of such type of non-sulphide deposit is the Skorpion deposit in Namibia. Here, the non-sulphide ore is hosted by arkosic meta-arenites and the acid-neutralising break-down reaction of feldspar and mica has formed non-sulphide ore, which consists mainly of sauconite (a zinc-smectite) (KÄRNER & BORG, 2001; BORG ET AL., 2003)

Neutralising reactions result in a pH-increase within the pore fluids and the release and re-precipitation of metal cations from the carbonate host rock, such as Ca^{2+}, Mg^{2+}, and minor amounts of $Fe^{2+/3+}$. These cations commonly participate in the formation of secondary minerals. The in-

crease in pH is accompanied by the precipitation of various (metal-bearing) minerals. Additionally, the newly formed minerals interact in several ways with the metal-bearing aqueous solution. Firstly, the precipitates are able to buffer the aqueous solutions within different ranges of pH (BLOWES & PTACEK, 1994) (Tab. 17) and secondly, the precipitates inhibit the acid-neutralisation reaction with the carbonates of the host rock due to an 'armouring' of the carbonate minerals (HUMICKI, 2004; HUMINICKI & RIMSTIDT 2004). Although an immediate neutralisation by highly reactive carbonate host-rocks (pH of 7 and above) might be expected, the oxidation of sulphides and the 'armoring' of the carbonate minerals result in an oxidation front, which shows a stabilised low pH, ranging approximately from pH 4 to pH 6 (YANFUL & ORLANDEA, 2000).

Tab. 17: The hydrolysis of different secondary Fe(III)-phases releases different amounts of H^+-ions into the aqueous solution and act as a buffer to the geochemical system within the oxidation zone.

Phase	Equatation	Moles H^+	
am. $Fe(OH)_3$(s)	$Fe^{3+} + 3H_2O \rightleftarrows Fe(OH)_3 + 3H^+$	3	R10
ferrihydrite	$10Fe^{3+} + 60H_2O \rightleftarrows Fe_2O_3 \bullet 9H_2O \downarrow + 30H^+$	3	R11
goethite	$Fe^{3+} + 2H_2O \rightleftarrows FeO(OH) \downarrow + 3H^+$	3	R12
hematite	$2Fe^{3+} + 3H_2O \rightleftarrows Fe_2O_3 \downarrow + 6H^+$	3	R13
schwertmannite	$8Fe^{3+} + SO_4^{2-} + 14H_2O \rightleftarrows Fe_8O_8(OH)_6SO_4 \downarrow + 22H^+$	2.75	R14
jarosite	$3Fe^{3+} + K^+ + 2SO_4^{2-} + 6H_2O \rightleftarrows KFe_3(SO_4)_2(OH)_6 \downarrow + 6H^+$	2	R15

am. $Fe(OH)_3$ = amorphous ferric hydroxide, Reactions R10 to R15 after DOLD ET AL. (1999A)

Carbonate minerals and H^+ ions are consumed as a result of the neutralisation, releasing dissolved cations (Ca^{2+} and Mg^{2+}) and mainly bicarbonate HCO_3^- (reactions R16 and R17) into the solution. The carbonate and bicarbonate may react and bond with metal ions such as Cd^{2+}, Mn^{2+}, Zn^{2+}, Pb^{2+}, and others and precipitate these elements as secondary minerals. However, the precipitation of secondary carbonates is highly dependent on the pH of the aqueous solution and requires high pH values.

$$H_2CO_3 \rightleftarrows H^+ + HCO_3^- \qquad \text{R16}$$

$$HCO_3^- \rightleftarrows H^+ + CO_3^{2-} \qquad \text{R17}$$

R16 and R17 after FREEZE & CHERRY (1979)

5.3 Important processes of metal-fractionation

The process of the formation of non-sulphide zinc ore has been examined, with a particular focus on the metal separation process that is a crucial factor in the formation of red and white zinc ore. The results of our investigations show, that multiple processes occur simultaneously during the formation of these different ore types: (1) the armoring effect of minerals (reaction inhibition of galena and calcite), (2) metal sorption onto HFO, and (3) different mineral solubilities and stabilities of various Zn- and Pb-minerals.

5.3.1 Armoring of galena

Observations from the Iranian deposits of Mehdi Abad and Irankuh have shown a preferential corrosion and oxidation of pyrite and sphalerite compared to galena. In most cases, galena is rimmed by anglesite containing abundant sub mm-sized galena inclusions. The size of the anglesite-coating is commonly up to 150 µm and more. These minerals are commonly associated with cerussite, which occurs in the immediate vicinity to- or is partly intergrown with the anglesite. In contrast to galena, other sulphides are less common within the oxidation zone of a sulphide ore body and their occurrence is commonly dependent on the stage of oxidation. Under the assumption that the sulphide ore consists mainly of a pyrite-sphalerite-galena paragenesis, the exclusive occurrence of galena or different oxidation stages of the sulphides suggest different reactivities within the oxidation process. Thus, the relative reactivity for these minerals at Mehdi Abad and Irankuh can be qualitatively characterised as:

pyrite > sphalerite > galena

These empirical field observations are similar to those of oter authors , such as MEGAW ET. AL (1996) and laboratory experiments with varying pH values from 2 to 6 (JAMBOR, 1994). The pH-values used in these laboratory experiments are characteristic for a proposed oxidation zone of carbonate-hosted sulphide Zn-Pb deposits. Thus, the observations of samples from oxidised ores of several Iranian deposits are in agreement with these laboratory results of KAKOVSKY & KOSIKOV (1975) .

The reactivity of pyrite, galena and sphalerite is highly variable and shows differences between the theoretically proposed and the observed reactivity. This reflects the different conditions under which oxidation occurs (e.g. gossans, abiotic, biotic, saturated-, unsaturated zone) (JAMBOR, 1994).

Under the presence of sulphate ions and low-ph conditions (Fig. 97) Pb^{2+} -ions precipitate as anglesite. Anglesite has a low solubility especially in SO_4^{2-} -bearing aqueous solutions (K_s=1.53·10^{-8} mol^2·l^{-2}, FAURE, 1998) and forms (more or less in situ) a coating onto undissolved galena and protects galena from an intensive direct contact with oxidising reagents (Fig. 98). This “protective” coating is probably one explanation for the apparent resistance of galena during the oxidation process. The solubility of zinc sulphates, such as zincosite, in contrast, is much higher and the related zinc- and sulphate concentrations would not be reached with the considered hypothetical initial solution. The precipitation of insoluble lead minerals starts with anglesite at low (acidic) pH values and changes to insoluble carbonates, such as cerussite or hydrocerussite. The formation of cerussite or hydrocerussite is determined by the partial pressure of CO_2. The formation of hydroce-

russite is limited to relatively low P_{CO2} (log p_{CO2}< -1.85 kPa, INGWERSEN, 1990), at higher pH values (approximately at pH 6.2). Thus, lead forms insoluble minerals over the full relevant range of pH, and P_{CO2} , which occur in the acidic oxide zone of sulphide deposits and the basic environment of carbonate host rocks.

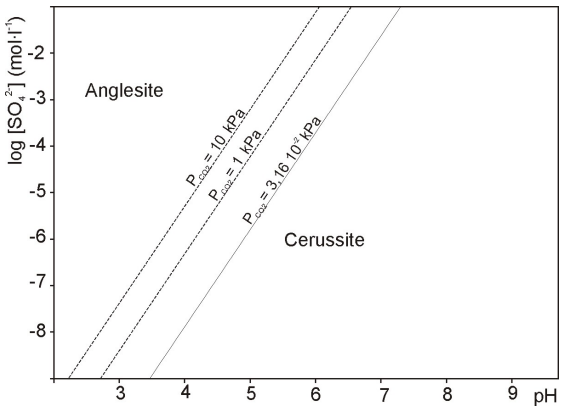

Fig. 97: Stability fields of Anglesite and Cerussite (25 °C, 100 kPa, calculated with Phreeqc). The lines show the phase boundary for different CO_2 partial pressures. Anglesite is stable even at low sulphate concentrations and at low pH. (atmospheric P_{CO2} = $3.16 \cdot 10^{-2}$ kPa)

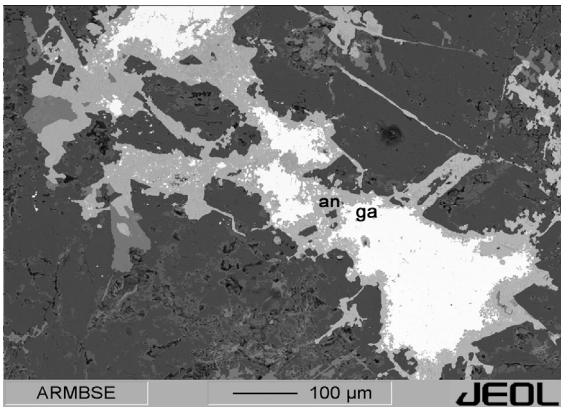

Fig. 98: SEM backscatter image of galena-relicts (**ga**) within dolomite. The galena is partly oxidised to anglesite (**an**). The anglesite encloses the galena and forms a coating, which inhibits the galena from further oxidation. Sphalerite and pyrite are absent, due to their complete oxidation.

Thus, the relative resistivity of galena within the oxidation process is best explained by armouring effects. Armored galena have been observed on samples from Mehdi Abad, Irankuh, and Ku-e-Surmeh and have also been described for other oxidised sulphides by several other authors as well, e.g. JEONG & LEE, (2003). The immediate precipitation of anglesite under acidic conditions results in two effects: i) the reaction inhibition by 'armoring' and thus prevention of a fast oxidation of galena, and ii) the concentration of Pb^{2+} ions within the aqueous solution is limited by the solubility of anglesite (log_a Pb^{2+} < -3.5 mol*l^{-1}).

5.3.2 Armoring of calcite

The neutralisation of sulphuric acid by calcite, as described in reaction R9, leads to the precipitation of gypsum, accompanied by the precipitation of Fe-oxihydroxides due to raised pH values. In general, this leads to a strongly adhesive encrustation of calcite and/or other minerals and to a partially or almost totally suppressed reactivity of the encrusted minerals (HUMINICKI, 2004; HUMINICKI & RIMSTIDT 2004; WILKINS ET AL., 2001).

Recent investigations of HUMICKI (2004), HUMINICKI & RIMSTIDT (2004), WILKINS ET AL. (2001), YANFUL & ORLANDEA (2000) and others have focussed on the reaction between sulphuric acid and carbonates and the effects of precipitation of gypsum coatings on the surface of calcite. Experiments that have measured the rate of calcite dissolution in conjunction with gypsum and/or iron hydroxide precipitation on the surface of calcite show that gypsum rather than iron hydroxide coatings may influence the neutralisation in slowing down the dissolution rate of the limestone in a car-

bonate host rock (Fig. 99). The isolation of calcite from further reaction by gypsum prevents the limestone from generating any additional alkalinity in the system (HAMMARSTROM, 2002).

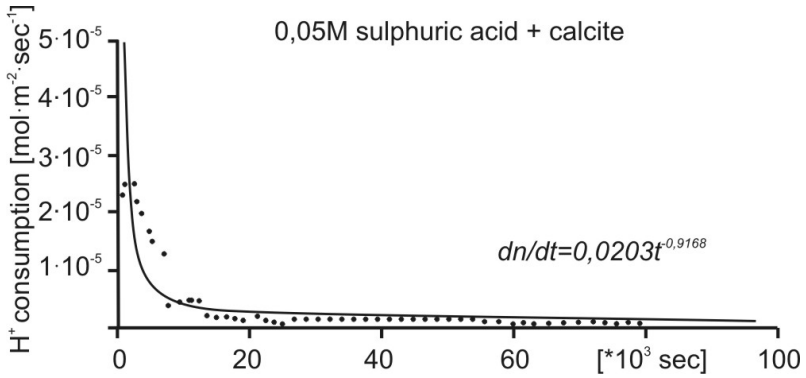

Fig. 99: The rate of calcite dissolution (measured as proton consumption) decreases rapidly with time. This is an effect of the $CaSO_4$-coating of calcite. The oxidation of a sulphide ore body is a long lasting process, which is reflected in high values on the time-axis of this diagram - associated with low H+ consumption rates of the calcite. (after Huminicki, 2004)

These observations are highly relevant for any oxidation- and metal-fractionation model of non-sulphide zinc deposits. As a result of the decreased reactivity of gypsum-coated carbonates, the pH-value of the metal-bearing aqueous solutions increase along the fluid path over a long distance. This provides the possibility for the metals to fractionate and precipitate spatially separately, depending on the pH of the solution.

The concentration of SO_4^{2-} ions is highly increased during the oxidation of sulphides (oxidation of galena, sphalerite, reactions, R6 to R9) and the associated generation of sulphuric acid due to the oxidising of pyrite (reaction R1and R2). The solubility of gypsum in these acidic SO_4^{2-}-rich fluids is much less than in pure water due to the common ion effect (*Le Chatelier's Principle*) (formula F 3). Under these conditions, gypsum is insoluble and forms a stable coating.

After the oxidation of the sulphides, the SO_4^{2-} concentration decreases rapidly, gypsum becomes much more soluble and is transported out of the (karst- and non-sulphide zinc) systems. The solubility of gypsum under normal aqueous conditions ($K_{sp}=1.9 \cdot 10^{-4}$) is higher than the solubility of calcite and dolomite.

$$CaCO_3 + 2H^+ + SO_4^{2-} + 2H_2O \rightarrow CaSO_4 \cdot 2H_2O \downarrow + H_2CO_{3(aq.)}$$ after WILKINS ET AL. (2001), R9

$$K_{sp} = \frac{a_{Ca^{2+}} a_{SO_4^{2-}}}{a_{CaSO_4}} \approx \left[Ca^{2+}\right]\left[SO_4^{2-}\right] = 1,9 * 10^{-4}$$ F 3

An additional mechanism for the armoring of limestone is the precipitation of Fe-oxihydroxides. The mechanisms, by which Fe-oxihydroxides armour limestone is still poorly understood. However, the reactivity of Fe-armoured limestone has been estimated to range from 4% to 62% compared to the reactivity of 'fresh' limestone (SUN ET AL., 2000).

The difference in the effectiveness for the armoring of carbonate minerals by either gypsum- or ferrihydrite-coatings is due to the geochemical origin and genesis of both types of coatings. Gypsum precipitates close to or immediately onto the carbonates as a result of a neutralisation reaction, whereas ferrihydrite has to be transported as insoluble particles towards the calcite to be available for armoring. A combination of both armoring mechanisms is presumably particularly effective to maintain a stable acidic environment within the oxidation zone of a carbonate-hosted sulphide ore body. Thus, the dissolution of primary and the precipitation of secondary minerals and the metal transport within the active oxidation zone is modelled for these most common conditions.

Contrary to expectations, which would suggest an immediate neutralisation within the highly reactive host carbonates (pH of 7 and above), the oxidation of sulphides and the armoring of the carbonates results in an oxidation front, which shows stable low pH values, ranging from approximately pH 4 to pH 6. Observations of sulphide- and carbonate-bearing mine tailings show, that the oxidation of sulphides leads to low pH values within a carbonate-dominated environment due to armoring effects (YANFUL & ORLANDEA, 2000). Long-term experiments by several authors, such as YANFUL & ORLANDEA, (2000), have shown the effects of limestone armoring to the neutralisation of acid mine drainage (ARD). The added limestone lost its effectiveness for neutralisation after a couple of years, as a result of the precipitation of secondary minerals onto the limestone particles.

5.3.3 Metal sorption onto ferrihydrite

Cu, Cd, Pb, Zn and As can be adsorbed onto Fe-oxyhydroxides (goethite, ferrihydrite) and this process of cation–adsorption onto hydrous ferric oxides is highly dependent on the pH level of the aqueous solution (MARTINEZ & MCBRIDE, 2001; DZOMBAK & MOREL, 1990). The chemical behaviour and mobility of metal cations are largely controlled by their interaction with these iron-oxides (TRIVEDI ET AL., 2003). Ferric hydroxides have specifically high surface areas (up to 600 m^2g^{-1}) (Lee & Saunders, 2003). This high surface area, associated with the affinity of ferric iron hydroxides to Me(II)-ions, results in a highly effective adsorption process controlled by pH and metal concentration.

Lead and zinc show different degrees of absorption onto ferrihydrites as shown in. The quantitative binding of Pb(II)-ions onto ferrihydrite reaches its maximum and the saturation of the ferrihydrite at approximately pH 5.5 (DYER ET. AL, 2003; RUTHERFORD, 2002). In contrast to lead, quantitative zinc adsorption starts at higher pH values, ranging from approximately pH 5.5 to 7.5 (DZOMBAK & MOREL, 1990). This is an additional, important reason for the metal separation and fractionation of lead and zinc within non-sulphide ore bodies. Most of the lead within the oxidation front is adsorbed under acidic condition onto hydrous ferric oxides. Under these acidic conditions however, zinc remains mobile in the aqueous solution and is, consequently, transported further (vertically or laterally) to distal areas. The pH increases slightly due to the neutralisation inhibition by the $CaSO_4$ and Fe-oxyhydroxide armoring of the carbonate host rock. As a result, zinc precipitates in distal (commonly deeper) portions of the supergene system, which are commonly free of hydrous ferric oxides and lack any substantial secondary lead accumulations.

Fe-oxyhydroxides occur as nanometre-sized colloidal precipitates. These colloidal precipitates can be transported in aqueous solutions into spatially deeper or to more distal levels (RUTHERFORD, 2002) dependent on the (acid-) karst system, fault systems and the general porosity and perme-

ability of the host rock. Thus, it is important to note that the occurrence of red Fe-oxides alone is not a sufficient indicator of a sulphide (proto-) ore that existed originally at this position.

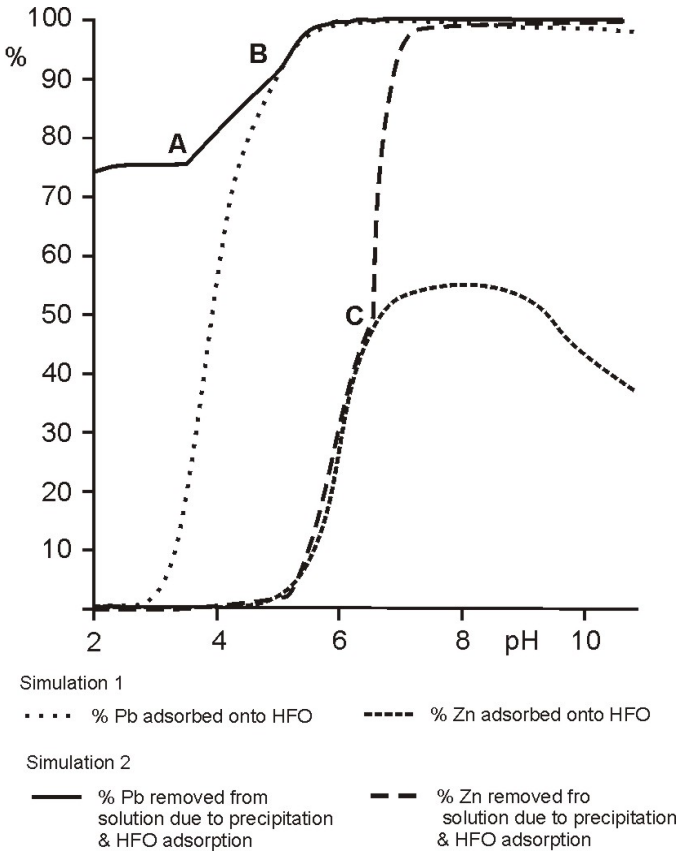

Fig. 100:
PHREEQC precipitation and adsorption simulation of a hypothetical metal-rich, which contains 2.4 10^{-2} mol Zn, 1.6 10^{-5} mol Pb. In **simulation 1** the Zn-Pb solution is in reaction and equilibrium with hydrous ferric oxides (HFO). The adsorption curves of Zn^{2+} and Pb^{2+} show clearly the dependence of the amount of adsorption to the pH. The quantitative adsorption of lead starts at approximately pH 3, and zinc at pH 5. **Simulation 2** is more realistic and shows the effect of the additional removement of Zn and Pb due to the precipitation of anglesite, cerussite, and hydrozincite. Until Point A nearly 75 % of lead have been removed from the solution due to the precipitation of anglesite. At point (**A**) additional adsorption effects take account and the concentration of lead reaches the adsorption isotherme at point (**B**). Zinc does not form insoluble sulphate minerals. Thus, zinc is removed from solution due to adsorption effects exclusively. At point (C) precipitation of hydrozincite starts and most portion of the zinc is removed from solution.

The sorption of metal-ions as well as carbonate-ions onto hydrous ferric oxides (HFO) is a function of pH (DZOMBAK AND MOREL, 1990). HFO is also called amorphous ferric hydroxide, or amorphous iron hydroxide and is a precipitate, which forms upon rapid hydrolysis-precipitation from ferric iron solutions. Hydrous ferric oxide is a poorly crystalline, highly porous solid with a large surface area from 200 m^2g^{-1} to approximately 750 m^2g^{-1}. The mineral-to-water interface of HFO has a pH-dependent charge and is highly reactive (HOFMANN ET AL., 2004). The reactive surfaces of metal oxides, such as hydrous ferric oxide in natural waters are predominantly covered by carbonate species (CO_3^{2-}, HCO_3^-). The lower availability of sorption sites affects sorption of other metals such as Cd, Cu, Ni, Pb, Zn and As and thus influences the mobility of these heavy metals in the natural environment.

The adsorption onto HFO plays an important role for the oxidation processes of Fe-rich Zn-(Pb) sulphide ores. The high amount of iron within the initial sulphide ore is a requirement for the formation of two different types of non-sulphide ore: the red zinc ore and the white zinc ore. The results of the calculated metal sorption (Fig. 100) onto HFO supports the explanation of several aspects and phenomena related to the formation of the red zinc ore and the white zinc ore. It is possible to envisage several scenarios of pH for the oxidation zone. The most interesting range of pH reflects acidic conditions of approximately pH 5 to 6.5 within the oxidation zone, where several effects interact. By applying the effects of HFO adsorption to the hypothetical Zn-Pb-Fe-rich solution of an oxidation zone, one can assume that HFO is able to adsorb up to 3 % of the zinc from the solution

and additionally adsorb up to 18% lead from this solution. In contrast to zinc, which is exclusively bound to HFO, the biggest portion of lead is removed from the solution due to the precipitation of anglesite. Thus, the final aqueous solution, which leaves the oxide zone is still rich in zinc but shows only traces of lead.

The ability of HFO to bind particularly zinc within the oxidation front depends on the local characteristics of each oxidation front.

5.4 Formation of hemimorphite, smithsonite, and hydrozincite, occurrence and mechanisms

5.4.1 Hemimorphite

Hemimorphite occurs as the most common zinc hydrosilicate mineral in all of the Iranian non-sulphide zinc deposits examined in this study. Other secondary zinc silicates, such as sauconite or willemite are rare or absent. In most cases, hemimorphite occurs in veins and open spaces of the 'white-' and 'red zinc-ore', within fault zones and -breccias and in the matrix of fault breccias as

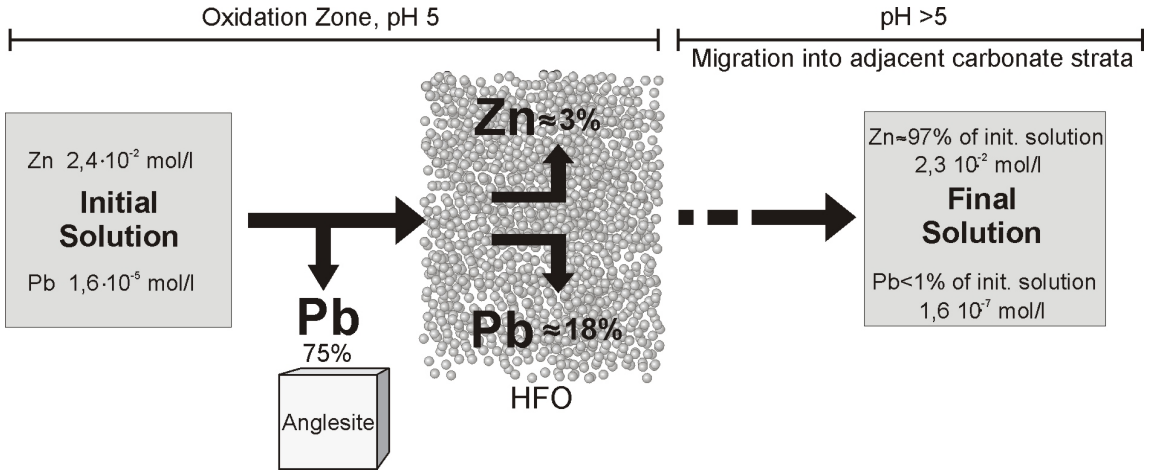

Fig. 101: Schematic processes and mass balance for precipitation and adsorption of Zn and Pb within an HFO-rich oxidation zone at pH=5. Zn and Pb are adsorbed by HFO. Lead, additionally, precipitates as Anglesite within the oxidation zone. Calculated data are based on a hypothetical Zb-Pb-Fe rich solution (see also Methods).

euhedral crystals, which have grown perpendicular to the underlying surface of fractures and spaces (Fig. 102). The size of the hemimorphite crystals ranges from sub-mm up to several millimetres. In some cases, several generations of hemimorphite can be distinguished. This phenomenon of several stages of hemimorphite precipitation is common, especially at the Mountain Ore Body (MOB) of Mehdi Abad (REICHERT & BORG, 2003), but also visible at Irankuh.

Zinc carbonates are soluble under acidic conditions and start to precipitate as smithsonite/hydrozincite at approximately pH 6.5 , depending on the P_{CO2} and the activity of Zn^{2+} (Fig. 103 and Fig. 104). Zinc silicate minerals will form if silica is available and the partial pressure of CO_2 is

low (Fig. 104). Hemimorphite is not commonly observed as a first stage mineral within the paragenetic sequence. Observations from Mehdi Abad and Irankuh (and reports for carbonate host rocks by TAKAHASHI, 1960 and others) have shown that hemimorphite is related to late or even last stages of non-sulphide mineralisation processes growing within fractures and open spaces of the 'white-' and 'red zinc-ore' Fig. 102 growing over long periods

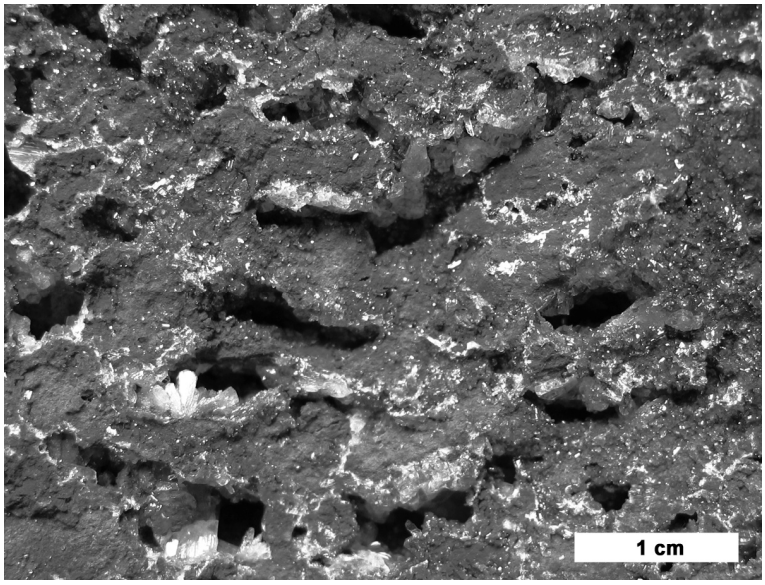

Fig. 102: Hemimorphite (white/colourless), which grewed in open spaces of a red zinc ore. Hemimorphite occurs as a late stage mineral locally in large quantities.

The quantitative precipitation of hemimorphite and other zinc-silicates is dependent on the availability of silica. For this reason, it is necessary to consider the geochemical behaviour of such fluids with respect to SiO_2 as well. The solubility of silica phases increases drastically from crystalline quartz to amorphous silica (DOVE & RIMSTIDT, 1994). H_4SiO_4 is a weak acid and dissociates appreciably about two pH units above neutrality (DOVE & RIMSTIDT, 1994). The carbonate dissolution process within a 'closed' system consumes enough H^+ to increase the solubility of SiO_2 significantly. The availability of dissolved silica is limited by the solubility of SiO_2 in water and the slow dissolution rate of SiO_2. Thus, silica within natural waters is not sufficient for an effective and quantitative binding of zinc. The biggest portion of zinc will precipitate as carbonates. Calculations with PHREEQC (Tab. 20) show, that SiO_2 concentration in carbonate-buffered solutions reaches $9.6 \cdot 10^{-4}$ mol$\cdot$l^{-1} for crystalline quartz and up to $2.0 \cdot 10^{-3}$ mol$\cdot$l^{-1} for amorphous quartz (chert). Thus, chert provides the highest concentrations of SiO_2 in aqueous solution. The low concentrations of dissolved silica lead to the precipitation of small amounts of Zn-silicates only, and, consequently, zinc precipitates at the oxidation stage predominantly as zinc carbonates from the supergene fluids.

Hemimorphite is less soluble than hydrozincite over a pH range from 5 up to approximately 7.6 under atmospheric pressure logP_{CO2}= -1.5 kPa (Fig. 103). Under these conditions, hemimorphite is more stable than hydrozincite and should precipitate. However, the stability fields occur close together and can be shifted easily by varying the P_{CO2} values and by the chemistry of the mineral assemblage in equilibrium with the aqueous solution (Tab. 18).

According to Tab. 18, an intimate association of dolomite/calcite with smithsonite and/or hydrozincite results in ph-values, which do not reach the stability of hemimorphite. The 'white zinc ore', found in numerous deposits, consists predominantly of smithsonite and/or hydrozincite. Thus, the phases, which are in equilibrium with the aqueous solution, are limited to smithsonite and/or hydrozincite. The resulting pH values for the equilibrium with aqueous solutions are lower with re-

spect to the calcite/dolomite-dominated mixtures (Tab. 18). Here, the stability of hemimorphite is reached for log_P_{CO2} < -0.5 kPa. Higher values of P_{CO2} (log_P_{CO2} > -0.5 kPa) support the precipitation of hydrozincite or smithsonite. Thus, the precipitation of hemimorphite is limited to relatively low P_{CO2} values, which occur preferentially in arid climates with low biological activities within the soil and deep groundwater tables.

Tab. 18: pH values for equilibrated mineral associations dependent on P_{CO2}.

Log P_{CO2} [kPa]	**-1.5**	**-1**	**-0.5**	**0**	**0.5**	**1**
pH value for dolomite/sm/hy association	8.28	7.95	7.62	7.30	6.97	6.65
pH values for calcite/sm/hy association	8.18	7.85	7.53	7.2	6.88	6.55
PH values for sm/hy association	7.42	7.2	6.96	6.73	6.46	6.14

sm: smithsonite, hy: hydrozincite, equilibrium reaction calculated with PHREEQC.

The data and calculations presented by TAKAHASHI (1960), MCPHAIL ET AL. (2003) and INGWERSEN (1990) indicate that the zinc silicates hemimorphite and willemite are the least soluble and most stable Zn-minerals in a pH range less then pH 7 (at atmospheric P_{CO2}) compared with zinc carbonates. Thus, hemimorphite can be interpreted as a mineral, formed under acidic to slightly basic conditions and thus should precipitate as the earliest non-sulphide zinc mineral.

In general, hemimorphite was formed after the oxidation of a sulphide ore, probably as a result of dissolution and re-precipitation of precursor zinc carbonate minerals. An exception, in which hemimorphite can be assumed as a quantitatively important first stage mineral, is the Mountain Ore Body (MOB) of Mehdi Abad. Here, at the MOB, hemimorphite occurs in large quantities and at least two different stages for the formation of hemimorphite are distinguishable (REICHERT ET AL., 2003).

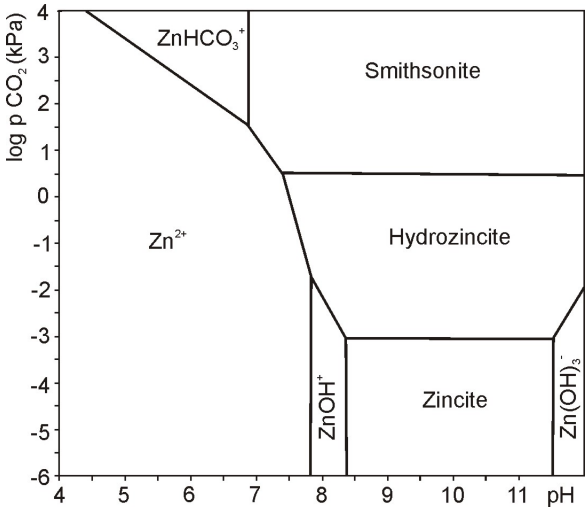

Fig. 103: Stability of zinc carbonates in the chemical system Zn-O-H-C dependent to P_{CO2} and the pH. The activity of zinc is a(Zn)= 10^{-5} (after MCPHAIL ET AL. (2003)

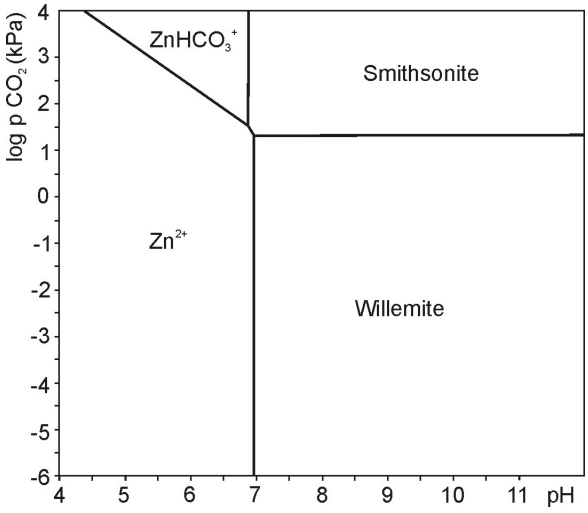

Fig. 104: Zinc mineral stabilities dependent to pH and p_{CO2} for a silica and carbonate containing solution. Smithsonite becomes stable at relative high partial pressures of CO_2 (p_{CO2}> 3.16 kPa) in the chemical system Zn-O-H-C-Si (after MCPHAIL ET AL. (2003).

5.5 Geochemical genetic model for carbonate-hosted non-sulphide deposits

5.5.1 A metallogenetic model for carbonate hosted non-sulphide zinc deposits

The model attempts to explain the genesis of carbonate-hosted non-sulphide zinc deposits sensu lato and related ore types, such as red zinc ore and the white zinc ore sensu stricto and is primarily adapted to carbonate-hosted non-sulphide zinc deposits with a distinct karst- and acid-karst breccia zone. Good examples for this type of deposit are the Mountain Ore Body (MOB) of Mehdi Abad and the Kohladarvazeh pit within the Irankuh deposit. These share similar typical geological attributes, resulting in the occurrence of the same types of non-sulphide zinc ore. At least three important factors for the genesis of this type of non-sulphide zinc deposit can be distinguished:

(i) The first important feature is a proto-sulphide ore close to surface. All of the investigated Iranian deposits are characterised by sulphide ore at or closely below the surface due to intensified exhumation rates, and which can easily be reached by supergene meteoric fluids and by oxygen. The (present) depths of the sulphide ore ranges from 10's of meters (Irankuh) to 130 meters and more (Mehdi Abad). The near-surface and partly exposed position of the sulphides in areas of high topographic relief are important factors that support a fast and effective oxidation process.

(ii) Secondly, the presence of karst-originated breccia clasts seems to be important for the formation of large quantities of non-sulphide ore. The breccia clasts are characterised by high surface area, high porosity and good permeability that allows metal-carrying groundwater to penetrate easily. The non-sulphide zinc minerals precipitated from these fluids and now form pore-filling cements to the karst fragments

(iii) The third important factor in the investigated deposits is the proximity of an aquiclude or aquifuge, such as shales (Irankuh, Kuh-e-Surmeh (REICHERT & BORG, 2002), shaly limestone (Mehdi Abad: Mountain Ore Body) and schists (Angouran) (DALIRAN & BORG, 2004). The aquiclude acts as a nearly impermeable and insoluble barrier for meteoric water, the groundwater system, and the metal-delivering fluids. This hydraulic barrier stops descending fluids, such as meteoric recharge from the surface and leads to a mixing with the local aquifer. These mixing processes can result in an increased capability to dissolve calcite and thus causes additional karst processes. The underlying aquiclude leads to a "ponding" of fluids in front of the hydraulic barrier.

These geological features suggest a general process of oxidation and the formation of non-sulphide zinc ore that can be explained in several stages:

At a first step, the sulphide-ore-bearing carbonate sequence was uplifted and the overburden eroded. Subsequently, the carbonate sequence reached a near surface environment and was penetrated by meteoric water and groundwater. This activated karst processes in the saturated zone and the adjacent strata. Extensive karst processes, supported by numerous faults and fractures, have affected the carbonate host rock. Partitioning of the bedding planes and the related fractures might have been additionally used by meteoric water for karst-processes.

The karst system supported the influx of oxygen and thus supported the oxidation process of the sulphide ore. Bedding planes and related (karst-) fractures additionally act as conduits for the supergene Zn-(Pb-) bearing fluids and the metal-bearing supergene fluids migrated to the underlying

breccia zone. The volume of the karst breccia zone and the related high surface area of the breccia-clasts provided a highly reactive surface and excellent porosity for the precipitation of the non-sulphide ore. A high portion of the non-sulphide zinc ore occurs as a cement to breccia clasts that originated from karst-collapse and the size of the breccia clasts ranges from sub-centimetre up to several decimetres.

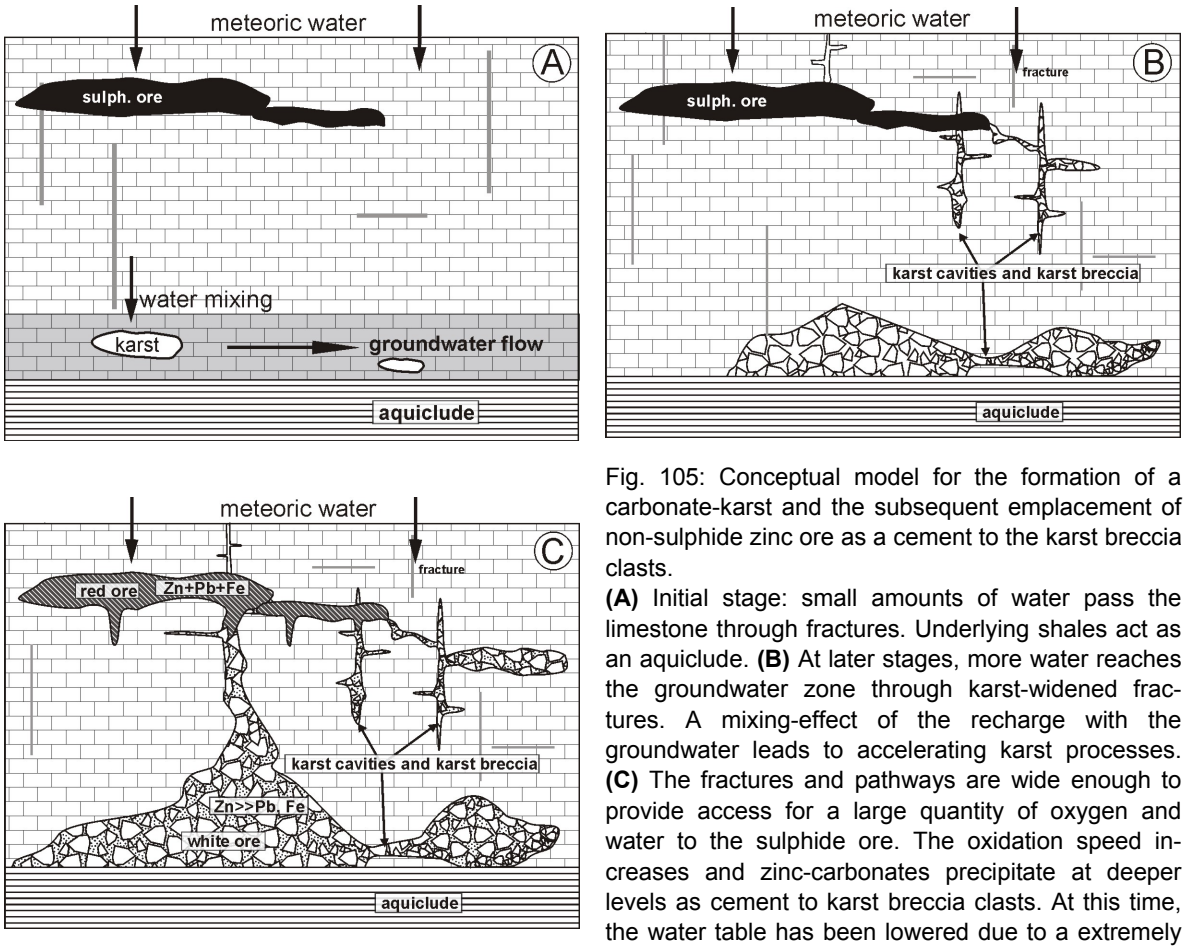

Fig. 105: Conceptual model for the formation of a carbonate-karst and the subsequent emplacement of non-sulphide zinc ore as a cement to the karst breccia clasts.
(A) Initial stage: small amounts of water pass the limestone through fractures. Underlying shales act as an aquiclude. **(B)** At later stages, more water reaches the groundwater zone through karst-widened fractures. A mixing-effect of the recharge with the groundwater leads to accelerating karst processes. **(C)** The fractures and pathways are wide enough to provide access for a large quantity of oxygen and water to the sulphide ore. The oxidation speed increases and zinc-carbonates precipitate at deeper levels as cement to karst breccia clasts. At this time, the water table has been lowered due to a extremely arid climate.

Typical massive and disseminated sulphide ores contain iron, which is bound to pyrite, sphalerite, and Cu-Fe-sulphides. Most of the iron, released during the oxidation process precipitates as largely insoluble hydrous ferric oxides (goethite, ferrihydrite) (reaction R3 & R4). The oxidation front and the adjacent areas are characterised by low pH-values, due to the precipitation of $CaSO_4$ (reaction R9) and subsequent coating of the calcite/dolomite host rock. This coating inhibits the neutralisation of sulphuric acid as described above. The pH-value should be relatively stable over a broad spatial range of the oxidation front and the adjacent regions and deeper levels, which are typically affected by the acidic fluids with low pH values. The low pH-value (pH<5) within the oxidation front, in turn, is important for the sorption of metals onto these ferrihydrites and, as a consequence, the metal fractionation processes.

5.5.2 Theoretical studies on the precipitation of secondary supergene minerals

The solubility and the precipitation of secondary minerals are predominantly triggered by pressure, temperature, P_{CO2}, pH, and element concentration of different species within the aqueous solution (TAKAHASHI, 1960). The Eh (oxidation-reduction potential) is not related to the stability boundaries and the precipitation of these minerals, since there is no change in the valences of the elements during the (re-) precipitation process (TAKAHASHI, 1960). Temperature and pressure of supergene conditions have been assumed to be constant at 25 °C and 101.3 kPa. Thus, the controlling factors involved in the formation of the most common secondary minerals (anglesite, cerussite, smithsonite, hydrozincite, hemimorphite, Fe-oxihydroxides, gypsum, calcite, dolomite) can be assumed as pH, total carbon dioxide in solution (dependent on the P_{CO2}), concentration of silica, sulphur (predominantly as SO_4^{2-}), and the concentration of the (metal-) cations (Ca^{2+}, Mg^{2+}, Zn^{2+}, Pb^{2+}, Fe^{3+}).

The occurrence of minerals is determined by their solubility, which can be calculated for equilibrium conditions. A mineral starts to precipitate under equilibrium conditions if its solubility limit is reached and the saturation index Si_[mineral] equals 0. These individual conditions for various minerals will be described below.

Smithsonite and hydrozincite

Fig. 103 shows the stability field for zinc carbonates at different P_{CO2} values, which depend on the mineral stability, on the pH value and the influence of the P_{CO2}. Generally, an increase of P_{CO2} leads to an increased stability of Zn- and Pb-carbonates within the relevant pH interval for a carbonate environment/host rocks. This effect is due to the raised activity of HCO_3^- and CO_3^{2-} ions within the aqueous solution.

The most common zinc carbonate hydroxide mineral at Irankuh and the MOB of Mehdi Abad is hydrozincite ($Zn_5(CO_3)_2(OH)_6$). Smithsonite ($ZnCO_3$) is detectable in most of the non-sulphide mineralised samples, but occurs only in subordinated amounts compared to hydrozincite. The reason for this disproportion between hydrozincite and smithsonite is the influence of the partial pressure of CO_2. The precipitation of smithsonite is restricted to relatively high P_{CO2} values (log P_{CO2} ≈ 0.2 kPa) TAKAHASHI (1960). Thus, regarding the atmospheric P_{CO2} value (Tab. 19), it is not possible to precipitate smithsonite from an aqueous solution, which is in equilibrium with the atmosphere. The atmospheric P_{CO2} is much lower (SIGG & STUMM, 1989) as the minimum conditions required for the precipitation of smithsonite ($\log P(CO_2)_{atm} << \log P(CO_2)_{soil} << \log P(CO_2)_{smithsonite}$)(Tab. 19).

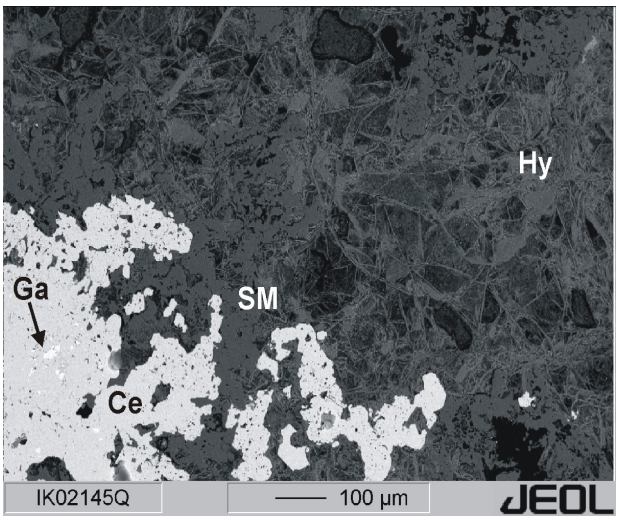

.Fig. 106: BSE image of partly oxidised sulphide ore. The most common non-sulphide zinc minerals are smithonite and hydrozincite. Relics of galena (Ga) are surrounded by cerussite (Ce). Massive and anhedral smithsonite (Sm) is overgrown (or was altered to) hydrozincite (Hy). The formation of smithsonite indicates the presence of high CO_2 partial pressures most likely at a precursor stage. However, the overgrown and smithsonite replacing hydrozincite at later/last stages indicate that hydrozincite became more stable. The process of alteration of smithsonite to hydrozincite is believed to be still active today and caused by open fractures and thus by equilibrium processes with the atmospheric P_{CO2}. (Irankuh, Sample IK02145)

Tab. 19: Typical values of P_{CO2} within the atmosphere, soils and partial pressure for smithsonite precipitation.

atmospheric log P_{CO2} (1)	**soil log P_{CO2} (2)**	**minimum log P_{CO2} – smithsonite (3)**
0…-2 kPa (actual log P(CO_2)= -1.5kPa)	0.5…5 kPa	0.24 kPa (15 °C) 1.4 kPa (40 °C)

(1) SIGG & STUMM, 1989; (2) after SCHEFFER & SCHACHTSCHABEL, 2002; GRYSCHKO & HORLACHER, 1997, (3) AFTER TAKAHASHI, 1960;

A logP_{CO2} = 0.2 kPa (at 15 °C) is valid for the formation of smithsonite according to the equation (after TAKAHASHI, 1960):

$$5ZnCO_3 + 3H_2O \leftrightarrow 2Zn_5(CO_3)_2(OH)_6 + 3CO_2 \qquad \text{R18}$$

The reaction would be driven to the right in case of logP_{CO2} < 0.2 kPa and hydrozincite would precipitate. These conditions are common for aqueous solutions, which are in equilibrium with the atmosphere, such as surface near solutions in unsaturated zones.

In contrast to these equilibrium conditions, aqueous solutions at deeper levels or water-saturated zones are in disequilibrium with the atmospheric CO_2 and reach values, which are favourable for the precipitation of smithsonite. Increasing carbonate concentrations as well as a high P_{CO2} tend to stabilise smithsonite and other carbonate-bearing minerals (MCPHAIL ET AL., 2003). Thus, the dominance of hydrozincite in the non-sulphide deposits of Iran-Kuh, and Mehdi Abad, Kuh-e-Surmeh (REICHERT & BORG, 2002), support the thesis of (near-) equilibrium conditions with the atmosphere.

All these examined non-sulphide zinc deposits are near-surface examples or are situated on the flanks of high topographic relief mountain ranges, associated with faults and intensively brecciated host-rocks. However, the occurrence of corroded traces of smithsonite, mostly replaced by hydrozincite within these three observed deposits suggests periods of raised P_{CO2} during which this early smithsonite was formed.

5.5.3 Possible reasons for high CO_2 partial pressures for the formation of smithsonite

Several sources of CO_2 are possible to explain the elevated P_{CO2} and thus the disequilibrium with the atmosphere The authors consider that the biggest portion of smithsonite as having been produced during the early stages of formation of the non-sulphide zinc deposits - contemporaneous with the oxidation of the sulphide ore body. The smithsonite in samples of Mehdi-Abad and Irankuh shows textures of corrosion and alteration to hydrozincite, which is the most common zinc carbonate mineral at the investigated non-sulphide deposits. The present atmospheric and climatic related P_{CO2} conditions in Iran favour the formation of hydrozincite only. As seen above, the precipitation and stability of smithsonite is limited to sufficiently high P_{CO2}. Since the formation of smithsonite is limited to high partial pressures of carbon dioxide, one has to consider additional sources of CO_2 that was available during its formation.

One well-known source of carbon dioxide are biological processes. These processes consume O_2 and oxidise mainly organic carbon to CO_2. The partial pressure of the biological induced CO_2 is able to increase up to values that reach the stability field of smithsonite. However, thick organic soil coverage in a humid climate on top of the oxidising sulphide ore consumes oxygen and thus hinders/inhibits the oxidation process of the sulphides.

Another important additional source of CO_2 is probably from the generation during the neutralisation of the acidic aqueous solution, derived from the oxidation process of the sulphide ore. This acidic solution reacts with the carbonates of the host rock (PALMER & PALMER, 2000; RITCHIE, 1994; LAPAKKO, 2002). The results of his reaction are gypsum (and other salts), water and carbon dioxide. The highest portion of the CO_2 generated through this neutralisation reaction dissolves in the aqueous solution as $H_2CO_3^0$. The dissolved $H_2CO_3^0$ can degas CO_2 to achieve equilibrium with the pore gasses. This process has been measured at carbonate-bearing sulphide mine tailings. Here, carbon dioxide increases from 0.15 vol. % at surface near tailing regions to concentrations as high as 24 vol. % within the tailings (GERMAIN ET AL. 1994) that is equivalent to a partial pressure of log-P_{CO2}=1.38 kPa.

$$CaCO_3 + 2H^+ + SO_4^{2-} \rightleftarrows H_2CO_3^o + CaSO_4(s)\cdot 2H_2O \qquad \text{pH>6.4} \qquad \text{R19}$$

$$CaCO_3 + 2H^+ + SO_4^{2-} \rightleftarrows HCO_3^- + H^+ + CaSO_4(s)\cdot 2H_2O \qquad \text{pH<6.4} \qquad \text{R20}$$

Thus, one can consider that H_2CO_3 dissociation to H_2O and CO_2 increases the partial pressure of CO_2 not only locally at the oxidation zone of the sulphide ore, but also adjacent to the oxidation zone due to four principal processes. These processes can be postulated as:

(1) Immediate degassing of CO_2 as a result of the equilibration with the pore gas

(2) Transport of CO_2 mainly dissolved as H_2CO_3 into adjacent areas of the host rock and thus the time-delayed degassing of CO_2

(3) Diffusion of CO_2 through the open pores of the host rock and/or karst spaces. The time-delayed degassing of CO_2 is due to a slow equilibrium reaction

The neutralisation processes is favoured here as the main source of carbon dioxide, which caused the high partial pressures of CO_2 and thus precipitation of the first-stage smithsonite. This CO_2-source is independent of the climate and is available even at low temperatures (which additionally support the formation of smithsonite). The high partial pressure of carbon dioxide is active as long as the oxidation process is in progress. Thus, it is possible to generate high P_{CO2} in an arid climate without or with low biological activities only. Additionally, a vegetation- and soil-free surface would support an effective penetration of oxygen to the sulphide and the effective formation of a non-sulphide ore body.

5.5.4 Anglesite and cerussite

The solubility of anglesite in pure water is relatively high and results in calculated activities of Pb^{2+} and SO_4^{2-} of approximately log_a = -3.5 mol*l^{-1} (Fig. 107). However, the solubility is dependent on the activity of SO_4^{2-}. Thus, additional SO_4^{2-} ions will decrease the solubility of anglesite and therefore decreases the activity of lead within the aqueous solution to $a_{Pb}=10^{-5}$ mol*l^{-1} (Fig. 108). Additional sources of SO_4^{2-} ions are the generation sulphuric acid during the oxidation process and/or the presence of gypsum and other SO_4^{2-} bearing minerals.

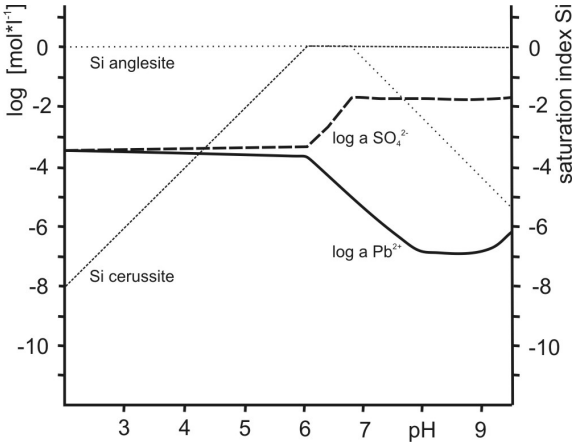

Fig. 107: Lead- and sulphate (SO_4^{2-}) concentration and saturation indices (Si) of anglesite and cerussite for an aqueous solution, which is in equilibrium with atmospheric P_{CO2} (Log_P_{CO2}=-1.5 kPa) dependent on the pH of the solution. The solubility of anglesite, which is reflected by log_a of Pb^{2+}, is relatively high (compared with the diagram on the right side) and the concentration of lead starts to decrease by reaching Si_[cerussite]=0 and cerussite starts to precipitate. (data & numerical simulation: PHREEQC)

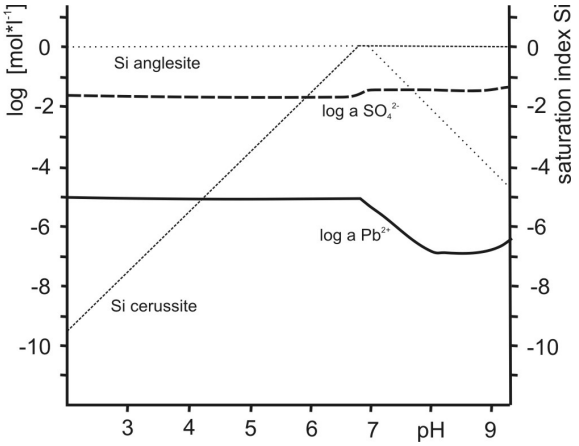

Fig. 108: Lead- and sulphate (SO_4^{2-}) concentration and saturation indices (Si) of anglesite and cerussite for an aqueous solution, which is in equilibrium with atmospheric P_{CO2} (Log_P_{CO2}=-1.5 kPa) and gypsum dependent to the pH of the solution. Here, the solubility of anglesite is relatively low (reflected by low log_a of Pb^{2+}), which is due to the high activity of SO_4^{2-} released from gypsum. The concentration of lead decreases by reaching Si_[cerussite] =0 due to precipitation of cerussite. (data & numerical simulation: PHREEQC)

Calculations with PHREEQC indicate, that the presence of gypsum (and of course other sulphate sources) is able to force anglesite to precipitate at even lower concentrations of Pb^{2+} compared to anglesite's precipitation in pure water. The equitation R21 is shifted to the right side and the resulting concentrations of Pb^{2+} decrease in order to fulfil the formula F 4.

$$Pb^{2+} + SO_4^{2-} \rightleftarrows PbSO_4 \downarrow \qquad \text{R21}$$

$$K_{sp} = \frac{a_{Pb^{2+}} a_{SO_4^{2-}}}{a_{PbSO_4}} \approx \left[Pb^{2+}\right]\left[SO_4^{2-}\right] = 1{,}58 * 10^{-8} \qquad \text{(FAURE, 1998)} \qquad \text{F 4}$$

After the oxidation of the sulphide ore, the pH value tends to change to basic conditions and cerussite becomes more stable then anglesite, according to figure Fig. 104. Thus, anglesite will be replaced by cerussite according to the following equitation R22 (after SANGAMESHWAR & BARNES, 1983):

$$PbSO_4 + H_2CO_3 \rightleftarrows PbCO_3 + SO_4^{2-} + 2H^+ \qquad \text{R22}$$

Reaction R22 shows the dependence of the activities of pH, H_2CO_3 and SO_4^{2-}. Active oxidation processes are associated with high activities of both SO_4^{2-} and H^+, which shifts the reaction to the left. After the oxidation process, the concentration of SO_4^{2-} decreases an pH will increase, which supports the formation of cerussite.

The armoring process and reaction inhibition of galena due to coating with anglesite/cerussite results in a decreased reactivity of galena (Fig. 98). Thus, the de facto reactivity of galena is much lower than the proposed theoretical rate, which would suggest that galena should be supposedly 5-times more reactive compared to sphalerite (ZEMAN, 1985). It is known, that the behaviour of sulphide oxidation, especially the oxidation of galena and sphalerite is highly dependent on the geochemical environment (pH, host rock geochemistry, hydrology) and is often different from the proposed theoretical values (JAMBOR, 1994).

5.5.5 Hydrocerussite

The investigations of the non-sulphide zinc deposits Mehdi Abad and Iran-Kuh, and Kuh-e-Surmeh (REICHERT & BORG, 2002) show either trace amounts or no hydrocerussite ($Pb_3(OH)_2(CO_3)_2$). Hydrocerussite also lacks on the Angouran non-sulphide zinc deposit (Iran), which was shown by studies by DALIRAN & BORG (2004). Non-sulphide zinc deposits of the United States from HEYL & BOZION (1963), and HEYL (1963 AND 1964), from Sardinia from BONI ET AL (2003) and investigations of KÄRNER (2003) and BOLAND ET AL. (2003) at Shaimerden/Kazakstan, of REYNOLDS ET AL (2003) at Mae Sod, and MULLER (1972) at Beltana are other examples of similar rare occurrence of hydrocerussite.

The scarcity of hydrocerussite can be explained by its stability parameters and the formation of hydrocerussite can be described as an equilibrium reaction as shown in reaction R23:

$$3PbCO_3 + H_2O \leftrightarrow Pb_3(OH)_2(CO_3)_2 + CO_2 \qquad \text{R23}$$

(MERCY ET AL., 1998)

The formula and thermodynamic/geochemical analysis indicate that the formation of hydrocerussite is highly dependent on the partial pressure P_{CO2} and the temperature. ESSINGTON ET AL (2004)

show, that the formation of hydrocerussite is favoured at P_{co2} equal or less than the atmospheric P_{co2} at 25 °C. Partial pressures of CO_2 above the atmospheric level of approximately $10^{-1.5}$ kPa lead to the precipitation of cerussite instead of hydrocerussite.

The lack of hydrocerussite in all examined carbonate hosted non-sulphide zinc deposits might be due to the relatively high P_{CO2}, which is equal or higher than the atmospheric P_{CO2} and the relatively low temperatures of the groundwater and in the host rock. Thus, the conditions, which are necessary for the formation of hydrocerussite, have not - or only very locally been reached.

5.5.6 Climatic effects

Acidic waters in carbonate host rocks, as a result of oxygen path oxidation with water-dissolved oxygen, are uncommon. In most cases, the concentration of dissolved oxygen in groundwater is insufficient to produce acidity greater than the alkalinity of the groundwater (DREVER, 1997). Thus, for an effective and fast oxidation, additional O_2 has to be introduced into the system, e.g. via faults and the drainage effects of karstification. Beside the geochemical parameters of the host rock such as limestone and dolomite, climatic and morphologic effects are other important factors for an effective oxidation process and the formation of supergene non-sulphide zinc deposits. These factors will be discussed for several scenarios below.

Climatic influence to geochemical systems and oxidation processes

The oxidation of sulphide ore bodies occurs usually in a ‘near surface’ environment. Water is readily available, as well as oxygen, nitrogen, carbon dioxide, and biological activities can also occur within this zone.

At a first stage, the meteoric water with no significant concentrations of metal ions is in equilibrium with the atmosphere. The gasses O_2 and CO_2 dissolve, depending on the temperature and on their related partial pressure P_{O2} and P_{CO2}. Although other gasses are available in the atmosphere and in equilibrium with the meteoric water, gasses other than O_2 and CO_2 are not important for the geochemical behaviour of water during the oxidation of sulphides and the precipitation of non-sulphide minerals and are thus not included in the present geochemical models.

Biological activity is a possible source for disequilibrium of soil and host rock pores with the atmosphere. An example might be the relatively high partial pressure of CO_2 within soil horizons of humid climates (SCHEFFER & SCHACHTSCHABEL, 2002). The P_{CO2} within soils is variable, significantly elevated and not in equilibrium with the atmospheric CO_2 partial pressure. Thus, the P_{CO2} of deeper levels of the host rock is often significantly elevated compared to the atmosphere and has to be included in geochemical models.

Above the groundwater table, the downward percolating rainwater interacts with the atmosphere as well as with soil and regolith before the meteoric water reaches and oxidises the sulphide ore. The chemistry of the water changes dramatically during this interaction and this modification plays an important role for further oxidation, dissolution, and transport processes. There are at least two different systems, in which water can be in equilibrium: i) equilibrium with atmospheric CO_2 and

carbonates and ii) equilibrium with atmospheric CO_2 and elevated P_{CO2} of soils and carbonates of the host rock. These hydraulic systems can be described either as 'closed' or 'open' systems.

Within an '**open**' system, water is able to equilibrate continuously with the atmosphere. Highly porous rocks and under-saturated conditions provide these 'open' conditions to seepage water and descending fluids.

A predominantly '**closed'** system is characterised by minute fissures and pores, filled with capillary water. The exchange of gasses is inhibited and, consequently, the system is not atmosphere-equilibrated. The P_{CO2} within the water is able to drop down to zero and pH increase rapidly or P_{CO2} may increase due to regional e.g. microbiological induced disequilibria.

These 'open' and 'closed' systems can be modelled by PHREEQC. Especially two drastically different scenarios are interesting to look at and these are either humid or arid climates.

- A humid climate is characterised by thick soil cover of the bedrock with biological activity supported by high annual precipitations of >500 mm. Thus, the soils show a highly increased P_{CO2} due to (micro-) biological activities. The seepage rates are high and the groundwater level is generally higher than in arid influenced regions.
- An (hyper-) arid climate shows generally low biological activities and is characterised by a low mean annual precipitation between 0-50 mm (hyper arid) or 50-200 mm (arid) (LLOYD, 1986). Therefore, the biological activity within the soil is rather limited compared to humid conditions. As a result of these limited biological processes, the P_{CO2} of such soils is nearly equal to that of the atmosphere.

Humid climate, 'open' system:

In a region with soil covered limestone and carbonate rocks, water that infiltrates through the soil approaches saturation with dissolved carbonates while still in contact with abundant CO_2. This reaction consumes CO_2 especially during contact with and dissolution of calcite from carbonate host rocks. The consumed gasses will be rapidly replenished by CO_2 from the overlying soil and/or atmosphere (PALMER & PALMER, 1995). This process stabilises the pH and leads to slightly increased pH-values. The pore water is characterised by relatively high CO_2 and low O_2 concentrations.

Humid climate, 'closed' system:

The first equilibrium reactions of the meteoric water within the closed system are similar to the open system. The water is in equilibrium with the atmosphere and the raised partial pressure of CO_2 of the soil. However, in contrast to the open system, here the dissolution of calcite/dolomite consumes most of the dissolved CO_2. Due to the lack of atmospheric CO_2 within the small fissures and the water-filled pores, the pH value increases drastically. The pore water is characterised by low CO_2 and O_2 concentrations (APPELO & POSTMA, 2005).

Arid climate, 'open' system:

An arid climate is characterised by low rates of precipitation (rainfall) and only subordinate biological activities within soils and associated with P_{CO2} and P_{O2} values similar to those of the atmosphere. The meteoric fluids are in equilibrium with the atmosphere. The pH is slightly increased and the fluids are relatively rich in dissolved O_2.

Arid climate, 'closed' system:

Similar to a "closed" system in a humid environment, the pH increases due to the dissolution process of calcite. However, in contrast to the humid climate, the concentrations of O_2 in water are higher, due to the lack of O_2-consuming organisms within the soil.

It is important to note, that the climate as well as the local geology (fragmentation, karstification) of the carbonate host rocks influence the O_2 and CO_2 concentrations of the descendent fluids, and thus, influence the pH and the ability of the fluid to dissolve the carbonate host rock. Calculations with PHREEQC have shown that arid environments provide best conditions for the oxygen-driven oxidation of sulphide ores (Tab. 20). The oxidation by Fe(III) is not included here, since Fe(III) itself is provided by oxygen and affects the oxidation process only on a regional scale. In arid environments, the dissolved O_2 reaches its maximum concentration, compared to other climates, and will not be consumed by biological activities within soils. The moderate to low rates of meteoric precipitation results in slow velocities of the seepage water and optimal conditions for equilibration with both the atmosphere and the host rocks. The groundwater table of arid climates is commonly low. This will lead to an opening of the water-filled pores and joints after an individual rainfall event and will thus provide an inward flow of gasses (O_2, CO_2) to any available sulphide ore body. This system will commonly change to a highly permeable system due to (karstic) dissolution processes of the carbonate host rock. Such a drained system allows continuous O_2 diffusion from the surface into the ore-bearing zones within the (water-) unsaturated zone. In this case, the oxidation rate of the sulphides is less limited by the O_2 concentration within the water but rather by the thickness of the overlying unsaturated zone. The possible depth of oxidation tends to deeper regions compared with oxidation processes, which are influenced by a humid climate. This is in agreement with observations of HEYL & BOZION (1962). The resulting sulphate and metal concentration within the fluids would be highly increased (APPELO & POSTMA, 2005) and pH decreases according to the generation of sulphuric acid.

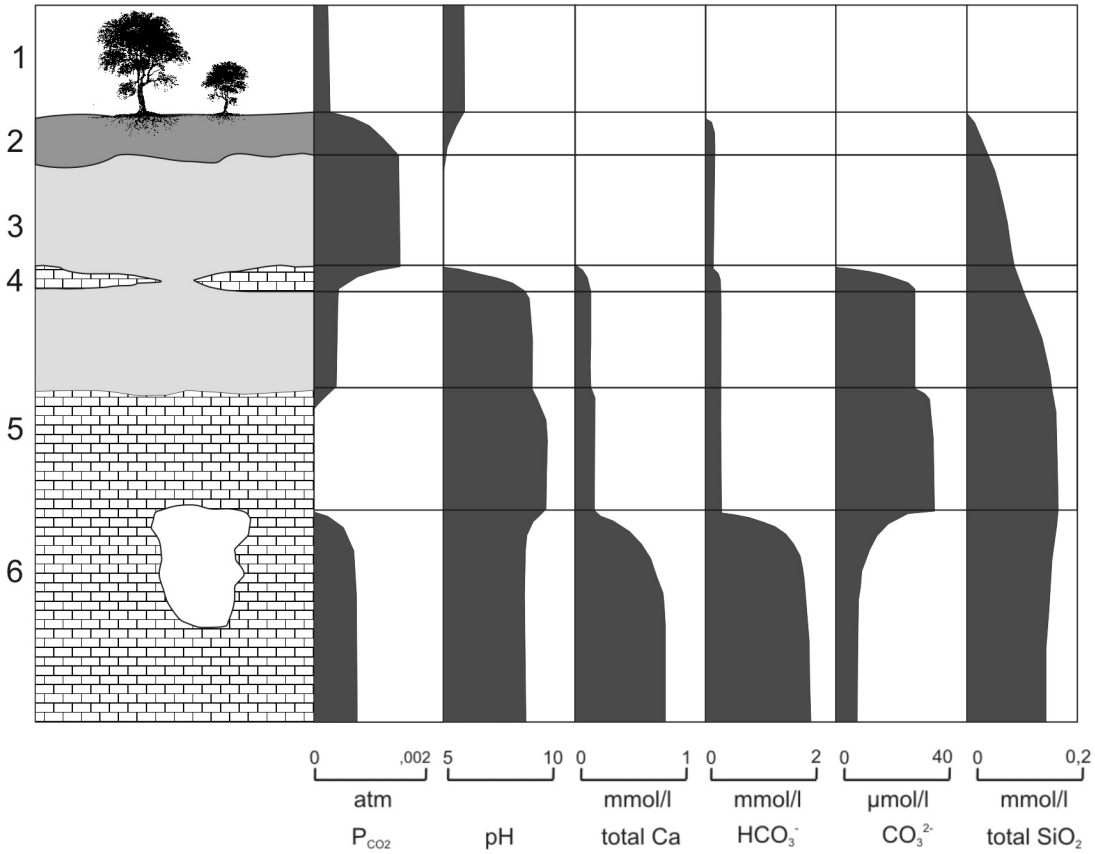

Fig. 109: Several stages of equilibrium reactions of descent fluids/seepage water in contact with silicates and/or carbonates. (modified after PALMER & PALMER, 1995)

(1): Equilibrium reaction with atmospheric O_2 and CO_2 **(2):** Water infiltrates the soil and reaches equilibrium with the CO_2 partial pressure of the soil. The pH value decreases, HCO_3^- and CO_3^{2-} concentration increases due to the dissolved CO_2. **(3/4):** Seepage water becomes isolated from soil, SiO_2 dissolves. The value of pH increases due to intercalated carbonates and solubility of SiO_2 increases significant. **(5):** $P(CO_2)$ decreases to 0 due to the 'closed' system, the high amount of carbonates, pH increases. **(6):** P_{CO2} increases due to the equilibrium reaction with CO_2 rich atmosphere in (karstic) spaces within the carbonate host rock, pH decreases and solubility increases due to the low pH and the high availability of CO_2.

Due to the limited availability of water in arid and hyper-arid climates, the fluids, which have been generated during the oxidation process, would be highly enriched in zinc and other metals. These high metal concentrations support an effective precipitation of non-sulphide base metal minerals. The low velocity seepage rates would generate aqueous solutions with high metal concentrations, the residence time of the fluid is relatively long and the oxidation process is more complete due to the mixed sources of oxygen: water-dissolved oxygen and oxygen, which has been provided by diffusion processes within the joints and pores of the host rock. These high element concentrations support an effective precipitation process within the carbonate host rock. Thus, an arid or semi-arid climate provides best conditions for the (slow, but effective) oxidation of a sulphide ore and also provides the best conditions for the preservation of a non-sulphide ore-body.

Tab. 20: Result of geochemical simulations with PHREEQC code. Seepage water has been modelled for different climates to simulate the capability to dissolve CO_2/O_2 and the ability of those waters to dissolve carbonates and SiO_2. Due to their different solubility, SiO_2 is divided into crystalline quartz and amorphous SiO_2. Simulations have shown that arid conditions provide the best environment for an effective oxidation of sulphide ores by dissolved O_2 and provide additional SiO_2 for the formation of zinc-silicates. Especially amorphous SiO_2 achieves high concentrations in aqueous solutions.

	Arid climate with amorphous SiO_2		**Arid climate with quartz-SiO_2**		**Humid climate with, soil coverage, amorphous SiO_2**		**Humid climate with, soil coverage, quartz-SiO_2**	
	closed	open	closed	open	closed	open	closed	open
Log P_{CO2} atm	-1.5	-1.5	-1.5	-1.5	-1.5	-1.5	-1.5	-1.5
Log P_{CO2} soil	-1.5	-1.5	-1.5	-1.5	0.5	0.5	0.5	1
Log P_{O2} atm.	1.7	1.7	1.7	1.7	1	1	1	
pH	9.03	8.2	9.66	8.3	7.6	6.9	7.6	7
PE	11.5	12.3	10.9	12.3	12.8	13.5	12.9	13.6
Total [SiO_2]	**$2.0 \cdot 10^{-3}$**	**$1.8 \cdot 10^{-3}$**	$1.4 \cdot 10^{-4}$	$9.6 \cdot 10^{-5}$	**$1.8 \cdot 10^{-3}$**	**$1.8 \cdot 10^{-3}$**	$9.4 \cdot 10^{-5}$	$9.4 \cdot 10^{-5}$
[Ca^{2+}]	$1.4 \cdot 10^{-4}$	$4.9 \cdot 10^{-4}$	$1.4 \cdot 10^{-4}$	$4.8 \cdot 10^{-4}$	$1.0 \cdot 10^{-3}$	$2.4 \cdot 10^{-3}$	$1.0 \cdot 10^{-3}$	$2.4 \cdot 10^{-3}$
[O_2]	**$2.7 \cdot 10^{-4}$**	**$2.6 \cdot 10^{-4}$**	**$2.5 \cdot 10^{-4}$**	**$2.5 \cdot 10^{-4}$**	$1.3 \cdot 10^{-4}$	$1.3 \cdot 10^{-4}$	$1.3 \cdot 10^{-4}$	$1.3 \cdot 10^{-4}$

concentrations [mol/l], Log P in **[kPa]**

fields of high/optimum concentrations of the specific element shown in grey

Climate change influenced Iran through the times and thus was one of the driving forces for changing mineral stabilities (Tab. 21). Especially the stability of hemimorphite is dependent on the P_{CO2} (e.g. as a result of biological processes) and thus indirectely influenced by temperatures and rainfall.

Tab. 21: . A provisional chronology of Quaternary climate in the southwestern part of the Arabian region. (after SADIQ & NASIR (2002)

Epoch	**Date in years**	**Climate**
Holocene	0-700	Hyperarid
	700-5,500	Slightly moist
	5,500-6,000	Hyperarid
	6,000-10,000	Wet (pluvial)
Late Pleistocene	10,000-17,000	Hyperarid
	17,000-36,000	Wet (pluvial)
	36,000-70,000	Arid
	70,000-270,000	Moist
	270,000-325,000	Arid
Middle Pleistocene	325,000-560,000	Wet
	560,000-700,000	Arid
Early Pleistocene	700,000-2,500,000	Wet humid (pluvial)

5.5.7 Numerical simulation of precipitation processes within a carbonate host rock

The aqueous solution, on which the computer model is based upon, represents a hypothetical acidic fluid, which was formed during the oxidation process of a primary pyrite-galena-sphalerite-bearing sulphide ore (see Methods section). The resulting theoretical initial solution has been allowed to equilibrate under different geochemical conditions with respect to P_{CO2} and host rock composition (dolomite-calcite).

Scenario A: Low P_{CO2} and limestone host rock (limestone or marble)

The scenario A simulates the reaction of a near-surface aqueous solution, which is in equilibrium with the atmospheric P_{CO2} (log P_{CO2}= -1.5 kPa), and which migrates from the oxidation zone through reactive limestone. The following assumptions have been made for this simulation: An initial solution (as described in Tab. 4) reacts with limestone (99% $CaCO_3$ and 1% $CaMg(CO_3)_2$). This geochemical system continuously equilibrates with the atmospheric P_{CO2}.

The first and most important reaction within the highly acidic environment is the precipitation of anglesite (Fig. 110). All simulations (scenario A and scenario B) show a rapid and immediate precipitation of anglesite. Thus, after the first equilibrium reaction, the activity of Pb^{2+} within the aqueous solution never reaches the initial value of $2.8 \cdot 10^{-2}$ mol·l^{-1} (loga_Pb^{2+} = -1.5 mol·l^{-1}) but decreases to approximately loga_Pb^{2+} = -5.5 mol·l^{-1}. This effect is due to the precipitation of anglesite, which is nearly insoluble under the influence of the high activity of sulphate ions (Fig. 110). The immediate precipitation of anglesite and the associated process of lead-immobilisation have been discussed in detail above. Zinc, in contrast, remains dissolved under these acidic conditions with its initial activity of a_Zn^{2+} = $3.8 \cdot 10^{-1}$ mol·l^{-1} (loga_Zn^{2+} = -0.42 mol·l^{-1}). These results prove and support the assumptions of a highly different mobility of zinc and lead. Lead remains immobile within the oxidation zone, whereas zinc becomes mobile due to the oxidation of the sulphide minerals and migrates to levels that are more distal. The continuous neutralisation reaction leads to the precipitation of gypsum, which decreases the activity of sulphate ions (Fig. 110).

The pH of the initial solution increases up to pH= 6.4. At this pH willemite becomes stable and precipitates up to pH= 7.71 at which point the final equilibrium of the aqueous solution with the limestone is reached. The amount of willemite, which primarily precipitates at this stage of the non-sulphide ore formation, is very low due to the low solubility and thus low availability of silica in water. Thus, the precipitation of willemite shows no visible effect on the activity of Zn^{2+}.

Hydrozincite becomes stable at pH= 6.4 according to the saturation index of this mineral and precipitates within the pH-range from pH= 6.4 to pH= 7.7. This precipitation consumes most of the dissolved zinc. Within this pH-range, the activity of zinc decreases from initial loga_Zn^{2+} = -1.6 mol·l^{-1} down to loga_Zn^{2+} = -5.9 mol·l^{-1}. The saturation index of smithsonite never reaches the necessary saturation (Si_smithsonite = 0) to precipitate this zinc carbonate. Thus, smithsonite is not stable and does not form under these conditions. As described above, smithsonite is associated

with high values of approximately log_P_{CO2} = 0.5 kPa, which is not given here. Cerussite becomes stable at pH 7.2 and its formation decreases the activity of Pb^{2+} ions down to loga_Pb^{2+} = -6.6 mol·l^{-1} at the end of the neutralisation. The final composition of the aqueous solution is given in the following table (Tab. 22):

Tab. 22: Hypothetic composition of an initial- and final solution according to geochemical modelling of scenario A.

	initial	final		initial	final
pH	1	6.7	**Fe**	$1.7 \cdot 10^{-3}$ mol·l^{-1}	$1.2 \cdot 10^{-12}$ mol·l^{-1}
pe	4	12.9	**Zn**	$2.4 \cdot 10^{-2}$ mol·l^{-1}	$1.1 \cdot 10^{-6}$ mol·l^{-1}
Temperature	25 °C	25	**Pb**	$1.6 \cdot 10^{-6}$ mol·l^{-1}	$2.7 \cdot 10^{-7}$ mol·l^{-1}
Log P_{CO2}	-1.5 kPa	-1.5 kPa	**SO_4^{2-}**	0.14 mol·l^{-1}	$1.2 \cdot 10^{-2}$ mol·l^{-1}
Ca^{2+}	0.0 mol·l^{-1}	$1.6 \cdot 10^{-2}$ mol·l^{-1}	**Mg^{2+}**	0.0 mol·l^{-1}	$1.2 \cdot 10^{-3}$ mol·l^{-1}

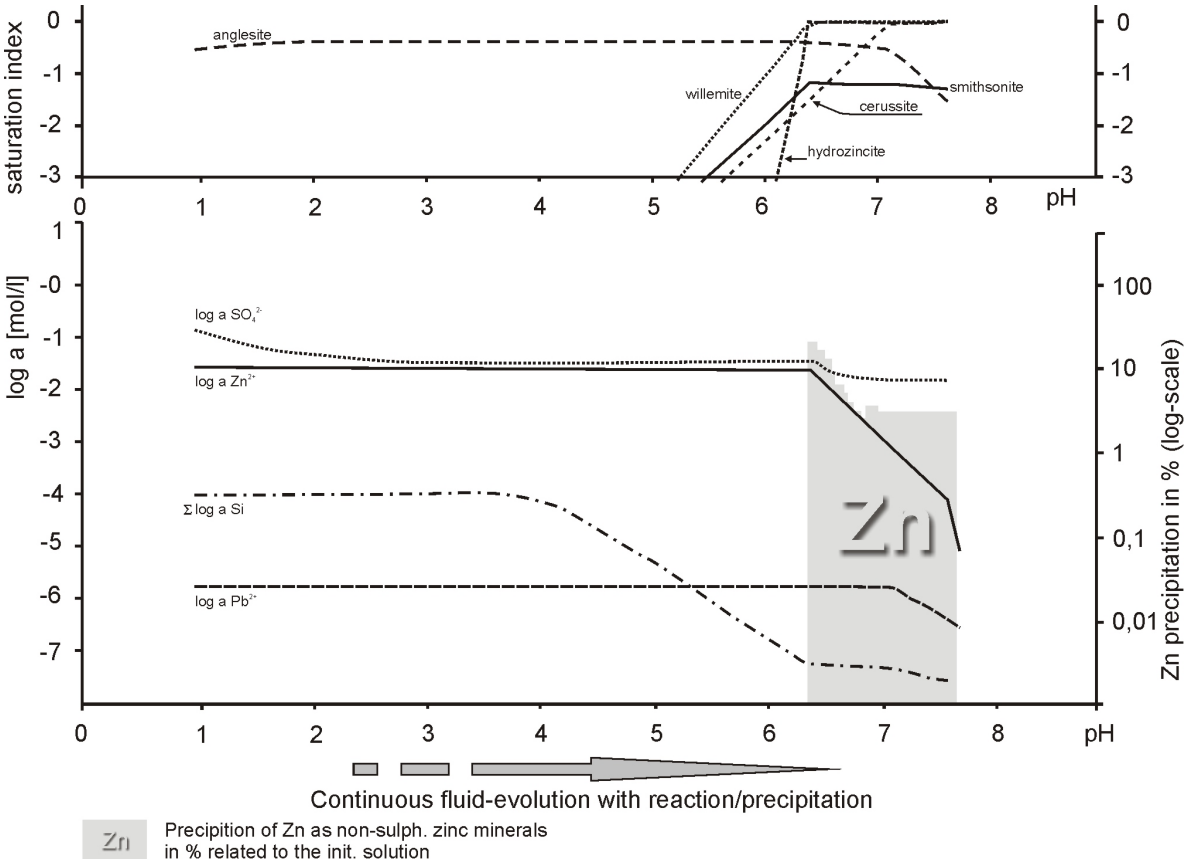

Fig. 110: Activities and saturation indices of a continuous pH dependent fluid evolution, produced by application of the PHREEAC program. The solution is in equilibrium with atmospheric CO_2 (log_P_{CO2} = -1.5 kPa).

Scenario B: High P_{CO2} and limestone host rock (limestone or marble)

The initial conditions for the aqueous solution and the mineralogy of the host rock of the second model are identical to those from 'Scenario A'. However, in contrast to 'Scenario A', the P_{CO2} is assumed to be relatively high at log P_{CO2} = 0.5 kPa, which can be reached e.g. due to biological activity or caused by the neutralisation reaction of acidic solutions with the carbonate host rock or easily due to CO_2 degassing due to neutralisation processes.

The modelling of the neutralisation process (Fig. 111 and Tab. 23) and the behaviour of anglesite precipitation are similar to 'Scenario A'. Most of the lead precipitates as anglesite because of the first equilibrium reaction. Concentration of sulphate ions is relatively low, due to the precipitation of anglesite and gypsum. Zinc is soluble and remains within the aqueous solution. Smithsonite reaches the saturation index Si_smithsonite= 0 at pH 6and precipitates. Hydrozincite gets close to saturation, but does not reach this point and does not precipitate. The precipitation of smithsonite occurs within the pH range of pH= 6 up to pH= 6.7, but most quantity of smithsonite precipitated between pH 6 and 6.4. After precipitation of smithsonite, the final concentration of dissolved zinc has been decreased from initial $loga_{Zn}$= -1.6 mol·l^{-1} to final $loga_{Zn}$= -3.95 mol·l^{-1}. Cerussite is stable, according to the raised P_{CO2} and thus precipitation of cerussite starts at pH=6.2. The stability of cerussite and its precipitation leads to a final activity of lead of $loga_{Pb}$= -6.7 mol·l^{-1}.

Tab. 23: Hypothetical composition of an initial- and a final solution, according to geochemical modelling of scenario B.

	initial	final		initial	final
pH	1	6.7	**Fe**	$1.7 \cdot 10^{-3}$ mol·l^{-1}	$1.6 \cdot 10^{-12}$ mol·l^{-1}
pe	4	13.9	**Zn**	$2.4 \cdot 10^{-2}$ mol·l^{-1}	$1.1 \cdot 10^{-4}$ mol·l^{-1}
Temperature	25 °C	25	**Pb**	$1.6 \cdot 10^{-6}$ mol·l^{-1}	$2.2 \cdot 10^{-7}$ mol·l^{-1}
Log P_{CO2}	0.5 kPa	0.5 kPa	**SO_4^{2-}**	0.14 mol·l^{-1}	$1.6 \cdot 10^{-2}$ mol·l^{-1}
Ca^{2+}	0.0 mol·l^{-1}	$1.65 \cdot 10^{-2}$ mol·l^{-1}	**Mg^{2+}**	0.0 mol·l^{-1}	$1.3 \cdot 10^{-3}$ mol·l^{-1}

Most of the zinc (85%) precipitated as smithsonite within the pH interval pH 6.0 to 6.3 and only traces of willemite precipitated due to the low concentration of SiO_2 within the solution.

The result of this model is close to the observations from different non-sulphide zinc deposits. Smithsonite is proposed to be the main first-stage zinc-mineral during the oxidation stage (associated with logP_{CO2}>0.5 kPa) and only subordinate amounts of zinc silicates are expected at this stage. Cerussite occurs, but only in traces due to its immobile behaviour within the oxidation zone and the low concentration within the initial solution. Anglesite should not precipitate outside the oxidation zone, since cerussite is more stable under the higher pH-P_{CO2} conditions.

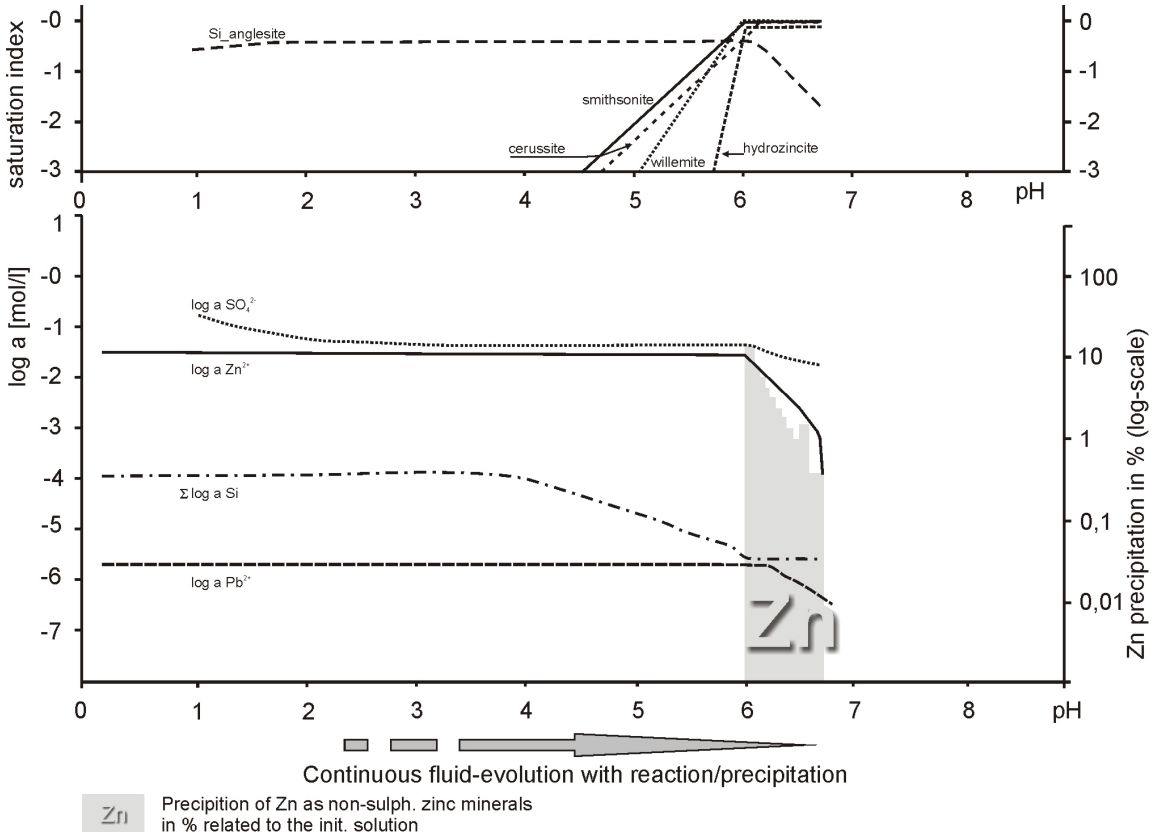

Fig. 111: Activities and saturation indices of a continuous pH dependent fluid evolution, produced by application of the PHREEAC program. The solution is in equilibrium with atmospheric CO_2 (log_P_{CO2} = 0.5 kPa).

The case scenario of an arid climate with limited soil coverage and low quantities of meteoric water should be discussed here in detail. These conditions suit the examinated Iranian non-sulphide zinc deposits and should be applicable to similar deposits. The most important processes for the sulphide oxidation, metal separation, and mineral precipitation can be summarised as followed.

Stage-I: oxidation stage

The oxidation of pyrite occurs in a surface near position. Carbon dioxide as well as oxygen penetrate and migrate through the soil and the host rock pores and spaces (Fig. 112) to the sulphide ore. Oxygen is partly consumed by organisms. The organic metabolism reduces the P_{O2} and increases the P_{CO2}. The oxygen reaches the sulphide ore and reacts with the pyrite and other sulphides. The products of this oxidation influence the geochemical behaviour of the oxidation system in several important ways: The gypsum- and hydrous ferric oxide armoured carbonates of the host rock are inhibited from a fast neutralisation reaction with the acidic solution and this establishes and stabilises an acidic low pH within the oxidation zone and the adjacent strata in spite of the carbonate host rock, which usually provides high capabilities to neutralise acidic solutions.

The hydrous ferric oxides are characterised by a high surface area, which is capable to adsorb metal ions (Ca^{2+}, Pb^{2+}, Zn^{2+}, Mg^{2+}, and other ions). This sorption process is highly pH-dependent. The pH values within the oxidation zone triggers the ability of HFO to adsorb zinc from the aqueous

solution. However, the zinc concentration of the aqueous solution is still high in contrast to lead, which has been removed from solution due to both processes the precipitation of anglesite and the adsorption to HFO. It can be assumed that up to 40% of the initial dissolved zinc is adsorbed onto HFO and 60 % leaves the oxidation zone and migrates into adjacent/deeper areas. Lead in contrast remains within the oxidation zone and only 1% is able to escape from the oxidation zone.

The neutralisation of the sulphuric acid with the carbonates of the host rock lead to the formation/liberation/degassing of CO_2, which equilibrates with the open pores, that increases the local P_{CO2}. Part of the CO_2 remains dissolved within the aqueous solution and is transported into adjacent areas. Subsequent degassing forms a CO_2-rich 'halo', which surrounds the oxidation zone and furthermore the local adjacent area. These high P_{CO2} levels indicate the lacking equilibrium with atmospheric CO_2 and should only be stable as long the oxidation (and neutralisation) process is active.

Smithsonite and/or hydrozincite start to precipitate at deeper levels, due to a progressing neutralisation and increasing pH-values of the migrating aqueous solution. Since the oxidation-stage is associated with a highly elevated P_{CO2} the formation of the high-P_{CO2} zinc carbonate smithsonite predominates over the precipitation of the low-P_{CO2} zinc carbonate hydrozincite. The 'stage-I smithsonite' precipitates as massive botryoidal layers (e.g. at Angouran; GILG ET AL. 2003; BORG ET AL., IN PREP.) or as a fine crystalline matrix of carbonate (karst-) breccia clasts of the limestone/dolomite host rock. Minor amounts of zinc precipitate as 'stage-I zinc-silicates', such as hemimorphite or willemite. The amount of zinc-silicate precipitation is limited by the low SiO_2 concentration within the aqueous solution. Lead precipitates in small quantities as anglesite and/or cerussite according to its low concentration.

In an exclusively carbonate-dominated environment, zinc precipitates as smithsonite or as hydrozincite. The stability and the occurrence of these zinc carbonates are dependent on the partial pressure of CO_2. Hydrozincite precipitates at relatively low P_{CO2}, which indicates in most cases equilibrium of the aqueous solutions and the pore space with the atmosphere and the atmospheric P_{CO2} - typical for the unsaturated zones as a near-surface precipitation.

Stage-II: post oxidation stage

The post-oxidation stage starts with a change of the entire geochemical system (Fig. 113). At this stage, the sulphide ore has been completely oxidised and/or occurs as a small remnant. The generation of acidic fluids stops and the neutralisation process ends at this stage. The consequence of these changes is a successive lowering of the sulphuric acid-derived sulphate ion concentration. The solubility of sulphates, such as gypsum and anglesite increases with these lowering concentrations due to *Le Chatelier's Principle (*MORTIMER, 1987*)*. Gypsum starts to dissolve and is removed over time and anglesite starts to dissolve as well. The increasing pH value favours the precipitation of cerussite instead of anglesite, thus anglesite becomes unstable an dissolves or is replaced with cerussite. The liberation of Pb leads to the formation of late-stage cerussite crystals within fractures and open spaces, which were form during this post oxidation stage and are common at MOB of Mehdi Abad and Irankuh - Kolahdarvazeh Mine.

Zinc carbonate minerals become stable within the former oxidation zone since the pH value has

risen to neutral and alkaline conditions. Under these conditions zinc is immobile an will remain at this Fe-rich zone and here forms secondary zinc minerals such as hydrozincite, smithsonite and zinc-silicates.

Now the P_{CO2} is changed now back to 'normal' conditions, which are equilibrium-near with the atmosphere. The low P_{CO2} changes the stability of the zinc carbonate minerals. Thus, smithsonite becomes unstable, whereas hydrozincite reaches its stability. At this point, the stage-I hydrozincite starts to replace the stage-I smithsonite. Additionally, hydrozincite starts to precipitate within the former oxidation zone.

In most cases, the formation of large quantities of zinc silicates (hemimorphite/willemite) is not associated with the oxidation stage of sulphide ores. As long as the oxidation process is still active, only subordinate amounts of zinc silicates (willemite, hemimorphite) will precipitate. In most cases, the formation of zinc silicates becomes an important process at the post-oxidation stage. Zinc silicates, such as hemimorphite or willemite precipitate in open spaces and pores and are commonly intimately associated with the red- or white zinc ore (smithsonite/hydrozincite). Hemimorphite is common in systems, which are able to provide sufficient concentrations of silica. The successive contact with SiO_2-bearing descending fluids leads to the formation of zinc silicates over the time. The amount of hemimorphite within the examinated deposits seems to correlate with the availability of SiO_2. Thus, the MOB, which contains chert-rich limestone, shows high amounts of late-stage hemimorphite, whereas hemimorphite is less common at Irankuh, since the SiO_2 content within host rock and the overlying strata is much lower.

The stage I and stage II processes should result in a non-sulphide zinc deposit with an ideal zonation pattern of two spatially separated and geochemically different types of zinc ore: the 'red zinc ore' (within the former oxidation zone) and the 'white zinc ore'.

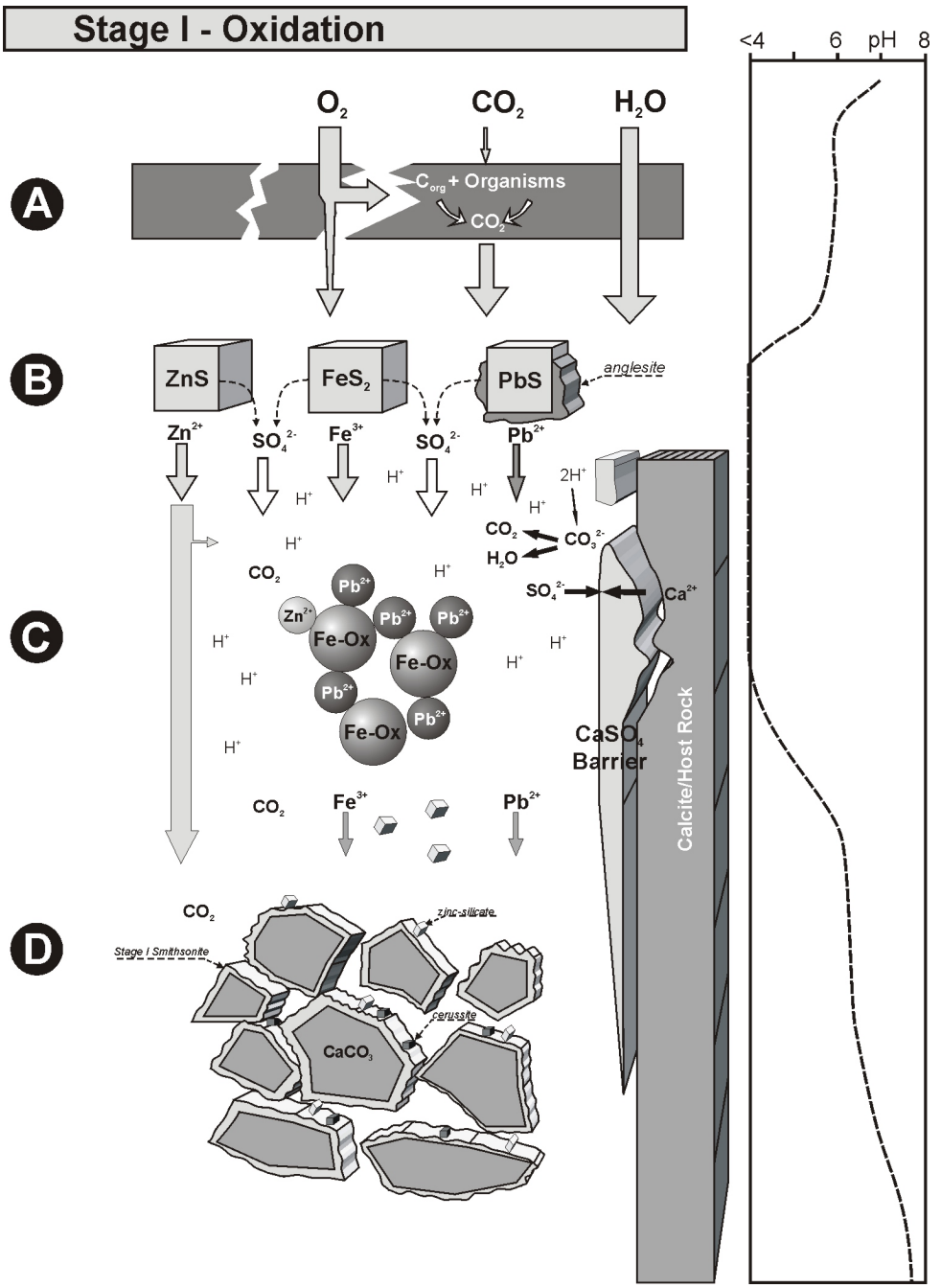

Fig. 112: Stage-I: Oxidation. **(A):** Descendent fluids (rain fall) partly penetrate an organic cover/soil. This process is associated with the partial loss of dissolved oxygen (HERBERT, 1999) and the increase of the CO_2 partial pressure P_{CO2}. This water reaches the sulphide ore. **(B):** The sulphide ore is in contact with atmospheric O_2 and CO_2 due to diffusion of these gasses. The sulphide ore is oxidised and this process is associated with acidic pH values, the release of sulphuric acid, and the precipitation of hydrous ferric oxides. The ph is low (<4). **(C):** The reaction of sulphuric acid with the adjacent carbonate host rock forms a $CaSO_4$ - and Fe-oxihydroxide-barrier, which inhibits the carbonate from further neutralisation reactions. This process stabilises the low pH of the oxidation zone. Lead precipitates as anglesite and is partly adsorbed from aqueous solution onto ferric hydrous oxides, whereas Zn^{2+} ions remain mobile and migrate into deeper levels. The pH is still acidic and increases moderately due to the $CaSO_4$ coating of the carbonates. (**D):** The pH increases, zinc silicates, such as hemimorphite will precipitate. However, due to low SiO_2 concentrations, the amount of zinc silicates is very low. Smithsonite, and/or hydrozincite start to precipitate at higher pH values as a cement of the carbonate breccia fragments. Only minor amounts of cerussite and other Pb-minerals precipitate, due to low Pb concentrations of the aqueous solution.

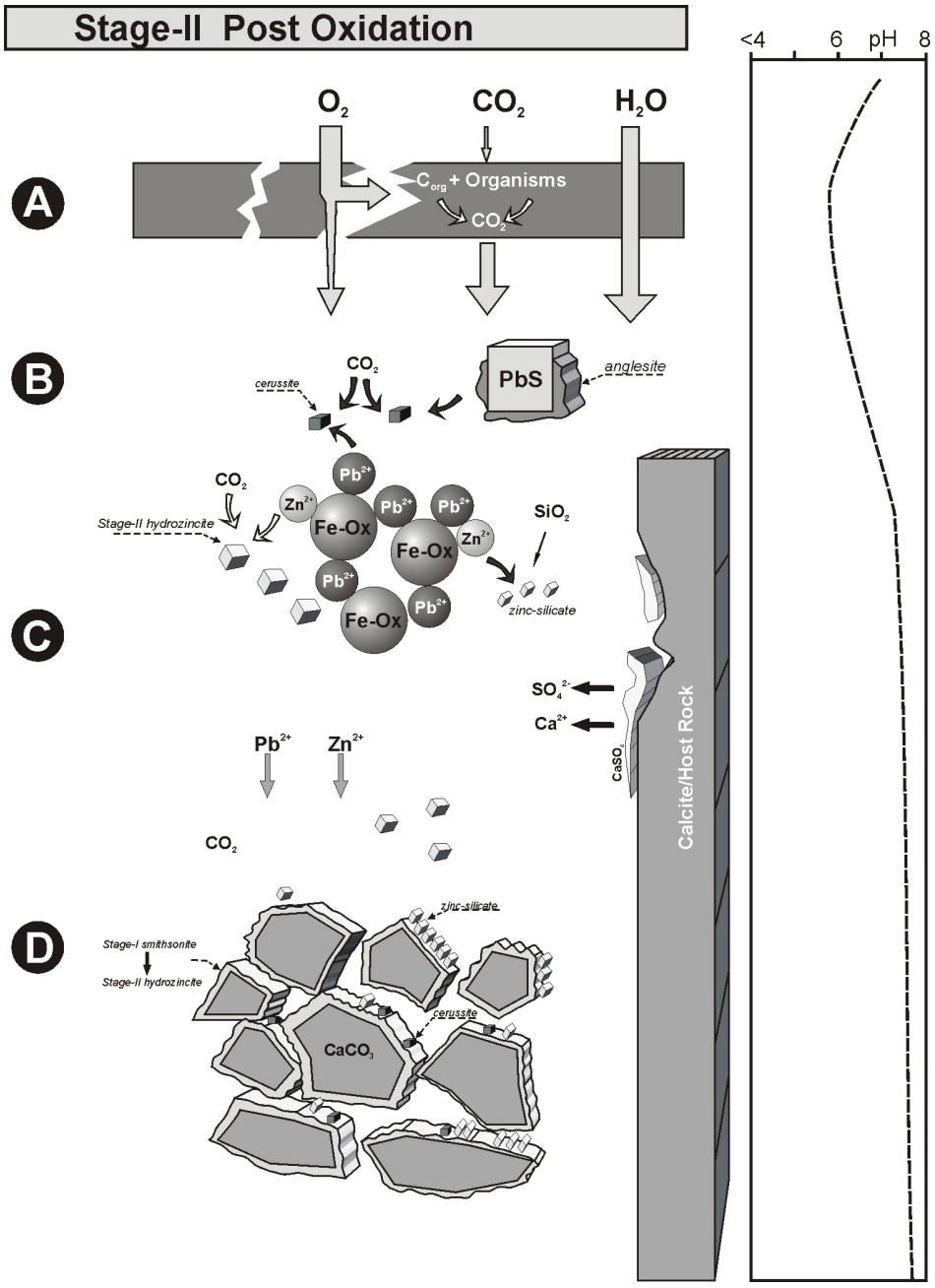

Fig. 113: Stage-II: (A): Descendent fluids (rain fall) partly penetrate an organic cover. This water reaches the former oxidation zone. (B): Most part of the sulphide ore is oxidised by now. P_{CO2} is relatively low, compared with stage-1 and is in equilibrium with the atmosphere. The pH within the former oxidation zone has changed to neutral or alkaline conditions. No or only minor amounts of galena are present, rimmed by an anglesite coating. Anglesite is replaced by cerussite due to changed P_{CO2}. Zinc precipitates as hydrozincite. Smithsonite will precipitate only if the P_{CO2} is high enough, probably due to microbiological metabolism. (C): The gypsum armoring of stage-I dissolves and is washed out of the system. The higher pH-values support the solubility of SiO2 and zinc-silicates start to precipitate successively. The mobility of Fe, Zn and Pb is low, which limits their quantitative transport. (D): Due to the lack of CO2 generating reactions the PCO2 decreases and smithsonite becomes unstable and is replaced by hydrozincite.

5.6 Interpretation of the Mehdi Abad deposit

Mountain Ore Body of Mehdi Abad

No clear indications for the sulphide protor of the MOB have been identified, which might be due to the thorough oxidation, folding, and faulting of the strata and solution collapse. The non-sulphide mineralising and ore-modifying processes at the MOB of Mehdi Abad appear to be relatively young or have continued until relatively recently. Mineralised breccias of tectonic and solution collapse origin document the earlier stages of the non-sulphide mineralisation. Locally, the open, partly mineralised pore-, fracture-, and breccia-spaces contain extremely delicate dissolution textures and euhedral supergene non-sulphide zinc minerals without any deformation by folding or gravitational compaction. The processes of ore formation, partial dissolution, and re-precipitation have only been terminated and 'mummified' by the current arid to hyper-arid climate.

The ore occurs in a carbonatic host-rock, which consist of limestone or dolomitc limestone. Most of the fault-breccias show a high content of zinc and lead within the matrix of the breccia, whereas the wallrock shows relatively low concentration of base metals. All examined and sampled adits show a high content of hemimorphite. This appears rather surprising, because of the carbonate dominated environment and the carbonatic host-rock. However, the high content of hemimorphite implies a source for the silicate, which is productive enough to deliver this quantity. Two sources of SiO_2 are capable to deliver these quantities. One possible source for the silicate may be the chert-bearing members of the Abkou Formation (K_a^{sh1}, K_a^{sh2}), which hosts the non-sulphide ore of the MOB. Another source is probably the strata of the Sangestan Fm., which are (a) underlying the Abkouh and Taft Formation and (b) are lateral located to the southwest of the Black-Hill Fault. The Sangestan Formation consists, among others, of fine-grained quartzitic-feldspatic sandstones, and sandy shales. The origin of the silica from the Sangestan Formation might imply ascendant or lateral fluid systems. This fluid-transport is possible by using the faults as pathways for the ascending fluids. However, the chert-bearing member of the Abkou Formation is the favoured and more probable source of the silica. As shown above, the chert is able to interact easily with the descending meteoric fluids. It is presumed that the precipitation of hemimorphite is a long lasting process, due to low SiO_2 concentrations within aqueous solutions. Thus, the formation of hemimorphite is supposed to occur successively after the oxidation stage of the sulphide ore, as a result of dissolution and corrosion processes of hydrozincite and smithsonite and the re-precipitation as hemimorphite.

The following stages are suggested, to be important for the formation of the non-sulphide zinc ore of the MOB:

At the **first stage (oxidation stage),** Fe-oxihydroxides, zinc- (hydro-) carbonates (hydrozincite, smithsonite) and minor amounts of hemimorphite precipitated and two distinct and spatial separated ore types have been formed due to metal mobilisation- and separation processes : the red zinc ore and the white zinc ore. The P_{CO2} at this stage was relatively high, due to the oxidation of pyrite and the subsequent neutralisation reaction with the carbonate host rock. Thus, the non-sulphide zinc ore was smithsonite dominated. The red zinc ore was formed, which mainly consisted of smithsonite, goethite (and other Fe-oxihydroxides), hemimorphite and Pb-bearing minerals. The

white zinc ore has been formed distal to the red zinc ore trapped in karst collapse breccias and within pores and open spaces of the host rock. At this stage, the white zinc ore was also smithsonite dominated, due to a proposed halo effect of a high P_{CO2}.

At a **second stage (post oxidation stage),** the generation of CO_2 has stopped and smithsonite became unstable and was replaced by hydrozincite due to lower P_{CO2}. The lowered P_{CO2} initiated also the alteration of the hemimorphite. Early-stage related hemimorphite became unstable at this point and was partly replaced by hydrozincite.

The **third stage** has led to the cessation of the hemimorphite dissolution/alteration. The stability-field changed again in favour of hemimorphite. The climate changed to the present arid to hyper-arid climate, and hemimorphite became more stable again and euhedral hemimorphite-II precipitated within fractures and open spaces, locally overgrowing the earlier mineral phases. This process is apparently still active

The reasons for the changing mineral stabilities are presumably a change of pH and P_{CO2} as an immediate result of the ending of the oxidation and acid/CO_2 generating process. P_{CO2} and pH changes are additionally a result of a changed climate, which might have been led to a rise in P_{CO2}, possibly due to microbial CO_2 production within the soil profile and groundwater of the palaeo-weathering surface under a more humid climate (REICHERT & BORG, 2004).

Valley Ore Body of Mehdi Abad

The geochemical evolution of the VOB is completely different from the MOB. At least three different stages of (tectonic or collapse) displacement and mineralisation can be interpreted.

The **first stage,** which has influenced the strata of Taft Formation, is characterised by paleo-karst and partly collapse of the limestone of the Taft Formation.

A **second phase** is associated with the dolomitisation of the carbonate rock. This dolomitisation is probably genetically linked with the emplacement of the sulphide ore and barite. The sulphide ore occurs as a filling of fractures and as cement of the carbonate/dolomite breccia. However, the sulphide ore itself occurs regionally limited as breccia fragments, cemented by sulphide ore. The syn-mineralising brecciation is possibly due to the dolomitisation of the carbonate host rock. A dolomitisation of a limestone is commonly associated with a decrease of volume (WEYL, 1960) (approximately 13 vol. %). This volume reduction has led to regional collapse processes and an increased permeability. This collapse has involved both: dolomite as well as the sulphide ore. The results are angular sulphide clasts at the VOB sulphide ore. The sulphide mineralisation was associated with the dolomitisation process, resulted in a subsequent (partial) collapse of dolomite and sulphide ore and cementation with new sulphides. The occurrences of deformed and broken barite crystals support the thesis of dolomite collapse and are most likely due to one single event, which has affected the entire region of Mehdi Abad. This hypothesis is based on a constant Ba-Sr ratio in all analysed samples of VOB and MOB, whereas different barite mineralising events should be distinguishable by different Ba-Sr ratios. Barite occurs as mm- to cm-sized crystals within the breccia as well as massive barite (Black Hill). This barite is common within the (sulphide and non-sulphide) ore-bearing strata of the VOB as well as in strata of the non-sulphide ore-bearing MOB. This barite

mineralisation is

The **third** Phase started with the oxidation of the sulphide protore. In contrast to the MOB the oxidation process of the VOB is still active and is actually limited to the upper sulphide zone of the VOB. The most portion of the non-sulphide zone overlies the sulphides of the VOB.

The metallogenetic source for both sulphides the (thoroughly oxidised) sulphide protore of the MOB and the sulphides of the VOB is not solved. One can assume a **separate sulphide mineralising phase** that has probably delivered Zn- and Pb-rich (hydrothermal) fluids for the protore of the MOB or has overprinted the geochemically parameters (such as As, Cd, Tl content) of the MOB. This would explain the geochemically different behaviour of the MOB with regard to the VOB. Another possible mechanism to achieve these geochemical differences is a possible lateral-separated position during the emplacement of the sulphide protore. Thus, the different REE pattern and the Element fingerprint were generated as a function of the proximity to the vent. A subsequent thrusting and stacking after the sulphide ore emplacement has finally resulted in the present vicinity of the MOB and VOB.

5.7 The interpretation of the Kolahdarvazeh mine data

Non-sulphide zinc-(lead-) mineralisation of the Kolahdarvazeh mine occurs predominantely as cement of a dolomite breccia. This feature is similar to the Mehdi Abad deposit. However, the geochemical evolution is completely different compared to the MOB and the VOB of Mehdi Abad and represents a special case in non-sulphide ore formation. The main difference between the Kolahdarvazeh mine and Mehdi Abad is the low amount of Fe sulphides within the sulphide protor of the Koladahrvazeh mine. This fact results in a completely different geochemical behaviour of the oxidising sulphide ore. The potential of such a low-Fe sulphide ore to generate sulphuric acid is highly limited. Only small quantities of sulphuric acid were generated during the oxidation stage. This low acidity would have led to a nearly immediate neutralisation with a limited armouring effect due to the low quantity of precipitated gypsum. Furthermore, the low amount of Fe-oxihydroxides should also not have played a significant role for the metal separation process. Thus, the main portion of the non-sulphide ore is assumed to be formed as an in situ direct replacement of the sulphide ore. The geochemical analyses of the Kolahdarvazeh mine support this theory. Especially the REE pattern as well as the composition of the sulphide ore compared to the non-sulphide ore shows no signs of separation processes of mobile zinc from immobile Fe (Pb). The non-sulphide ore in fact shows nearly the same element composition compared to the sulphide protor. The lack of acidity and the lacking liberation of CO_3^{2-} ions from neutralisation reactions has been balanced by the incorporation of supergene (meteoric) delivered carbonate ions. This is reflected by relatively low $\delta^{13}C$ values compared to Mehdi Abad. The low $\delta^{13}C$ values of the non-sulphide zinc ore of the Kolahdarvazeh mine suggest an important role of organic and meteoric CO_2.

The formation of non-sulphide mineralised dolomite breccias in the proximity of the Kolahdarvazeh fault is the result of a long lasting and successive dissolution process of the primary non-sulphide ore and reprecipitation nearby the Kolahdarvazeh fault. The karstification and the zinc-enrichment of the dolomite host rock have been accompanied by numerous faults and fractures. Additionally

the bedding of the dolomite and limestone dips towards the Kolahdarvazeh Fault. The partition of the bedding plains and the related fractures could have been additionally used for karst processes and as conduits by the Zn-(Pb-) bearing fluids. Black shales limit the deposit to the south at the contact of the Kolahdarvazeh fault and also underly the ore bearing dolomite strata. The shales might have acted as an impermeable and insoluble barrier for the ore-delivering fluids and the ground water system. This hydraulic barrier stopped the fluid flow and led to the 'ponding' of the fluids in front of the hydraulic barrier (Fig. 114).

The oxidation process of the sulphide protor is supposed to be relatively short, due to the highly fractured dolomite and the exposed location at a flank of a mountain ridge. The oxygen reaches the sulphides easily, and is not adsorbed by a deep soil horizon or hindered by a thick overlying (alluvial) cover. Thus, the following steps are proposed for the formation of the non-sulphide orebody of the Kolahdarvezeh mine:

At a **first stage** the sulphide protor has been oxidised in a fast and effective way. The non-sulphide ore has been formed as a result of a direct sulphide replacement. Only a small amount of zinc was mobilised and precipitated distal from the sulphides as cement of collapse breccias.

The **second stage** is characterised by successive dissolution of the primary non-sulphide zinc minerals according to their solubility. The mobilised zinc was transported with supergene, meteoric driven fluids towards the Kolahdarvazeh fault. Here, a concentration process and the high surface of a karst collapse breccia led to the reprecipitation of non-sulphide zinc minerals. However, a white zinc ore is the dominating type at the Irankuh mining district.

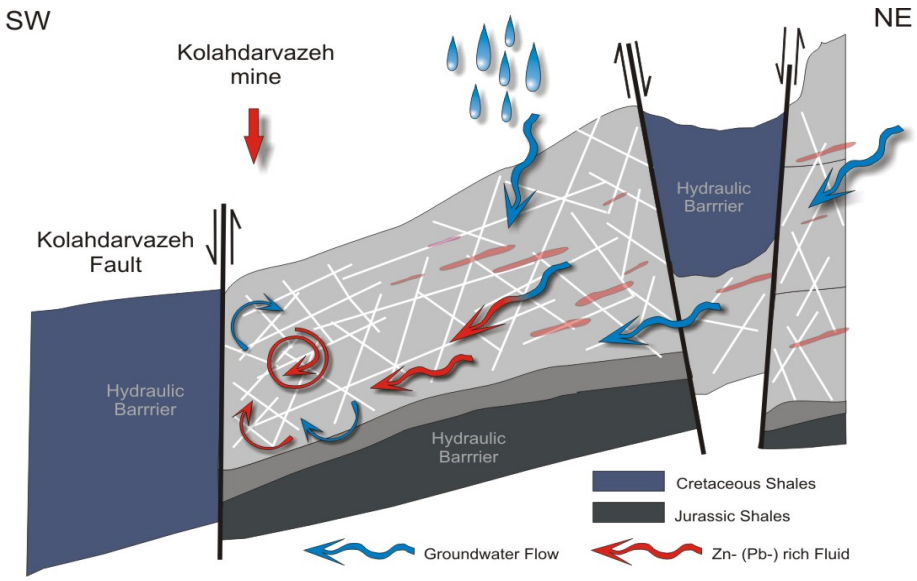

Fig. 114: Schematic model of the fluid-flow processes, during the genesis of the Kolahdarvazeh deposit. The impermeable and insoluble shales might have been acted as a barrier for supergene fluids, which interacted with the sulphide-ore of the dolomite/limestone. The ore has been oxidised, zinc became mobile and has been transported along fractures and faults towards the Kolahdarvazeh fault. This led to the ponding of the fluids in front of the hydraulic barrier. The result was a highly effective karst- and non-sulphide mineralising process.

6 Conclusions

Although various non-sulphide zinc deposits worldwide differ in individual aspects, there are a number of common features and interpreted genetic mechanisms that are proposed to be more or less always present during the oxidation and metal-separation process.

The oxidation process necessary to form a non-sulphide zinc deposit is triggered by numerous factors of which the most important are: the climate, and the tectonic setting and the geometrical position of the sulphide protore (Fig. 115). The efficiency of the precipitation apparently increases if an aquitard or aquifuge is present and underlies the sulphide ore.

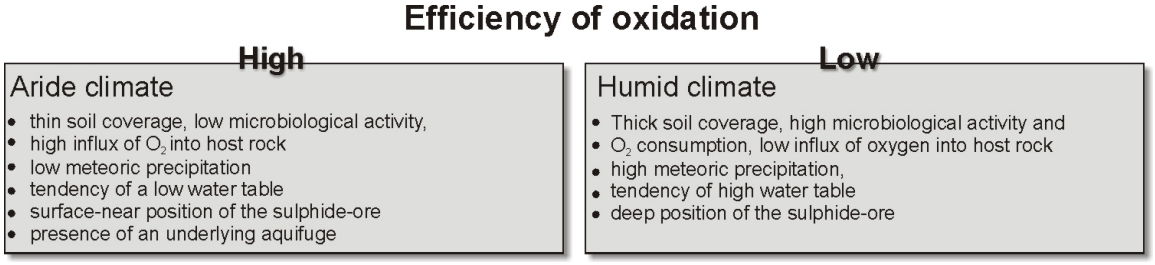

Fig. 115: Overview of parameters that influence descent both the oxidation of the sulphide protore and the formation of a non-sulphide ore body.

A near-surface position and a (hyper-) arid environment particularly support the formation of high-grade non-sulphide zinc ores, whereas a humid climate and a deep position of a sulphide protore should normally reduce the effectiveness of the accumulation of non-sulphide zinc minerals. A tectonically induced, rapid uplift process (DALIRAN & BORG, 2005) and the associated erosion process of the overlaying strata is one of the most effective ways to move a sulphide ore to a surface-near position. The suitable climate as well as crustal uplift and the resulting near-surface position are main factors for the large number of well-developed and well-preserved Iranian non-sulphide zinc deposits (DALIRAN & BORG, 2005). Most of the Iranian non-sulphide zinc deposits are typically influenced by an arid- or hyper-arid climate.

Beside the climatic and geometrical aspects of the genesis of non-sulphide zinc deposits the local stratigraphic sequence influences the metallogenetic process as well. Especially the occurrence of an aquifuge seems to be important. The aquifuge acts in two possible ways:

1) The aquifuge and the related groundwater table support karst-processes e.g. as a result of water mixing effects with different concentrations of CO_2. This results in karst related breccias, which are able to act as a voluminous trap with a highly reactive surface area derived from the breccia clasts. These breccia filled cavities act as a geochemical trap for the dissolved zinc of the descent aqueous solutions and leads to the concentration of the zinc within a regional limited region and thus prevents that zinc disperses over a wide range. These carbonate breccias with non-sulphide zinc minerals as matrixes are a common type of non-sulphide zinc ore both in the examined Iranian deposits and other examples worldwide.

2) An underlying aquitard or aquifuge focuses the fluids within well-defined and locally limited strata. Common strata, which act as an aquitard, are shales, shaly limestone and other strata with low permeability.

The spatial position, the climate, and the lithostratigaphic setting provide the physical parameters for the oxidation process. However, the geochemical processes and the resulting non-sulphide zinc ore are highly dependent on the composition of the sulphide protore. In most cases, Zn- and Pb-mineralised rocks (sphalerite, galena) are associated with large quantities of iron-bearing minerals, mainly pyrite. The iron content is most likely one of the key features of the sulphidic protore that triggers the evolution and geochemical behaviour of the oxygen-driven oxidation process in several ways (Fig. 116). The most important effect to the geochemical behaviour of the oxidation zone related to the formation of a non-sulphide zinc ore is the amount of iron bound in pyrite rather than in the sphalerite. Only the oxidation of pyrite and similar sulphides (arsenopyrite, chalcopyrite) is capable to influence the geochemical system in all of these four ways:

1. Generation of sulphuric acid and low pH values,
2. Increased P_{CO2} due to acid-neutralisation by host-rock carbonates,
3. Generation of sulphate ions
4. Precipitation of hydrous ferric oxides

The strength and influence of these four points depend on the availability of oxygen and water, which represent the key driving forces of the oxidation process and control its effectiveness.

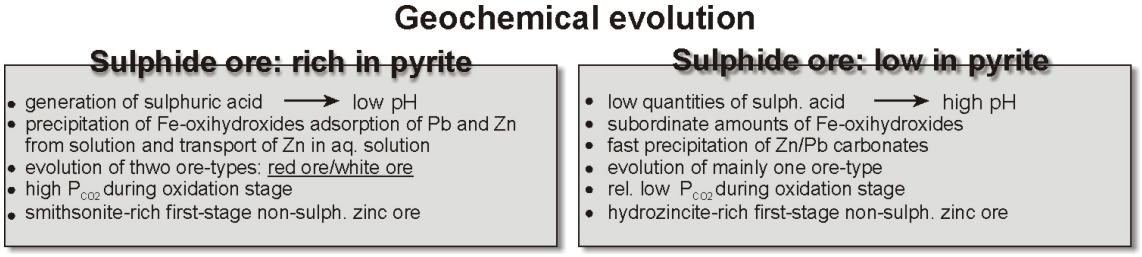

Fig. 116: The geochemical behaviour and the formation of non-sulphide zinc deposits are dependent on the initial composition of the sulphide protore. The concentration of iron (mainly bound to pyrite) influences the pH, sulphate concentration and the amount of Fe-oxihydroxides. All of them are important parameters that control the mineralogy and formation of non-sulphide zinc minerals in different ways.

Sulphuric acid, as a product of pyrite oxidation reacts with calcite/dolomite with subsequent precipitation of gypsum as the product of this neutralisation reaction. The development of gypsum crystals, which growt onto the calcite leads to the armoring of calcite. Furthermore, the insoluble Fe-oxyhydroxides attached to the calcite build an additional barrier between the calcite and the acidic solution and thus intensify the armouring effect. As a result, the armouring effect lowers the reactivity of the limestone/dolomite and stabilises low pH-values within the carbonate host rock, especially within the oxidation zone.

The formation of the ‘white-‘ and ‘red zinc ore’ are the result of aqueous transport processes coupled with a gradual increase of the pH-value due to neutralisation reactions and adsorption effects. The paragenetic sequence of the precipitated minerals is highly dependent on the P_{CO2} and is

dominated by oxides, hydroxides (mainly Fe-bearing minerals), sulphates, such as gypsum and anglesite, and carbonates (smithsonite, hydrozincite, cerussite, and others), especially at higher pH-values while the oxidation process is in progress. The process of the armoring of limestone and other carbonates is known and described for acid mine drainage systems. Thus, it is reasonable to apply these armoring processes to the oxidation of sulphide ore and the formation of non-sulphide ore.

7 References

Alavi, M. (1994): Tectonics of the Zagros orogenic belt of Iran: New data and interpretations: Tectonophysics, v. 229, p. 211–238

Alavi, M. (2004): Regional stratigraphy of the Zagros Fold-Thrust Belt of Iran and its proforeland evolution. American Journal of Science. 304 (1), p. 1-20

Allen, J.R. & Matthews, R.K. (1982): Isotope signatures associated with early meteoric diagenesis. Sedimentology, v. 29, p. 297-817.

Allen, M., Jackson, J., & Walker, R. (2004): Late Cenozoic reorganization of the Arabia-Eurasia collision and the comparison of short-term and long-term deformation rates: Tectonics, v. 23, p. 16.

Alsharhan, A.S., Rizk, Z.A., Nairn, A.E.M., Bakhit, D.W. & Alhajari, S.A. (2001): Hydrogeology of an arid region: The Arabian Gulf and Adjoining Areas. Elsevier, Amsterdam, 368 p.

Ankomah, A.B. (1992): Magnesium and pH Effect on Zinc Sorption by Goethite. Soil Science, v. 154, 3, p. 206-213

Appelo, C.A.J. & Postma, D. (2005): Geochemistry, groundwater and pollution. Amsterdam: Balkema.

Appelo, C.A.J., Verweij, E. & Schäfer, H. (1998): A hydrogeochemical transport model for an oxidation experiment with pyrite/calcite/exchangers/organic matter containing sand. Applied Geochemistry, 13 (2), p. 257-268

Attendorn, H.G. & Bowen, R.N. C. (1997): Radioactive and Stable Isotope Geology. Chapman and Hall, London, 522 p.

Azari, K. & Sethna, S.F. (1994): Geology and ore localization study of the zinc-lead sulphide deposit of Central Valley Mehdiabad-EH-Bahadoran, Yazd Province, Iran. Proceeding of Fourth Mining Symposium of Iran. 10th-14th Sept. 1994, Exploration, v. 1

Barton, P.B. & Toulmin, P. (1966). Phase relations involving sphalerite in the Fe-Zn-S system. Economic Geology, 61(5), p. 815-849

Berberian, M. & King, G.C.P. (1981): Towards a Paleogeography and tectonic evolution of Iran: Can. J. Earth Sci. 18, p. 210-265

Berberian, M. (1981) : Active faulting and tectonics of Iran, in Gupta, H. K., and Delany, F. M., editors, Zagros-Hindu Kush-Himalaya Geodynamic Evolution: American Geophysical Union Geodynamic Series, v. 3, p. 33–69

Bertorino, G., Caredda, A.M. & Zuddas, P. (1995): Weathering of Pb-Zn mine tailings in pH buffered environment. Water Rock Interaction. Proceedings of the 8th International Symposium on Water-Rock Interaction, 1995, p. 859-862

Blowes, D.W. & Ptacek, C.J. (1994): Acid-neutralization mechanisms in inactive mine tailings. In: Jambor, J.L. & Blowes, D.W. (eds.): Short Course Handbook on Environmental Geochemistry of Sulfide Mine Waste. Mineralogical Association of Canada, Nepean, v. 22, p. 271-291.

Boland, M.B., Kelly, J.G., and Schaffalitsky, C., 2003, The Shaimerden supergene zinc deposit, Kazakhstan: Economic Geology, v.98 (4), p. 787-795.

Boni, M. & Large, D. (2003): Non-sulphide Zinc Mineralisation in Europe: An Overview. Economic Geology, v.98(4), p. 715-729

Boni, M. (2003): Non-sulphide zinc deposits: a new (old) type of economic mineralization. SGA News, 15, August 2003, p. 6-11

Boni, M., Gilg, H.A., Aversa, G. & Balassone, G. (2003): The "Calamine" of SW Sardinia (Italy): geology, mineralogy and stable isotope geochemistry of a supergene Zn-mineralization: Economic Geology, v.98 (4), p. 731-748.

Borg, G. (2002a): Sauberes Zinkerz aus der Wüste. Scientia Hallensis, 1/2002

Borg, G. (2002b): The good, the bad and the ugly – a maturity index for supergene non-sulphide deposits. 2002 GSA-Annual Meeting, Denver, Abstracts, v. 34, no. 6, p. 287

Borg, G., Daliran, F., Armstrong, R., Woodhead, J.D., Friese, K., Sadeghi, M., Walter, J. & Vennemann, T. (in prep.): The Hypogene Emplacement and Supergene Modification History of the Angouran Zinc Deposit, NW-Iran – a Holistic Approach

Borg, G., Kärner, K., Buxton, M., Armstrong, R. & Schalk, W.v.d. (2003): Geology of the Skorpion non-sulphide deposit, southern Namibia. Economic Geology 98, p. 749–771.

Boyle, D.R. (1993). Oxidation of Massive Sulphide Deposits in the Bathurst Mining Camp, New Brunswick. In Alpers, C.N. & Blowes, D.W. eds. (1994): Environmental Geochemestry of Sulphide Oxidation. p. 535-550

BRGM, (1993). Mehdiabad Lead-Zinc Deposit, Prefeasibility Study. Unpubl. internal report.

BRGM, (1994). Mehdiabad Lead-Zinc Deposit, Prefeasibility Study. Geological Assessment Report. Unpubl. internal report.

Brindley, GW & Brown, G -Eds- (1980): Crystal Structures of Clay Minerals and Their X-ray Identification. Mineralogical Society, London, 495 p.

Brugger, J., McPhail, D. C., Wallace, M. & Waters, J. (2003): Formation of Willemite in Hydrothermal Environments. Economic Geology; June 2003; v. 98; no. 4; p. 797-818

Cabala, J. (2001): Development of oxidation in Zn-Pb deposits in Olkusz area. In: Mineral Deposits at the Beginning of the 21st century. Balkema. p. 121-124

Cerling, T.E. (1984): The stable isotopic composition of modern soil carbonate and its relationship to climate. Earth Planet. Sci. Lett. 71, p. 229-240.

Choquette, P.W. & James, N.P.(1990): Limestones – the burial diagenetic environment. In: I.A. McIlreath & D.W. Morrow (Eds.): Diagenesis. Geoscience Canada Reprint Series 4, Ottawa, p. 75-111.

Christidis, G. E. (1998). Comparative Study of the Mobility of Major and Trace Elements During Alteration of an Andesite and a Rhyolite to Bentonite, in the Islands of Milos and Kimolos, Aegean, Greece. Clays and Clay Minerals, v. 46, 4, p. 379-399

Coniglio, M., Myrow,P. & White, T. (1996): Stable oxygen and carbon isotope compositional fields for skeletal and diagenetic components in New Zealand Cenozoic nontropical carbonate sediments and limestones: a synthesis and review. New Zealand Journal of Geology and Geophysics, 1996, v. 39, p. 93-10

Craig, J.R. & Scott, S.D. (1974): Sulfide phase equilibria. In P.H. Ribbe, Ed., Sulfide Mineralogy, v. 1, cs1–cs104. Reviews in Mineralogy, Mineralogical Society of America, Washington, D.C.

Cramer, J.J., Nesbitt, H.W. (1983). Mass-Balance Relations and Trace-Element Mobility During Continental Weathering of Various Igneous Rocks. Sci. Géol., Mém., 73, p. 63-73

Criss, R.E. (1995): Stable isotope distribution. variations from temperature, organic and waterrock interactions. In T.J. Ahrens, ed., Global Earth Physics: A Handbook of Physical Constants, 1, p. 292-307, American Geophysical Union, Washington, D.C.

Dabirrahmani, H. (1984): Zur Quartärgeologie des Beckens von Riz und benachbarter Beckenstrukturen bei Esfahan (Iran). Unpubl. PhD Thesis, Technische Hochschule Aachen.

Daliran, F. & Borg, G. (2005). Characterisation of the nonsulphide zinc ore at Angouran, Northwestern Iran, and its genetic aspects. In: Mao, J. and Bierlein, F.P. (Eds.) Mineral Deposit Research: Meeting the Global Challenge. v. 2, 913-916.

Daliran, F. & Borg, G. (2004): "Non-sulphide Zinc Deposits, Iran- A Preliminary Study of the Zinc Ores at Angouran Mine, NW-Iran". BGR, Hannover, open file report

Davies, J.F., Prevec, S.A., Whitehead, R.E. & Jackson, S.E. (1997): Variations in REE and Srisotope chemistry of carbonate gangue, Castellanos Zn-Pb deposit, Cuba. Chemical Geology 144 (1998), p. 99-119

Davoudzahdeh, M. (1997): Iran. In: Moores, E.M. & Fairbridge, R.W. (1997): Encyclopedia of Europeean and Asian regionla geology. Chapman & Hall, London.

Dixon, C.J., & Pereira, J., (1974): Plate Tectonics and Mineralization in the Tethyan Region. Mineral. Dep. 9: 185-198.

Dold, B (2003): Enrichment processes in oxidizing sulphide mine tailings: Lessons for supergene ore formation. SGA New 16: 7.

Dold, B., Fontboté, L., & Wildi, W. (1999a): Detection and distribution of ferric oxyhydroxides and oxyhydroxide sulfates in sulfide mine tailings; their importance to selective metal retention and acid production. Mine, Water and Environment, 1999 IMWA Congress, Sevilla, Spain, v. 2, p. 525-526.

Dold, B., Fontboté, L., Wildi, W. (1999b): Selective metal retention by ferric oxyhydroxides and oxyhydroxide sulfates in sulfide mine tailings and influence of climate to element mobility. SMPG.

Domènech, C., De Pablo,J., & Ayora,C. (2002): Oxidative dissolution of pyritic sludge from the Aznalcóllar mine (SW Spain). Chemical Geology, V. 190, 1-4, p. 339-353

Dove, P.M. & Rimstidt, J.D. (1994):Silica-Water Interactions. In: Heaney, P.J., Prewitt, C.T. & Gibbs, G.V. eds. (1994) Silica, pysical behavior, geochemistry and materials applications. Reviews in Mineralogy, v. 29, p. 259-308

Drever, J.I. (1997): The geochemistry of natural Waters: surface and groundwater environments. 3rd. ed., Prentice-Hall International (UK)

Duchesne, J.C., Rouhart, A., Schoumacher, C. & Dillen, H. (1983): Thallium,Nickel, Cobalt and Other Trace Elements in Iron Sulfides from Belgian Lead-Zinc Vein Deposits.

Dyer, J.A., Trivedi,P., Scrivner,N.C. & Sparks,D.L. (2003): Lead Sorption onto Ferrihydrite. 2. Surface Complexation Modeling. Environ. Sci. Technol., 37, p. 915-922

Dzombak, D.A. & Morel, F.M.M. (1990): Surface Complexation Modeling, Hydrous Ferric Oxide. John Wiley & Sons, New York

Essington, M.E., Foss, J.E. & Roh. Y. (2004): The soil mineralogy of lead at Horace's Villa. Soil Science Society of America Journal. 68(3): 979-993

Faure, G. (1998): Principles and Applications of Geochemistry, 2nd ed., Prentice Hall, 600p.

Fedo, C.M., Nesbitt,H.W., Young, G.M. (1995). Unraveling the effects of potassium metasomatism in sedimentary rocks and paleosols, with implications for paleoweathering conditions and provenance. Geology, 23, 10, p. 921-924

Ferreira Da Silva, Fonseca E.C., Matos J. X., Patinha, C., Reis P.,. Santos Oliveira J. M (2005): The effect of unconfined mine tailings on the geochemistry of soils, sediments and surface waters of the lousal area (Iberian Pyrite Belt, Southern Portugal). Land Degradation & Development, v. 16, p. 213-228

Förstner, U. & Wittmann, G.T.W. (1983): Metal Pollution in the Aquatic Environment. Berlin-Heidelberg-New York (Springer-Verlag).

Freeze, R.A. & Cherry, J.A. (1979): Groundwater, Englewood Cliffs, NJ: Prentice-Hall.

Gazea, B., Adam, K. & Kontopoulos, A (1996): Passive systems for the treatment of Acid Mine Drainage, Minerals Engineering Journal, v. 9, No.1, p. 23-42

Germain, M.D., Tassé, N. & Bergeron, M., (1994): Limit to self-neutralization in acid mine tailings: the case of East-Sullivan, Québec, Canada. In: Blowes, D.W. & Alpers, C.N. (eds), Environmental Geochemistry of Sulfide Oxidation. American Chemical Society, Symposium Series 550, p. 365-379

Ghazanfari, F. (1999): Zn-Pb mines and deposits in Iran. Unpubl. Report

Ghazban, F., McNutt, R.H. & Schwarcz, H.P. (1994): Genesis of Sediment-Hosted Zn-Pb-Ba Deposits in the Irankuh District, Esfaha Area, West-Central Iran. Economic Geology, v.89, 1994, p. 1262-1278

Ghorbani M., Tajbakhsh, P. & Khoie, N. (2000): Lead and Zinc Deposits in Iran. GSI Book No 75:512

Gilg, H.A. & Boni, M. (2004): Stable isotope studies on Zn and Pb carbonates: Could they play a role in mineral exploration? -in: Applied Mineralogy, Developments in Science and Technology, v. 2, M. Pecchio, F.R.D. Andrade, L.Z D'Agostino, H. Kahn, L.M. Sant'Agostino, M.M.M.L. Tassinari (Editors), ICAM-BR, São Paulo, p. 781-784.

Gilg, H.A., Allen, C., Balassone, G., Boni, M., Moore, F. (2003): The 3-stage evolution of the Angouran Zn “oxide”-sulfide deposit, Iran. In: Eliopoulos, D.G. et al. (Eds.) Mineral exploration and sustainable development. Millpress, Rotterdam, p. 77–80

Gryschko, R. & Horlacher, D. (1997): Bodenversauerung; Ursachen – Auswirkungen – Maßnahmen. Landesanstalt für Umweltschutz Baden-Württemberg, Karlsruhe

GSI (Geological Survey of Iran) (1988). Geological studies on the Mehdiabad Lead and Zinc Project. (Internal report)

Haas, N.C. & Scheff, P.A. (1990): Estimation of Averages in Truncated Samples. Environ. Sci. Technol., 24, p. 912-919

Hammarstrom, J.M. (2002): Mineralogical characterisation of limestone reacted with acid mine drainage in a pulsed limestone bed treatment system. Abstract, Denver Annual Meeting (October 27-30, 2002)

Hangi, R.D. & Paarlberg, N. (1996): Silver Distribution in Iron Sulfides at the Buick and Brushy Creek Mines, Viburnum Trend, Southeast Missoury. In: Carbonate-Hosted Lead-Zinc Deposits. Sangster, D.F. (ed.), SEG Special Publications No.4, p.577-587

Haskin, L.A., Haskin, M.A., Frey F.A. , & Wildman T.R. (1968): Relative and Absolute terrestrial abundances of the rare earth. In: Ahrens,L.H. (ed.): Origin and distribution of the elements, v. 1. Pergamon, Oxford, p. 889-911

Herbert, R.B. (1999): Sulphide oxidation in mine waste deposits, a review with emphasis on dysoxic weathering. . MiMi-report. Mitigation of the environmental impact from mining waste (MiMi). MiMi Print, Lulea, Sweden

Hessami, K., Koyi, H.A., Talbot, C.J., Tabassi, H. & Shabanian, E.. (2001): Progressive unconformities within an evolving foreland fold-thrust belt, Zagros Mountains, J. geol. Soc. Lond., 158, 969–981.

Heyl, A.V. & Bozion, C.N. (1960): Varieties of supergene zinc deposits in the United States; Article 2, B2 – B5.

Heyl, A.V. & Bozion, C.N. (1962): Oxidized zinc deposits of the United States. Part 1. General Geology. Geological Survey Bulletin 1135-A, 52p

Heyl, A.V. (1963) Oxidized zinc deposits of the United States; Part 2, Utah. U.S. Geological Survey Bulletin, B1 – B104.

Heyl, A.V. (1964) Oxidized zinc deposits of the United States; Part 3, Colorado. U.S. Geological Bulletin, C1 – C98.

Hitzman, M.W., (2001): Zinc oxide and zinc silicate deposits – a new look. Geological Society of America, Program with Abstracts, v.33, p.1-336

Hitzman, M.W., Reynolds, N.A., Sangster, D.F., Allen, C.R., & Carman, C. (2003): Clasification, genesis and exploration guides for non-sulphide zinc deposits. Economic Geology, v.98(4), p. 685-714

Hoefs, J. (1997): Stable Isotope Geochemistry. 4th Edition, Springer-Verlag, Berlin. 214 p.

Hofmann, A., Pelletier, M. Michot, L., Stradner, A., Schurtenberger, P. & Kretschmar, R. (2004): Characterisation of pores in hydrous ferric oxide aggregates formed by freezing and thawing. Jour. of solid and Interface Science, 271, p. 163-173

Huminicki, D.M. (2004): The Effect of secondary precipitates on the dissolution rate of calcite in AMD solutions. Abstract, Ninth Annual Geoscience Student Research Symposium, 18-19 March 2004, Blacksburg, Virginia

Huminiki, D.M.C. & Rimstid, J.D. (2004): The Effect of Secondary Precipitates on the Dissolution Rate of Calcite in Acid Mine Drainage Solutions. Department of Geosciences, Virginia Polytechnic Institute and State University, Blacksburg

Ingwersen, G. (1990): Die sekundären Mineralbildungen der Pb-Zn-Cu-Lagerstätte Tsumeb, Namibia. Unpublished PhD.-thesis, University Stuttgart

ITOK International (Ltd) (2005): http://www.itokgroup.com

Jambor, J.L. (1994): Mineralogy of Sulfide-rich Tailings and Their Oxidation Products., in Environmental Geochemistry of Sulfide Mine-wastes, Mineralogical Association of Canada Short Course v. 22., p. 59-102.

Jeong, G.Y. & Lee, B.Y. (2003): Secondary mineralogy and microtextures of weathered sulfides and manganoan carbonates in mine waste-rock dumps, with implications for heavy-metal fixation. American Mineralogist, 2003, 88, p. 1933-1942.

Jun,C., Hongtao,W. & Huayu,L. (1996): Behaviours of REE and other trace Elements During Pedological Weathering – Evidence from Chemical Leaching of Loess and Palae osol from the Luochuan Section in Central China. Acta Geologica Sinica, v.9,3, p. 290-302

Kakovsky,M. & Kosikov,Y.M. (1975): Study of kinetics of oxidation of some sulphide minerals. Obogashch. Rud. 20, p.18-21 (in Russian language)

Kärner, K. & Borg, G.(2001): Relationship between non-sulphides and sulphides at the Skorpion zinc deposit, Namibia. GSA-Conference 2001, Boston.

Kärner, K. (2003): Mineralogical and geochemical observations on the non-sulphide zinc deposit Shaimerden, Northern Kazakhstan. In: Eliopoulos, D. G. et al. (eds.): Mineral Exploration and Sustainable Development. v. 1, 85–88, Millpress, Rotterdam.

Kärner, K. (2006): The Metallogenesis of the Skorpion Non-Sulphide Zinc Deposit, Namibia. Unpupl. Ph.D. Thesis, Martin-Luther-University Halle-Wittenberg

Khalili, M. (1997): Petrography, Mineralchemistry and Geochemistry of Shir-Kuh Granite Southwest of Yazd Central Iran. Unpubl. PhD Thesis, University Hamburg

Kimball, B.A., Callender, E. and Axtmann, E.V. (1995): Effects of Colloids on Metal Transport in a River Receiving Acid Mine Drainage, Upper Arkansas River, Colorado, U.S.A.: Applied Geochemistry, v. 10, p. 285-306

Kolker, A. & Nordstrom, D.K. (2001). Occurrence and Micro-Distribution of Arsenic in Pyrite. USGS Workshop on Arsenic in the Environment, February 21-22, Denver

Lapakko, K., 2002, Metal Mine Rock and Waste Characterization Tools: An Overview, International Institute for Environment and Development.

Large, D. (2001): The Geology of nonsulphide zinc deposits – an overview. Erzmetall, 54, p. 264 – 274.

Leach, D.L., Viets, J.B., Foley-Ayuso, N., Klein, D.P. (1986). Mississippi Valley-Type Pb-Zn Deposits. In Bray, E.A. ed., 'Preliminary Compilation of descriptive geoenvironmental mineral deposit models.': U.S. Geological Survey Open File Report 95-831.

Leaman, P. & Staude, J.M. (2002): Metallogenetic evolution of the western Tethys of Turkey and Iran. Metal Mining Agency of Japan, Mineral Resources Information Center, p. 15-16

Lee,M.K. & Saunders,J.A. (2003): Effects of pH on Metals precipitation and sorption: Field bioremediation and geochemical modelling approaches. Vadose Zone J., v. 2, p. 177-185

Lloyd, J.W. (1986) "A review of aridity and groundwater", Hydrology Processes, 1, p. 63-78.

Lohmann, K.C., 1988, Geochemical patterns of meteoric diagenetic systems and their application to studies of paleokarst, in James, N.P., and Choquette, P.W., eds., Paleokarst: New York, Springer-Verlag, p. 58-80

MacLean,W.H. & Barret,T.J. (1993): Lithogeochemical techniques using immobile elements. J. of geochemical Exploration, 48, p. 109-133

Marie, J.St., Kesler, S.E and Allen, C.A. (2001). Origin of iron-rich Mississippi Valley-type deposit. Geology, 29, p. 59-62

Martinez, C.E. & McBride,M.B. (2001): Cd, Cu, And Zn Coprecipitates in Fe Oxide Formed At Different pH: Aging Effects on Metal Solubility And Extractability by Citrate. Enviironmental Toxicology and Chemistry, 20, 1, p. 122-126

Matthes, S. (1996): Mineralogie. Springer-Verlag Berlin, Heidelberg, New York

Mazumdar, A., Tanaka, K. Takahashi, T. & Kawabe, I. (2003): Characteristics of rare earth element abundances in shallow marine continental platform carbonates of Late Neoproterozoic successions from India. Geochemical Journal, v37 (2), p. 277-289

McCall, G.J.H., (1998): The geotectonic history of the Makran and adjacent areas of southern Iran: Journal of Asian Earth Sciences, v. 15, p. 517–531

McLennan, S.M. (1989). Rare Earth Elements in Sedimentary Rocks: Influence of Provenance and Sedimentary Processes. In Lipin, B.R. & McKay,G.A., eds. (1989): Geochemestry and Mineralogy of Rare Earth Elements. Mineralogical Society of America, p. 169-200

McPhail, D.C., Summerhayes, E., Welch, S. & Brugger, J. (2003): The geochemistry of zinc in the regoloith. In: Roach I.C. ed. 2003. Advances in Regolith, p. 287-291. CRC LEME

Megaw, P.K.M., Barton, M.D., & Islas-Falce, J. (1996): Carbonate-hosted Lead-Zinc (Ag, Cu, Au) deposits of Northern Chihuahua, Mexico, in Sangster, D.F., ed.: Society of Economic Geologists, Special Publication No. 4, 1996, p. 277-289

Mehdiabad Zinc Company (1995): http://www.mehdiabadzinc.com

Mercy, M.A., Rock P.A., Casey, W.H. & Mokarram, M.M. (1998): Gibbs energies of formation for hydrocerrusite [Pb(OH)2.(PbCO3)2(s)] and hydrozincite {[Zn(OH)2]3.(ZnCO3)2(s)]} at 298 K and 1 bar from electrochemical cell measurements. American Mineralogist 83(7-8), p. 739-745.

Middelburg, J.J., Van Der Weijden, C.H. & Woittiez,J.R.W. (1988). Chemical Processes Affecting the Mobility of Major, Minor and Trace Elements During Weathering of Granitic Rocks. Chemical Geology, 68, p. 253-273

Miura, N. & Kawabe, I. (2000): Dolomitization of limestone with MgCl2 solution at 150°C: Preserved original signatures of rare earth elements and yttrium as marine limestone. Geochemical Journal, v. 34, p. 223 – 227

Mohajjel, M. (1997): Structure and tectonic evolution of Palaeozoic - Mesozoic rocks, Sanandaj-Sirjan Zone, western Iran. Unpub. PhD thesis, University of Wollongong.

Momenzadeh, M. (1976): Stratabound lead-zinc ores in the lower Cretaceous and Jurassic sediments in the Malayar-Isfahan district (west central Iran). Diss. Univ. Heidelberg: 300 p, Heidelberg.

Monthel, J. (1994): Mehdi Abad Lead-Zinc Project, Prefeasibily Study – Geological Assessment Report. BRGM, unpubl. internal report

Moore, DM & Reynolds, RC (1997): X-ray diffraction and the identification and analysis of clay minerals. 2nd Edition. Oxford University Press, 378 p.

Mortimer, C.E. (1987): Chemie. Georg Thieme Verlag Stuttgart, New York

Nelson, C.S. & Smith, A.M. (1996): Stable oxygen and carbon isotope compositional fields for skeletal and diagenetic components in New Zealand Cenozoic nontropical carbonate sediments and limestones: a synthesis and review. NZ J. Geol. Geophys., 39, p. 93- 107

Nosratian, J. (1991). Geological Map of Mehdi Abad. Based on the topographical Map Mehdi Abad-Yazd, 1:2000. (1987)

Palmer, A.N. & Palmer, M.V. (1995): Geochemistry of capillary seepage in Mammoth Cave. Proc. Of the 4th Mammoth Cave Science Conf., Mammoth Cave, KY, 1995, p. 119-133

Palmer, A.N. & Palmer, M.V. (2000): Hydrochemical interpretation of cave patterns in the Guadalupe Mountains, New Mexico and West Texas: Journal of Cave and Karst Studies, v. 62, no. 2, p. 91-108.

Parkhurst, D.L. & Appelo, C.A.J. (1999): User's guide to PHREEQC (version 2) USGS Water-Resources Investigations Report 99-4259, USGS, Denver, Colorado, USA.

Parr, J.M. (1992). Rare-earth element distribution in exhalites associated with Broken Hill-type mineralisation at the Pinnacles deposit, New South Wales, Australia. Chemical Geology, 100, p. 73-91

Peter, J.M. & Godfellow,W.D. (1996): Mineralogy,bulk and rare earth element geochemistry of massive sulphide-assotiated hydrothermal sediments of the Brunswick Horizon, Bathurst Mining Camp, New Brunswick. Ca. J. Earth Sci. 33, p. 252-283

Qing, H. & Mountjoy, E.W. (1994): Rare earth element geochemistry of dolomites in the Middle Devonian Presqu'ile barrier, Western Canada Sedimentary Basin: implications for fluid-rock ratios during dolomitization. Sedimentology, v.41,4, p.787, doi:10.1111/j.1365-3091.1994.tb01424.x

Rastad, E. (1981): Geological, Mineralogical, and Facies Investigations on the Lower Cretaceous Stratabound Zn-Pb-(Ba-Cu) Deposits of the Irankuh Mountain Range, Esfahan, West Central Iran. Unpubl. PhD Thesis, Ruprecht-Karl-University Heidelberg

Rastad, E., Fontbote, L. & Amstutz, G.C. (1980): Relations between tidal flat facies and diagenetic ore fabrics in the stratabound Pb-Zn-(Ba-Cu) deposits of Irankuh, Esfahan, West Central Iran. Universidad de Bercelona, Instituto de Investigationes Geologicas Dipretacion Provincial, Revista, v. 34, p. 311-323

Reichert, J., Borg, G. & Rashidi, B. (2003): Mineralogy of calamine ore from the Mehdi Abad zinc-lead deposit, Central Iran. In: Eliopoulos, D. G. et al. (eds.): Mineral Exploration and Sustainable Development. v. 1, p. 97–100, Millpress, Rotterdam.

Reichert, J. & Borg, G. (2002). Lithological and structural controls on non-sulfide zinc ores at Kuh-e-Surmeh, Zagros Fold Belt, SW Iran. Denver Annual Meeting (October 27-30, 2002) GSA-Conference 2002, poster presentation.

Rimstidt J. D., Chermak J. A., & Gagen P. M. (1994) Rates of reaction of galena, sphalerite, chalcopyrite, and arsenopyrite with Fe(III) in acidic solutions. The Environmental Geochemistry of Sulfide Oxidation, A.C.S. Symp. Series, p. 2-13.

Ritchie, A.I.M. (1994): The Waste-rock Environment, in: Environmental Geochemistry of Sulfide Mine-Wastes, Mineralogical Association of Canada Short Course Handbook (J.L. Jambor and D.W. Blowes, eds.), v. 22, p. 133-161

Rollinson, H.R. (1993). Using Geochemical Data: Evaluation, Presentation, Interpretation. Longman Group UK Limited

Runnells, D.D. and Rampe, J.J. (1989): Natural clean-up of a stream contaminated by mine and mill wastes: A reaction analogous to liming in water treatment, in Miles D.L., ed., Proceed-

ings of the 6th International Symposium on Water-Rock Interaction, Malvern, 3-8 August 1989, Rotterdam: A.A. Balkema, p. 597-598

Rutherford, N. (2002): Interaction of pH, Redox and Solution Chemistry in Exploration Geochemistry. ALS Chemex News, 2, 2002

Saaltink, M.W., Domènech,C., Ayora,C. & Carrera, J. (2002): Modelling the oxidation of sulphides in an unsaturated soil, Mine Water Hydrogeology and Geochemistry, Geological Society, London, Special Publications, 198, p. 187-204

Sadiq A. M. & Nasir S. J. (2002): Middle Pleistocene karst evolution in the State of Qatar, Arabian Gulf. Journal of Cave and Karst Studies 64(2), p. 132-139.

Salmon S. & Malmström M. (2002): Steady state, geochemical box model of a tailings impoundment: Application to Impoundment 1, Kristineberg, Sweden, and prediction of effect of remediation. Report in series of the MISTRA research programme: Mitigation of the environmental impact from mining waste, Stockholm, Sweden, MiMi 2002:2

Salmon, S.U. (2003): Geochemical modelling of Acid Mine Drainage in Mill Tailings: Quantification of Kinetic Processes From Laboratory to Field Scale. Ph.D. KTH Land and Water Resource Engeneering

Sangameshwar, S.R. & Barnes,H.L. (1983): Supergene processes in zinc-lead-silver sulfides ores in carbonates, Economic Geology, 78, 1379-97

Sattarzadeh,Y., Cosgrove, J.W. & VITA-FINZI, C. (2002): The geometry of structures in the Zagros cover rocks and its neotectonic implications. In: Clift, P.D. et al. (Eds): The Tectonic and Climatic Evolution of the Arabian Sea Region. Geological Society Special Publication 195, p. 205–217.

Scheffer, F. & Schachtschabel, P. (2002): Lehrbuch der Bodenkunde. Spektrum Akademischer Verlag Heidelberg, Berlin

Schippers,A. (2003): Long-term anaerobic microbial processes in remediated mine tailings. MiMi-report. Mitigation of the environmental impact from mining waste (MiMi). MiMi Print, Lulea, Sweden

Schwartz, M. (2000): Cadmium in Zinc Deposits: Economic Geology of a Polluting Element. Econ. Geol. Review, 42, 2000, p. 445-469

Scott, S.D. & Barnes, H.L. (1971). Sphalerite Geothermometry and Geobarometry. Economic Geology, 66, 1971, p. 653-669

Seal, R.R. II, Foley, N.K., and Wanty, R.B., 2002, Introduction to Geoenvironmental Models of Mineral Deposits: in Progress on Geoenvironmental Models for Selected Mineral Deposit Types, Seal R.R., II, and Foley, N.K., eds., USGS Open-file Report 02-195, p. 1-7.

Sharp, Z.D. (1999): Application of stable isotope geochemistry to low-grade metamorphic rocks. In: Low-Grade Metamorphism (Frey M & Robinson D; Eds). Blackwell Science, p. 227-260.

Shufeng, Y., Chengzao, J., Hanlin, C., Guoqi, W., Xiaogan, C., Dong, J., Ancheng, X & Shaojie, G. (2002): Tectonic evolution of Tethyan tectonic field, formation of Northern Margin basin and explorative perspective of natural gas in Tarim Basin. Chinese Science Bulletin, V.47, p. 34-41

Sigg, L. & Stumm, W. (1989): Aquatische Chemie – Eine Einführung in die Chemie wässriger Lösungen und natürlicher Gewässer. Verl. Der Fachvereine; Stuttgart: Teubner, 1994)

Stöcklin, J (1968): Structural history and tectonics of Iran: A review. Amer Assoc Petrol Geol Bull 52, p. 1229-1258.

Stumm, W. & Morgan, J.J. (1996): Aquatic Chemistry, Chemical Equilibria and Rates in Natural Waters, 3rd ed. John Wiley & Sons, Inc., New York, 1022p.

Sun, Q., McDonald, L.M. Jr. & Skousen, J.G., (2000). Effects of Armoring on Limestone Neutralization of AMD. Proceedings of the 2000 West Virginia Mine Drainage Task Force Symposium. Morgantown, WV. 4-5 April 2000, 10 p.

Takahashi, T. (1960). Supergene Alteration of Zinc and Lead Deposits in Limestone. Economic Geology, v. 55, 6, p. 1084-1115

Taylor, S.R. & McLennan, S.M. (1985): The continental crust: its composition and evolution. 312 p.

Trivedi, P., Dyer, J.A. & Sparks, D.L. (2003): Lead Sorption onto Ferrihydrite. 1. A Macroscopic and Spectroscopic Assessment. Environ. Sci. Technol., 37, p. 908-914

Valley, J. W.; Taylor Junior, H. P.; O'Neil, J. R. (1986): Stable isotope geochimistry of metamophic rocks. Revs. Mineralogy, 16, p. 445-489.

Veizer, J., Hoefs, J., (1976): The nature of $^{18}O/^{16}O$ and $^{13}C/^{12}C$ secular trends in sedimentary carbonate rocks. Geochim. Cosmochim. Acta 40, p. 1387–1395.

Voegelin, A., Barmettler, K. & Kretzschmar, R. (2003): Heavy-metal release from contaminated soils: Comparison of column leaching and batch extraction results. J. Environmental Quality, 32, p. 865-875

Wellmer, F.W. (2002): Leachable supergene Base and Precious Metal Deposits Worldwide. Erzmetall, 55, 1, p. 25-33

Weyl, P.K. (1960): Porosity through dolomitization--Conservation-of-mass requirements. J. Sed. Petrology, v. 30(1), p. 85-90

Wilkins, S.J., Compton, R.G., Taylor, M.A., & Viles, H.A (2001): Channel Flow Cell Studies of the Inhibiting Action of Gypsum on the Dissolution Kinetics of Calcite: A Laboratory Approach with Implications for Field Monitoring. J. Colloid Interface Sci., 236, p.354-361.

Williamson, M.A. & Rimstidt, J.D. (1994): The kinetics and electrochemical rate-determining step of aqueous pyrite oxidation: Geochimica et Cosmochimica Acta, v. 58, p. 5443-5454.

Yanful, E.K. & Orlandea, M.P. (2000): Controlling acid drainage in a pyritic mine waste rock. Part II – Geochemistry of drainage. Water, Air and Soil Pollution Journal, v. 124, 3-4, December, p. 259-283.

Zahedi, M. (1976): Explanatory text of the Esfahan quadrangle map. 1:250,000. Iran Geological Survey, 49 p.

Zeman, J. (1985): Supergene alteration of sulfides, II. A laboratory electrochemical study. Scripta Fac. Sci. Nat. Univ. Purk. Brun., v.15,2, p. 115-136

Zeng, N., Izawa, E., Motomura, Y. & Lai,L. (2000): Silver Minerals and paragenesis in the Kangjiawan Pb-Zn-Ag-Au Deposit of the Shuikoushan Mineral District, Hunan Province, China. Can. Mineral., v. 38, p. 11-22

8 Appendix

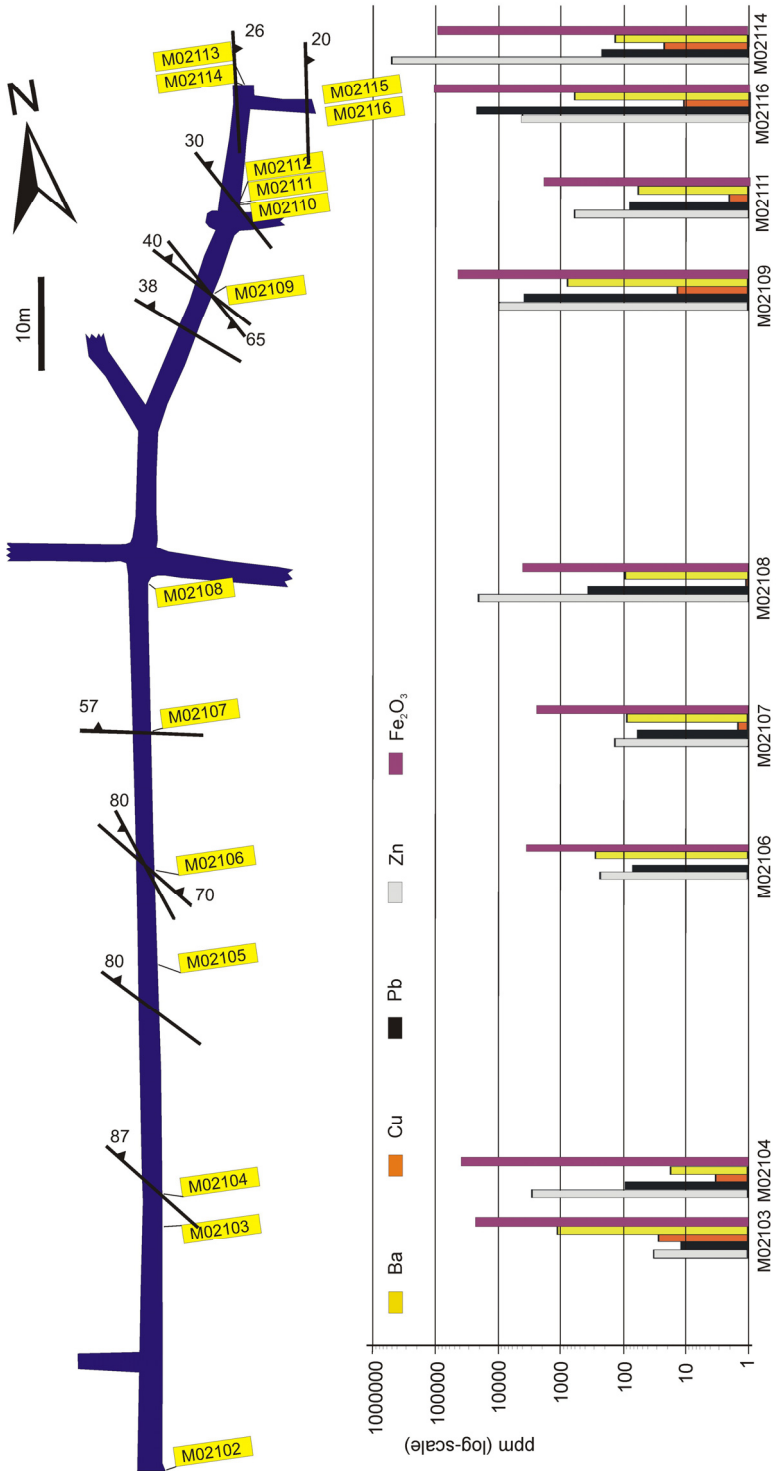

Fig. A. 1: Mehdi Abad, MOB: Schematic map of the base level adit (No. 1) with faults, and location of sample points. The graph (logarithmic scale on y-axis) shows the concentration of Zn, Pb, Ba, and Cu of selected samples. (after NOSRATIAN, 1991)

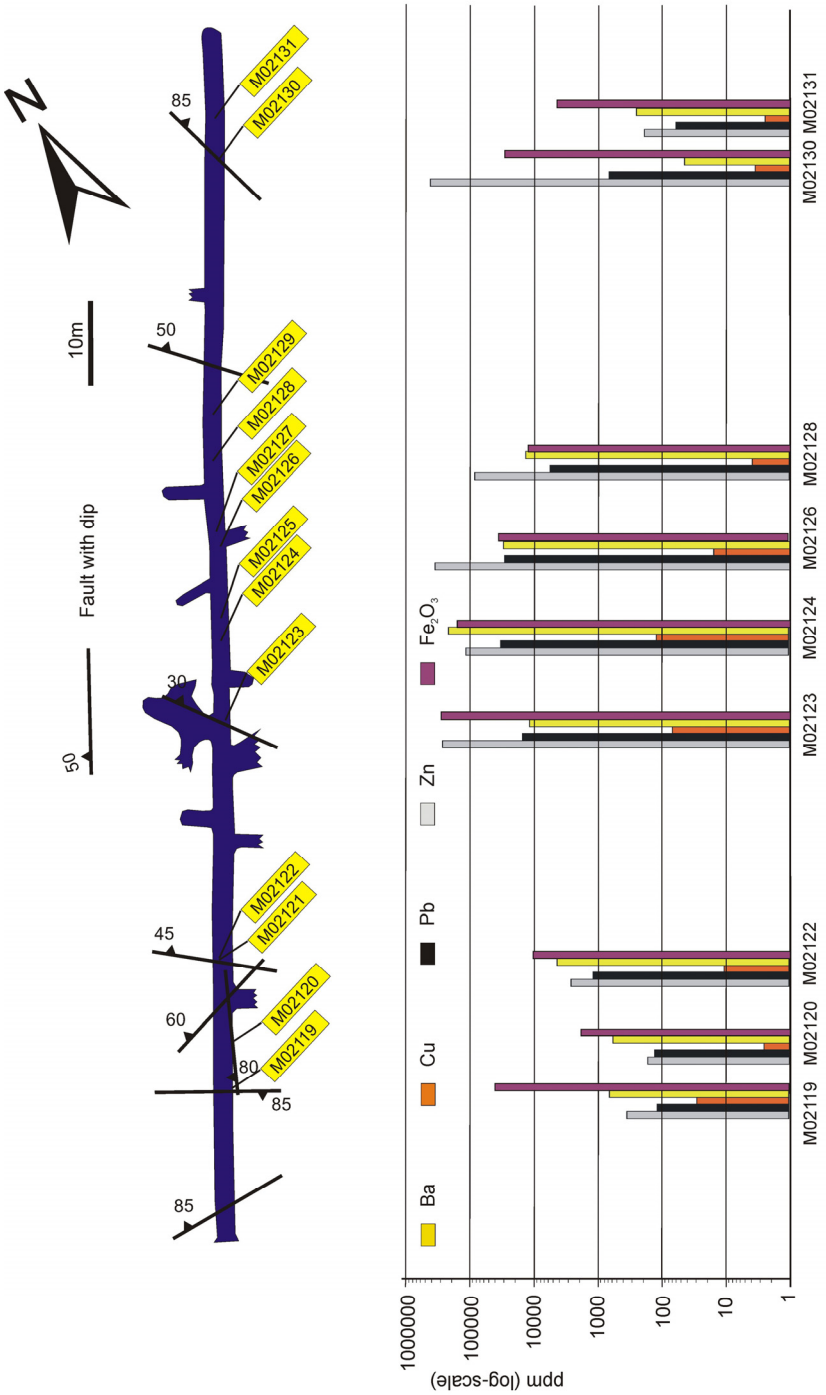

Fig. A. 2: Mehdi Abad, MOB: Schematic map of the mid level adit (No. 2) with faults, and location of sample points. The graph (logarithmic scale on y-axis) shows the concentration of Zn, Pb, Ba, and Cu of selected samples. (Map after NOSRATIAN, 1991)

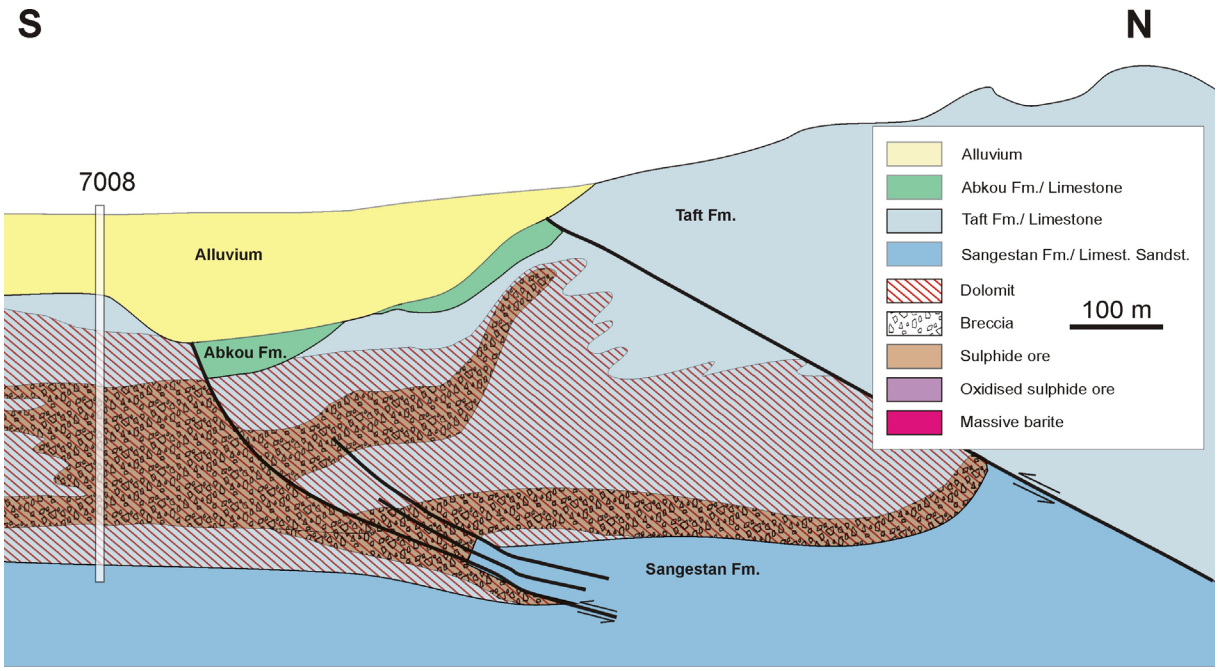

Fig. 117: Mehdi Abad, VOB: Stratigraphic position of bore hole no. 7008. The sulphide ore is mainly associated with the brecciated dolomite of the Taft Formation. The breccia as well as the barren host rock appears dolomitised. (Graphic modified after BRGM, 1994)

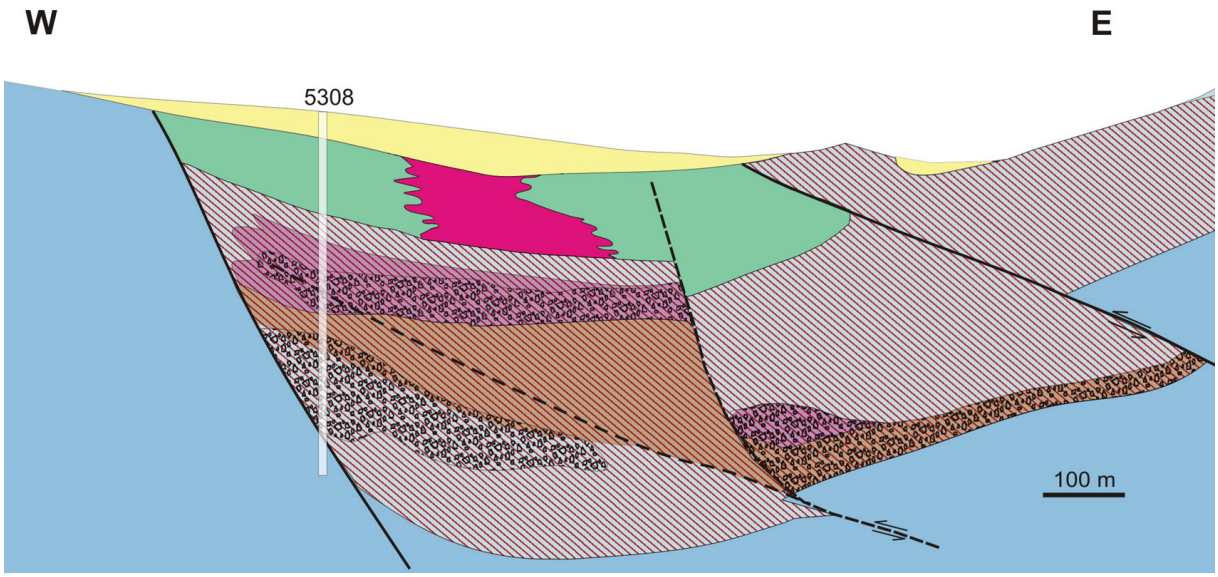

Fig. 118: Mehdi Abad, VOB: Stratigraphic position of bore hole no. 5308. Here the sulphide ore is partly oxidised. Dolomitisation has apparently affected the limestones of the Taft Formation exclusively. The strata of the Abkou Formation, which shows regionally massive barite mineralisation, have not been influenced by subsequent dolomitisation processes. (Graphic modified after BRGM, 1994)

Sample	Location	Borehole No.	Depth	Local	Lithology	Comments
5204-122a	Mehdi Abad	5204	-122	VOB	dolomite	breccia, oxidised
5204-122b	Mehdi Abad	5204	-122	VOB	dolomite	breccia, oxidised
5204-153	Mehdi Abad	5204	-153	VOB	dolomite	breccia, oxidised
5204-159	Mehdi Abad	5204	-159	VOB	dolomite/limestone	fault breccia
5204-173	Mehdi Abad	5204	-173	VOB	gossan	barite veins
5204-185	Mehdi Abad	5204	-185	VOB	dark grey dolomite	
5204-194	Mehdi Abad	5204	-194	VOB	dark grey limestone	intercalations of shale
5204-225	Mehdi Abad	5204	-225	VOB	limestone with intercalated shales	
5308-045	Mehdi Abad	5308	-45	VOB	gossan	oxidised
5308-156	Mehdi Abad	5308	-156	VOB	gossan barite-rich	oxidised
5308-167	Mehdi Abad	5308	-167	VOB	gossan barite-rich	oxidised
5308-189	Mehdi Abad	5308	-189	VOB	gossan barite-rich	oxidised
5308-196	Mehdi Abad	5308	-196	VOB	Barite	oxidised
5308-212	Mehdi Abad	5308	-212	VOB	Barite/sulphides	sulphide ore
5308-226	Mehdi Abad	5308	-226	VOB	Barite	oxidised
5308-247	Mehdi Abad	5308	-247	VOB	sulphides, barite	sulphide ore
5308-265	Mehdi Abad	5308	-265	VOB	sulphides, barite	sulphide ore
5308-275	Mehdi Abad	5308	-275	VOB	sulphides, barite	breccia
5308-394	Mehdi Abad	5308	-394	VOB	shale	breccia
5308-431	Mehdi Abad	5308	-431	VOB	siltstone, barite	
M02104	Mehdi Abad			MOB	dolomite	
M02108	Mehdi Abad			MOB	limestone	fault breccia
M02109	Mehdi Abad			MOB	limestone	fault breccia
M02113	Mehdi Abad			MOB	limestone	
M02114	Mehdi Abad			MOB	non-sulph. ore	red ore
M02115	Mehdi Abad			MOB	limestone	fault breccia
M02116	Mehdi Abad			MOB	limestone	fault breccia
M02123	Mehdi Abad			MOB	non-sulph. ore	red ore
M02124	Mehdi Abad			MOB	non-sulph. ore	red ore
M02125	Mehdi Abad			MOB	non-sulph. ore	red ore
M02126	Mehdi Abad			MOB	non-sulph. ore	red ore
M02127	Mehdi Abad			MOB	non-sulph. ore	red ore
M02128	Mehdi Abad			MOB	limestone	breccia
M02129	Mehdi Abad			MOB	non-sulph. ore	white ore
M02130	Mehdi Abad			MOB	mylonite	fault zone
M02132	Mehdi Abad			MOB	non-sulph. ore	red ore
M02133	Mehdi Abad			MOB	non-sulph. ore	red ore
M02134	Mehdi Abad			MOB	non-sulph. ore	red ore
M02135	Mehdi Abad			MOB	non-sulph. ore	white ore
M02136	Mehdi Abad			MOB	non-sulph. ore	white ore

	%	%	%	%	%	%	%	%	%	%	%	%	ppm	%	%	%
Sample	**SiO2**	**Al2O3**	**Fe2O3**	**MgO**	**CaO**	**Na2O**	**K2O**	**TiO2**	**P2O5**	**MnO**	**Cr2O3**	**LOI**	**Ba**	**SUM (Oxides+LOI+Ba)**	**TOT/C**	**TOT/S**
5204-122a	0.18	0.12	1.28	8.12	44.74	0.00	0.02	0.00	0.02	0.83	0.00	43.90	514	99.28	12.30	0.01
5204-122b	0.22	0.15	3.66	16.63	32.74	0.00	0.02	0.00	0.06	1.24	0.00	44.20	1426	99.09	12.60	0.00
5204-153	0.42	0.42	8.91	11.81	28.77	0.03	0.02	0.02	0.07	7.57	0.00	39.80	1658	98.03	11.70	0.01
5204-159	19.21	6.49	8.12	5.00	10.38	0.07	2.06	0.34	0.04	2.28	0.01	19.80	120466	87.25	4.38	3.10
5204-173	6.16	0.55	45.95	0.23	0.13	0.01	0.21	0.03	0.02	9.48	0.00	9.60	137736	87.75	0.16	3.12
5204-185	17.03	2.41	25.01	5.55	10.62	0.03	0.81	0.13	0.05	8.61	0.00	28.80	0	99.06	9.19	0.53
5204-194	14.09	1.56	1.71	1.78	42.65	0.00	0.56	0.09	0.03	0.40	0.00	36.80	26	99.68	10.40	0.13
5204-225	47.51	8.14	3.71	2.95	15.09	0.44	2.26	0.45	0.14	0.12	0.01	17.90	532	98.77	4.71	0.12
5308-045	46.82	3.80	25.71	0.35	0.19	0.06	0.99	0.19	0.08	2.29	0.01	7.00	67944	95.08	0.13	1.71
5308-156	44.08	0.35	19.02	1.09	0.68	0.00	0.05	0.01	0.04	2.28	0.00	6.90	148196	91.05	0.64	3.58
5308-167	0.98	0.03	22.43	0.21	0.02	0.00	0.00	0.00	0.00	2.31	0.00	4.00	290601	62.43	0.75	6.95
5308-189	5.27	0.20	62.35	0.24	0.02	0.01	0.00	0.00	0.04	0.69	0.00	7.50	147706	92.82	0.17	3.53
5308-196	0.16	0.00	10.72	0.00	0.01	0.00	0.00	0.00	0.00	0.01	0.00	1.00	494743	67.16	0.07	11.90
5308-212	10.57	0.00	4.21	0.12	0.02	0.01	0.00	0.00	0.00	0.24	0.00	7.70	225379	48.06	0.44	15.20
5308-226	12.18	0.03	5.96	0.26	0.07	0.00	0.00	0.00	0.00	0.76	0.00	4.10	408074	68.93	1.07	10.30
5308-247	3.57	0.24	43.90	1.89	0.44	0.03	0.08	0.01	0.01	6.90	0.00	27.60	62662	91.67	8.89	3.44
5308-265	14.47	0.14	19.45	0.78	0.19	0.01	0.03	0.00	0.03	2.67	0.00	14.30	211922	75.74	3.70	9.24
5308-275	7.65	0.14	35.46	1.30	0.35	0.00	0.04	0.00	0.02	4.92	0.02	21.00	154589	88.17	6.28	5.90
5308-394	18.29	3.46	38.74	2.28	0.49	0.08	1.06	0.18	0.04	8.33	0.01	26.10	5241	99.64	8.02	0.56
5308-431	56.49	7.07	9.07	1.01	0.33	0.05	1.76	0.37	0.09	0.99	0.03	12.20	73301	97.64	1.78	1.98
M02104	2.27	1.17	4.50	16.40	30.69	0.05	0.22	0.06	0.20	0.12	0.00	44.00	17	99.68	12.22	0.18
M02108	1.31	0.11	0.42	0.16	52.71	0.05	0.02	0.00	0.03	0.21	0.00	42.00	92	97.04	11.64	0.00
M02109	7.17	1.44	4.37	0.67	45.94	0.01	0.31	0.07	0.04	0.06	0.01	38.30	768	98.48	10.09	0.38
M02113	4.52	0.93	0.75	0.55	51.33	0.01	0.25	0.04	0.03	0.08	0.01	41.00	245	99.53	11.35	0.00
M02114	27.43	1.87	11.74	0.26	0.25	0.04	0.51	0.08	0.06	0.12	0.01	9.70	131	52.09	0.05	0.00
M02115	4.88	0.47	1.07	0.44	46.08	0.02	0.13	0.02	0.01	0.13	0.02	38.10	36	91.38	10.19	0.00
M02116	28.78	7.96	14.05	1.14	21.54	0.24	1.99	0.39	0.12	0.04	0.01	20.90	754	97.25	4.65	0.40
M02123	14.93	0.31	29.98	0.03	0.08	0.01	0.04	0.01	0.03	0.06	0.00	11.10	12730	58.01	0.14	0.33
M02124	5.97	0.20	16.73	0.02	0.09	0.00	0.02	0.01	0.03	0.01	0.00	10.10	229464	58.80	0.10	5.27
M02125	2.15	0.64	58.92	0.06	0.34	0.05	0.03	0.03	0.05	0.01	0.00	13.80	53701	82.09	0.18	1.41
M02126	21.90	1.60	3.54	0.08	0.09	0.00	0.17	0.08	0.01	0.60	0.01	12.40	33168	44.20	0.61	0.81
M02127	2.41	0.42	2.76	0.21	0.28	0.00	0.02	0.02	0.02	0.25	0.02	25.40	46919	37.07	4.61	1.15
M02128	5.52	1.58	1.33	0.49	39.43	0.06	0.05	0.08	0.04	0.07	0.00	35.50	13996	85.72	8.85	0.35
M02129	20.81	4.16	3.19	0.49	3.98	0.57	0.69	0.21	0.07	0.10	0.00	15.80	7254	50.88	1.41	0.34
M02130	10.56	0.69	3.02	0.78	0.48	0.02	0.18	0.04	0.00	0.21	0.01	27.90	47	43.91	7.32	0.00
M02132	15.28	0.39	29.08	0.07	1.20	0.00	0.08	0.02	0.11	0.07	0.00	11.10	5412	58.01	0.35	0.13
M02133	18.93	3.14	21.94	0.29	0.69	0.17	0.58	0.13	0.07	0.10	0.00	11.30	632	57.43	0.25	0.09
M02134	6.06	0.21	16.71	0.15	3.14	0.13	0.03	0.01	0.00	0.11	0.00	23.50	4072	50.52	4.45	0.12
M02135	24.82	1.05	1.02	0.13	0.20	0.00	0.26	0.05	0.00	0.08	0.00	9.00	10550	37.79	0.11	0.26
M02136	28.26	9.78	1.00	0.88	0.78	0.01	0.22	0.03	0.00	0.01	0.00	14.20	6042	55.86	0.03	0.10

	ppm	ppm	ppm	ppm	ppm	ppm	ppm	ppm	ppm	ppm	ppm	ppm	ppm	ppm	ppm	ppm
Sample	**Ni**	**Co**	**Cs**	**Sc**	**Ga**	**Hf**	**Nb**	**Rb**	**Sn**	**Sr**	**Ta**	**Th**	**Tl**	**U**	**V**	**W**
5204-122a	2.4	33.5	0.0	0.0	0.0	0.0	<0.05	0.8	<1	30.5	0.0	<0.1	0.4	0.8	8.0	796.8
5204-122b	3.5	14.7	0.1	0.0	1.0	0.0	<0.05	0.7	1.0	52.2	0.3	0.2	0.8	0.9	10.0	1946.5
5204-153	6.2	11.1	0.0	1.0	5.6	0.0	<0.05	0.5	<1	131.2	0.7	0.4	0.1	3.1	42.0	3846.2
5204-159	26.6	6.5	9.5	5.0	10.0	3.2	6.30	75.2	<1	2063.4	1.2	6.1	18.1	4.4	77.0	10.0
5204-173	17.0	9.1	0.7	1.0	7.9	0.8	0.70	5.5	<1	2776.7	1.3	0.5	15.4	3.6	8.0	2655.8
5204-185	11.3	10.1	2.4	2.0	9.8	1.3	2.50	26.0	<1	57.3	0.3	2.8	1.7	3.8	21.0	1047.1
5204-194	11.5	16.3	1.4	2.0	2.6	1.3	1.70	16.1	<1	207.8	0.3	2.1	0.7	0.9	16.0	1309.9
5204-225	24.4	26.9	7.2	9.0	10.0	4.9	9.10	91.9	2.0	140.6	2.0	9.2	0.3	2.1	66.0	7824.8
5308-045	45.0	9.0	7.2	1.0	6.7	1.3	3.50	48.9	1.0	1161.4	0.4	2.6	4.9	5.1	55.0	24.3
5308-156	1.7	24.3	0.0	1.0	2.7	0.7	0.80	2.1	<1	3142.4	2.6	0.2	0.3	1.3	<5	5088.2
5308-167	3.6	40.5	0.0	0.0	2.2	2.2	<0.05	0.0	<1	5881.4	3.3	<0.1	5.7	0.4	<5	976.7
5308-189	3.1	18.3	0.0	0.0	0.8	0.0	<0.05	0.0	<1	3333.0	1.5	0.2	0.1	3.8	9.0	1626.9
5308-196	0.1	6.5	0.0	0.0	0.0	2.8	<0.05	0.0	<1	8521.8	6.0	<0.1	<0.1	0.1	<5	1249.6
5308-212	0.9	28.2	0.1	0.0	0.9	0.6	<0.05	0.0	<1	5443.0	2.4	<0.1	2.3	0.3	<5	2590.9
5308-226	0.5	9.3	0.0	1.0	0.7	2.3	<0.05	0.0	<1	9830.5	4.2	<0.1	0.7	0.0	<5	1897.0
5308-247	1.9	20.0	0.3	0.0	5.1	0.0	<0.05	2.4	<1	1578.7	0.7	0.2	1.2	1.9	7.0	1671.1
5308-265	0.8	24.0	0.2	1.0	4.6	0.8	<0.05	1.1	<1	5532.8	1.7	<0.1	1.3	1.4	5.0	3719.7
5308-275	5.0	21.1	0.0	0.0	2.5	0.0	0.60	1.5	<1	4104.5	1.0	0.4	1.5	2.2	10.0	2151.2
5308-394	12.7	13.4	4.0	3.0	12.5	1.1	3.70	49.0	<1	175.6	0.3	3.1	1.1	2.3	40.0	571.3
5308-431	12.3	24.9	4.4	4.0	12.4	2.5	8.40	94.5	2.0	2095.1	1.5	7.0	0.4	3.0	63.0	3457.8
M02104	31.2	6.2	1.1	2.0	1.0	0.0	1.10	8.8	<1	97.0	0.0	1.7	3.0	0.0	30.0	9.6
M02108	15.8	32.9	0.0	0.0	0.0	0.0	<0.05	0.5	<1	83.2	0.3	0.3	36.7	0.4	<5	1786.3
M02109	12.6	12.8	3.7	2.0	1.4	0.0	1.00	15.9	<1	151.8	0.3	0.9	9.3	2.3	49.0	1130.5
M02113	1.8	6.3	2.2	1.0	1.0	0.0	0.60	12.6	<1	203.0	0.2	0.6	6.3	0.9	14.0	1229.3
M02114	23.0	23.7	3.3	3.0	2.8	0.0	0.60	20.4	3.0	42.1	0.3	1.3	348.4	2.4	35.0	1236.3
M02115	40.4	4.7	0.9	1.0	1.1	0.0	0.80	6.6	3.0	137.9	0.0	0.3	65.8	1.1	7.0	26.3
M02116	4.1	3.3	14.1	6.0	11.9	2.1	6.00	95.9	1.0	205.8	0.5	4.2	219.9	5.2	92.0	76.9
M02123	38.7	13.9	0.2	0.0	1.1	0.0	<0.05	1.6	<1	192.1	0.2	<0.1	197.9	8.7	18.0	665.5
M02124	24.2	7.7	0.0	0.0	1.6	0.0	<0.05	0.5	<1	4028.6	1.0	0.5	7.4	8.8	8.0	27.6
M02125	58.2	5.8	0.0	0.0	1.5	0.0	<0.05	0.8	<1	1037.6	0.5	0.8	22.6	8.4	24.0	806.9
M02126	56.4	17.4	1.1	0.0	2.3	<0,5	1.40	7.3	<1	646.0	0.3	1.2	26.8	6.7	29.0	4.6
M02127	71.1	33.1	0.0	0.0	1.6	<0,5	<0,5	0.0	<1	894.1	0.5	0.5	42.5	6.1	10.0	2429.0
M02128	18.4	7.1	0.0	1.0	2.3	0.5	0.90	2.6	<1	414.5	0.6	1.1	17.0	1.8	22.0	1096.1
M02129	43.5	10.3	2.4	4.0	7.0	1.1	3.50	35.3	<1	201.9	0.4	4.2	57.3	8.1	54.0	314.2
M02130	109.5	23.9	1.2	1.0	1.7	0.6	0.80	7.4	1.0	15.5	0.0	0.4	43.0	0.9	12.0	324.9
M02132	34.4	33.9	0.5	1.0	1.0	0.0	<0.05	2.7	1.0	128.8	0.3	0.4	92.2	5.0	10.0	2141.8
M02133	123.9	56.8	2.6	4.0	3.8	1.1	2.30	22.9	<1	45.9	0.3	2.1	42.7	7.9	42.0	1724.1
M02134	143.6	29.3	0.0	0.0	0.0	0.0	<0.05	0.7	<1	97.0	0.0	0.2	29.8	24.4	22.0	317.0
M02135	26.0	43.9	2.2	2.0	1.7	0.0	0.90	10.9	<1	206.4	0.1	0.8	33.1	2.4	20.0	895.2
M02136	189.1	10.3	2.1	5.0	1.5	<0,5	<0,5	8.2	<1	279.6	0.0	0.6	19.2	2.1	15.0	91.5

	ppm	ppm	ppm	ppm	ppm	ppm	ppm	ppm	ppm	ppm	ppm	ppm	ppm	ppm	ppm	ppm	ppm
Sample	**Zr**	**Y**	**La**	**Ce**	**Pr**	**Nd**	**Sm**	**Eu**	**Gd**	**Tb**	**Dy**	**Ho**	**Er**	**Tm**	**Yb**	**Lu**	**Mo**
5204-122a	1.3	0.50	0.80	2.10	0.11	0.4	<0,1	<0.05	0.15	0.03	0.14	<0.05	<0.05	<0.05	0.1	0.02	0.4
5204-122b	1.2	0.90	1.50	3.50	0.23	0.6	0.30	<0.05	0.30	0.02	0.20	<0.05	0.13	<0.05	0.1	<0.01	0.8
5204-153	5.9	2.70	5.50	8.40	0.72	3.2	0.70	0.82	0.78	0.07	0.46	0.09	0.24	<0.05	0.2	0.02	2.1
5204-159	89.1	10.00	19.20	28.70	2.72	11.7	2.10	0.98	2.36	0.27	2.38	0.30	0.95	0.2	1.1	0.20	3.1
5204-173	5.5	2.30	6.10	6.20	0.50	2.1	0.80	<0.05	1.18	0.07	1.22	0.05	0.11	<0.05	0.3	0.01	5.7
5204-185	50.8	9.10	11.40	20.30	2.03	8.9	1.90	1.58	2.35	0.33	2.00	0.34	0.78	0.1	0.9	0.10	1.7
5204-194	36.0	6.50	6.80	15.10	1.38	5.6	1.20	0.29	1.35	0.22	0.88	0.19	0.67	0.1	0.7	0.11	0.6
5204-225	156.3	17.50	25.80	46.10	4.99	20.3	4.30	0.81	3.56	0.56	3.23	0.79	1.89	0.3	1.7	0.20	0.5
5308-045	37.9	6.70	16.30	22.50	1.96	7.8	1.30	<0.05	1.01	0.16	1.51	0.19	0.66	0.1	0.8	0.13	2.2
5308-156	5.1	1.90	2.90	3.40	0.21	0.7	0.50	2.01	1.04	0.06	1.39	<0.05	0.07	<0.05	0.1	0.02	1.2
5308-167	0.5	3.30	5.00	2.80	0.24	1.2	0.90	<0.05	2.01	0.13	2.34	0.05	0.13	<0.05	0.1	0.01	2.7
5308-189	1.8	2.70	3.30	4.50	0.26	1.3	0.70	1.59	1.33	0.09	1.39	0.07	0.14	<0.05	0.2	0.02	1.3
5308-196	0.0	5.50	7.50	3.10	0.14	0.5	1.30	<0.05	2.76	0.09	3.34	<0.05	<0.05	<0.05	0.2	0.01	2.5
5308-212	1.0	1.60	3.80	3.30	0.10	<0,1	0.40	4.52	1.23	0.03	1.43	<0.05	<0.05	<0.05	0.1	<0.01	0.8
5308-226	0.0	4.20	7.30	4.30	0.31	1.5	1.40	0.34	2.28	0.10	3.24	<0.05	0.05	0.1	0.2	<0.01	1.3
5308-247	2.7	1.50	4.30	5.30	0.40	1.5	0.40	0.79	0.69	0.05	0.72	<0.05	0.12	<0.05	0.1	0.02	1.8
5308-265	1.4	2.70	3.80	3.10	0.15	<0,1	0.70	<0.05	1.35	0.05	1.84	<0.05	0.08	<0.05	0.1	0.02	2.0
5308-275	1.7	2.60	2.20	1.80	0.22	1.1	0.60	<0.05	1.20	0.06	0.65	0.07	0.09	<0.05	0.2	0.02	5.3
5308-394	43.2	5.20	8.10	10.90	0.89	2.7	0.50	0.70	0.75	0.18	0.64	0.16	0.64	0.1	0.7	0.11	4.0
5308-431	73.0	11.20	22.70	34.20	3.60	12.4	2.00	<0.05	2.53	0.33	2.73	0.38	1.32	0.2	1.4	0.22	1.6
M02104	15.7	10.40	4.00	9.30	1.10	5.2	1.30	0.39	2.30	0.29	1.75	0.37	0.90	0.1	0.8	0.11	0.3
M02108	1.1	11.90	6.70	2.50	0.89	4.1	0.80	0.23	1.08	0.09	0.87	0.21	0.51	0.1	0.6	0.06	0.8
M02109	14.4	5.90	6.00	11.60	1.17	5.4	0.90	0.24	0.85	0.15	0.76	0.19	0.40	<0.05	0.5	0.06	2.3
M02113	9.2	5.90	5.30	7.90	0.84	3.8	0.60	0.15	0.79	0.08	0.41	0.15	0.37	0.1	0.4	0.05	0.4
M02114	13.1	11.60	12.60	16.40	2.40	10.9	1.60	0.40	1.96	0.21	1.31	0.37	0.67	0.1	0.8	0.11	4.0
M02115	5.5	14.60	7.30	8.30	1.63	8.3	1.50	0.88	1.90	0.32	1.66	0.29	0.71	0.1	0.6	0.09	0.8
M02116	69.2	8.10	18.90	29.00	3.03	9.8	1.30	0.40	1.12	0.22	1.02	0.26	0.75	0.1	1.1	0.15	2.7
M02123	2.4	8.50	4.20	10.70	1.66	8.5	1.60	0.57	1.82	0.31	1.97	0.30	0.67	0.1	0.6	0.05	7.2
M02124	1.8	4.20	3.70	2.50	0.30	1.4	1.00	<0.05	1.52	0.09	1.63	0.08	0.17	<0.05	0.2	0.01	9.3
M02125	7.6	10.20	7.20	8.60	1.50	7.9	1.70	0.83	2.20	0.23	1.54	0.24	0.41	0.1	0.5	0.08	51.2
M02126	17.7	3.40	5.10	9.60	0.68	3.0	0.40	<0.05	0.57	0.04	0.48	0.10	0.19	<0.05	0.2	0.04	1.8
M02127	4.8	3.60	3.50	11.70	0.59	2.7	0.80	<0.05	0.90	0.06	0.74	0.07	0.12	<0.05	0.3	<0.01	3.5
M02128	15.5	6.20	6.70	9.70	1.09	5.4	0.70	0.13	0.97	0.13	0.87	0.17	0.46	<0.05	0.4	0.03	0.7
M02129	49.4	7.50	8.60	21.60	1.60	7.0	1.10	0.23	1.38	0.20	0.95	0.27	0.70	0.1	0.7	0.07	2.5
M02130	12.0	4.70	2.50	3.70	0.67	3.5	0.80	0.16	0.93	0.09	0.69	0.11	0.28	<0.05	0.3	0.07	1.1
M02132	4.4	6.40	4.00	8.90	1.18	8.6	1.70	0.47	1.53	0.22	1.53	0.20	0.60	0.1	0.5	0.05	2.7
M02133	28.9	7.00	5.30	13.70	1.55	7.6	1.40	0.64	1.32	0.24	1.71	0.25	0.83	0.1	0.8	0.15	7.2
M02134	2.8	6.80	5.50	15.80	1.26	5.9	1.20	0.29	1.18	0.17	0.89	0.18	0.42	0.1	0.4	0.07	3.5
M02135	10.9	1.00	0.80	9.10	0.36	2.4	0.10	<0.05	0.33	0.05	0.44	0.06	0.14	<0.05	0.2	0.03	1.1
M02136	7.2	1.20	<0,5	5.30	0.13	0.8	0.20	<0.05	0.29	0.05	0.16	0.07	0.10	<0.05	0.1	0.03	0.4

	ppm	ppm	ppm	ppm	ppm	ppm	ppm	ppm					
Sample	**Cu**	**Pb**	**Zn**	**As**	**Cd**	**Sb**	**Bi**	**Ag**					
5204-122a	29.6	2011.4	2927.0	33.0	5.5	1.8	0.0	0.2					
5204-122b	15.7	219.9	4194.0	47.0	7.5	1.4	0.0	0.5					
5204-153	1204.3	3137.4	6606.0	76.0	26.1	208.0	0.2	14.4					
5204-159	197.6	13617.9	37164.0	317.0	161.7	71.0	0.2	15.0					
5204-173	487.9	6796.5	33345.0	240.0	73.8	178.5	5.0	10.3					
5204-185	12.0	186.2	6017.0	22.0	10.4	13.5	0.1	0.6					
5204-194	20.0	38.30	205.0	28.0	0.8	3.3	0.1	0.2					
5204-225	8.4	64.60	152.0	15.0	0.4	1.0	0.2	0.2					
5308-045	128.3	25943.4	1434.0	469.0	3.2	70.6	0.2	13.6					
5308-156	321.8	12157.7	9782.0	29.0	50.7	51.5	0.7	34.3					
5308-167	2435.0	36603.2	4750.0	208.0	19.6	216.6	3.1	66.1					
5308-189	378.9	15717.5	2899.0	203.0	3.5	53.3	0.2	11.3					
5308-196	1959.3	2782.0	386.0	30.0	0.4	26.4	11.6	18.2					
5308-212	248.6	31243.9	133392.0	17.0	583.3	534.2	0.6						
5308-226	2420.1	5102.5	1636.0	10.0	9.9	15.9	21.5	9.3					
5308-247	114.9	7123.0	30438.0	2.0	133.1	12.9	0.6	8.9					
5308-265	265.5	32920.3	58299.0	5.0	280.0	64.5	0.1	36.4					
5308-275	1447.3	12556.0	9391.0	15.0	33.2	29.1	5.0	10.7					
5308-394	64.1	1450.7	963.0	20.0	2.9	16.0	1.5	3.5					
5308-431	1793.4	3301.4	121.0	7.0	0.3	13.4	3.9	4.8					
M02104	3.2	90.90	2933.0	50.0	59.2	3.8	0.1	0.2					
M02108	1.1	357.1	20266.0	71.0	488.0	1.2	0.0	3.4					
M02109	13.1	3640.8	9228.0	1549.0	85.0	164.9	0.1	4.6					
M02113	3.8	92.00	2738.0	168.0	12.4	70.0	0.0	1.3					
M02114	21.5	211.8	471300.0	7114.0	16.1	274.6	0.0	0.3					
M02115	4.9	1784.8	63697.0	895.0	2004.1	64.0	0.0	0.8					
M02116	12.1	29428.6	5506.0	11545.0	34.6	250.1	0.3	0.7					
M02123	69.2	16238.5	300000.0	7687.0	70.1	197.4	0.1	3.2					
M02124	124.3	35064.4	99999.0	27387.0	127.7	1474.1	0.1	7.1					
M02125	95.2	35786.1	124000.0	24767.0	370.7	959.8	0.1	4.7					
M02126	15.8	31754.2	389900.0	6612.0	63.8	129.5	0.1	4.6					
M02127	3.3	30755.4	461253.0	6404.0	395.2	183.4	0.1	1.0					
M02128	3.9	5784.1	89818.0	1116.0	844.6	110.0	0.0	0.4					
M02129	7.0	24713.4	434320.0	1543.0	134.5	371.4	0.1	1.5					
M02130	3.6	702.3	472105.0	906.0	654.4	17.2	0.1	0.7					
M02132	133.4	4179.5	292344.0	6323.0	147.2	307.0	0.1	43.8					
M02133	38.3	8490.7	375258.0	2453.0	93.3	299.4	0.1	3.7					
M02134	4.9	5764.6	380608.0	5635.0	1600.8	75.2	0.0	0.5					
M02135	58.2	1904.8	99999.0	564.0	121.9	46.9	0.1	9.4					
M02136	200.4	1103.6	383200.0	199.0	44.6	19.7	0.0	2.8					

Sample	Location	Borehole No.	Depth	Local	Lithology	Comments
M02111	Mehdi Abad			MOB	limestone	
7006-117	Mehdi Abad	7006	-117	VOB	dolomite	barite veins
7006-267	Mehdi Abad	7006	-267	VOB	dolomite	with massive barite
7006-268	Mehdi Abad	7006	-268	VOB	dolomite	breccia
7006-275	Mehdi Abad	7006	-275	VOB	dolomite	
7006-291	Mehdi Abad	7006	-291	VOB	dolomite	
7006-303x	Mehdi Abad	7006	-303	VOB	shaly limestone	breccia
7006-317x	Mehdi Abad	7006	-307	VOB	shaly limestone	breccia
7006-330	Mehdi Abad	7006	-330	VOB	shale	breccia
7006-330x	Mehdi Abad	7006	-330	VOB	shale	breccia
7006-336	Mehdi Abad	7006	-336	VOB	shale	
7016-167	Mehdi Abad	7016	-167	VOB	dolomite/barite	sulphide ore
7016-197	Mehdi Abad	7016	-197	VOB	shale	mylonite with sulphides
7016-202x	Mehdi Abad	7016	-202	VOB	shaly limestone	sulphides
7016-65x	Mehdi Abad	7016	-65	VOB	gossan	
7016-75	Mehdi Abad	7016	-75	VOB	gossan	highly oxidised
7018-145a	Mehdi Abad	7018	-145	VOB	dolomite	breccia
7018-171	Mehdi Abad	7018	-171	VOB	dolomite	
7018-171a	Mehdi Abad	7018	-171	VOB	dolomite	sulphide ore
7018-188	Mehdi Abad	7018	-188	VOB	dolomite	
7018-194	Mehdi Abad	7018	-194	VOB	dolomite	breccia
7018-204a	Mehdi Abad	7018	-204	VOB	dolomite	sulphide ore
7018-360	Mehdi Abad	7018	-360	VOB	limestone/dolomite	partly oxidised
7018-370a	Mehdi Abad	7018	-370	VOB	shaly limestone/dolomite	sulphides
7018-370ab	Mehdi Abad	7018	-370	VOB	shales	
7018-370b	Mehdi Abad	7018	-370	VOB	shales	sulphides
7101-103	Mehdi Abad	7101	-103	VOB	gossan	barite rich
7101-131	Mehdi Abad	7101	-131	VOB	gossan	
7101-141	Mehdi Abad	7101	-141	VOB	barite, some dolomite	barite with galena Fe-Ox rich
7101-179x	Mehdi Abad	7101	-179	VOB	gossan	barite veins
7101-267	Mehdi Abad	7101	-267	VOB	gossan	galena, sulphides, barite veins
7101-356	Mehdi Abad	7101	-356	VOB	sulphides, barite	sulphide ore
7101-404	Mehdi Abad	7101	-404	VOB	sulphides, barite	sulphide ore with barite veins
7101-417	Mehdi Abad	7101	-417	VOB		barite veins, some galena
K02100	Ilrankuh			Goushfil Pit	dolomite with sulphide ore	
K02101	Ilrankuh			Goushfil Pit	dolomite	
K02102	Ilrankuh			Goushfil Pit	shales	
K02103	Ilrankuh			Goushfil Pit	dolomite	fault zone
K02104	Ilrankuh			Goushfil Pit	shales	fault zone
K02111	Ilrankuh			Goushfil Pit	shales	sulphides, partly oxidised, fault zone
K02114	Ilrankuh			Koladahrvazeh	dolomite	non-sulphide zinc mineralised

Sample	SiO2	Al2O3	Fe2O3	MgO	CaO	Na2O	K2O	TiO2	P2O5	MnO	Cr2O3	LOI	Ba	SUM (Oxides+LOI+Ba)	TOT/C	TOT/S
M02111	1.40	0.12	0.24	0.47	54.20	0.04	0.03	<0.01	0.03	0.05	0.01	43.10	60	99.70	11.93	0.01
7006-117	0.95	0.20	4.05	9.39	18.12	0.06	<0.02	<0.01	<0.01	1.03	<0.001	28.10	188881	83.00	7.63	4.74
7006-267	0.59	0.36	4.30	17.90	30.68	0.05	<0.02	0.01	0.04	1.75	<0.001	43.70	90	99.40	12.86	0.19
7006-268	0.57	0.43	4.36	17.27	30.80	0.03	<0.02	0.02	0.02	2.79	<0.001	42.50	106	98.81	12.67	0.50
7006-275	3.32	0.64	6.24	14.95	30.00	0.04	0.14	0.03	0.02	2.49	<0.001	39.20	600	97.13	12.20	1.05
7006-291	1.32	1.04	3.83	16.69	30.64	0.03	<0.02	0.05	0.29	3.02	0.00	42.50	32	99.42	12.30	0.01
7006-303x	19.86	0.53	27.76	1.27	0.73	0.02	0.10	0.03	<0.01	7.75	0.00	21.20	53002	85.17	6.56	5.06
7006-317x	20.03	2.72	38.34	1.87	0.80	0.04	0.72	0.13	<0.01	9.70	0.00	24.90	6050	99.93	8.23	0.59
7006-330	17.97	0.40	38.82	1.33	0.65	0.02	0.12	0.01	<0.01	10.76	<0.001	25.80	300	95.92	8.05	1.69
7006-330x	17.83	0.36	37.39	1.29	0.59	0.02	0.08	<0.01	<0.01	10.35	<0.001	25.50	510	93.48	7.98	2.56
7006-336	67.20	9.66	4.03	2.22	3.82	0.12	2.93	0.58	0.10	0.46	0.01	7.80	190	98.96	2.00	0.37
7016-167	4.50	1.05	40.58	1.49	0.48	0.05	0.27	0.05	0.02	6.83	0.00	27.20	24373	85.25	8.38	5.32
7016-197	15.88	3.46	22.88	1.07	0.35	0.05	1.22	0.17	0.03	4.47	0.00	17.90	103290	79.01	4.83	7.32
7016-202x	1.77	0.75	40.80	1.59	0.64	0.03	0.17	0.03	0.02	7.71	<0.001	27.00	52373	86.36	8.38	4.63
7016-65x	32.43	1.80	40.84	0.37	0.14	0.04	0.48	0.08	0.23	5.24	0.00	7.20	91533	99.07	0.10	1.75
7016-75	52.69	4.14	24.24	0.57	0.15	0.08	1.19	0.21	0.09	3.48	0.00	7.00	45849	98.97	0.11	0.85
7018-145a	1.65	0.20	1.57	19.15	30.46	0.04	0.02	<0.01	0.01	0.46	<0.001	46.00	1471	99.73	13.24	0.03
7018-171	1.27	0.27	2.13	18.88	29.88	0.04	0.04	<0.01	0.02	0.67	<0.001	45.30	40	98.52	13.05	0.16
7018-171a	1.37	0.26	1.39	6.51	10.96	0.02	0.04	<0.01	0.03	0.24	<0.001	1.50	100	22.34	5.10	11.08
7018-188	1.35	0.44	3.01	18.16	29.92	0.04	0.13	0.01	0.02	1.02	0.00	40.50	1791	94.81	12.01	0.86
7018-194	0.48	0.28	2.61	17.28	32.38	0.01	0.06	<0.01	0.02	1.03	<0.001	43.90	560	98.12	13.24	0.04
7018-204a	2.31	0.41	3.27	16.78	28.85	0.03	0.11	0.01	0.01	1.20	0.00	40.60	55	93.59	11.83	0.60
7018-360	2.00	0.65	7.57	0.83	29.06	0.06	0.17	0.03	0.02	23.24	<0.001	24.30	5260	88.52	6.61	0.01
7018-370a	3.40	0.85	41.53	4.12	1.82	0.05	0.21	0.04	<0.01	11.28	<0.001	31.50	210	94.82	9.85	1.94
7018-370ab	6.39	1.83	41.98	4.63	1.41	0.04	0.45	0.07	0.01	11.42	0.00	31.50	45	99.75	10.04	0.39
7018-370b	3.25	0.81	42.67	4.17	1.63	0.03	0.19	0.04	<0.01	11.54	<0.001	30.90	230	95.26	10.04	2.10
7101-103	26.53	0.15	1.28	0.05	0.08	0.01	0.03	0.01	0.01	0.12	0.00	1.00	366625	70.21	0.10	9.02
7101-131	8.14	0.15	54.37	0.09	0.06	0.01	0.05	<0.01	<0.01	4.49	<0.001	9.30	82227	85.85	0.49	1.97
7101-141	0.31	<0.03	15.99	0.03	0.03	0.01	0.06	<0.01	0.01	0.16	<0.001	9.80	255385	54.92	1.16	8.10
7101-179x	4.21	<0.03	26.65	0.24	0.05	0.02	0.05	<0.01	<0.01	1.47	<0.001	7.90	200581	63.00	1.23	7.58
7101-267	1.87	0.04	21.05	1.14	0.26	0.01	0.06	<0.01	<0.01	2.44	<0.001	21.00	87653	57.67	4.22	14.67
7101-356	4.98	0.07	27.87	1.17	0.25	0.01	0.11	<0.01	0.01	5.53	<0.001	28.60	3500	68.99	5.89	10.73
7101-404	11.19	0.41	23.81	1.05	0.36	0.03	0.09	0.02	0.04	3.15	<0.001	17.20	180500	77.51	4.36	7.17
7101-417	20.50	0.71	43.42	1.50	0.53	0.04	0.19	0.03	0.06	5.04	<0.001	24.70	20900	99.05	7.88	0.39
K02100	9.73	0.60	1.41	5.05	8.29	0.02	0.16	0.04	0.06	0.07	<0.001	7.00	144256	48.54	3.57	12.34
K02101	0.39	0.11	0.88	20.97	32.09	0.05	0.04	<0.01	0.05	0.24	<0.001	44.80	24	99.62	12.78	<0.01
K02102	77.39	11.24	2.16	0.42	0.25	0.23	2.64	0.72	0.07	<0.01	0.01	3.30	320	98.47	0.25	1.63
K02103	1.51	0.72	2.65	18.90	31.05	0.02	0.23	0.03	0.04	0.76	0.00	42.50	120	98.43	12.40	0.59
K02104	56.54	15.93	1.11	1.41	3.66	0.21	4.29	0.79	0.13	0.05	0.01	7.00	56964	97.51	1.49	1.58
K02111	6.63	0.76	4.94	0.86	5.03	0.01	0.20	0.03	<0.01	1.28	0.00	29.50	4298	49.73	6.67	3.17
K02114	0.51	0.14	1.10	18.61	30.04	0.01	<0.02	<0.01	0.01	0.18	<0.001	46.30	25	96.91	12.78	<0.01

Sample	Ni	Co	Cs	Sc	Ga	Hf	Nb	Rb	Sn	Sr	Ta	Th	Tl	U	V	W
M02111	0.4	41.7	0.2	1.0	<0,5	<0,5	<0,5	1.5	5.0	209.8	0.2	0.2	3.3	0.6	<5	1121.9
7006-117	1.6	10.2	<0,1	2.0	1.0	<0,5	<0,5	<0,5	<1	4526.0	1.1	<0.1	0.1	2.8	47.0	1013.1
7006-267	2.8	5.9	<0,1	< 1	1.1	<0,5	<0,5	<0,5	<1	55.4	0.3	0.4	0.1	0.8	27.0	1061.4
7006-268	2.3	11.0	<0,1	2.0	1.6	<0,5	<0,5	0.8	<1	35.8	0.7	0.5	0.8	1.5	23.0	3318.1
7006-275	5.0	46.6	0.6	1.0	2.5	<0,5	0.70	5.9	<1	77.3	0.4	0.6	1.4	3.1	15.0	2088.8
7006-291	7.1	10.6	0.2	1.0	2.9	<0,5	1.20	1.0	<1	59.8	0.5	0.7	0.1	2.9	41.0	2331.3
7006-303x	2.8	14.1	0.4	1.0	5.7	<0,5	0.80	3.9	<1	1325.5	0.1	0.9	1.9	2.7	18.0	149.2
7006-317x	7.1	9.7	2.4	2.0	9.9	0.8	2.60	28.1	<1	186.8	0.2	2.2	0.7	5.4	40.0	124.8
7006-330	3.5	8.0	0.5	1.0	7.8	<0,5	<0,5	5.0	<1	12.6	0.3	0.2	0.8	0.9	5.0	2395.1
7006-330x	3.9	11.3	0.2	1.0	8.8	<0,5	<0,5	2.9	<1	15.7	<0,1	0.3	1.4	0.9	<5	171.6
7006-336	20.9	34.2	9.3	9.0	13.1	5.3	12.10	113.7	2.0	61.5	0.9	7.0	0.9	2.0	76.0	547.1
7016-167	4.4	10.4	1.2	1.0	6.6	<0,5	0.60	11.5	<1	1099.1	0.4	1.1	3.8	3.5	31.0	1106.0
7016-197	6.3	12.5	5.3	4.0	9.8	1.4	3.20	50.6	<1	2932.9	0.2	3.1	4.8	18.8	38.0	1085.9
7016-202x	5.3	14.6	0.7	1.0	7.2	<0,5	1.00	6.9	<1	1439.5	0.2	0.8	5.2	1.9	12.0	45.9
7016-65x	18.1	20.1	2.9	1.0	6.8	0.7	1.70	23.0	1.0	1959.0	0.1	1.6	2.9	9.2	91.0	154.4
7016-75	10.9	20.9	5.7	4.0	11.3	1.3	4.70	58.0	1.0	1072.8	0.7	4.1	1.8	3.6	47.0	1901.4
7018-145a	7.5	1.6	<0,1	< 1	1.0	<0,5	<0,5	<0,5	<1	58.4	<0,1	<0.1	0.4	0.6	8.0	4.6
7018-171	2.5	17.0	<0,1	1.0	0.6	<0,5	<0,5	0.6	<1	33.9	0.5	0.4	0.1	1.5	10.0	2891.8
7018-171a	4.6	10.0	<0,1	1.0	0.8	<0,5	<0,5	1.1	<1	30.6	0.2	0.2	1.6	1.5	10.0	1139.3
7018-188	15.5	0.6	0.4	< 1	<0,5	<0,5	<0,5	3.8	<1	59.3	<0,1	0.4	2.0	2.2	12.0	8.0
7018-194	5.5	15.8	<0,1	2.0	0.5	<0,5	<0,5	2.1	<1	32.3	0.7	<0.1	0.3	1.8	20.0	3707.3
7018-204a	5.0	13.9	0.2	< 1	1.1	<0,5	<0,5	2.6	<1	40.8	<0,1	<0.1	0.3	1.5	19.0	262.8
7018-360	1.2	20.5	0.6	3.0	12.7	<0,5	1.00	5.4	<1	689.9	0.9	1.1	2.2	12.6	15.0	3898.5
7018-370a	3.0	5.4	1.0	1.0	8.9	<0,5	0.80	7.7	<1	15.7	0.3	0.6	0.4	1.4	11.0	1368.4
7018-370ab	5.8	10.1	2.1	2.0	10.5	0.6	1.30	18.9	<1	12.9	0.5	1.1	0.6	2.7	25.0	2140.6
7018-370b	3.7	5.4	1.3	< 1	9.6	<0,5	0.80	7.9	<1	15.7	0.3	0.4	0.5	1.8	11.0	1413.6
7101-103	44.7	0.3	0.1	< 1	2.6	<0,5	<0,5	1.4	<1	8661.6	1.1	0.2	1.3	0.3	6.0	14.3
7101-131	2.7	18.5	0.1	1.0	3.8	<0,5	<0,5	1.0	<1	1344.7	0.4	0.2	0.2	1.1	5.0	1729.4
7101-141	0.3	6.7	0.2	1.0	1.4	0.6	<0,5	0.6	<1	8001.0	1.2	<0.1	0.4	0.3	5.0	421.9
7101-179x	3.3	32.5	<0,1	< 1	2.2	<0,5	<0,5	0.6	<1	5977.6	0.5	<0.1	10.5	0.7	5.0	56.4
7101-267	3.1	23.6	0.3	1.0	3.0	<0,5	<0,5	0.7	<1	2315.3	0.4	<0.1	6.4	0.5	<5	1178.4
7101-356	1.4	22.8	0.3	1.0	6.1	<0,5	<0,5	0.8	<1	44.5	0.7	0.2	7.0	1.0	10.0	3785.8
7101-404	12.4	22.6	0.3	4.0	2.6	<0,5	0.60	3.3	<1	3252.5	0.5	0.4	0.5	0.7	11.0	1032.1
7101-417	4.4	15.1	0.3	2.0	3.5	<0,5	0.90	7.3	<1	353.9	0.5	0.8	8.5	0.9	12.0	2739.5
K02100	23.3	60.5	0.4	3.0	17.6	<0,5	0.60	5.7	<1	6792.5	0.7	0.5	0.7	0.9	15.0	1063.9
K02101	0.9	11.7	<0,1	1.0	0.6	<0,5	<0,5	1.1	<1	94.1	0.4	<0.1	0.2	0.4	7.0	2225.0
K02102	21.5	31.0	5.3	11.0	13.4	8.4	14.50	110.2	2.0	69.3	2.1	12.8	0.7	2.8	116.0	5588.6
K02103	4.1	7.8	0.6	2.0	0.9	<0,5	0.90	8.3	<1	76.7	0.4	0.8	0.4	1.6	11.0	1980.3
K02104	22.2	19.9	10.5	19.0	20.3	5.4	15.90	168.5	3.0	1131.7	1.9	13.5	2.6	3.1	132.0	4585.2
K02111	63.2	37.1	1.0	4.0	5.5	<0,5	0.80	8.3	<1	88.8	0.3	0.5	5.1	2.9	14.0	1099.4
K02114	2.7	7.2	<0,1	1.0	<0,5	<0,5	<0,5	<0,5	<1	78.2	0.1	0.1	11.5	1.4	5.0	751.6

Sample	Zr	Y	La	Ce	Pr	Nd	Sm	Eu	Gd	Tb	Dy	Ho	Er	Tm	Yb	Lu	Mo
M02111	1.7	3.20	2.10	2.40	0.34	1.4	0.10	0.11	0.38	0.04	0.29	0.07	0.17	<0.05	0.2	0.03	0.3
7006-117	0.9	1.90	5.00	2.20	0.26	1.2	0.90	0.00	1.49	0.08	0.51	<0.05	0.09	<0.05	0.1	0.03	1.6
7006-267	3.1	4.20	4.60	5.90	0.78	3.0	0.70	1.17	1.02	0.15	0.53	0.12	0.28	<0.05	0.2	0.04	0.3
7006-268	4.2	4.50	5.10	7.10	0.70	3.7	0.60	1.03	0.84	0.12	0.56	0.08	0.24	<0.05	0.2	0.03	0.4
7006-275	9.3	4.50	6.30	7.70	0.82	3.6	0.80	0.93	0.88	0.13	0.53	0.09	0.27	<0.05	0.2	0.03	0.6
7006-291	12.0	6.90	13.00	20.40	2.15	9.0	2.10	3.58	1.97	0.27	1.03	0.15	0.35	0.1	0.4	0.07	0.3
7006-303x	9.1	2.90	15.60	22.40	2.11	9.5	1.80	<0.05	1.37	0.14	0.64	0.08	0.18	<0.05	0.2	0.03	0.7
7006-317x	28.7	4.90	21.30	30.30	2.73	10.7	1.70	1.59	1.39	0.18	0.64	0.13	0.44	0.1	0.4	0.07	2.7
7006-330	3.3	2.70	3.00	6.00	0.59	3.3	0.80	1.39	0.76	0.10	0.37	0.06	0.15	<0.05	0.1	0.02	0.7
7006-330x	2.9	2.30	2.50	4.80	0.57	2.6	0.60	1.19	0.65	0.08	0.45	0.06	0.13	<0.05	0.2	0.03	0.7
7006-336	183.1	22.10	25.30	52.40	5.52	24.6	4.10	0.94	4.11	0.74	3.66	0.75	2.37	0.3	2.1	0.34	0.4
7016-167	11.1	2.30	5.70	6.70	0.64	2.3	0.60	<0.05	0.65	0.06	0.43	0.08	0.23	<0.05	0.2	0.05	2.8
7016-197	45.2	5.40	17.60	25.80	2.56	10.3	1.90	<0.05	1.67	0.16	1.07	0.13	0.48	0.1	0.7	0.09	2.5
7016-202x	7.8	3.40	5.80	9.30	0.88	3.6	1.00	0.53	0.89	0.12	0.59	0.11	0.27	<0.05	0.3	0.04	1.1
7016-65x	15.2	6.90	11.60	13.10	1.31	6.0	2.70	<0.05	2.60	0.29	1.54	0.18	0.53	0.1	0.4	0.08	9.8
7016-75	48.8	6.20	26.30	24.80	2.03	6.8	1.60	<0.05	1.86	0.21	1.19	0.22	0.66	0.1	0.6	0.10	3.3
7018-145a	0.9	1.10	1.10	1.10	0.16	<0,1	0.20	0.08	0.27	0.03	0.11	<0.05	0.10	<0.05	0.1	0.01	0.4
7018-171	2.0	2.20	2.00	3.30	0.41	1.1	0.50	0.35	0.48	0.08	0.43	0.06	0.16	<0.05	0.2	0.02	0.3
7018-171a	3.1	1.10	0.70	1.80	0.22	0.8	0.20	0.16	0.26	0.03	0.21	<0.05	0.08	<0.05	0.2	<0.01	0.5
7018-188	4.9	2.60	2.40	3.90	0.44	2.3	0.40	0.41	0.67	0.07	0.39	0.07	0.17	<0.05	0.2	0.03	0.3
7018-194	2.0	2.60	2.00	3.10	0.41	1.8	0.50	0.36	0.68	0.07	0.44	0.07	0.16	<0.05	0.2	<0.01	0.4
7018-204a	3.4	5.00	4.30	9.20	0.96	4.6	1.30	1.03	0.85	0.13	0.94	0.11	0.31	<0.05	0.4	0.04	0.2
7018-360	10.7	18.00	22.70	31.80	3.49	17.4	4.20	5.16	4.99	0.48	2.59	0.43	1.02	0.1	0.7	0.10	5.3
7018-370a	9.4	4.80	6.60	12.00	1.27	6.1	1.60	2.40	1.88	0.17	0.85	0.12	0.33	<0.05	0.3	0.04	1.1
7018-370ab	17.9	6.20	9.70	16.10	1.64	7.7	1.60	2.16	1.78	0.23	1.19	0.17	0.39	0.1	0.4	0.06	1.4
7018-370b	9.4	5.00	6.90	11.70	1.36	7.1	1.80	2.56	2.11	0.21	0.95	0.13	0.33	<0.05	0.3	0.05	1.0
7101-103	3.5	0.60	7.60	0.60	0.07	<0,1	1.50	2.86	2.52	0.03	0.82	<0.05	<0.05	<0.05	0.1	<0.01	4.1
7101-131	2.3	0.80	2.60	1.80	0.14	0.5	0.50	0.88	0.72	0.03	0.38	<0.05	0.06	<0.05	0.1	0.01	3.1
7101-141	<0,5	0.60	11.30	1.50	0.07	0.6	2.20	7.09	3.64	0.03	1.27	<0.05	<0.05	<0.05	0.2	0.01	1.7
7101-179x	0.5	0.90	7.40	1.90	0.20	0.7	1.80	1.90	2.44	0.05	0.71	<0.05	<0.05	<0.05	0.1	<0.01	6.5
7101-267	1.1	1.00	5.90	6.80	0.65	3.3	1.00	1.07	1.39	0.04	0.38	<0.05	<0.05	<0.05	<0.05	<0.01	2.2
7101-356	2.1	3.10	4.50	7.20	0.75	3.3	1.10	1.51	0.94	0.10	0.58	0.05	0.18	<0.05	0.1	0.02	1.5
7101-404	5.5	2.90	6.80	4.80	0.48	1.8	1.90	2.26	2.70	0.13	1.13	0.08	0.21	<0.05	0.2	0.01	2.3
7101-417	6.9	2.70	5.80	10.80	1.11	5.0	1.40	1.67	1.49	0.12	0.60	0.09	0.19	<0.05	0.1	0.03	0.8
K02100	5.3	2.30	4.70	1.90	0.27	1.7	2.10	0.00	2.81	0.13	1.01	0.06	0.16	<0.05	0.2	0.02	1.4
K02101	1.1	2.40	0.90	1.90	0.26	1.5	0.30	0.21	0.44	0.07	0.40	0.06	0.17	<0.05	0.1	0.02	0.1
K02102	289.5	19.80	36.60	82.40	8.40	28.8	5.00	0.89	3.53	0.58	3.31	0.71	2.00	0.4	2.2	0.36	0.8
K02103	9.9	4.20	2.80	5.90	0.65	2.0	0.60	0.46	0.81	0.11	0.55	0.12	0.30	<0.05	0.3	0.03	0.9
K02104	163.5	26.30	40.60	85.60	8.69	30.4	5.80	0.76	5.41	0.79	4.95	0.95	2.59	0.5	2.6	0.46	0.8
K02111	10.6	13.50	3.00	4.50	0.73	4.4	1.60	1.53	1.95	0.30	1.34	0.28	0.55	0.1	0.5	0.05	4.8
K02114	<0,5	2.20	0.80	1.00	0.18	0.8	0.20	0.07	0.32	0.04	0.25	<0.05	0.14	<0.05	0.1	0.02	0.2

Sample	Cu	Pb	Zn	As	Cd	Sb	Bi	Ag					
M02111	2.0	81.10	642.0	25.0	15.0	5.9	<0,1	3.3					
7006-117	60.5	16500.0	9270.0	46.0	38.1	35.5	0.1	69.7					
7006-267	5.2	340.0	5957.0	17.0	11.9	8.2	0.1	0.3					
7006-268	22.8	2574.6	7655.0	55.0	12.3	7.7	0.1	1.5					
7006-275	5.3	2854.2	18186.0	106.0	27.8	8.4	0.1	1.9					
7006-291	2.2	330.0	5381.0	7.0	13.7	12.3	0.1	0.3					
7006-303x	34.5	15800.0	61295.0	48.0	250.0	35.8	0.1	28.2					
7006-317x	5.4	1345.5	4307.0	27.0	10.5	14.6	0.1	1.3					
7006-330	37.1	4303.3	31584.0	43.0	150.1	34.5	0.1	13.0					
7006-330x	74.3	14200.0	50390.0	65.0	255.8	55.8	0.1	26.7					
7006-336	6.6	25.50	76.0	26.0	0.1	5.7	0.4	0.4					
7016-167	95.3	35300.0	62007.0	49.0	268.9	123.8	0.2	66.6					
7016-197	63.8	38600.0	85314.0	173.0	362.1	105.0	0.2	84.4					
7016-202x	53.6	30100.0	43891.0	179.0	197.9	130.4	0.1	67.1					
7016-65x	3276.4	535.9	5042.0	208.0	6.8	144.5	5.9	7.6					
7016-75	1889.7	1082.8	3513.0	73.0	7.1	40.1	15.0	2.2					
7018-145a	2.8	533.3	3305.0	22.0	4.2	3.3	0.1	0.2					
7018-171	1.6	592.7	9364.0	4.0	17.6	2.1	0.1	0.8					
7018-171a	61.9	378000.0	110600.0	8.0	310.3	1054.1	0.1						
7018-188	14.6	1427.1	26275.0	8.0	29.1	5.4	0.1	1.6					
7018-194	4.2	1178.5	9896.0	24.0	10.5	24.6	0.1	0.9					
7018-204a	4.0	1681.8	44901.0	19.0	86.3	8.0	0.1	2.2					
7018-360	13.9	1084.2	21739.0	35.0	24.3	2.8	0.1	10.0					
7018-370a	1.4	6086.5	38780.0	11.0	137.4	6.2	0.1	0.1					
7018-370ab	1.4	822.2	5703.0	5.0	13.6	4.4	0.1	0.1					
7018-370b	1.2	6094.4	38850.0	11.0	139.3	6.4	0.1	0.1					
7101-103	108.3	8294.1	1415.0	192.0	1.8	39.6	1.8	51.3					
7101-131	1262.3	41100.0	32504.0	394.0	106.1	38.3	1.2	10.8					
7101-141	597.3	108900.0	25669.0	151.0	170.1	337.8	7.8	147.1					
7101-179x	2954.6	14500.0	54665.0	1628.0	213.2	51.3	14.1	28.5					
7101-267	2289.6	105300.0	234900.0	189.0	634.0	150.2	12.1	130.5					
7101-356	358.1	142200.0	172500.0	251.0	555.5	618.6	0.1						
7101-404	971.9	10000.0	17229.0	110.0	57.7	405.9	15.5	88.0					
7101-417	515.0	4601.1	1667.0	235.0	2.3	14.7	5.4	11.9					
K02100	128.9	121400.0	127100.0	110.0	164.1	411.5	0.1	117.0					
K02101	1.0	204.0	842.0	9.0	1.6	3.0	0.1	0.3					
K02102	11.7	149.2	2585.0	72.0	1.4	9.9	0.2	0.5					
K02103	11.1	306.0	9574.0	39.0	15.8	13.4	0.1	5.2					
K02104	42.6	724.7	692.0	19.0	1.1	46.4	0.5	2.7					
K02111	83.1	17200.0	343600.0	234.0	233.0	51.0	0.1	27.0					
K02114	13.5	2828.1	20573.0	38.0	231.1	15.6	0.1	0.5					

Sample	Location	Borehole No.	Depth	Local	Lithology	Comments
K02117	Ilrankuh			Koladahrvazeh	non-sulph. ore	white ore
K02118	Ilrankuh			Koladahrvazeh	dolomite breccia	white ore
K02120	Ilrankuh			Koladahrvazeh	dolomite	
K02121	Ilrankuh			Koladahrvazeh	dolomite	
K02122	Ilrankuh			Koladahrvazeh	white zinc ore	
K02128	Ilrankuh			Koladahrvazeh	white zinc ore	
K02131	Ilrankuh			Koladahrvazeh	oxide ore	
M02138	Mehdi Abad			VOB	dolomite	oxidised
M02139	Mehdi Abad			VOB	limestone	oxidised
M02140	Mehdi Abad			VOB	gossan	
M02141	Mehdi Abad			Felsite	gossan	
M02143	Mehdi Abad			VOB	dolomite	
M02144	Mehdi Abad			VOB	shale	
M02145	Mehdi Abad			VOB	red zinc ore	non-sulphide ore
M02147	Mehdi Abad			VOB	red zinc ore	non-sulphide ore
M02148	Mehdi Abad			VOB	shales, shaly limestone	
M02151	Mehdi Abad			VOB	dolomite	oxidised
M02152	Mehdi Abad			VOB	dolomite	mineralised, oxidised
M7008-205	Mehdi Abad	7008	-205	VOB	dolomite	sulphides
M7008-216	Mehdi Abad	7008	-216	VOB	dolomite	barite veins
M7008-266	Mehdi Abad	7008	-266	VOB	dolomite	breccia, with sulphides
M7008-295	Mehdi Abad	7008	-295	VOB	dolomite	breccia, with sulphides
M7008-302	Mehdi Abad	7008	-302	VOB	dolomite	breccia with barite veins and sulphides
M7008-309	Mehdi Abad	7008	-309	VOB	dolomite	breccia with barite veins and sulphides
M7008-314	Mehdi Abad	7008	-314	VOB	dark grey dolomite, shaly intercalations	barite, sulphides
M7008-330	Mehdi Abad	7008	-330	VOB	grey dolomite	sulphide ore, barite
M7008-371	Mehdi Abad	7008	-371	VOB	shaly limestone	barite
IK02107	Ilrankuh			Goushfil Pit	dolomite	
IK02108	Ilrankuh			Goushfil Pit	shales	weathered
IK02109	Ilrankuh			Goushfil Pit	mylonite	fault zone
IK02110	Ilrankuh			Goushfil Pit	dolomite	mineralised
IK02112	Ilrankuh			Goushfil Pit	shales	
IK02125	Ilrankuh			Koladahrvazeh	white-ore	
IK02126	Ilrankuh			Koladahrvazeh	white-ore	
IK02127A	Ilrankuh			Koladahrvazeh	white-ore	
IK02127B	Ilrankuh			Koladahrvazeh	white-ore	
IK02129	Ilrankuh			Koladahrvazeh	white-ore	
IK02130	Ilrankuh			Koladahrvazeh	massive barite	
IK02132	Ilrankuh	DDH64	-110	Koladahrvazeh	dolomite	
IK02133	Ilrankuh	DDH64	-13	Koladahrvazeh	dolomite	sulphides, partly oxidised
IK02134A	Ilrankuh	DDH64	-16.4	Koladahrvazeh	dolomite	

Sample	SiO2	Al2O3	Fe2O3	MgO	CaO	Na2O	K2O	TiO2	P2O5	MnO	Cr2O3	LOI	Ba	SUM (Oxides+LOI+Ba)	TOT/C	TOT/S
K02117	0.42	0.06	0.11	0.62	0.49	<0.01	<0.02	<0.01	<0.01	0.05	<0.001	34.20	2993	36.29	8.76	0.07
K02118	0.34	0.05	1.64	14.41	22.27	0.02	0.02	<0.01	0.02	0.12	<0.001	42.80	3187	82.05	11.52	0.09
K02120	0.21	0.05	0.28	21.05	31.77	0.05	<0.02	<0.01	0.04	0.08	<0.001	46.10	142	99.64	12.78	<0.01
K02121	0.44	0.10	0.33	21.67	32.52	0.06	<0.02	<0.01	0.03	0.09	<0.001	44.30	305	99.59	13.17	<0.01
K02122	1.58	0.04	1.86	8.17	15.04	0.01	<0.02	<0.01	0.02	0.40	<0.001	32.00	2413	59.40	9.09	0.08
K02128	17.94	0.04	0.89	0.23	0.32	0.01	0.02	<0.01	<0.01	0.06	<0.001	10.70	7637	31.06	1.17	0.24
K02131	0.10	<0.03	0.44	0.26	0.33	<0.01	<0.02	<0.01	<0.01	0.03	<0.001	29.60	4549	31.29	7.93	0.16
M02138	4.20	1.01	22.23	5.07	14.61	2.03	0.27	0.03	0.04	7.11	<0.001	28.30	383	84.95	5.03	0.34
M02139	11.38	1.81	19.47	0.36	22.26	0.03	0.53	0.09	0.01	7.22	0.00	23.00	377	86.20	4.69	0.05
M02140	1.78	0.60	46.04	2.57	6.09	0.52	0.16	0.02	0.02	18.16	<0.001	15.60	5912	92.22	2.12	0.44
M02141	3.64	0.78	50.41	0.19	0.29	0.72	0.27	0.03	0.06	16.60	0.00	12.80	5389	86.39	0.13	0.16
M02143	29.02	8.94	4.13	8.86	18.57	0.10	2.70	0.43	0.10	0.59	0.01	26.00	230	99.47	7.03	0.24
M02144	65.26	12.24	4.06	1.85	2.51	0.12	2.92	0.71	0.10	0.25	0.01	9.30	396	99.38	1.85	1.74
M02145	2.10	0.85	44.20	1.30	0.25	0.17	0.22	0.03	0.02	24.48	<0.001	12.90	1102	86.65	0.17	0.05
M02147	3.32	1.51	48.79	1.28	0.45	0.20	0.47	0.07	0.05	22.15	0.00	11.00	6134	89.98	0.19	0.08
M02148	54.57	9.32	3.11	4.50	8.91	0.11	2.66	0.52	0.16	0.48	0.01	14.20	226	98.57	3.63	0.23
M02151	6.77	1.42	6.07	11.35	23.56	0.11	0.39	0.07	0.02	2.18	0.00	38.40	1593	90.52	10.16	0.18
M02152	6.32	0.95	6.05	13.99	30.32	<0.01	0.25	0.04	0.06	2.24	<0.001	38.00	97	98.23	11.44	<0.01
M7008-205	1.32	0.48	6.86	12.07	19.31	0.03	<0.02	0.02	0.04	1.32	<0.001	32.00	120494	86.91	8.79	4.04
M7008-216	0.34	0.08	3.61	12.34	21.81	0.01	<0.02	<0.01	0.01	1.40	<0.001	34.50	95896	84.83	9.57	3.80
M7008-266	1.11	0.66	1.78	6.09	10.03	<0.01	0.07	0.04	0.01	0.97	0.00	8.30	151812	46.01	4.79	13.09
M7008-295	1.42	0.79	1.43	8.27	14.28	0.03	0.10	0.05	0.02	0.31	0.00	15.50	132410	56.99	6.10	8.87
M7008-302	1.32	1.04	4.91	17.13	25.76	0.04	0.05	0.06	0.11	1.35	0.00	40.80	32576	96.21	10.79	1.11
M7008-309	0.71	0.30	1.83	10.65	17.18	<0.01	0.10	0.02	0.02	0.53	<0.001	22.30	154480	70.89	7.11	7.84
M7008-314	2.84	0.95	3.78	11.96	22.55	0.02	0.32	0.05	0.05	1.44	0.00	34.40	57302	84.77	10.28	3.26
M7008-330	0.89	0.18	46.58	2.10	0.92	0.02	0.05	<0.01	<0.01	10.97	<0.001	30.80	3042	92.87	9.67	2.18
M7008-371	13.27	0.39	34.52	1.26	0.61	0.02	0.10	0.02	<0.01	6.19	<0.001	21.60	116951	91.04	6.75	3.09
IK02107	9.85	1.75	5.01	11.90	19.66	0.06	0.44	0.10	0.02	1.13	0.00	29.00	63875	86.06	8.96	4.11
IK02108	76.02	11.52	0.93	0.40	0.03	0.20	2.94	0.66	0.06	<0.01	0.01	4.50	1346	97.42	0.29	0.81
IK02109	37.44	2.09	11.26	0.26	0.31	0.05	0.50	0.11	0.02	0.06	0.00	14.80	171	66.93	1.05	18.59
IK02110	1.23	0.38	7.60	10.88	20.66	0.02	0.08	0.02	<0.01	2.32	<0.001	30.20	91340	83.60	9.16	4.37
IK02112	60.01	16.41	5.26	1.87	1.87	0.18	3.63	0.83	0.15	0.07	0.01	6.00	633	96.37	1.35	0.10
IK02125	18.57	0.11	2.51	0.12	0.17	0.01	<0.02	<0.01	0.01	0.41	<0.001	14.60	314	36.56	0.81	0.06
IK02126	16.07	0.02	5.85	0.03	0.02	<0.01	<0.02	<0.01	0.01	0.17	<0.001	15.00	1784	37.37	1.07	0.09
IK02127A	20.32	0.02	0.84	0.83	1.24	<0.01	<0.02	<0.01	0.03	0.28	<0.001	10.00	2843	33.88	1.34	0.09
IK02127B	21.23	0.03	1.05	0.77	1.10	0.01	<0.02	<0.01	0.04	0.17	<0.001	10.10	2628	34.79	1.23	0.07
IK02129	1.40	0.08	0.97	0.23	0.07	<0.01	<0.02	<0.01	<0.01	0.14	<0.001	28.40	459	31.36	5.26	0.01
IK02130	1.11	0.13	1.12	0.56	0.15	<0.01	<0.02	0.01	<0.01	0.21	<0.001	23.50	148220	43.35	4.72	4.67
IK02132	0.09	0.02	0.57	22.47	29.48	0.02	<0.02	<0.01	<0.01	0.13	<0.001	44.80	118	97.60	12.93	0.01
IK02133	0.42	0.03	0.77	15.62	21.58	0.02	<0.02	<0.01	<0.01	0.12	<0.001	44.70	433	83.32	11.61	0.12
IK02134A	0.08	0.02	0.42	23.90	30.98	<0.01	<0.02	<0.01	<0.01	0.11	<0.001	43.10	69	98.64	12.83	0.01

Sample	Ni	Co	Cs	Sc	Ga	Hf	Nb	Rb	Sn	Sr	Ta	Th	Tl	U	V	W
K02117	3.4	12.1	<0,1	< 1	<0,5	<0,5	<0,5	<0,5	<1	6.1	0.1	<0.1	0.3	0.3	<5	566.7
K02118	6.8	10.3	<0,1	< 1	<0,5	<0,5	<0,5	<0,5	<1	70.5	0.4	<0.1	0.7	1.0	10.0	1868.7
K02120	0.1	5.4	0.1	< 1	<0,5	<0,5	<0,5	<0,5	<1	76.0	0.2	<0.1	0.3	1.2	<5	1151.1
K02121	2.4	14.5	<0,1	< 1	<0,5	<0,5	<0,5	<0,5	<1	90.4	0.4	<0.1	0.2	1.0	<5	1614.8
K02122	0.1	10.0	<0,1	< 1	<0,5	<0,5	<0,5	<0,5	<1	87.8	0.3	<0.1	4.1	3.9	<5	1216.0
K02128	2.6	16.7	<0,1	< 1	1.6	<0,5	<0,5	0.9	<1	66.2	0.4	<0.1	0.3	3.0	<5	1852.6
K02131	1.1	10.5	0.1	< 1	1.4	<0,5	<0,5	0.9	<1	60.0	0.2	<0.1	0.6	0.7	<5	1084.5
M02138	8.9	10.4	0.7	1.0	4.2	<0,5	0.80	7.0	<1	152.4	0.2	1.7	1.5	3.3	14.0	730.1
M02139	10.1	17.6	2.1	2.0	6.4	0.9	2.00	17.0	<1	65.9	0.3	1.8	17.9	3.6	27.0	831.2
M02140	13.8	40.5	1.1	1.0	9.6	<0,5	0.50	5.3	<1	373.5	0.2	0.5	2.6	3.0	7.0	444.3
M02141	8.7	65.1	0.9	2.0	10.1	<0,5	0.90	8.3	<1	104.0	0.8	0.7	14.3	10.3	14.0	3400.7
M02143	13.0	15.1	11.3	9.0	15.0	2.8	8.40	104.1	1.0	134.7	0.7	8.8	1.4	2.4	74.0	1084.0
M02144	39.8	95.5	31.3	11.0	16.4	6.5	13.10	124.6	2.0	70.2	1.2	10.8	2.5	4.2	98.0	1312.8
M02145	32.8	60.2	0.8	1.0	12.0	<0,5	<0,5	5.0	<1	330.7	0.2	0.6	0.5	3.6	12.0	780.4
M02147	42.7	63.1	1.4	2.0	12.0	<0,5	1.30	10.9	<1	1645.6	0.6	1.4	2.9	6.8	23.0	2508.3
M02148	12.4	21.6	10.8	11.0	14.7	5.5	10.40	98.9	2.0	73.5	2.0	8.3	1.0	2.9	81.0	7042.9
M02151	21.4	1.6	1.6	1.0	4.4	0.6	1.00	14.4	<1	69.1	0.1	1.4	2.9	3.2	18.0	4.0
M02152	4.9	22.7	0.8	1.0	3.8	<0,5	0.80	8.9	<1	70.0	0.3	0.7	0.3	2.0	14.0	974.3
M7008-205	4.9	9.4	0.1	<1	2.0	<0,5	<0,5	0.6	<1	2955.1	0.9	0.6	0.1	4.2	31.0	1083.1
M7008-216	2.6	10.2	<0,1	1.0	1.4	<0,5	<0,5	0.9	<1	2311.3	0.8	0.2	0.1	0.7	9.0	2504.9
M7008-266	8.4	5.3	0.3	<1	2.6	0.7	0.80	3.6	<1	3818.7	0.9	0.7	1.0	1.2	32.0	732.1
M7008-295	8.4	7.0	0.4	2.0	1.7	0.7	0.80	5.1	<1	3188.0	1.0	0.5	0.5	1.5	56.0	1119.6
M7008-302	8.6	9.7	0.3	2.0	2.9	0.5	1.10	2.5	<1	703.9	0.6	0.9	0.1	2.0	115.0	2093.4
M7008-309	1.3	5.0	0.6	<1	1.1	0.8	<0,5	4.1	<1	3234.7	1.0	0.5	0.4	2.5	18.0	841.2
M7008-314	8.8	19.5	1.1	2.0	2.4	0.7	1.10	12.6	<1	1059.0	1.1	1.2	2.5	9.0	43.0	4580.6
M7008-330	2.2	22.7	0.3	<1	9.3	<0,5	<0,5	2.3	<1	69.3	0.4	<0.1	0.6	1.7	7.0	2120.2
M7008-371	1.0	13.9	0.4	<1	5.4	<0,5	<0,5	4.4	<1	2414.7	0.5	0.6	0.1	1.5	9.0	1427.9
IK02107	15.1	11.3	1.3	2.0	4.7	0.9	2.00	17.8	<1	1917.8	0.8	2.2	5.6	2.0	30.0	272.8
IK02108	14.9	37.0	5.1	10.0	15.2	6.5	14.50	122.1	2.0	78.4	1.6	14.7	0.9	4.0	102.0	3910.3
IK02109	103.2	51.1	1.3	2.0	10.3	1.2	2.60	20.9	9.0	14.4	0.3	3.3	1.2	0.7	17.0	1102.9
IK02110	15.2	10.2	0.5	1.0	2.5	<0,5	<0,5	4.0	<1	4551.2	0.9	0.3	5.4	1.0	14.0	1104.3
IK02112	52.7	33.8	11.8	18.0	20.5	6.2	16.80	146.6	2.0	75.9	1.6	17.0	1.5	5.9	130.0	2302.9
IK02125	4.1	18.3	<0,1	1.0	0.7	<0,5	<0,5	1.2	<1	77.7	0.2	<0.1	6.3	12.9	<5	2367.0
IK02126	1.6	5.4	<0,1	<1	0.8	<0,5	1.10	<0,5	<1	135.6	<0,1	0.1	7.4	3.6	<5	930.4
IK02127A	4.8	25.4	<0,1	1.0	0.8	<0,5	<0,5	<0,5	<1	22.0	0.2	<0.1	7.8	2.3	<5	1979.5
IK02127B	3.6	9.4	<0,1	<1	0.8	<0,5	<0,5	<0,5	<1	28.8	<0,1	<0.1	2.6	1.7	<5	267.3
IK02129	6.8	2.4	<0,1	<1	2.4	<0,5	<0,5	<0,5	<1	24.6	<0,1	0.1	1.4	0.7	<5	28.0
IK02130	5.1	6.9	<0,1	<1	1.8	0.8	<0,5	<0,5	<1	5451.6	0.8	0.5	2.9	0.7	<5	264.2
IK02132	2.2	11.6	<0,1	1.0	<0,5	<0,5	<0,5	<0,5	<1	86.7	0.4	<0.1	<0.15	0.4	<5	2688.8
IK02133	3.6	10.0	0.1	<1	0.6	<0,5	<0,5	<0,5	<1	82.4	0.2	<0.1	0.7	1.2	<5	1152.3
IK02134A	1.3	9.2	<0,1	1.0	<0,5	<0,5	<0,5	<0,5	<1	64.1	0.3	<0.1	<0.15	<0,1	<5	1594.9

Sample	Zr	Y	La	Ce	Pr	Nd	Sm	Eu	Gd	Tb	Dy	Ho	Er	Tm	Yb	Lu	Mo
K02117	<0,5	1.60	0.80	<0,5	0.14	0.6	0.20	0.00	0.22	0.02	0.16	<0.05	0.11	<0.05	0.1	<0.01	0.1
K02118	<0,5	2.10	0.90	0.60	0.12	0.5	0.20	0.00	0.30	0.05	0.18	<0.05	0.14	<0.05	0.1	<0.01	1.0
K02120	<0,5	0.70	<0,5	<0,5	0.04	<0,1	<0,1	0.00	0.08	0.02	0.05	<0.05	<0.05	<0.05	<0.05	<0.01	0.3
K02121	<0,5	0.60	<0,5	<0,5	0.05	<0,1	<0,1	<0.05	<0.05	<0.01	0.00	<0.05	<0.05	<0.05	<0.05	<0.01	0.2
K02122	<0,5	0.80	<0,5	<0,5	0.06	<0,1	<0,1	<0.05	0.10	0.01	0.07	<0.05	<0.05	<0.05	<0.05	<0.01	1.7
K02128	1.7	0.20	0.50	0.50	0.06	0.5	<0,1	<0.05	0.10	<0.01	0.06	<0.05	<0.05	<0.05	<0.05	<0.01	0.5
K02131	<0,5	0.20	<0,5	0.50	0.08	<0,1	<0,1	<0.05	<0.05	<0.01	<0.05	<0.05	<0.05	<0.05	<0.05	<0.01	2.1
M02138	9.7	6.60	9.00	14.30	1.50	6.5	1.40	1.54	1.81	0.24	1.16	0.17	0.40	0.1	0.3	0.05	3.6
M02139	31.8	6.20	9.00	15.80	1.69	7.1	1.40	1.05	1.44	0.20	0.99	0.19	0.50	0.1	0.5	0.08	2.3
M02140	5.1	9.00	10.90	16.10	1.63	7.7	2.00	3.30	2.95	0.35	1.54	0.25	0.54	0.1	0.4	0.05	1.9
M02141	8.2	8.10	15.10	20.30	2.29	9.4	2.50	4.36	3.10	0.40	1.80	0.27	0.57	0.1	0.5	0.08	2.4
M02143	89.4	24.30	25.60	53.60	5.73	21.4	4.20	1.04	4.32	0.74	4.05	0.74	1.99	0.3	1.8	0.28	0.1
M02144	225.5	25.90	29.70	59.70	6.74	24.8	5.20	1.04	4.14	0.79	4.34	0.84	2.35	0.4	2.5	0.40	0.9
M02145	9.9	8.20	13.70	19.10	2.61	11.4	2.90	3.15	3.54	0.39	1.70	0.28	0.71	0.1	0.5	0.07	3.3
M02147	15.0	9.40	13.10	18.60	2.04	8.5	2.20	2.12	2.68	0.32	1.39	0.25	0.58	0.1	0.5	0.08	6.1
M02148	182.5	24.00	27.60	56.20	6.02	22.2	5.10	1.05	4.95	0.71	3.98	0.82	2.25	0.4	2.2	0.35	0.5
M02151	16.4	7.50	7.20	9.20	1.24	5.1	1.00	0.86	1.64	0.19	0.89	0.18	0.40	0.1	0.3	0.05	4.0
M02152	11.0	3.80	4.00	7.10	0.81	3.1	0.80	0.45	1.01	0.11	0.52	0.10	0.27	<0.05	0.2	0.04	1.0
M7008-205	5.2	5.20	7.50	7.90	0.87	4.0	1.10	1.78	1.42	0.14	1.37	0.10	0.28	0.1	0.3	0.05	1.4
M7008-216	0.7	3.70	5.80	6.20	0.57	2.4	0.60	0.44	0.99	0.10	1.07	0.08	0.17	<0.05	0.2	0.03	0.4
M7008-266	9.7	3.00	5.70	5.80	0.48	1.8	0.70	0.25	0.95	0.10	1.33	<0.05	0.18	<0.05	0.2	0.04	0.5
M7008-295	10.2	3.40	6.40	7.60	0.62	2.6	0.70	<0.05	0.86	0.12	1.13	0.07	0.16	<0.05	0.2	0.04	0.3
M7008-302	13.6	6.40	9.00	14.60	1.35	5.5	1.20	1.39	1.26	0.17	0.87	0.18	0.37	0.1	0.4	0.08	0.5
M7008-309	3.9	3.10	6.30	4.60	0.48	2.1	0.60	0.43	0.88	0.08	1.34	<0.05	0.12	<0.05	0.1	0.03	0.5
M7008-314	14.4	7.10	14.50	21.60	2.07	9.0	2.00	4.17	1.84	0.25	1.48	0.17	0.44	0.1	0.4	0.08	2.3
M7008-330	1.5	4.80	4.70	6.80	0.78	3.0	0.90	1.83	0.95	0.16	0.68	0.12	0.25	<0.05	0.2	0.04	1.9
M7008-371	5.3	3.10	4.40	5.10	0.49	2.6	0.80	0.83	1.21	0.12	1.13	0.07	0.15	<0.05	0.1	0.02	1.1
IK02107	20.2	10.20	6.50	13.10	1.45	6.7	2.50	1.14	2.46	0.36	1.93	0.29	0.72	0.1	0.6	0.08	6.7
IK02108	233.0	20.60	36.90	77.10	7.70	31.0	4.90	1.07	3.68	0.68	3.26	0.76	1.97	0.3	2.3	0.36	0.9
IK02109	40.2	6.00	5.80	12.90	1.27	6.1	1.30	0.44	1.39	0.18	1.07	0.22	0.58	0.1	0.5	0.09	0.6
IK02110	4.1	8.30	3.10	5.30	0.78	3.8	1.90	5.51	2.21	0.30	2.10	0.28	0.51	0.1	0.4	0.07	1.9
IK02112	190.4	29.00	41.20	85.10	9.48	37.1	6.50	1.38	5.04	0.94	4.86	1.11	2.78	0.5	2.7	0.47	0.6
IK02125	0.5	0.30	0.50	0.50	0.06	<0,1	<0,1	<0.05	<0.05	0.01	<0.05	<0.05	<0.05	<0.05	<0.05	<0.01	2.7
IK02126	<0,5	0.20	<0,5	<0,5	0.05	<0,1	<0,1	<0.05	<0.05	0.01	<0.05	<0.05	<0.05	<0.05	<0.05	<0.01	3.5
IK02127A	<0,5	0.40	<0,5	1.20	0.05	<0,1	<0,1	<0.05	0.07	0.01	0.08	<0.05	<0.05	<0.05	<0.05	<0.01	2.4
IK02127B	<0,5	0.40	<0,5	0.80	0.06	<0,1	<0,1	0.06	<0.05	<0.01	<0.05	<0.05	<0.05	<0.05	<0.05	<0.01	1.6
IK02129	1.1	0.40	0.50	0.80	0.07	<0,1	<0,1	<0.05	<0.05	0.01	<0.05	<0.05	<0.05	<0.05	<0.05	<0.01	2.4
IK02130	1.9	1.50	2.60	0.70	0.07	<0,1	0.40	0.80	0.68	0.04	1.15	<0.05	<0.05	<0.05	<0.05	0.02	3.3
IK02132	0.5	0.50	<0,5	<0,5	0.04	<0,1	<0,1	<0.05	<0.05	<0.01	<0.05	<0.05	<0.05	<0.05	<0.05	<0.01	0.3
IK02133	0.7	0.50	<0,5	<0,5	0.06	<0,1	<0,1	<0.05	<0.05	<0.01	0.09	<0.05	<0.05	<0.05	<0.05	<0.01	0.7
IK02134A	<0,5	0.50	<0,5	<0,5	0.05	<0,1	<0,1	<0.05	<0.05	<0.01	0.06	<0.05	<0.05	<0.05	<0.05	<0.01	0.2

Sample	Cu	Pb	Zn	As	Cd	Sb	Bi	Ag					
K02117	218.9	1334.5	497300.0	10.0	>2000	4.9	0.1	0.6					
K02118	30.3	1512.0	136300.0	113.0	205.8	44.8	0.1	3.7					
K02120	1.4	81.60	493.0	8.0	1.2	9.0	0.1	0.4					
K02121	0.8	89.50	222.0	12.0	0.3	0.8	0.1	0.3					
K02122	38.2	47000.0	237700.0	393.0	1009.6	23.9	0.1	12.3					
K02128	60.7	60600.0	436000.0	214.0	18.8	250.9	0.1	23.9					
K02131	49.3	225800.0	350600.0	136.0	308.1	643.4	0.1	5.4					
M02138	2.7	19900.0	90592.0	140.0	265.8	14.5	0.1	2.0					
M02139	38.9	23600.0	84195.0	469.0	192.7	63.0	0.1	3.9					
M02140	2.3	453.6	45749.0	160.0	254.4	4.2	0.1	1.7					
M02141	2.9	32100.0	74661.0	532.0	164.8	123.0	0.1	1.5					
M02143	21.8	204.6	863.0	20.0	1.4	7.0	0.2	0.1					
M02144	138.2	106.9	1103.0	129.0	1.0	18.2	0.3	0.6					
M02145	9.7	10637.2	80707.0	254.0	480.4	9.6	0.1	9.7					
M02147	1.9	5670.0	61025.0	58.0	418.9	4.2	0.1	20.3					
M02148	5.1	114.6	974.0	9.0	1.4	4.0	0.3	0.2					
M02151	4.5	6834.4	62443.0	43.0	383.9	53.3	0.1	0.8					
M02152	1.0	483.8	10255.0	19.0	8.2	36.4	0.1	0.1					
M7008-205	31.2	15600.0	10200.0	12.0	34.9	41.8	0.1	43.5					
M7008-216	25.3	18900.0	26000.0	1.0	99.6	13.8	0.1	29.5					
M7008-266	258.2	59300.0	177300.0	5.0	691.5	85.8	0.1	168.9					
M7008-295	57.3	106800.0	93600.0	2.0	399.4	36.3	0.1	65.3					
M7008-302	42.8	1751.0	11700.0	24.0	53.6	54.7	0.1	6.4					
M7008-309	49.5	11400.0	51400.0	8.0	205.0	42.5	0.1	75.4					
M7008-314	33.5	5090.5	29900.0	139.0	127.2	45.1	0.1	11.0					
M7008-330	<0,1	1127.8	40400.0	12.0	118.8	5.9	0.1	3.8					
M7008-371	610.6	456.2	734.0	99.0	2.5	231.2	4.2	7.0					
IK02107	14.9	1918.8	19200.0	122.0	22.6	17.0	0.1	5.6					
IK02108	7.2	784.0	2870.0	60.0	4.6	21.1	0.2	1.0					
IK02109	218.3	2875.4	264800.0	714.0	440.5	152.6	0.1	14.5					
IK02110	6.7	3425.4	28800.0	38.0	65.6	7.6	0.1	3.2					
IK02112	46.5	49.20	290.0	21.0	0.1	6.8	0.3	0.1					
IK02125	52.0	96900.0	478300.0	515.0	507.8	101.1	0.1	7.3					
IK02126	102.9	166700.0	408500.0	927.0	26.8	151.4	0.1	45.2					
IK02127A	20.2	6057.2	517800.0	142.0	177.8	228.0	0.1	0.7					
IK02127B	24.0	5028.2	510600.0	157.0	174.4	222.0	0.1	0.6					
IK02129	256.2	214200.0	430900.0	201.0	452.7	1170.0	0.1	23.6					
IK02130	241.7	50000.0	322200.0	106.0	623.5	787.0	0.1	9.2					
IK02132	3.1	752.2	2598.0	7.0	8.8	12.9	0.1	0.8					
IK02133	29.3	25700.0	100600.0	48.0	81.5	108.3	0.1	10.3					
IK02134A	1.0	106.4	326.0	2.0	1.4	1.1	0.1	0.4					

Sample	Location	Borehole No.	Depth	Local	Lithology	Comments
IK02134B	Ilrankuh	DDH64	-16.4	Koladahrvazeh	shales	
IK02135	Ilrankuh	DDH64	-50.5	Koladahrvazeh	non-sulph. ore	
IK02139	Ilrankuh	DDH64	-96.8	Koladahrvazeh	non-sulph. ore	
IK02140	Ilrankuh	DDH64	-97	Koladahrvazeh	non-sulph. ore	
IK02141	Ilrankuh	DDH64	-109.5	Koladahrvazeh	non-sulph. ore	
IK02142	Ilrankuh	DDH64	-111	Koladahrvazeh	dolomite	parltly non-sulph. Minerals
IK02143	Ilrankuh	DDH64	-111.5	Koladahrvazeh	dolomite	sulphides
IK02145	Ilrankuh	DDH64	-112.5	Koladahrvazeh	non-sulph. ore	
IK02149	Ilrankuh	DDH40	-77	Koladahrvazeh	dolomite	
IK02151	Ilrankuh	DDH40	-74.5	Koladahrvazeh	non-sulph. ore	
IK02151grey	Ilrankuh	DDH40	-74.5	Koladahrvazeh	dolomite	
IK02154	Ilrankuh	DDH40	-54.2	Koladahrvazeh	dolomite/shale	contact zone
IK02155	Ilrankuh	DDH40	-45	Koladahrvazeh	dolomite	partly non-sulphide minerals
IK02156	Ilrankuh	DDH40	-40.5	Koladahrvazeh	non-sulph. ore	
IK02158	Ilrankuh			Koladahrvazeh	dolomite	barite rich
IK02159	Ilrankuh			Koladahrvazeh	non-sulph. Ore	malachite bearing
IK02160	Ilrankuh	DDH10G		Goushfil Pit	dolomite	
IK02161	Ilrankuh	DDH10G	-156	Goushfil Pit	dolomite	
IK02162	Ilrankuh	DDH10G	-149	Goushfil Pit	dolomite	partly sphalerite
IK02164	Ilrankuh	DDH10G	-117	Goushfil Pit	dolomite	sulphides, pyrite, partly oxidised
IK02166	Ilrankuh	DDH10G	-72	Goushfil Pit	shales and limestone	fault
IK02170	Ilrankuh	DDH10G	-25	Goushfil Pit	highly alterated, gossan	
IK02171	Ilrankuh	DDH10G	-20	Goushfil Pit	non-sulph. ore	gossan
IK02172	Ilrankuh	DDH10G	-15	Goushfil Pit	alterated, limestone	fault zone
IK02173	Ilrankuh	DDH10G	-12	Goushfil Pit	barite	
IK02174	Ilrankuh	DDH10G	-8	Goushfil Pit	gossan	
IK02175	Ilrankuh	DDH10G	-5	Goushfil Pit	dolomite	oxidised
M02155	Mehdi Abad			VOB	barite	black hill
M02156	Mehdi Abad			VOB	barite	black hill
M02157	Mehdi Abad			VOB	barite	black hill
M02158	Mehdi Abad			VOB	barite	black hill
M02159	Mehdi Abad			VOB	barite	black hill
M02160	Mehdi Abad			VOB	barite	black hill

Sample	SiO2	Al2O3	Fe2O3	MgO	CaO	Na2O	K2O	TiO2	P2O5	MnO	Cr2O3	LOI	Ba	SUM (Oxides+LOI+Ba)	TOT/C	TOT/S
IK02134B	55.39	14.53	5.70	2.36	4.85	0.73	3.51	0.71	0.14	0.07	0.01	10.60	255	98.64	2.68	0.32
IK02135	1.73	0.11	1.05	3.42	4.82	0.02	<0.02	<0.01	<0.01	0.12	0.00	20.40	179549	51.73	5.07	6.13
IK02139	12.23	0.03	1.04	9.25	14.00	<0.01	<0.02	<0.01	<0.01	0.21	<0.001	28.10	1999	65.11	6.46	0.10
IK02140	10.64	0.09	0.96	0.22	0.15	0.03	<0.02	0.01	0.02	0.16	<0.001	17.20	33600	33.24	2.50	0.97
IK02141	0.14	0.04	0.83	11.93	16.55	0.03	<0.02	<0.01	<0.01	0.15	<0.001	37.40	266	67.12	10.38	1.65
IK02142	0.18	0.02	2.23	18.11	26.08	<0.01	<0.02	<0.01	<0.01	0.41	<0.001	44.00	97	91.06	11.81	0.02
IK02143	0.15	0.05	0.60	13.26	17.89	0.01	<0.02	<0.01	<0.01	0.11	<0.001	14.20	27	46.29	8.67	10.69
IK02145	0.23	0.04	0.48	0.47	0.24	0.01	<0.02	<0.01	<0.01	0.08	<0.001	31.10	56	32.66	6.88	0.13
IK02149	0.24	0.06	2.12	21.78	30.55	0.01	<0.02	<0.01	<0.01	0.30	<0.001	43.40	18	98.47	13.68	0.46
IK02151	0.09	0.02	0.42	4.42	5.89	<0.01	<0.02	<0.01	<0.01	0.07	<0.001	18.80	96	29.71	6.05	11.32
IK02151grey	0.16	0.10	1.37	16.36	22.88	0.01	0.02	<0.01	<0.01	0.21	<0.001	21.30	71	62.43	10.20	7.84
IK02154	13.25	4.08	2.16	4.46	6.52	0.03	1.05	0.19	0.05	0.09	0.00	12.90	100348	55.99	4.32	11.94
IK02155	0.33	0.06	1.70	8.95	13.97	<0.01	<0.02	<0.01	<0.01	0.14	<0.001	9.00	90630	44.28	6.23	13.89
IK02156	2.00	0.73	3.81	1.52	2.51	<0.01	0.19	0.03	0.01	0.02	<0.001	10.60	191316	42.78	1.18	24.17
IK02158	0.31	0.05	3.26	12.73	17.63	<0.01	<0.02	<0.01	<0.01	0.20	<0.001	27.60	194143	83.47	7.91	4.99
IK02159	0.52	0.05	6.64	0.36	0.08	0.01	<0.02	<0.01	<0.01	0.91	<0.001	30.50	27	39.09	8.14	0.02
IK02160	0.41	0.19	10.36	15.67	28.08	0.04	0.05	0.01	<0.01	2.49	<0.001	33.20	28	90.51	11.52	3.92
IK02161	0.59	0.34	3.72	19.49	30.92	0.04	0.10	0.02	<0.01	1.56	<0.001	42.10	2810	99.20	13.16	0.32
IK02162	0.57	0.33	3.03	20.67	31.06	0.02	0.09	0.02	<0.01	1.18	<0.001	40.70	251	97.71	13.06	0.96
IK02164	1.41	0.19	30.79	8.77	25.57	<0.01	0.03	0.01	0.02	1.64	0.00	26.60	14710	96.69	7.73	2.03
IK02166	8.29	4.53	9.14	12.89	24.52	0.08	1.18	0.24	0.02	3.06	0.00	32.70	8496	97.60	10.00	1.53
IK02170	1.58	0.67	14.68	0.42	0.11	<0.01	0.13	0.03	0.02	1.86	0.00	26.90	62085	53.35	6.50	1.99
IK02171	4.12	1.46	41.18	0.08	0.01	0.02	0.29	0.12	0.03	0.05	0.01	9.30	228555	82.19	0.07	5.68
IK02172	12.22	6.90	11.11	0.33	0.13	0.09	1.63	0.41	0.06	0.56	0.01	13.20	276624	77.54	0.13	8.55
IK02173	1.54	0.48	0.53	0.03	0.03	<0.01	0.14	0.03	<0.01	0.02	<0.001	2.30	578144	69.66	0.07	13.89
IK02174	7.21	2.27	9.84	0.10	0.02	0.02	0.58	0.13	0.02	<0.01	0.00	5.70	433948	74.35	0.05	11.22
IK02175	1.37	0.54	7.36	14.60	27.43	0.03	0.16	0.02	<0.01	2.49	<0.001	39.60	3982	94.06	11.21	0.12
M02155	12.96	0.02	0.09	0.01	0.01	<0.01	<0.02	<0.01	<0.01	<0.01	<0.001	4.40	402612	62.40	0.12	12.25
M02156	22.39	0.09	28.89	0.05	0.16	0.02	<0.02	<0.01	<0.01	0.82	0.00	3.80	246693	83.79	0.07	6.20
M02157	0.09	0.02	0.02	0.01	0.01	<0.01	<0.02	<0.01	0.01	<0.01	<0.001	0.05	596815	66.78	0.01	13.59
M02158	18.83	0.03	2.29	0.01	0.02	0.01	<0.02	<0.01	<0.01	<0.01	<0.001	0.80	465897	74.01	0.03	11.22
M02159	60.68	1.82	1.49	0.04	0.04	0.02	0.34	0.13	0.67	<0.01	0.00	4.30	160181	87.43	0.08	4.35
M02160	7.97	0.81	9.73	0.23	0.34	0.06	0.22	0.04	0.03	1.40	<0.001	25.00	320930	81.66	0.19	11.11

Sample	Ni	Co	Cs	Sc	Ga	Hf	Nb	Rb	Sn	Sr	Ta	Th	Tl	U	V	W
IK02134B	38.2	21.4	18.5	15.0	18.8	4.2	11.00	131.8	2.0	113.9	1.1	10.7	2.8	1.8	106.0	2442.7
IK02135	3.2	6.7	<0,1	<1	0.8	0.8	<0,5	<0,5	<1	4405.8	1.5	0.1	1.6	4.2	<5	626.3
IK02139	2.1	16.0	<0,1	<1	0.6	<0,5	<0,5	<0,5	<1	67.7	<0,1	<0.1	5.3	0.5	16.0	231.8
IK02140	12.3	9.3	<0,1	<1	2.6	<0,5	<0,5	0.6	<1	438.9	0.3	<0.1	2.2	53.2	<5	1284.4
IK02141	2.1	5.3	0.1	<1	1.7	<0,5	<0,5	0.5	<1	126.4	<0,1	<0.1	1.0	0.3	<5	151.8
IK02142	3.2	20.2	<0,1	<1	1.1	<0,5	<0,5	<0,5	<1	64.8	0.2	<0.1	6.8	<0,1	<5	1143.6
IK02143	1.4	3.6	0.4	<1	2.9	<0,5	<0,5	0.5	<1	62.2	<0,1	<0.1	2.5	0.1	5.0	276.8
IK02145	3.8	2.5	<0,1	<1	2.6	<0,5	<0,5	<0,5	<1	67.1	<0,1	<0.1	2.2	1.1	<5	35.9
IK02149	17.0	31.3	<0,1	1.0	0.8	<0,5	<0,5	<0,5	<1	99.1	0.2	<0.1	<0.15	0.1	<5	801.5
IK02151	5.2	12.9	<0,1	1.0	0.6	<0,5	<0,5	<0,5	<1	272.1	0.4	0.1	4.6	0.4	<5	2377.5
IK02151grey	5.4	14.5	0.1	1.0	0.8	<0,5	<0,5	0.9	<1	69.5	0.4	<0.1	1.7	0.2	10.0	2674.2
IK02154	21.5	116.5	4.4	5.0	6.2	1.7	2.90	40.0	<1	4096.4	0.4	2.6	2.6	1.0	31.0	727.7
IK02155	4.2	5.2	<0,1	<1	1.7	<0,5	<0,5	<0,5	<1	2756.5	0.6	<0.1	2.6	0.2	<5	191.1
IK02156	9.5	3.2	1.0	1.0	3.3	0.7	<0,5	7.0	<1	7870.1	0.7	0.5	8.6	0.3	5.0	136.8
IK02158	2.8	3.8	<0,1	<1	1.0	0.8	<0,5	<0,5	<1	3538.7	1.9	0.1	1.4	0.6	<5	1287.8
IK02159	9.4	15.3	<0,1	<1	4.4	<0,5	<0,5	<0,5	<1	3.2	0.1	<0.1	9.0	6.8	<5	456.5
IK02160	6.2	8.5	<0,1	1.0	2.2	<0,5	<0,5	1.3	<1	69.8	<0,1	0.1	1.4	1.4	14.0	388.5
IK02161	3.0	5.6	0.3	<1	2.0	<0,5	<0,5	3.1	<1	154.2	<0,1	0.1	1.1	1.4	10.0	257.5
IK02162	6.9	9.2	0.2	1.0	1.7	<0,5	<0,5	3.1	<1	93.8	0.2	0.2	2.2	1.3	9.0	849.3
IK02164	43.4	23.6	<0,1	1.0	1.7	<0,5	<0,5	1.2	<1	380.0	0.5	0.4	3.9	1.8	6.0	2016.8
IK02166	19.6	12.1	7.0	7.0	7.4	1.4	2.90	43.9	<1	173.2	0.5	3.2	2.6	4.0	61.0	1398.5
IK02170	140.5	15.4	0.9	1.0	3.1	<0,5	<0,5	5.3	<1	1053.4	0.2	0.6	45.2	6.7	17.0	63.6
IK02171	10.1	2.1	0.9	1.0	7.6	1.0	1.90	10.4	<1	2660.8	1.1	1.8	4.1	5.4	45.0	238.7
IK02172	14.6	18.9	2.8	6.0	8.3	2.8	5.00	49.6	<1	7917.7	1.2	7.7	99.7	11.7	73.0	310.7
IK02173	1.9	2.3	0.2	<1	1.2	2.1	0.50	3.9	<1	16375.2	2.7	0.5	1.3	1.2	11.0	48.2
IK02174	3.4	3.6	0.9	1.0	4.5	1.8	1.80	16.3	<1	12444.1	1.2	2.1	3.5	3.0	40.0	503.7
IK02175	3.7	15.6	0.4	1.0	2.8	<0,5	<0,5	5.6	<1	419.6	<0,1	0.7	4.9	1.6	14.0	148.9
M02155	0.8	15.3	<0,1	1.0	0.7	1.2	<0,5	<0,5	<1	11753.1	1.4	<0.1	1.0	0.5	<5	2670.5
M02156	36.6	3.3	<0,1	<1	1.1	<0,5	<0,5	0.5	<1	4583.3	0.5	<0.1	262.9	2.2	6.0	21.9
M02157	0.1	4.4	<0,1	<1	<0,5	1.4	<0,5	0.5	<1	9113.2	3.0	<0.1	5.0	<0,1	<5	272.6
M02158	0.1	17.6	<0,1	1.0	0.8	1.4	<0,5	<0,5	<1	7221.6	1.6	<0.1	1.8	0.2	<5	1652.0
M02159	0.1	9.6	1.4	5.0	7.4	1.2	2.00	12.1	<1	3934.8	2.4	4.7	2.5	16.0	112.0	6615.3
M02160	19.5	31.6	2.4	<1	2.8	1.8	0.90	13.9	<1	8834.3	1.6	0.9	3.0	1.5	53.0	713.1

Sample	Zr	Y	La	Ce	Pr	Nd	Sm	Eu	Gd	Tb	Dy	Ho	Er	Tm	Yb	Lu	Mo
IK02134B	153.1	26.20	31.00	61.70	6.85	27.3	4.90	1.16	4.71	0.78	4.22	0.89	2.42	0.4	2.6	0.39	0.4
IK02135	0.6	1.80	2.90	<0,5	0.05	<0,1	0.40	<0.05	0.72	0.04	1.28	<0.05	<0.05	<0.05	<0.05	0.02	1.6
IK02139	0.9	0.80	0.50	<0,5	0.07	<0,1	<0,1	<0.05	0.07	<0.01	0.06	<0.05	0.05	<0.05	<0.05	<0.01	2.7
IK02140	2.2	0.70	1.70	1.50	0.15	<0,1	0.10	0.20	0.16	<0.01	0.30	<0.05	<0.05	<0.05	<0.05	<0.01	2.7
IK02141	0.6	0.60	0.70	0.70	0.10	<0,1	<0,1	<0.05	0.07	0.02	0.07	<0.05	<0.05	<0.05	<0.05	<0.01	1.1
IK02142	<0,5	1.10	0.60	0.60	0.12	<0,1	<0,1	<0.05	0.17	0.02	0.12	<0.05	0.08	<0.05	<0.05	<0.01	1.7
IK02143	0.7	0.80	0.50	0.60	0.08	<0,1	0.10	<0.05	0.11	0.01	0.05	<0.05	<0.05	<0.05	<0.05	<0.01	0.9
IK02145	0.9	0.30	<0,5	<0,5	0.06	<0,1	<0,1	<0.05	0.10	<0.01	0.05	<0.05	<0.05	<0.05	<0.05	<0.01	1.4
IK02149	0.5	1.40	<0,5	<0,5	0.06	<0,1	0.10	<0.05	0.23	0.03	0.19	<0.05	0.10	<0.05	0.1	0.02	0.3
IK02151	<0,5	0.30	<0,5	<0,5	0.02	<0,1	<0,1	<0.05	<0.05	<0.01	<0.05	<0.05	<0.05	<0.05	<0.05	<0.01	0.6
IK02151grey	1.2	0.60	<0,5	0.60	0.07	<0,1	<0,1	<0.05	0.07	0.02	<0.05	<0.05	<0.05	<0.05	0.1	0.01	0.5
IK02154	36.8	7.40	7.60	13.70	1.58	6.3	1.50	<0.05	1.42	0.20	1.69	0.22	0.62	0.1	0.7	0.09	2.5
IK02155	1.3	3.00	1.10	0.80	0.08	<0,1	0.40	<0.05	0.69	0.09	0.96	0.06	0.16	<0.05	0.1	0.02	0.4
IK02156	4.7	2.50	2.50	1.30	0.15	0.6	0.40	<0.05	0.89	0.06	1.37	<0.05	0.11	<0.05	0.1	0.02	0.4
IK02158	0.8	1.90	2.60	0.60	0.08	<0,1	0.30	<0.05	0.70	0.05	1.15	<0.05	0.06	<0.05	<0.05	0.01	1.6
IK02159	1.0	0.30	<0,5	0.90	0.05	<0,1	<0,1	<0.05	0.12	<0.01	0.07	<0.05	<0.05	<0.05	<0.05	<0.01	6.5
IK02160	2.3	1.90	1.00	2.00	0.31	1.1	0.40	0.62	0.52	0.06	0.34	0.05	0.14	<0.05	0.2	0.03	1.5
IK02161	3.9	1.70	1.20	2.10	0.25	1.0	0.40	0.23	0.38	0.06	0.21	<0.05	0.12	<0.05	0.1	0.02	1.1
IK02162	3.5	1.60	1.10	2.30	0.23	1.0	0.30	0.20	0.30	0.04	0.29	<0.05	0.12	<0.05	<0.05	0.02	0.8
IK02164	1.8	2.80	1.10	2.10	0.33	1.4	0.50	0.48	0.58	0.09	0.34	0.05	0.17	<0.05	0.1	0.02	2.2
IK02166	34.2	8.80	8.30	16.00	1.94	7.7	1.80	1.64	1.82	0.26	1.43	0.28	0.71	0.1	0.7	0.10	18.7
IK02170	11.8	5.50	2.30	3.60	0.52	2.7	1.30	1.47	1.51	0.20	1.23	0.18	0.41	<0.05	0.3	0.07	13.4
IK02171	20.3	3.60	6.40	7.00	0.67	2.6	0.60	<0.05	0.78	0.06	1.45	0.07	0.17	<0.05	0.3	0.05	7.6
IK02172	55.6	8.10	23.40	32.10	4.01	16.8	2.40	<0.05	1.69	0.22	2.63	0.22	0.59	0.1	0.8	0.14	36.6
IK02173	6.6	4.40	6.60	2.50	0.24	1.2	1.10	<0.05	1.60	0.10	2.96	<0.05	0.06	<0.05	0.1	0.04	1.7
IK02174	22.5	5.40	9.10	8.90	1.04	3.9	1.20	<0.05	1.45	0.12	2.40	0.07	0.23	0.1	0.4	0.07	11.2
IK02175	4.1	4.30	2.00	4.30	0.61	2.6	1.10	1.49	1.00	0.17	0.67	0.12	0.34	<0.05	0.3	0.04	2.5
M02155	<0,5	3.10	5.00	0.50	0.04	<0,1	0.60	<0.05	1.22	0.05	2.35	<0.05	<0.05	<0.05	0.1	<0.01	2.6
M02156	<0,5	3.00	3.50	1.80	0.20	0.8	0.60	<0.05	1.11	0.08	1.64	<0.05	0.06	<0.05	0.1	0.01	3.6
M02157	<0,5	4.10	6.30	<0,5	0.03	<0,1	0.90	<0.05	1.57	0.07	3.13	<0.05	<0.05	<0.05	0.1	0.01	0.2
M02158	<0,5	3.10	5.70	<0,5	0.02	<0,1	0.70	5.63	1.26	0.06	2.53	<0.05	<0.05	<0.05	0.1	0.01	5.0
M02159	23.4	5.80	14.30	29.00	4.40	21.9	8.10	9.85	6.00	0.48	2.33	0.14	0.30	0.1	0.4	0.06	2.3
M02160	10.1	5.20	8.70	4.80	0.47	1.4	0.90	3.37	1.56	0.13	2.44	0.07	0.20	0.1	0.2	0.06	2.2

Sample	Cu	Pb	Zn	As	Cd	Sb	Bi	Ag					
IK02134B	30.2	16.70	92.0	28.0	0.1	8.8	0.3	0.1					
IK02135	114.1	9177.2	230300.0	78.0	427.0	137.5	0.1	31.4					
IK02139	31.5	3624.5	282300.0	108.0	436.7	88.4	0.1	11.5					
IK02140	195.9	4906.8	511600.0	127.0	143.1	292.0	0.1	5.4					
IK02141	144.6	72100.0	201900.0	49.0	605.9	252.8	0.1	27.6					
IK02142	62.1	3150.2	56800.0	57.0	213.9	158.9	0.1	3.2					
IK02143	17.2	12800.0	221000.0	194.0	534.1	226.0	0.1	3.9					
IK02145	179.5	239800.0	391900.0	160.0	1390.5	748.0	0.1	61.4					
IK02149	1227.5	3464.6	3218.0	67.0	6.6	706.2	0.1	27.3					
IK02151	52.7	234700.0	329400.0	13.0	1331.8	263.5	0.1	6.0					
IK02151grey	77.2	2990.8	153100.0	29.0	243.1	59.5	0.1	11.1					
IK02154	14.7	19300.0	211700.0	90.0	1085.5	93.7	0.1	0.4					
IK02155	7.3	12900.0	228700.0	19.0	223.2	270.7	0.1	0.1					
IK02156	91.2	932.2	308400.0	441.0	450.2	212.6	0.1	1.9					
IK02158	133.1	2163.5	16400.0	116.0	55.7	95.0	0.1	5.1					
IK02159	>10000	15000.0	465600.0	1362.0	1706.8	>4000	0.1	87.1					
IK02160	12.7	1259.8	2646.0	130.0	5.7	17.6	0.1	3.9					
IK02161	2.6	426.8	967.0	11.0	1.8	6.2	0.1	1.0					
IK02162	3.0	2192.5	9192.0	18.0	16.4	9.9	0.1	3.7					
IK02164	115.2	1900.8	12500.0	683.0	11.6	82.9	0.1	116.6					
IK02166	13.0	1207.5	9227.0	24.0	11.8	9.0	0.1	2.6					
IK02170	91.1	6876.5	352800.0	171.0	744.6	240.0	0.1	22.8					
IK02171	39.4	9804.7	40700.0	586.0	33.1	21.1	0.1	5.4					
IK02172	33.4	25400.0	39900.0	1235.0	6.8	146.5	0.1	156.9					
IK02173	1.4	6836.8	2201.0	22.0	0.4	15.9	0.1	47.1					
IK02174	22.1	10800.0	6700.0	138.0	4.0	25.1	0.1	26.2					
IK02175	5.2	1954.6	38100.0	30.0	55.1	9.0	0.1	43.6					
M02155	1489.1	81500.0	225.0	76.0	2.3	360.0	0.1						
M02156	2292.8	1417.1	1121.0	43.0	2.6	18.3	4.8	35.9					
M02157	7.9	73.20	18.0	29.0	0.1	9.6	4.7	3.0					
M02158	525.8	3111.6	96.0	497.0	0.6	81.8	5.3	58.8					
M02159	98.8	9600.0	135.0	88.0	0.1	65.8	3.3	11.5					
M02160	66.5	66.30	350.0	82.0	1.5	15.5	1.5	1.7					